Finanziato dall'Unione europea NextGenerationEU | Ministero dell'Università e della Ricerca | Italiadomani PIANO NAZIONALE DI RIPRESA E RESILIENZA

multi-Risk sciEnce for resilienT commUnities undeR a changiNgclimate

Codice progetto MUR: **PE00000005** – CUP Lead Partner: F83C22001180002

Deliverable title: Report on field experiments in coastal, transitional and shallow hydrothermal vents area

Deliverable ID: DV 4.4.1

Due date: 15/02/2026

Submission date: 15/02/2026

AUTHORS

Annamaria Albanese (OGS), Rocco Auriemma (OGS), Laura Baldassarre (OGS), Elisa Banchi (OGS), Matteo Bazzaro (OGS), Margherita Burini (UNITS; OGS), Laura Caiazzo (ENEA), Raffaela Caprioli (ENEA), Federica Cassetti (UNIPA), Federica Cerino (OGS), Tamara Cibic (OGS), Giovanna Cilluffo (UNIPA), Cinzia Crovato (ENEA), Alessandra Davanzo (OGS), Michela D'Alessandro (OGS), Maurizio De Cassan (ENEA), Cinzia De Vittor (OGS), Giuseppa Di Bella (UNIME), Tommaso Diociaiuti (OGS), Nessim Douss (OGS), Valentina Esposito (OGS), M. Falzarano (UNISAPIENZA), Daniela Fornasaro (OGS), Marco Graziano (OGS), Marta Greco (UNIPA), Simona Iannucci (OGS), Martina Kralj (OGS), F. Litrenta (UNIME), Vincenzo Alessandro Laudicella (OGS), Sonia Manzo (ENEA), Maria Rita Montereali (ENEA), Federica Nasi (OGS), Vicenzo Nava (UNIME), Luisa Parrella (ENEA), Petrosillo Katiuscia (OGS, UNIPA), Alessandra Poletti (UNISAPIENZA), Marco Proposito (ENEA), Federica Relitti (OGS), Simona Retelletti Brogi (OGS), Lisa Sandri (OGS, UNIPA), Simona Schiavo (ENEA), Cosimo Solidoro (OGS), Franco Tassi (UNIFI), Lorenzo Toffanin (OGS), Agostino Tomasello (UNIPA), Cecilia D. Tramati (UNIPA), Geraldina Signa (UNIPA), Salvatrice Vizzini (UNIPA)

1 Technical references

Project Acronym	RETURN
Project Title	multi-Risk sciEnce for resilienT commUnities undeR a changiNg climate
Project Coordinator	Domenico Calcaterra UNIVERSITA' DEGLI STUDI DI NAPOLI FEDERICO II domcalca@unina.it
Project Duration	December 2022 – November 2025 (36 months)

Deliverable No.	DV 4.4.1
Dissemination level*	CO
Work Package	WP 4.4 – Multi risk assessment, and proof of concepts
Task	T4.4.1. - Climate change and environmental degradation. Field- and laboratory-scale experiments to assess synergistic/antagonistic effects and cumulative impact of multiple environmental degradation causes, including combined effects of warming, acidification, deoxygenation; heavy metals contaminations
Lead beneficiary	UNIPA
Contributing beneficiary/ies	OGS, ENEA

* PU = Public

PP = Restricted to other programme participants (including the Commission Services)

RE = Restricted to a group specified by the consortium (including the Commission Services)

CO = Confidential, only for members of the consortium (including the Commission Services)

1.1 Document history

Version	Date	Lead contributor	Description
0.1	15.02.2026	Salvatrice Vizzini (UNIPA)	Final version

2 Abstract

Climate change and environmental degradation are interconnected global challenges with far-reaching implications for biodiversity and ecosystem health. Marine and coastal environments, in particular, are exposed to an increasing number of stressors, such as warming, acidification, deoxygenation, and trace metal contamination. It is important to note that these stressors rarely act in isolation, while they interact in complex ways, producing effects that can amplify or mitigate their individual impacts. It is imperative to comprehend the interplay of these multifaceted effects to facilitate precise prediction of ecological responses and the formulation of efficacious mitigation strategies. This report presents a series of field- (Grado and Marano Lagoon, volcanic vents at the Aeolian Islands) and laboratory-scale experiments designed to investigate the cumulative impacts of multiple environmental stressors. The primary objective is to assess the nature and magnitude of interactions between the key drivers of degradation.

The benthic-pelagic ecosystem functioning of the Grado-Marano Lagoon, and its response to Hg contamination and O_2 depletion, were assessed through enclosures (June 2024), field samplings (June 2025) and experiments in aquaria (autumn 2025). In June 2024, 18 mesocosms were positioned in the most contaminated lagoon area. The dynamics of Hg, physical-chemical and biological variables were assessed in water and sediments at T0, after 96 hours (T1) and 10 days (T2), and compared to external sites. At T2, O2 concentration inside the mesocosms decreased (-48.1±7.3%) compared to T0, triggering changes in key benthic and pelagic biological processes. Benthic Primary Production and Community Respiration decreased by 21.4±2.2% and 63.4±2.9% respectively. In contrast, from T1 to T2, inorganic nutrients concentration increased in the water (P-PO_4 +84.6±6.9%, N-NH_4 +77.7±1.0%, Si-Si(OH) +59.7±3.6%) following organic matter remineralization by microbial activity (prokaryotic Heterotrophic C Production).

The combined effects of climate change (warming and acidification), sulphide, and trace metal contamination on photosynthesising and habitat-forming organisms and on their role as climatic refugia were studied using natural laboratories (hydrothermal vents). Two field surveys (September 2024 and May 2025) were carried out at Panarea vents and Salina controls to assess features of seawater, interstitial water, sediment, and the seagrass *Posidonia oceanica*. At impacted sites, pH ranged from 7.30–7.97 in the water column and 4.9–6.5 in interstitial waters. A 54°C anomaly was found in one site's sediments. High Hg and As levels were also observed. Stressors led to reduced leaf area, brown tissue, and fewer/shorter scales in *Posidonia*, plus 50% growth inhibition in the microalgae *Dunaliella tertiolecta* during the ecotoxicity test. Additionally, higher levels of trace element contamination and more negative carbon isotope values were also detected in the tissues of *P. oceanica* from Panarea than from Salina, revealing a high influence of hydrothermal emissions on contaminant exposure and carbon uptake dynamics.

The ecological interactions and physico-chemical transformations of four plastic typologies, of which two conventional (polyethylene, PE; and polypropylene, PP) and two biodegradable (Mater-Bi and polylactic acid, PLA), have been investigated through a field experiment in the Aeolian Archipelago. Stainless steel containers holding microplastic samples were deployed in seawater in September 2024 across six sites differing in levels of acidification, trace metal contamination, and temperature. Every four months samples have been collected to conduct analyses regarding physical and chemical degradation, biofouling, ecotossicological risk assessments, and the release-uptake of trace metals and other pollutants. Targeted analyses are also being carried out on the edible tissues of the fish species. Sites exhibited a pH gradient ranging from 7.51 at Baia di Levante (Vulcano), influenced by hydrothermal emissions, to 8.12 in Gelso (Vulcano), a reference site. Two non-indigenous molluscs, *Isognomon bicolor* and *Pinctada radiata* have settled and have been grown within the plastic boxes, confirming the role of plastics as refuge/ vector for non-indigenous species. Preliminary ATR-FTIR analysis revealed almost no chemical changes for PLA and HDPE over the different exposure times. In contrast, PP samples exhibited a 30% increased crystallinity that may be a consequence of annealing, while Mater-Bi samples indicated the loss of the stearamide additive.

The outcomes of this study enhance our understanding of ecosystem vulnerability under accelerating climate change and increasing anthropogenic pressures, providing critical insights into the projected impacts of future disturbance scenarios on sensitive ecosystems and key habitats that underpin essential ecosystem services.

3 Table of contents

3.1 List of Tables

3.2 List of Figures

Structure of the Deliverable

This Deliverable (D 4.4.1) of the task 4.4, entitled "Climate change and environmental degradation. Field- and laboratory-scale experiments to assess synergistic/antagonistic effects and cumulative impact of multiple environmental degradation causes, including combined effects of warming, acidification, deoxygenation and trace metal contaminations" is designed to provide a comprehensive overview of the activities carried out and of the results obtained.

Following this introductory section, the Deliverable is organised into three main sections, each dedicated to a specific case study (the Grado-Marano lagoon, the Panarea vents, and the Lipari/Vulcano vents), whose overarching aim is to investigate the interplay of key drivers of marine and coastal environmental degradation, including warming, acidification, deoxygenation, and trace metal contamination, and to assess how these stressors interact to influence ecosystem structure, function, and health.

Each section is structured into dedicated chapters, including an Introduction outlining the scientific background, rationale and specific objectives of the study; a Materials and Methods chapter detailing the study area, sampling strategy and analytical procedures adopted for the evaluation of the case specific issues; and Results, Discussion and Conclusions chapters, in which the main findings are presented and critically interpreted in the context of existing literature and site-specific conditions. The report concludes with a unified Conclusions section that integrates the main outcomes of the three case studies and highlights their broader ecological and environmental relevance, followed by a common References section.

4 Case study Grado-Marano Lagoon

4.1 Introduction

Lagoon systems represent global ecological hotspots due to their high primary productivity, and capacity to provide essential ecosystem services (Geppi *et al.*, 2023). Although they cover a relatively limited surface area, these systems play a crucial role in regulating biogeochemical cycles and carbon sequestration, with productivity rates ranging from 50 to 500 g C m^{-2} yr^{-1}, comparable to those of ocean upwelling zones (Knoppers, 1994; Kennish, 2015; Odum, 1983).

Lagoons not only support highly productive biological networks but also perform essential functions such as water purification, nutrient regulation, and carbon sequestration (Mitsch and Gosselink, 2015). Remarkably, their carbon storage potential per unit area often exceeds that of many terrestrial ecosystems (Heckbert *et al.*, 2011; Macreadie *et al.*, 2021), rendering them key natural allies in climate change mitigation. The loss of these functions would jeopardize not only local biodiversity but also the global climate balance (Béné *et al.*, 2011; Newton *et al.*, 2018; Uwadiae *et al.*, 2025).

The ecological structure of lagoons is highly dynamic and complex, shaped by strong physico-chemical gradients and seasonal environmental fluctuations (Bellino *et al.*, 2019; Ferrarin *et al.*, 2010). However, this very complexity also exposes them to vulnerability. Several disturbances such as contaminant loads, extreme weather events, or prolonged thermal stress, can trigger cascading effects that profoundly alter biological interactions and biogeochemical cycles, ultimately compromising system resilience (Ligorini *et al.*, 2023; Toffolo *et al.*, 2022).

Despite their importance, coastal lagoons remain underrepresented in ecosystem research studies (Martínez-Megías and Rico, 2022), compared to those focused on open ocean environments (Gilbert *et al.*, 2022). Even rarer are studies investigating the interaction between chronic contamination and climate stressors at the ecosystem scale (Gissi *et al.*, 2021), and very few have employed experimental field approaches, such as mesocosms, to simulate future scenarios (Ostrowski *et al.*, 2021).

In this context, the mercury-contaminated Grado-Marano Lagoon (Bettoso *et al.*, 2023) represents an ideal case study for investigating the interactions between historical human impacts and present-day climatic factors. In this study we adopted an innovative ecosystem-based experimental approach: we isolated specific lagoon sections during the warmest months of the year, limiting the horizontal exchanges with oxygen-enriched seawater under naturally elevated summer temperatures, to mimic the increase in the resident time of lagoon waters that occurs in its most confined areas in summer. We selected the second half of June to carry out the experiment, based on the oxygen data obtained from the Regional Agency for Environmental Protection of Friuli Venezia Giulia (ARPA FVG), indicating a progressive anticipation of hypoxic events in the last years, with their first occurrences already in June (Pittaluga *et al.* 2022).This particular kind of field mesocosm setup (Baldassarre *et al.*, 2023) allowed us to induce water stagnation and dissolved oxygen depletion, simulating potential future climate change scenarios. The mesocosms thus acted as "windows into the future," modelling a miniature lagoon system simultaneously exposed to thermal, hypoxic and Hg-contamination stress.

The study aimed at evaluating the functional resilience of a contaminated lagoon ecosystem subjected to the synergistic effect of multiple stressors. Specifically, our guiding questions were: Q1) *How do the key biological processes respond to increased hydrodynamic isolation, and does the latter lead to a shift in the trophic state of the system?* Q2) *Does the progressing isolation induce modifications in the pelagic-benthic coupling, and what are the implications for the overall ecosystem resilience?*

4.2 Materials and methods

4.2.1 Study Area

Covering an area of approximately 160 km² between the estuaries of the Isonzo River to the east and the Tagliamento River to the west, the Grado-Marano Lagoon system (Figure 4.2.2.1 A) is divided into two main sub-basins: the Marano Lagoon (western sector) and the Grado Lagoon (eastern sector). These can be further divided into functional sub-basins: Lignano, San Andrea, and Buso for Marano, and Morgo, Grado, and Primero for Grado (Acquavita *et al.*, 2015).

The two subsystems display pronounced morphological, bathymetric, and hydrodynamic differences (Ferrarin *et al.*, 2010). The Marano Lagoon is a semi-enclosed tidal basin, relatively deeper, with extensive saltmarsh areas and a dense network of channels, highly influenced by freshwater inputs (notably the Tagliamento River and several minor tributaries). In contrast, the Grado Lagoon is shallower, less affected by riverine inputs, more exposed to seawater influence, and characterized by weaker hydrodynamic circulation (Ferrarin *et al.*, 2010).

These structural differences are mirrored in strong heterogeneity of the physical-chemical parameters of water and sediments - temperature, salinity, dissolved oxygen, pH, turbidity, chlorophyll-*a* (Acquavita *et al.*, 2015) - and of sediment grain-size, which affects the distribution and availability of contaminants. Such conditions vary across spatial and temporal scales, both seasonally and interannually, exposing this system to the effects of global warming (Acquavita *et al.*, 2024).

A distinctive feature of the Grado-Marano Lagoon is its historical mercury (Hg) contamination, which represents a long-lasting environmental stressor deriving from past anthropogenic inputs (Bettoso *et al.*, 2023).

The Hg loads originate from two main sources:

- ☐ Mining-derived contamination (Dizdarevič, 2001), linked to the former Idrija mining district (Slovenia), one of the largest European cinnabar (HgS) deposits. Hg released by mining activities was carried downstream the Idrijca River, a tributary of the Isonzo, and ultimately reached the Adriatic coast. Coastal and tidal circulation mechanisms subsequently facilitated its transfer and accumulation, particularly in the eastern sector of the lagoon (Dizdarevič, 2001).
- ☐ Industrial contamination (Acquavita *et al.*, 2024 and references therein; Bettoso *et al.*, 2023), originating from the former chlor-alkali plant of Torviscosa (NE Italy). The facility remained in operation for several decades, and between 1949 and 1984 discharged approximately 190 tonnes of Hg into the Aussa-Corno River. The metal, bound to fine sediments, was subsequently accumulated mostly in the central sector of the lagoon (Acquavita *et al.*, 2024 and references therein; Bettoso *et al.*, 2023).

Although the primary sources of Hg discharge stopped decades ago, Hg contamination persists in surface sediments, where it can be remobilized and microbially transformed into methylmercury (MeHg) and released into the water column, particularly under hypoxic/anoxic or elevated-temperature conditions (Bettoso *et al.*, 2023).

In recent years, the lagoon has shown increasing vulnerability to climate change. Dissolved oxygen (DO) measurements conducted by ARPA FVG indicate a rising frequency of hypoxic events, particularly during summer and early autumn in areas with limited water circulation such as the innermost part of the Grado lagoon (Pittaluga *et al.* 2022).

4.2.2 Experimental design

The experiment was carried out in early summer, between 17 and 27 June 2024, under naturally high temperature conditions, to mimic a realistic thermal stress scenario. Three clusters of mesocosms (R1, R2, R3) (Figure 4.2.2.1 B) were deployed in the Primero sub-basin of the Grado Lagoon (45°42′06.5″ N, 13°24′44.1″ E, mean depth 0.72 m (Ferrarin *et al.*, 2010), (Figure 4.2.2.1 A) as independent spatial

replicates to capture natural variability. This site was specifically chosen because it represents the most contaminated area of the lagoon, with a total mercury concentration of 6.1 mg kg^{-1} (FM301; Bettoso et al., 2023). Each cluster was formed by six mesocosms, for a total of eighteen experimental units. At each sampling time, three mesocosms were sampled (with an additional external replicate at T_1 and T_2), one per cluster, while the remaining units hosted multiparametric probes and passive samplers for organic and inorganic contaminants (data not shown) or served as backup. The irregular spatial arrangement of mesocosms was due to the presence of patches of *Cymodocea nodosa* ((Figure 4.2.2.1 D) (Boscutti *et al.*, 2015; Cingano *et al.*, 2024). Mesocosms were placed on unvegetated lagoon beds to ensure that sampled sediments were not influenced by macrophytes, and once the nylon cylinders were raised (Fig. 1C), the direct influence of vegetation ceased due to the horizontal isolation of water inside the mesocosms. Each mesocosm (V = 1 m^3 ca.) consisted of a galvanized iron cylindrical frame (ø = 1 m) covered by a transparent nylon cylinder that allowed light penetration, maintaining photosynthetic activity. Lateral closure prevented horizontal water exchange, while it permitted vertical fluxes between air/water at the top, and water/sediment at the bottom ((Figure 4.2.2.1 C). Each structure was inserted into the lagoon bed for 50–60 cm in depth, limiting natural circulation and promoting water column stratification. With this set-up we were able to simulate conditions typical of a future climate change scenario (for more details see Baldassarre *et al.* 2023). The experiment began by raising the nylon cylinders to isolate the inner volumes, and sampling was performed at T_0 outside the mesocosms while internal and external conditions were still alike. T_1 was conducted after four days and T_2 after ten days, when oxygen levels inside the mesocosms showed a progressive decline. At both T_1 and T_2, samples were collected inside the mesocosms, one from each replicate cluster, and outside, in order to compare experimental conditions with natural ones. Only a single replicate was available for the external samples, due to the overall complexity of the experiment and the total time required to sample all variables at four points (3 mesocosms + 1 external point).

Dissolved oxygen (DO) was periodically monitored between sampling events to track any modifications inside the mesocosms and guide the timing of subsequent collections. Temperature (T), salinity (S), and conductivity (C) were continuously monitored throughout the experiment using Star-Oddi DST-CTD mini data loggers fixed to the structures: three placed inside the mesocosms (one per replicate) and one positioned externally, anchored to a mesocosm. During each sampling event, a YSI EXO2 multiparameter probe was additionally employed to measure T, S, pH, and DO concentration and saturation (O_2, mg L^{-1} and %), both inside and outside the sampled mesocosms. In parallel, at T_1 and T_2 external water and sediment samples were collected in close proximity to the mesocosms.

At each experimental time (T_0, T_1, T_2), water samples were collected first, in order to prevent contamination from sediment resuspension. Sampling was performed with a 5 L horizontal Niskin bottle, specifically designed for shallow lagoonal environments. Water aliquots were subsampled for the analysis of inorganic nutrients, chlorophyll-*a*, phytoplankton biomass (PB), and to estimate Gross Primary Production (GPPw) and Heterotrophic Carbon Production rates (HCPw).

Subsequently, surface sediment samples were collected using a manual HAPS corer (KC Denmark; inner Ø 14 cm, sampling area 154 cm^2, max depth 31 cm). For each mesocosm and for the external site, two sediment cores were obtained: the first one was extruded immediately on board, and the top (0–1 cm) homogenized sediment was subsampled for the following analyses: grain-size, Total Organic Carbon (TOC), Total Nitrogen (TN), and Gross Primary Production (GPPs). The second undisturbed core was transported to the laboratory within 2 h maintaining in situ temperatures. This core was subsampled with a plexiglass liner (inner Ø 3 cm) to estimate benthic community respiration (CR), while the surface layer (0–1 cm) of the remaining portion was collected separately, homogenized, and used for Heterotrophic Carbon Production (HCPs) and microphytobenthos (MPB) biomass analyses.

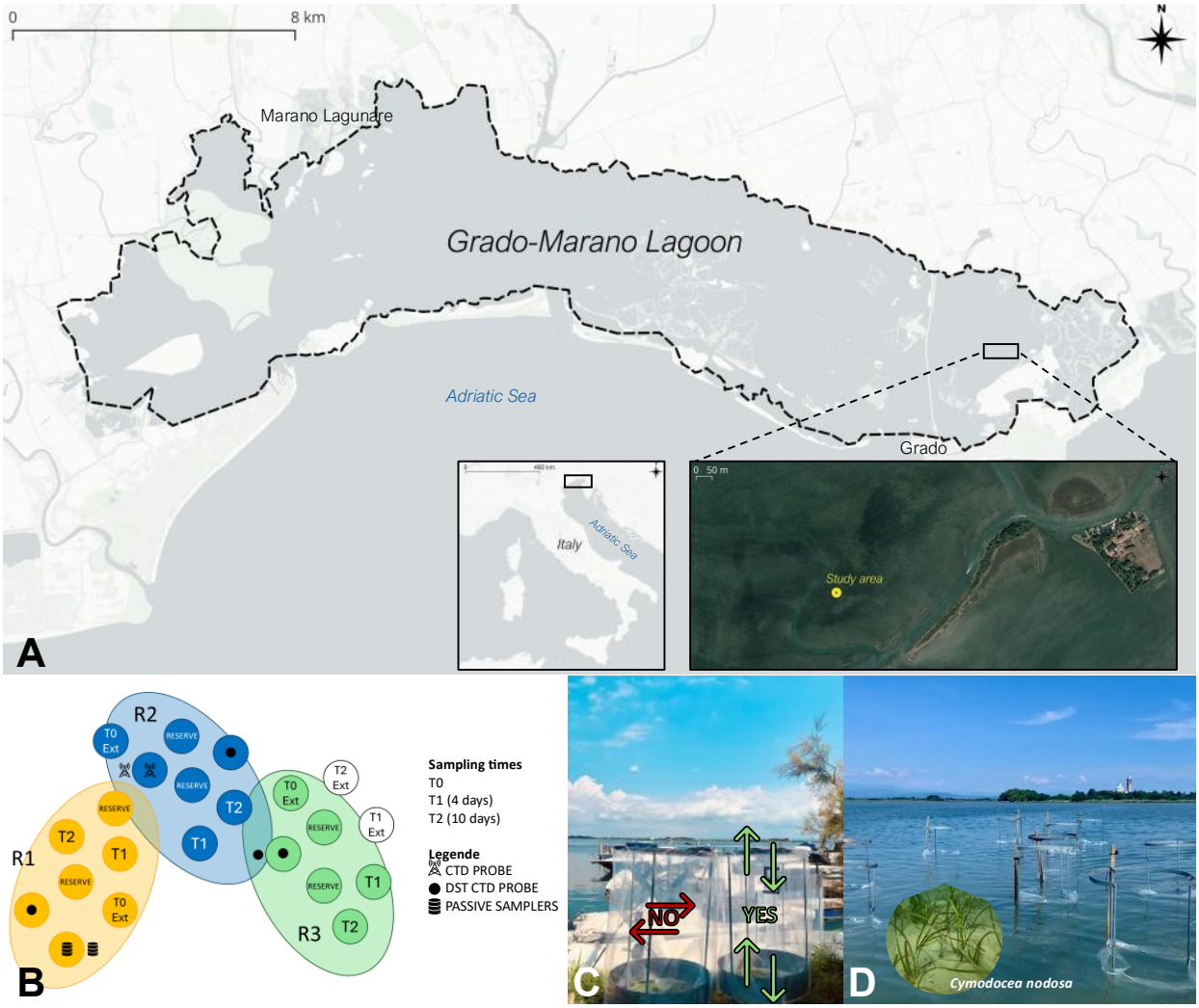

Figure 4.2.2.1. **(A)** Grado–Marano Lagoon (northern Adriatic Sea, Italy) showing the position of the study site. **(B)** Experimental set-up, illustrating the spatial arrangement of the mesocosms into three clusters (R1, R2, R3) and the sampling times (T_0, T_1, T_2). **(C, D)** Images of the mesocosms before their placement *in situ* (C) and before the beginning of the experiment (D); in the latter the occurrence of *Cymodocea nodosa* patches among the mesocosms is evidenced.

4.2.3 Chemical-physical and biological features of the water column

✓ *Inorganic nutrients*

Water samples for dissolved inorganic nutrients ($P\text{-}PO_4$, $N\text{-}NH_4$, $N\text{-}NO_2$, $N\text{-}NO_3$ and $Si\text{-}Si(OH)_4$) were pre-filtered on-board using pre-combusted glass-fiber filters with a 0.7 µm pore size (Whatman GF/F) and then collected in polyethylene vials that were acid-washed (HCl 1M) and rinsed with seawater. All samples were immediately frozen at -20°C and stored at this temperature until analysis. The analyses were conducted at room temperature using a four-channel QuAAtro SEAL Analytical, Continuous Flow Analyzer, as described by Hansen and Koroleff (1999). The detection limits for ammonium, nitrite, nitrate, phosphate, and silicate were 0.03, 0.01, 0.02, 0.01, and 0.02 µmol L^{-1}, respectively.

✓ *Chlorophyll*

Water subsamples for chlorophyll a (Chl *a*) determination were collected on board, kept in the dark, and maintained at 4 °C until filtration. In the laboratory, samples were filtered immediately onto 47 mm Whatman GF/F glass fiber filters, which were then stored at −20 °C. Chlorophyll a concentrations, corrected for phaeopigments, were quantified fluorometrically after extraction with 90% acetone and centrifugation in darkness, following the procedure described by Lorenzen and Jeffrey (1980), using a Perkin Elmer LS50B fluorometer.

✓ *Phytoplankton biomass (PB)*

For phytoplankton (2-200 µm) analysis, samples were collected in 500 mL-dark bottles and preserved with pre-filtered and neutralized 1.6% formaldehyde (Throndsen, 1978). Cell counts were performed following the Utermöhl method (Utermöhl, 1958), as applied in Zingone *et al.* (1990). A variable volume of seawater (10-50 mL) was settled depending on cell concentrations. Cell counts were performed using an inverted light microscope (Olympus IX71 and LEICA BMI3000B) equipped with phase contrast. Cells (minimum 200) were counted along transects (1–2) in a Utermöhl chamber at a magnification of 400×. In addition, one half of the chamber was also examined at a magnification of 200×, to obtain a more correct evaluation of less abundant phytoplankton taxa. Phytoplankton specimens were identified to the lowest possible taxonomic level using floras listed in Cibic *et al.* (2022a). The biovolume of phytoplankton cells was calculated according to Edler (1979) and Hillebrand et al. (1999). Cell volumes were converted to carbon content using the formula introduced by Menden-Deuer and Lessard (2000) and PB was expressed in µg C L^{-1}.

4.2.4 Chemical-physical and biological features of surface sediments

✓ *Grain-size*

A 10 – 25 g aliquot of homogenized sediment was collected from each core replicate. Small pebbles and shell fragments were separated from the sand and mud fractions by sieving at 2 mm. Each sample was pretreated with 10% hydrogen peroxide before being analyzed using the LS 13 320 Laser Diffraction Particle Size Analyzer, Beckman Coulter, USA. The data are presented as percentages of sand, silt, and clay, following the Udden-Wentworth grain-size classification (Wentworth, 1922).

✓ *Total Organic Carbon (TOC) and Total Nitrogen (TN)*

Sediment was freeze-dried, ground in a ceramic mortar, and then sieved through a 250 µm iron steel sieve (Endecotts LTD, UK). Triplicate subsamples, each weighing approximately 8 – 12 mg, were placed directly into silver and tin capsules using a microultrabalance with an accuracy of 0.1 µg. Before TOC analysis, the subsamples were treated in the capsules with increasing concentrations of HCl (0.1 N and 1 N) to remove the carbonate fraction (Nieuwenhuize *et al.*, 1994). Carbon (C) and nitrogen (N) contents were determined using a CHNO-S elemental analyzer (mod. ECS 4010, Costech, Italy), following the method of Pella and Colombo (1973). The instrument was calibrated using standard acetanilide (Costech, purity ≥ 99.5%), and empty capsules were analyzed to correct for blank values. Quality control was carried out with internal standards, and carbon measurements were also verified using the certified marine sediment reference material PACS-2 (National Research Council Canada, 2007). The relative standard deviations for three replicates were below 3%. TOC and TN concentrations were reported as weight percentages of C and N, respectively, on a dry sediment basis.

✓ *Microphytobenthos (MPB) biomass*

For MPB analyses, three aliquots of homogenized sediment (2 cm^3) were withdrawn using a syringe and directly fixed with 10 mL of formaldehyde (4% final concentration) buffered solution $CaMg(CO_3)_2$, in pre-filtered bottom seawater (0.2 µm filters). After manual stirring, 20 µL aliquots of the sediment suspension were drawn off from the slurries and placed into a counting chamber. Only cells containing pigments and not empty frustules were counted under a Leitz inverted light microscope following the protocol described by Franzo *et al.* (2015) and Cibic *et al.* (2022a). The qualitative identification of MPB assemblages was

carried out using floras listed in Cibic and Blasutto (2011). To estimate the biomass (expressed as µg cm^{-3}), the biovolume of MPB cells was calculated according to Hillebrand *et al.* (1999). Afterwards, the MPB biomass was obtained multiplying the abundance (cells cm^{-3}) by the carbon content of each counted cell using the formulas introduced by Menden-Deuer and Lessard (2000).

4.2.5 Biological processes in the pelagic and benthic compartments

✓ *Gross Primary Production (GPP)*

We estimated Gross Primary Production in water (GPPw) and surface sediments (GPPs) samples using the ^{14}C uptake method (Nielsen, 1952). The incubation time was kept to 1 hour, therefore in both cases a gross primary production rate was measured (Gazeau *et al.*, 2005).

To estimate GPPw, water samples were poured into 75-mL translucent and dark polycarbonate carboys (Nalgene) and stored in coolers in the dark for 30 minutes to halt any residual photosynthetic activity. Subsequently, 6 µCi (0.22 MBq) of $NaH^{14}CO_3$ (DHI, Denmark) was added per bottle. Three light and one dark samples per mesocosm/external reference were fixed on a rosette and incubated in situ, for 1h under natural light conditions. At the end of the incubation, samples were transferred to 100-mL bottles and supplemented with 320 µL of 5 N HCl (Cibic and Virgilio, 2011) to stop the photosynthetic activity and remove the residual labelled bicarbonate, not assimilated by the phototrophic plankton. Subsequently, samples were treated as described in (Cibic *et al.*, 2022a).

To estimate GPPs, for each mesocosm/external reference, an aliquot of 2.5 cm^3 of homogenized sediment was re-suspended in 50 mL of filtered seawater (0.22 µm filter) and 250 µL of ^{14}C ($NaH^{14}CO_3$, DHI, Denmark) were added to reach a final activity of 1 µCi mL^{-1} (37 kBq mL^{-1}) (Nielsen, 1952). The suspension was then transferred into two dark and three light 9 mL-glass vials. These samples were fixed on a rosette and incubated in situ for 1 h. Afterwards, 200 µL of HCl 5N were added immediately to stop the PP activity (Cibic and Virgilio, 2010). Subsequently, samples were treated as described by (Cibic *et al.*, 2008b).

Disintegrations per minute (DPM) were measured by a QuantaSmart TRI-CARB 2900 TR Liquid Scintillation Analyzer (Packard BioScience, USA) including quenching correction, obtained using internal standards. Carbon assimilation was calculated as described by (Gargas, 1975), assuming 5 % isotope discrimination. Activity of the added $NaH^{14}CO_3$ and inorganic carbon concentration (tCO_2) were calculated based on total alkalinity measured in the same samples. Photosynthetically available radiation (PAR) was recorded in the water column, using a Profiling Natural Fluorometer PNF-300A (Biospherical Instruments Inc., San Diego, CA, USA) before and after each incubation. Since incubations were carried out in different light conditions, GPPw and GPPs data were normalized for light intensity of 2000 µE, representing the average PAR value measured in situ during incubations.

✓ *Heterotrophic C Production (HCP)*

Heterotrophic prokaryotic carbon production (HCP) was assessed using the method of ^3H-leucine (Leu) incorporation, as described by Kirchman *et al.* (1985) for water samples and by van Duyl and Kop (1994) for sediment samples.

To estimate HCPw, for each replicate, three 1.7 mL water subsamples, along with one killed control (90 µL of 100% trichloroacetic acid - TCA), were spiked with 20 nM radiotracer (50.2 Ci $mmol^{-1}$; Revvity, Waltham, MA, USA) and incubated for 1 hour in the dark at *in situ* temperature. The extraction of ^3H-labeled proteins was performed using the microcentrifugation technique described by Smith and Azam (1992). Following the addition of 1 mL of scintillation cocktail (Ultima Gold™ MV; Packard), the radioactivity was measured using a Tri-Carb 4910TR Liquid Scintillation Analyzer (Revvity, Waltham, MA, USA). To estimate carbon biomass production, a conversion factor of 3.1 kg C mol^{-1} Leu incorporated was applied, assuming a 2-fold isotope dilution (Simon and Azam, 1989).

To estimate HCPs, each sediment sample (0.2 mL of 1:1 v/v slurry) was incubated with 6 µCi of ^3H-leucine (Revvity, Waltham, MA, USA) in the dark for 1h at in situ temperature; incubations were stopped by adding

80% ethanol (1.7 mL). After washing the samples twice with ethanol (80%) by mixing, centrifuging and supernatant removal, the sediment was transferred with ethanol (80%) onto a polycarbonate filter (0.2 µm mesh size). The filters were then washed twice with 5% TCA and heated in 2M NaOH for 2 h in a water bath at 100°C, cooled on ice and centrifuged at 425 g for 3 minutes. One mL of supernatant was transferred to scintillation vials; after the addition of 10 mL of Hionic Fluor (Revvity, Waltham, MA, USA) scintillation fluid, the activity in the sediments was determined by a Tri-Carb 4910TR Liquid Scintillation Analyzer (Revvity, Waltham, MA, USA). For each sample, three replicates and two ethanol-treated blanks were analyzed.

✓ *Community respiration (CR)*

Oxygen consumption rates were obtained through O_2 microprofiles conducted on intact sediment cores. The latter were kept in the dark and maintained at *in situ* temperature using a cryostat (Grant, model LT Ecocool 150). The O_2 microprofiles in steady-state conditions were acquired using an O_2 microsensor (Unisense Denmark, OX-100 standard) (Moya *et al.*, 2014), a Clark-type electrode with a protected cathode (Revsbech and Jorgensen, 1989; Revsbech, 2005), with a sensor tip diameter of 100 µm, and the agitation sensitivity < 2%. O_2 profiles were acquired at 100 µm depth intervals and subsequently processed using the Unisense SensorTrace Suite software (Logger+, Photo, Rate and Profiling) version 3.4.700 (Unisense, Aarhus, Denmark). To calculate CR (nmol cm^{-3} s^{-1}), porosity, temperature, and salinity data were manually added. Before acquiring each profile, the microsensor was polarized and calibrated using the Zero-oxygen calibration kit (Unisense). Areal oxygen respiration rates were calculated as described by Cibic *et al.* (2007a). By applying a respiratory quotient of 1, the oxygen data were converted to mg C m^{-2} h^{-1} to estimate the trophic status (autotrophy/heterotrophy) of the investigated area. Finally, net primary production (NPP) was estimated by subtracting CR from GPP (Cibic *et al.*, 2012b).

4.2.6 Statistical analysis

All statistical analyses and graphical outputs were performed using R (version 4.5.1; R Core Team, 2025). Temporal changes of variables in the mesocosms were assessed considering all three experimental times (T_0, T_1, and T_2), while comparisons between results obtained inside vs outside the mesocosms were conducted for T_1 and T_2, only. As only one replicate was available for the external environment, comparisons between internal (inside mesocosms) and external data were performed using a bootstrap analysis. For each comparison, the three individual internal replicate variables were resampled 27 times to generate an empirical distribution, from which confidence intervals and p-values for the external variable were estimated, following principles similar to those described by Dwivedi *et al.* (2017) for small-sample resampling analyses. Unlike Dwivedi *et al.* (2017), who resampled means of small-sample replicates, we directly resampled the individual internal replicates (three mesocosms), preserving their natural variability. The bootstrap analysis provided a qualitative output, indicating whether the difference between internal and external data was statistically significant ("yes") or not ("no"). Significance was assessed based on whether the external value fell outside the 95% confidence interval of the bootstrap distribution, with a "yes" result corresponding to a p-value < 0.05.

For univariate analyses of all physico-chemical and biological variables, one-way ANOVA was applied, followed by Tukey HSD post-hoc tests to compare replicates of the three experimental times (T_0, T_1, T_2). Correlations between variables were assessed using Spearman's rank correlation coefficient.

For multivariate analyses, biotic data were organized into separate matrices for water and sediments. Negative biotic values (e.g., CR and NPP) were transformed using the log_signed() function, to preserve the ecological meaning of negative values while compressing the scale. Principal Component Analysis (PCA) was performed on abiotic variables (temperature, pH, O_2%, salinity, $N–NO_3$, $N–NO_2$, $N–NH_4$, $Si–Si(OH)_4$, $P–PO_4$, Chl *a* for water; sand%, silt%, TC, TN, TOC, and C/N ratio for sediments) to explore environmental gradients among samples. Biotic variables (diatom, dinoflagellate, coccolithophore and flagellate biomass, GPPw and HCPw for water; MPB biomass, GPPs, CRs and HCPs for sediments) were then fitted as supplementary variables using the *envfit* function to assess their relationships with the abiotic gradients.

Two separate PCAs were performed, one on water and one on sediment variables. The significance of multivariate patterns was tested using ANOSIM, both for comparisons between internal and external data and the three experimental times. Additionally, separate PERMANOVA analyses were applied to abiotic matrices of water (temperature, pH, O_2%, salinity, N–NO_3, N–NO_2, N–NH_4, Si–$Si(OH)_4$, P–PO_4, Chl *a*,) and sediments (clay%, sand%, silt%, TC, TN, TOC, and C/N ratio) to assess temporal variations outside the mesocosms. . All analyses and graphical outputs were produced using R custom scripts. Details of all statistical tests are provided in the Supplementary Material.

4.2.7 Chemical analyses of inorganic trace elements, organic contaminants, and ecotoxicological responses

All procedures related to the chemical and ecotoxicological analyses of waters and sediments were performed by ENEA (Italian National Agency for New Technologies, Energy and Sustainable Economic Development) and are detailed in the following sections.

- ✓ *Trace elements*

During the sampling, seawater samples were filtered using a 0.45 µm membrane filter (Millex HA, Merck) and acidified with ultrapure 1% HNO3. Then, measurements were performed using Agilent 7800 ICP-MS, equipped with a UHMI (Ultra High Matrix Introduction) system for the analysis of complex matrices with high salt content and, in order to suppress interferences, in He and, for As and Fe, HeHe mode. A 0.1 mg L-1 of Rh solution was used as an internal standard to compensate for any variations in instrument efficiency that could influence the measurements during analysis.

The standard solutions used for the calibration curves were prepared by appropriately diluting a 10 mg L-1 multi-element standard solution - Environmental Calibration Standard solution, from Agilent Technologies - in a salt matrix consisting of 3.5% NaCl (99.99 SuprapurR, Merck) in H2O MilliQ and 1% di HNO3 (TraceSelectTM Ultra, Fluka), to simulate "artificial" seawater.

Quality measurements was evaluated by analyzing the following certified reference materials: CASS-5, CASS-6-Nearshore Seawater Certified Reference Materials for Trace Metals and other Constituents, and ERMCA403 seawater (element content). Sediments aliquots used for metal analyses (except Hg) were oven-dried (40°C) and then, sieved to 2 mm and finely ground. The determinations of trace metal content (except Hg) in sediments were obtained by a microwave-assisted acid digestion procedure, using an acid mixture of HNO3, HF and H2O2. After the acid digestion, the excess of unreacted hydrofluoric acid was removed by carefully evaporating the samples to near dryness, followed by re-dissolution in 1% HNO3. Then, the trace metals analyses were performed by an ICP-MS instrument (Agilent 7800). A multi-element calibration standard solution with a concentration of 10 µg mL-1 in nitric acid was diluted to the proper concentrations and used to prepare the calibration standard solutions. An internal standard mix solution (Bi, Ge, In, Li6, Sc, Tb, and Y in 5% HNO3, Agilent Techn.) was diluted and used to correct any matrix interference occurring during the ICP-MS analysis. The quality of the analytical data was assessed using procedural blanks and analyzing, with the same method adopted for the samples, two certified reference materials based on marine sediment (PACS-3 and MESS-4, National Research Council Canada, NRCC).

Sample sediments for Hg analyses were air-dried in a fume hood at room temperature and Hg determination in sediments was carried out directly on the dry sample, without any acidic pretreatments, by the automated Hg analyzer FKV AMA-254.

PACS-3 and MESS-4 certified reference materials were analyzed in the same conditions used for Hg measurements in sediments samples to evaluate the analytical quality of the provided data.

- ✓ *DGT (Diffusive Gradient in Thin films) for Metal (As, Cd, Cr, Co, Cu, Fe, Pb, Mn, Ni, V and Zn) and Hg measurements*

Immediately after the passive samplers withdrawn from the sea, the devices were rinsed thoroughly with Milli-Q water. Successively, in laboratory, the metals were eluted from the binding gel in 1 ml of 2M HNO3 for

24h. The obtained extracts were diluted with Milli-Q water and trace metal analysis was carried out by using ICP-MS (Agilent 7800). A blank resin was always considered. DGT performance was evaluated according to the method used by Zhang and Davison (Zhang and Davison, 1995). The concentrations of metals measured by DGT, in three replicates, were calculated using equations and parameters provided by Davison (2016).

Analysis of total mercury concentrations in DGT units was performed using AMA 254 mercury analyzer: the chelating resin was removed from the device and directly analyzed without further preparations. A blank resin was analyzed in the same conditions and its mercury content was always subtracted to the mercury quantity measured for the samples. The concentrations of mercury measured by DGT, in three replicates, were then calculated using equations and parameters provided by Davison (2016).

✓ *Hydrophobic organic contaminants*

Passive samplers (Semi-Permeable Membrane Devices, SPMDs) and water samples were collected to assess hydrophobic organic contaminants, including polycyclic aromatic hydrocarbons (PAHs), polychlorinated biphenyls (PCBs), organochlorine pesticides (OCPs), and organotin compounds (OTs). SPMDs, consisting of polyethylene membranes filled with triolein, were deployed to accumulate time-integrated contaminant concentrations. Sediment samples were freeze-dried prior to extraction, and seawater samples were filtered to remove particulate matter before solid-phase extraction (SPE).

i. SPMDs: Membranes were extracted twice for 24 h using 200 mL of *n*-hexane containing surrogate standards (deuterated PAHs, PCBs, and DDTs). Combined extracts were passed through anhydrous sodium sulfate and concentrated to a few milliliters. Hexane extracts were cleaned using a silica gel column (Merck 60, 70–230 mesh, activated at 250 °C for 16 h, 30 cm × 1 cm i.d.) following EPA Method 3630. Elution was performed in two fractions: F1 (PCBs, HCB, DDEs, aldrin, α- and β-endosulfan, isodrin) and F2 (PAHs, DDDs, DDTs, HCHs, dieldrin, endrin, heptachlor epoxide). Fractions were concentrated to 0.25 mL and spiked with *p*-terphenyl as the injection standard.

ii. Seawater: PAHs were extracted from 500 mL of seawater using C18 SPE cartridges (Supelco Supelclean Envi-18, 6 mL). Cartridges were conditioned with dichloromethane and methanol, equilibrated with organic-free water, and samples were passed through under vacuum. Elution was performed with 10 mL dichloromethane, followed by dehydration over sodium sulfate and concentration to a few milliliters using a vacuum rotary evaporator.

✓ *Analytical Determination*

All extracts were analyzed by gas chromatography–mass spectrometry (GC–MS, Agilent Technologies 7890A/5975C) equipped with a methyl-5% phenylsilicone capillary column. Detection was performed with a quadrupole mass spectrometer in electron impact (EI) mode at 70 eV using Selected Ion Monitoring (SIM). Helium (N55) was used as the carrier gas. Peak identification was based on retention times and isotopic mass ratios relative to reference standards. Response factors were checked periodically by injection of standard mixtures to account for instrument tuning variability. Quantification was performed using the internal standard calibration curve method. Detection limits were 0.1 μg kg^{-1} for PAHs, 0.01 μg kg^{-1} for PCBs and hexachlorobenzene, 0.05 μg kg^{-1} for other OCPs, and 0.03 μg kg^{-1} for organotin compounds. For PAHs, 2.5 g of sediment were extracted with *n*-hexane:acetone (1:1, v/v) using an Accelerated Solvent Extractor (ASE 200, Dionex) at 120 °C and 1500 psi for two cycles, followed by water washing and concentration over sodium sulfate with addition of 1 mL iso-octane. Cleanup was performed using silica gel column chromatography as described for SPMDs, with the PAH-containing fraction concentrated to 0.5 mL. PCBs and OCPs were extracted from 10 g of freeze-dried sediment with ASE under the same conditions, using PCB and DDT-d_8 surrogate standards. Hexane extracts were fractionated into F1 (PCBs, HCB, DDEs, aldrin, α- and β-endosulfan, isodrin) and F2 (DDDs, DDTs, HCHs, dieldrin, endrin, heptachlor epoxide), optionally further purified on silica gel pipettes with 40% sulfuric acid to remove aldrin. Fractions were concentrated to 0.25 mL and spiked with *p*-terphenyl. Organotin compounds were extracted from 2.5 g of freeze-dried sediment using ultrasound-assisted extraction with a methanolic tropolone solution and HCl, followed by dichloromethane partitioning, derivatization with

pentylmagnesium bromide, and cleanup on silica gel columns eluted with hexane:toluene (1:1 v/v), with the final extracts concentrated to 0.5 mL. Analytical Determination was performed as previously described.

✓ *Ecotoxicological assessment*

Toxicity tests, in triplicate, were carried out on seawater and sediment elutriates. For the preparation of sediment elutriate, Artificial SeaWater (ASW) (ASTM 1994) was added to the sediment in the ratio 4:1 (volume/dry weight) and placed in a shaker for 1 h at room temperature. Then, the mixture was centrifuged at 3,000 rpm (1,000×g) for 20 min and filtered (Ø 0.45 µm). For aqueous samples, a bioassay battery, consisting of three different species representing different trophic levels, algae *Dunaliella tertiolecta*, bacteria *Vibrio fischeri*, crustacean *Artemia salina*, was chosen.

i. *D. tertiolecta* test - The chronic test was carried out according to ISO 10253. The culture medium for algal growth was prepared according to ISO protocol. A screening with the undiluted (whole) sample was performed. An algal suspension at a concentration of 1×106 cells/mL was prepared. Then, an aliquot of algal suspension was added to each replicate to reach the final concentration of 1×104 cells/mL. Culture medium has been utilized as negative control (six replicates). The test flasks were placed in a thermostatic chamber at 20 °C with a light source in the 7,000– 8,000-lux range for 72 h. The cell density of each sample was measured after 72 h by the Burker chamber. The effect percentage for each sample was calculated with respect to the control.

ii. *salina* test - Cysts were hatched by using the procedure described in APAT IRSA-CNR (2003). The encysted organisms were first hydrated in a volume of ASW for 1 h at 25 °C at 3,000–4,000 lx. Then, the cysts were incubated for 24 h in the dark at the same temperature. Acute toxicity test (96 h) was conducted according to APAT-IRSA (2003). Ten nauplii were transferred in a beaker with 40 mL of sample. Each sample was tested in triplicate. The negative control consisted of six replicates of artificial seawater. The treatments were incubated at 25 °C with a light regime of 14:10 h light/dark. No food was provided during the exposure. Every 24 h, the number of the live individuals was recorded. The effect percentage for each sample was calculated with respect to the control.

iii. *Vibrio fischeri* test - Vibrio fischeri luminescence inhibition test was carried out using whole (undiluted) seawater and elutriate samples as a screening assessment. Each sample was mixed with the bacterial suspension and incubated according to the biolight toxy procedure. A negative control consisting of diluent (2% NaCl) was included in each test run. Luminescence was measured after 15 and 30 minutes of exposure using the Biolight toxy , following the manufacturer's instructions. Results were expressed as the percentage of luminescence inhibition relative to the control.

iv. *Toxicity test Battery Index (TBI)* - For each sample, the results of the different tests were integrated using the TBI (Manzo *et al.*, 2008). The TBI was calculated also for the seawater and elutriates samples separately. The effects on the chosen endpoints were expressed as percentage and classified. To calculate the TBI, the percentage of the effect (%E) on each endpoint was corrected to obtain the Score test Endpoint (SEi) using the following formula: SEi = %E (M x S) SCF where SCF (statistical correction factor) is the Students t-test between sample and control. The values of 0, 1, 2, 3, and 4 were attributed to SCF, corresponding to no differences ($p > 0.05$), biostimulation ($p < 0.05$), high biostimulation ($p < 0.01$), toxicity ($p < 0.05$), and high toxicity ($p < 0.01$), respectively; matrix (M) based on the ecological relevance of the matrices and on the level of sample manipulation equal to 2 for elutriate; severity (S) referred to the degree of effect that the bioassay endpoints measure. Mortality and bioluminescence inhibition are considered the most severe endpoints followed by algal growth and fertilization equal to 4 for algal growth, 3 for fertilization, and 5 for mortality and bioluminescence. SEi is expressed in a 0–100 scale relative to test battery utilized as follows: %SEi = SEi (%Em) / (SE max) where % Em is the maximum effect percentage observed corresponding to the maximum MS obtained, and SE max is the maximum Score test Endpoint calculated. The TBI is calculated according to the following formula: %TBI = (∑%Sei /N) where N is the number of endpoints. The ecotoxicological risk is defined as follows: absent (TBI <5%), low (5 < tbi <10%), moderate (10% <20%), high (20% <50%), very high (tbi>50%).

4.3 Results

4.3.1 Dynamics of chemical-physical variables in the water column

During the experiment, significant differences were observed between the inside and outside of the mesocosms, highlighting the effects of isolation, as well as a temporal evolution related to environmental conditions.

Dissolved oxygen was significantly lower inside compared to outside both at T_1 (96.73 ± 15.29% and 123.70%, respectively; $p < 0.05$) and at T_2 (107.07 ± 2.91% and 139.23%; $p < 0.05$) (Figure 4.3.1.1B, **Errore. L'origine riferimento non è stata trovata.**). Similarly, pH values were lower inside the mesocosms (T_1: 8.25 ± 0.07 and 8.37; T_2: 8.34 ± 0.03 and 8.47; $p < 0.05$) (Figure 4.3.1.1D, **Errore. L'origine riferimento non è stata trovata.**). Salinity, on the other hand, was lower inside at T_1 (25.70 ± 0.07 and 27.71; $p < 0.05$) but higher at T_2 (26.95 ± 0.14 and 25.23; $p < 0.05$) (Figure 4.3.1.1C, **Errore. L'origine riferimento non è stata trovata.**).

Over time, internal temperature (Figure 4.3.1.1A) decreased from T_0 (28.32 ± 0.91 °C) to T_1 (26.69 ± 0.19 °C;* $0.01 \leq p < 0.05$), and then slightly increased at T_2 (27.27 ± 0.21 °C; $p \geq 0.05$) (Figure 4.3.1.1A, **Errore. L'origine riferimento non è stata trovata.**). Dissolved oxygen significantly decreased from T_0 (196.23 ± 20.87%) to subsequent times (** $0.001 \leq p < 0.01$) (Figure 4.3.1.1B, **Errore. L'origine riferimento non è stata trovata.**). Salinity showed a progressive and significant increase from T_0 (22.07 ± 0.27) to T_1 (25.70 ± 0.07; *** $p < 0.001$) and T_2 (26.95 ± 0.14; *** $p < 0.001$) (Figure 4.3.1.1C, **Errore. L'origine riferimento non è stata trovata.**). Finally, pH decreased from T_0 (8.63 ± 0.05) to T_1 (8.25 ± 0.07; ** $0.001 \leq p < 0.01$), then slightly increased again at T_2 (8.34 ± 0.03; ** $0.001 \leq p < 0.01$) (Figure 4.3.1.1D, **Errore. L'origine riferimento non è stata trovata.**).

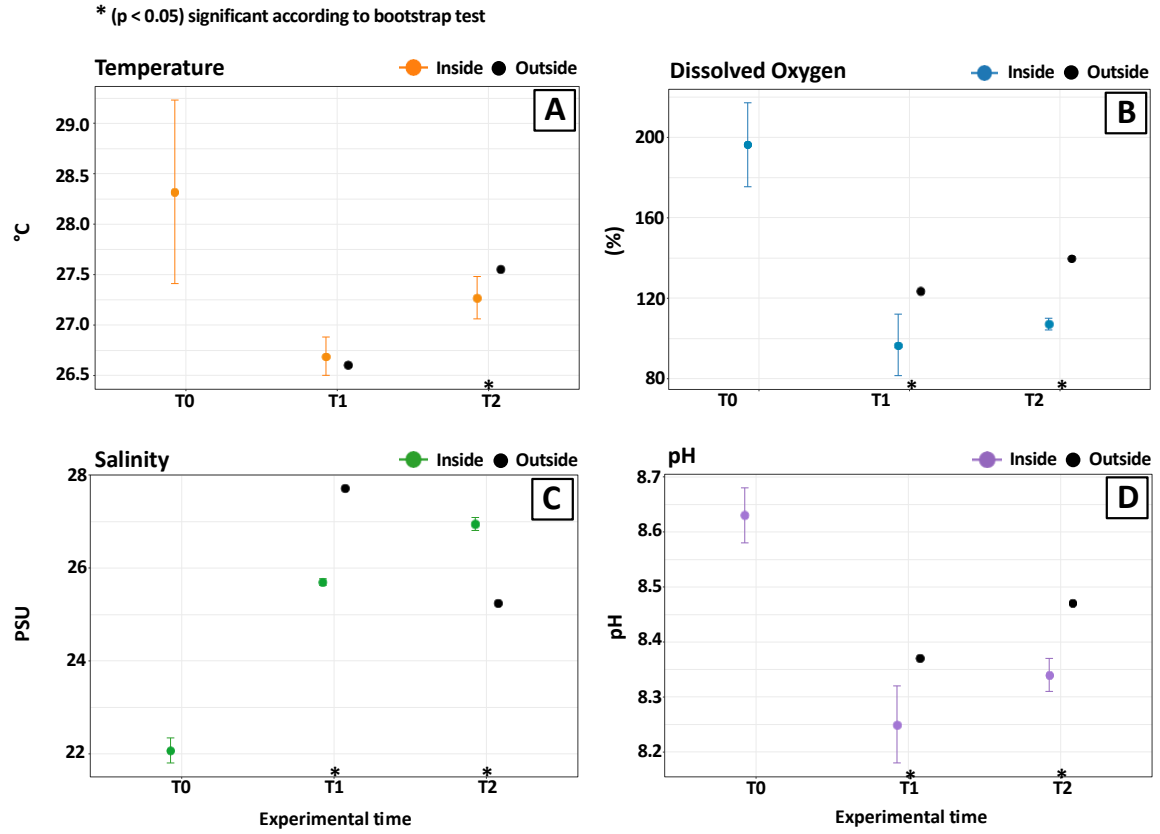

Figure 4.3.1.1 Temporal variations of the main physico-chemical parameters inside (colored points) and outside (black points) the mesocosms during the experiment (T_0, T_1, T_2). **(A)** Temperature, **(B)** Dissolved oxygen, **(C)** Salinity, and **(D)** pH. Error bars represent standard deviations (n = 3).

4.3.2 Inorganic nutrients in water

Nitrogenous nutrients (N-NO_3, N-NO_2 and N-NH_4) exhibited clear differences between the inside and outside of the mesocosms. Nitrate (N-NO_3) was significantly lower inside the mesocosms compared to the outside at T_1 (2.32 ± 0.17 µmol L^{-1} and 5.04 µmol L^{-1}, respectively; $p < 0.05$) and slightly lower at T_2 (1.28 µmol L^{-1} and 1.30 µmol L^{-1}; $p > 0.05$) (Figure 4.3.2.1A, Table 9.S1). Nitrite (N-NO_2) was also significantly lower inside at T_1 (0.24 ± 0.02 µmol L^{-1} and 0.32 µmol L^{-1}; $p < 0.05$), while at T_2 internal concentrations were slightly higher than external (0.21 ± 0.08 µmol L^{-1} and 0.16 µmol L^{-1}; $p > 0.05$) (Figure 4.3.2.1B, Table 9.S1). Ammonium (N-NH_4) was significantly higher inside than outside at both T_1 (6.00 ± 2.55 µmol L^{-1} and 1.73 µmol L^{-1}; $p < 0.05$) and T_2 (6.09 ± 1.01 µmol L^{-1} and 1.68 µmol L^{-1}; $p < 0.05$) (Figure 4.3.2.1C, Table 9.S1).

Considering the temporal evolution inside the mesocosms, N-NO_3 (Figure 4.3.2.1A, Table 9.S2) and N-NO_2 (Figure 4.3.2.1B, Table 9.S2) decreased significantly compared to T_0 (11.1 ± 1.09 µmol L^{-1} and 0.85 ± 0.07 µmol L^{-1}, respectively; *** $p < 0.001$, T_0-T_1 and T_0-T_2), whereas N-NH_4 increased significantly (1.36 ± 0.13 µmol L^{-1} at T_0; * $0.01 \leq p < 0.05$, T_0-T_1 and T_0-T_2) (Figure 4.3.2.1C, Table 9.S2).

Phosphate (P-PO_4) was at the lowest detectable concentrations at T_1 (0.01 ± 0.00 µmol L^{-1}) inside the mesocosms, equal to the external values, and increased at T_2 (0.06 ± 0.07 µmol L^{-1}), when it was significantly higher than outside (0.01 µmol L^{-1}; $p < 0.05$) (Figure 4.3.2.1D, Table 9.S1).

Silicate (Si-$Si(OH)_4$) was significantly higher inside compared to outside at T_1 (15.89 ± 7.02 µmol L^{-1} and 9.61 µmol L^{-1}; $p < 0.05$) and T_2 (17.11 ± 3.58 µmol L^{-1} and 10.34 µmol L^{-1}; $p < 0.05$) , while no significant

changes over time compared to T_0 (6.90 ± 0.39 µmol L^{-1}; $p \geq 0.05$) were observed (Figure 4.3.2.1E, Table 9.S1, Table 9.S2).

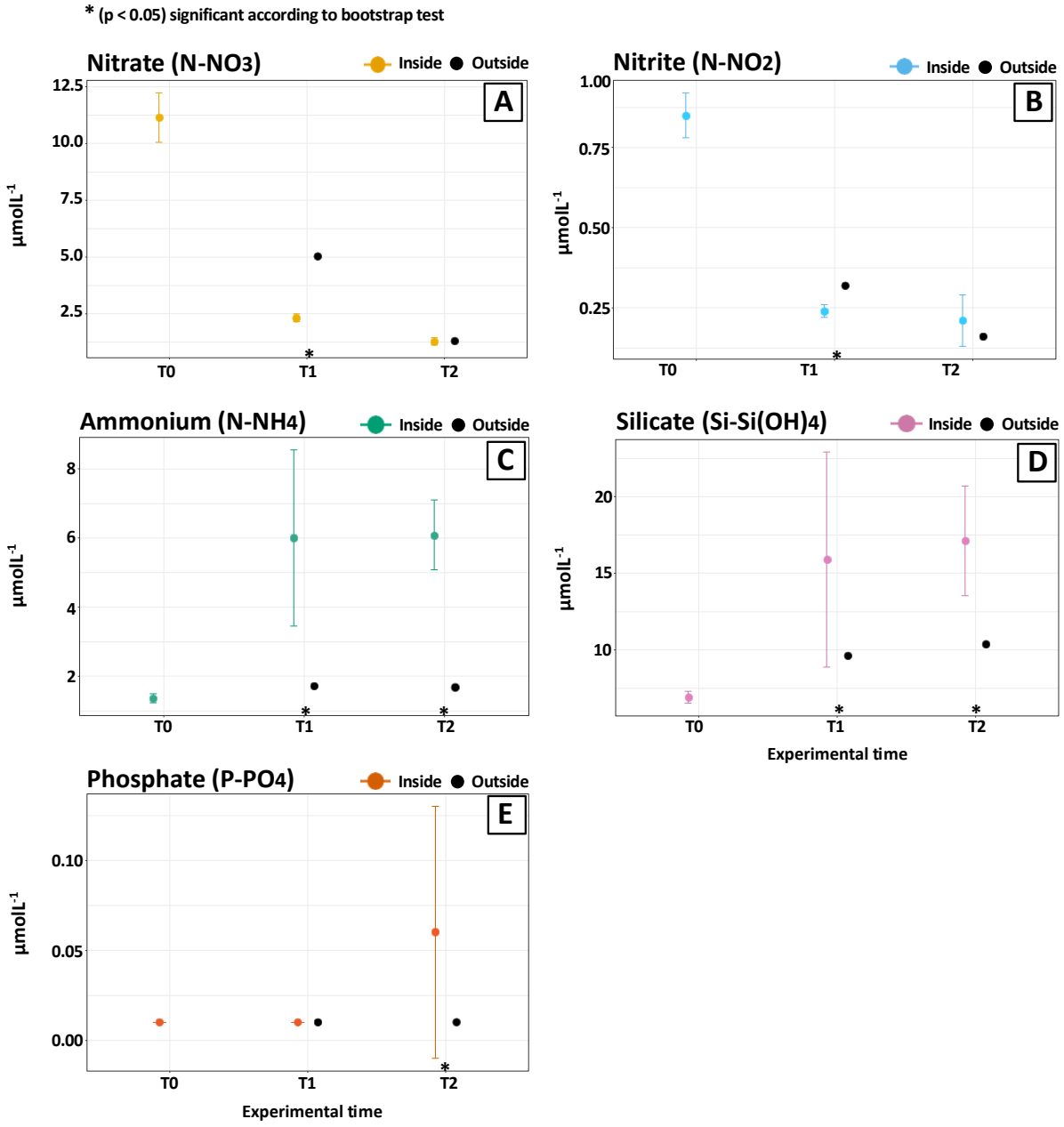

Figure 4.3.2.1 Concentrations of dissolved inorganic nutrients measured inside (colored points) and outside (black points) the mesocosms during the experiment (T_0, T_1, T_2). Error bars represent standard deviations (n = 3). Asterisks (*) indicate statistically significant differences according to the bootstrap test ($p < 0.05$). The analyzed nutrients include **(A)** nitrate ($N\text{-}NO_3$), **(B)** nitrite ($N\text{-}NO_2$), **(C)** ammonium ($N\text{-}NH_4$), **(D)**, silicate ($Si\text{-}Si(OH)_4$) and **(E)** phosphate ($P\text{-}PO_4$).

4.3.3 Chemical-physical features of the surface sediments

✓ *Grain-size*

At T_0, the sediments were predominantly sandy, with an average sand content of 48.47 ± 2.71%, followed by silt with 36.53 ± 2.37% and clay with 15.00 ± 0.78%. No significant differences were observed between T_0 and T_1 in sediment grain size distribution.

However, compared to T_1, a clear shift in grain size fractions was observed at T_2 in both internal and external sediments. Silt became the prevalent fraction, reaching 42.33 ± 6.66% inside the mesocosms and 45.20% outside. Correspondingly, the percentage of sand decreased to 39.40 ± 9.95% inside and 36.30% outside, whereas that of clay remained the lowest but increased slightly to 18.27 ± 3.32% inside and 18.5% outside the enclosures (Figure 9.S1).

✓ *Total Organic Carbon (TOC), Total Nitrogen (TN) and C/N*

Inside the mesocosms, TN, TOC, and C/N showed differences compared to external sediments. TN was significantly higher inside than outside at T_1 (2.27 ± 0.24 mg N g^{-1} dw and 1.89 mg N g^{-1} dw, respectively; $p < 0.05$), whereas no significant differences were observed at T_2 (1.94 ± 0.49 mg N g^{-1} dw and 1.93 mg N g^{-1} dw) (Figure 4.3.3.1A, Table 9.S1). TOC displayed a similar pattern, being higher inside at T_1 (18.49 ± 1.01 mg C g^{-1} dw and 16.65 mg C g^{-1} dw; $p < 0.05$), while at T_2 values were comparable between internal and external sediments (17.14 ± 2.80 mg C g^{-1} dw and 17.32 mg C g^{-1} dw) (Figure 4.3.3.1B, Table 9.S1). The C/N ratio was significantly lower inside at T_1 (9.56 ± 0.57 and. 10.27; $p < 0.05$), whereas at T_2 the difference was negligible (10.47 ± 1.08 and 10.48) (Figure 4.3.3.1C, Table 9.S1).

Considering temporal changes inside the mesocosms, TN slightly decreased from the beginning of the experiment (T_0: 2.42 ± 0.38 mg N g^{-1} dw) to T_2 (1.94 ± 0.49 mg N g^{-1} dw) (Figure 4.3.3.1A, Table 9.S2), as did TOC (T_0: 20.37 ± 3.65 mg C g^{-1} dw; T_2: 17.14 ± 2.80 mg C g^{-1} dw) (Figure 4.3.3.1B, Table 9.S2). The C/N ratio inside the mesocosms showed a slight decrease from T_0 (9.80 ± 0.30) to T_1 (9.56 ± 0.57), followed by an increase at T_2 (10.47 ± 1.08); however, none of these changes were statistically significant ($p \geq 0.05$) (Figure 4.3.3.1C, Table 9.S2).

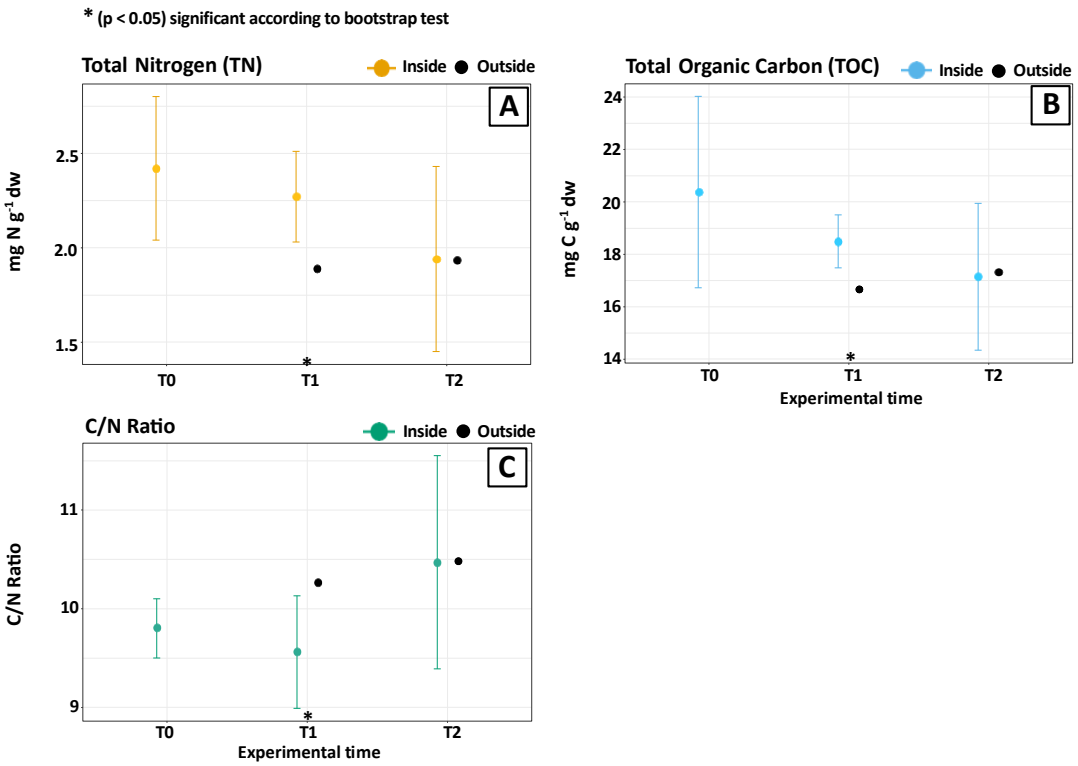

Figure 4.3.3.1. **(A)** Total nitrogen (TN), **(B)** total organic carbon (TOC), **(C)** and molar C/N ratio measured in sediments at T_0, T_1, and T_2. Colored points refer to results inside the mesocosms, black points the outside environment. Error bars indicate standard deviations (n = 3).

4.3.4 Chlorophyll a, Phytoplankton Biomass and Microphytobenthos Biomass

Inside the mesocosms, Chl *a* was slightly lower compared to the outside both at T_1 (1.57 ± 0.14 µg L^{-1} and 1.64 µg L^{-1}, respectively) and at T_2 (0.74 ± 0.07 µg L^{-1} and 0.79 µg L^{-1}) (Figure 4.3.4.1A, **Table S1**). Phytoplankton biomass (BP) showed a different pattern: at T_1, internal BP was lower than external (27.29 ± 1.62 µg C L^{-1} and 43.72 µg C L^{-1}; $p < 0.05$), whereas at T_2 it was slightly higher (6.66 ± 2.41 µg C L^{-1} and 5.44 µg C L^{-1}; $p > 0.05$) (Figure 4.3.4.1C, Table 9.S1). Among the phytoplankton groups, diatoms remained predominant throughout the experiment. Inside the mesocosms, their biomass was significantly lower than outside at T_1 (16.51 ± 3.00 µg C L^{-1} and 29.01 µg C L^{-1}; $p < 0.05$), but higher at T_2 (4.85 ± 1.70 µg C L^{-1} and 1.93 µg C L^{-1}; $p < 0.05$).

Dinoflagellates showed no significant differences between inside and outside at either time (T_1: 5.54 ± 3.76 µg C L^{-1} and 6.77 µg C L^{-1}; T_2: 0.90 ± 0.91 µg C L^{-1} and 1.52 µg C L^{-1}; $p > 0.05$). Coccolithophores contributed minimally to total biomass and were not significantly different at T_1 (0.07 ± 0.07 µg C L^{-1} and 0.09 µg C L^{-1}; $p > 0.05$), while they were slightly lower inside at T_2 (0.00 µg C L^{-1} and 0.04 µg C L^{-1}; $p < 0.05$). Flagellates were significantly less represented inside at both T_1 (5.17 ± 1.73 µg C L^{-1} and 7.85 µg C L^{-1}; $p < 0.05$) and T_2 (0.92 ± 0.29 µg C L^{-1} and 1.95 µg C L^{-1}; $p < 0.05$).Microphytobenthos (MPB) showed a steady increase from T_0 (82.32 ± 20.31 µg C cm^{-3}) to T_2 (135.25 ± 99.10 µg C cm^{-3}), consistently higher inside the mesocosms compared to outside (T_1: 87.66 ± 19.83 and 47.0 µg C cm^{-3}; $p < 0.05$; T_2: 135.25 ± 99.10 and 72.25 µg C cm^{-3}; $p > 0.05$) (Figure 4.3.4.1B, Table 9.S1).

Chl *a* increased from T_0 (1.06 ± 0.08 µg L^{-1}) to T_1 (1.57 ± 0.14 µg L^{-1}; ** $0.001 \leq p < 0.01$) and then decreased at T_2 (0.74 ± 0.07 µg L^{-1}; * $0.01 \leq p < 0.05$) (Figure 4.3.4.1A, Table 9.S2). BP followed a similar pattern, with diatoms remaining dominant throughout the experiment, showing a significant increase at T_1 (* $0.01 \leq p < 0.05$) followed by a marked decline at T_2 (** $0.001 \leq p < 0.01$) (Figure 4.3.4.1C, Table 9.S2).

Flagellates were stable between T_0 and T_1 ($p \geq 0.05$) but decreased significantly at T_2 (* $0.01 \leq p < 0.05$), whereas dinoflagellates exhibited lower values at T_1 and T_2, although differences were not statistically significant. (Figure 4.3.4.1C, Table 9.S2). MPB progressively increased throughout the experiment (Figure 4.3.4.1B, Table 9.S2).

Spearman correlations (Table 9.S3) highlighted consistent relationships among variables: BP and Chl *a* were strongly correlated with diatoms ($\rho = 0.81$). Chl *a* was negatively correlated with $P\text{-}PO_4$ ($\rho = -0.72$) and positively associated with water column primary production (GPPw, $\rho = 0.73$).

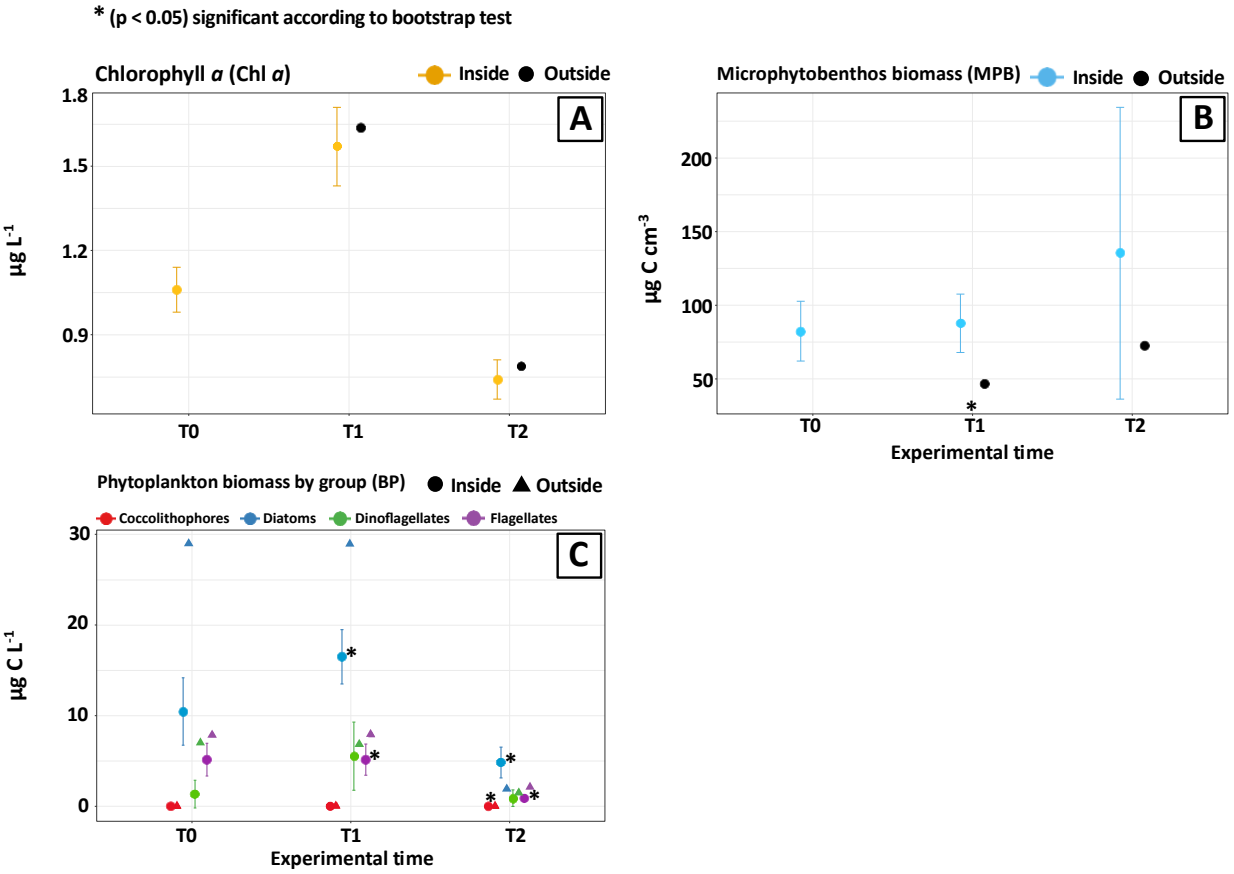

Figure 4.3.4.1. **(A)** Chlorophyll *a* (Chl *a*) in the water column, **(B)** microphytobenthic (MPB) biomass, and **(C)** phytoplankton biomass (BP) inside (colored points) and outside (black points) the mesocosms at T_0, T_1, and T_2. Error bars represent standard deviations (n = 3).

4.3.5 Dynamics of Primary Production and Community respiration

GPPw was slightly lower inside the mesocosms compared to outside both at T_1 (13.18 ± 2.04 µg C L^{-1} h^{-1} and 14.11 µg C L^{-1} h^{-1}, respectively; $p > 0.05$) and at T_2 (5.24 ± 0.73 µg C L^{-1} h^{-1} and 6.70 µg C L^{-1} h^{-1}; $p < 0.05$) (Figure 4.3.5.1A, Table 9.S1). In the sediments, both GPPs and NPPs were lower inside the mesocosms compared to outside at T_1 (7.04 ± 2.56 mg C m^{-2} h^{-1} and -4.33 ± 4.06 mg C m^{-2} h^{-1}; 13.98 mg C m^{-2} h^{-1} and 3.61 mg C m^{-2} h^{-1}; $p < 0.05$) and at T_2 (5.16 ± 2.61 mg C m^{-2} h^{-1} and -2.49 ± 1.04 mg C m^{-2} h^{-1}; 14.59 mg C m^{-2} h^{-1} and 5.09 mg C m^{-2} h^{-1}; $p < 0.05$) (Figure 4.3.5.1B, Table 9.S1), indicating a decrease in the benthic photosynthetic activity under confinement.

Over time, inside the mesocosms, GPPw rates increased compared to T_0 (5.57 ± 0.91 µg C L^{-1} h^{-1}), reaching a maximum at T_1 (** $0.001 \leq p < 0.01$) and then decreased at T_2 (** $0.001 \leq p < 0.01$) (Figure 4.3.5.1A, Table 9.S2). (GPPs (Figure 4.3.5.1B, Table 9.S2), displayed a progressive decrease from T_0 (17.42 ± 4.27 mg C m^{-2} h^{-1}) to T_1 (7.04 ± 2.56 mg C m^{-2} h^{-1}; *$0.01 \leq p < 0.05$) and T_2 (5.16 ± 2.61 mg C m^{-2} h^{-1}; ** 0.001

≤ p < 0.01), together with a reduction in community respiration rates (CRs) (T_0: −20.95 ± 3.18 mg C m^{-2} h^{-1}; T_1: −11.38 ± 1.64 mg C m^{-2} h^{-1}; * 0.01 ≤ p < 0.05; T_2: −7.66 ± 2.94 mg C m^{-2} h^{-1}; ** 0.001 ≤ p < 0.01). Consequently, negative NPPs values were obtained throughout the experiment (T_0: −3.54 ± 3.26 mg C m^{-2} h^{-1}; T_1: −4.33 ± 4.06 mg C m^{-2} h^{-1}; T_2: −2.49 ± 1.04 mg C m^{-2} h^{-1}).

Overall, correlation analyses (Table 9.S3) revealed consistent relationships between primary production processes and environmental variables: GPPw was inversely associated with temperature (ρ = −0.75), whereas in sediments GPPs and CRs were positively (ρ = 0.75) and negatively (ρ = −0.76) correlated, respectively, with total carbon (TC).

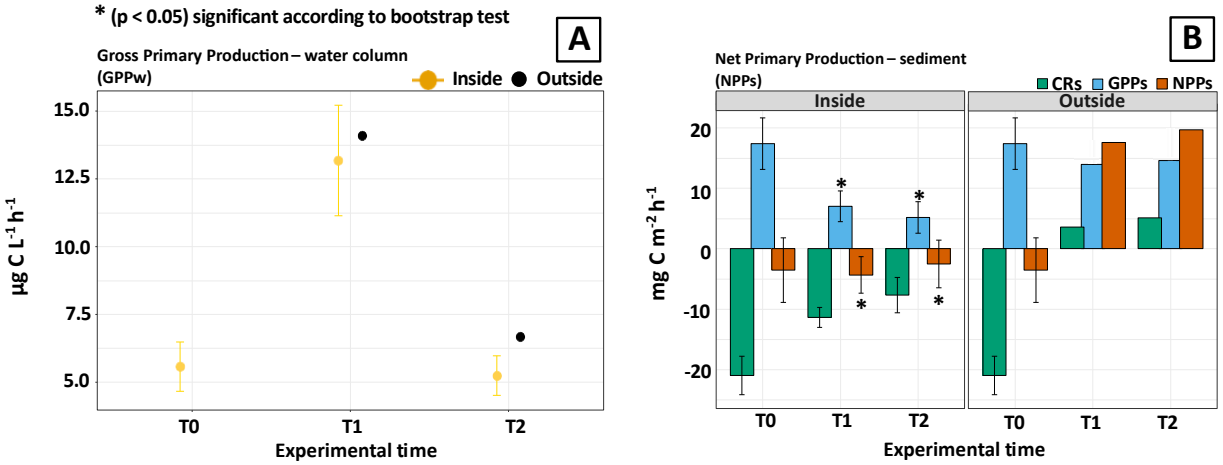

Figure 4.3.5.1. **(A)** Gross primary production in water (GPPw) inside (colored points) and outside (black points) the mesocosms at T_0, T_1, and T_2. **(B)** At T_0, the sample was the same for inside and outside conditions. Net primary production (NPP) estimated as the difference between gross primary production (GPPs) and community respiration (CRs) in sediments. Error bars represent standard deviations (n = 3).

4.3.6 Heterotropic Carbon Production (HCP) in Water and Sediment

Inside the mesocosms, HCPw was consistently higher than outside at T_1, with 9.22 ± 1.97 µg C L^{-1} h^{-1} (p < 0.05) inside compared to 7.25 µg C L^{-1} h^{-1} outside. At T_2, this pattern reversed, with external HCPw exceeding the internal values (12.3 µg C L^{-1} h^{-1} and 9.38 ± 2.70 µg C L^{-1} h^{-1}, respectively; p < 0.05) (Figure 4.3.6.1A, Table 9.S1). HCPs showed a similar dynamics: at T_1, internal values (3.24 ± 0.85 mg C m^{-2} h^{-1}; p < 0.05) were higher than the external one (2.23 mg C m^{-2} h^{-1}), whereas at T_2, external sediments displayed higher microbial activity than inside the mesocosms (4.33 mg C m^{-2} h^{-1} and 3.54 ± 2.27 mg C m^{-2} h^{-1}; p > 0.05) (Figure 4.3.6.1B, Table 9.S1).

Examining the temporal variability inside the mesocosms (p ≥ 0.05), HCPw slightly decreased compared to T_0 (10.56 ± 0.22 µg C L^{-1} h^{-1}), remaining similar both at T_1 (9.22 ± 1.97 µg C L^{-1} h^{-1}) and T_2 (9.38 ± 2.70 µg C L^{-1} h^{-1}) (Figure 4.3.6.1A, Table 9.S2), while HCPs showed a progressive increase from T_0 (2.80 ± 0.27 mg C m^{-2} h^{-1}) up to T_2 (3.54 ± 2.27 mg C m^{-2} h^{-1}) (Figure 4.3.6.1B, Table 9.S2).

Correlation analyses (Spearman) (Table 9.S3) did not reveal any significant relationships between HCP and the measured environmental variables; however, HCP was significantly higher inside compared to outside, suggesting a microbial response to the availability of fresh organic matter.

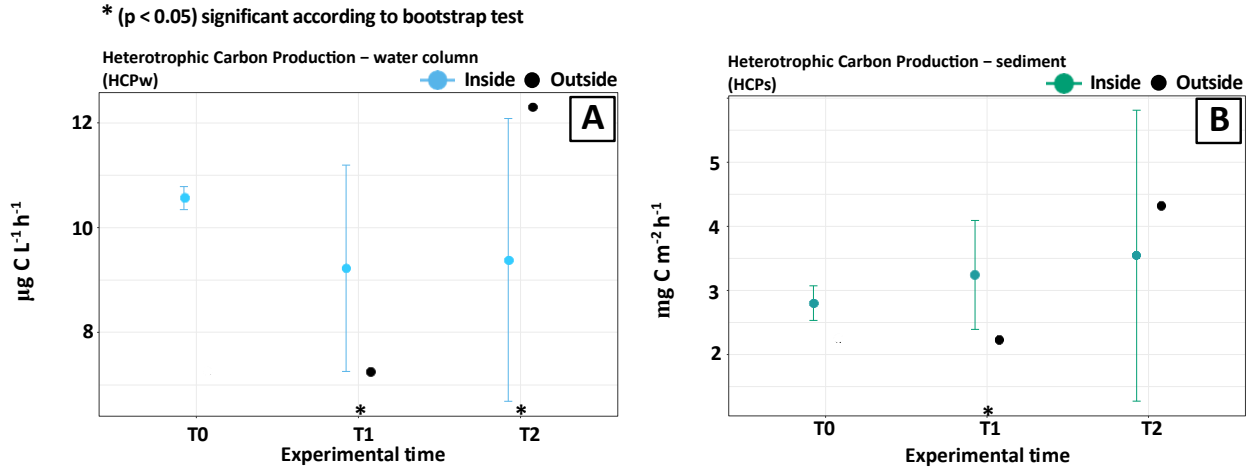

Figure 4.3.6.1. **(A)** Heterotrophic carbon production in water (HCPw) and **(B)** in sediments (HCPs) inside (colored points) and outside (black points) the mesocosms at T_0, T_1, and T_2. Error bars represent standard deviations (n = 3).

4.3.7 Response of lagoon ecosystem to progressive isolation from seawater

PCA calculated on abiotic data from the water column (Figure 4.3.7.1A) explained 82.4% of the total variance, with PC1 and PC2 accounting for 65.8% and 16.6%, respectively. PC1 was mainly positively correlated with O_2% (0.99), pH (0.97), and N-NO_2 (0.93), and negatively with N-NH_4 (−0.83) and salinity (−0.89). PC2 was primarily associated with Chl *a* (0.49) and P-PO_4 (0.33). Samples at T_0 were positioned in the first quadrant, reflecting high O_2%, pH, and oxidized N-compounds. At T_1, internal mesocosm samples were located in the third quadrant, associated with high salinity and Chl *a*, promoting major GPPw and BP fraction values. At T_2, internal samples were gathered in the second quadrant, driven by major N-NH_4 and P-PO_4 concentrations, indicating high degradation activities (HCPw). External T_1 and T_2 samples were slightly closer to the T_0 sample group, indicating more similar conditions to the initial ones. PERMANOVA confirmed significant differences among T_0, T_1, and T_2 ($F = 20.116$; $p = 0.005$; $R^2 = 0.87$).

The PCA of abiotic sediments variables (Figure 4.3.7.1B) accounted for 52.0% of the total variance considering the first two components (PC1: 42.0%, PC2: 34.5%). PC1 was strongly associated with TN (0.99) and TOC (0.92), while PC2 was explained by silt (−0.97) and sand (0.98). T_0 replicates were located in the first quadrant, representing organic matter-enriched sediments with high photosynthetic activity (GPPs). At T_1, internal replicates slightly shifted toward the second quadrant, mirroring progressively more heterotrophic conditions while the T_2 samples were gathered mostly in the lower part of the biplot, reflecting an increase in silt% and in the overall heterotrophic components (CRs and HCPs). External samples, particularly that of T_1, were far from the internal ones indicating different environmental conditions outside the mesocosms. PERMANOVA on sediment replicates did not reveal significant differences over time ($F = 1.231$; $p = 0.294$; $R^2 = 0.29$).

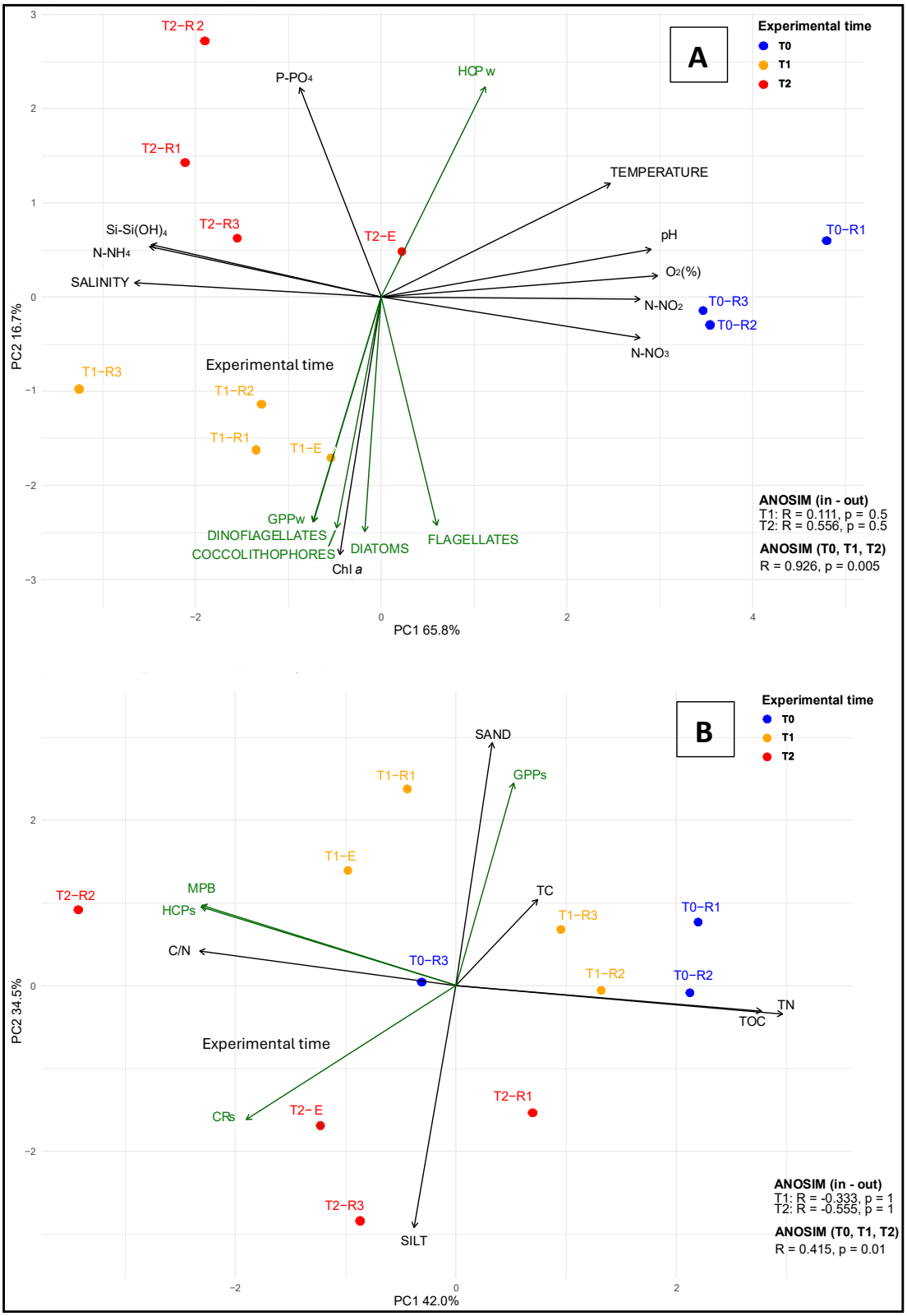

Figure 4.3.7.1. PCA of abiotic variables in water **(A)** and sediment **(B)** samples. Both biotic (green vectors) and abiotic (black vectors) variables are plotted to show their contributions to sample distribution. Points indicate samples at different experimental times (T_0, T_1, T_2) and distinguish between inside (-R1/R2/R3) and outside (-E) the mesocosms. ANOSIM tests confirm significant

differences between times and/or between inside and outside ($p < 0.05$). Vector length and direction indicate the strength and correlation of each variable with community composition.

4.3.8 Metal analyses in lagoon waters

The percentage distribution of metals in the waters sampled in the three experimental areas of the Grado lagoons at the two sampling times are showed in Figure 4.3.8.1. Site characterization revealed clear differences in metal distribution among the areas: at R1, Zn and Mn had the highest concentrations; at R2, Zn was the most abundant; whereas at R3, Mn was predominant, although the highest concentration of As was also detected there.

At the end of the experimental period, the same sites showed a marked change in the sampled waters (inside the mesocosms), with an increase in Mn and a sharp decrease in Fe at R1, while at R2 and R3 Zn was again the most represented metal.

The passive samplers placed inside and outside the mesocosms at R1 highlighted a different metal distribution compared to grab sampling, particularly showing the occurrence of Hg together with Fe and Zn, and to a lesser extent Mn. Inside the mesocosms, the passive sampler revealed the same prevalence of metals, although Hg was clearly increased at the expense of Zn. It is worth to note that occurrence of elements as Cd, Cr, Fe and Pb are detectable mostly or exclusively with these devices.

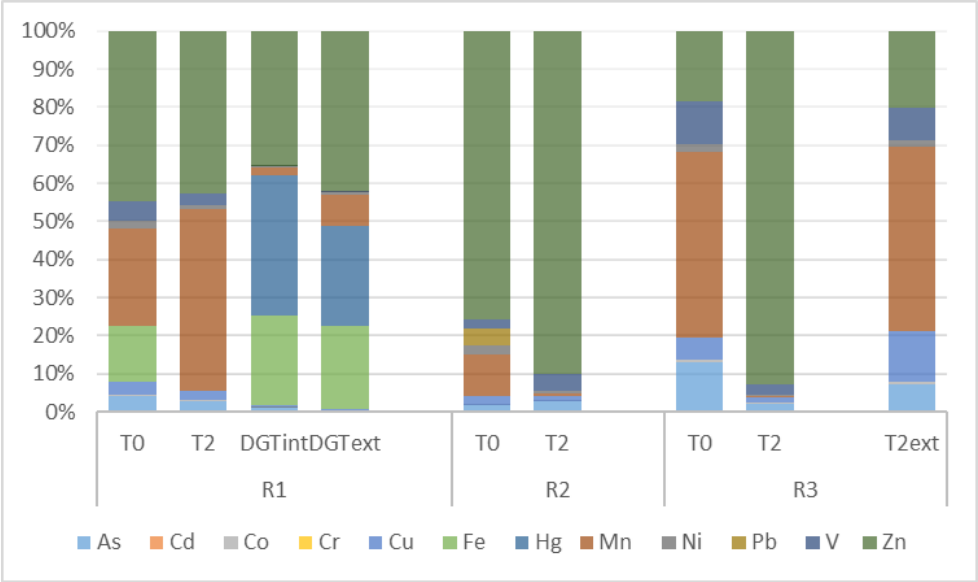

Figure 4.3.8.1. Percentage distribution of metals in the waters sampled in the three experimental areas of the Grado lagoons at the two sampling times.

4.3.9 Trace metal distribution and organic compounds in sediments

Metal distribution in lagoon sediments showed different patterns across the experimental sites (Figure 4.3.9.2). At R1, almost all major metals were present in comparable percentages, with clearly lower amounts of As, Pb, and Zn. At R2, higher concentrations of As and Cd were observed, while Zn was scarcely represented. At R3, by contrast, Zn was highly represented together with Pb. At T2, the surface sediments inside the mesocosms showed a clear change in metal distribution, likely attributable to the experimental conditions. At R1, the general pattern of several elements was maintained, but with a marked increase in Ni and Hg

and, to a lesser extent, As. At R2, Zn became more evident, whereas As, Cd, and Mn decreased, while Hg increased again. At R3, many metals decreased, with increases observed for Be, Cr, and Hg, whereas Pb and Zn were substantially reduced. Organic compounds measured in surface sediments showed different distributions after the experimental period, especially at R1 and R3. At R1, organic compounds were almost completely reduced, while TBT was the most represented compound inside the mesocosms. At R2, an increase in TPhT and TBT was observed. At R3, the high amount of TPhT measured at T0 was substantially reduced, with a concurrent increase in MPhT and DPhT. TBT was also reduced, with a slight increase in DBT and MBT.

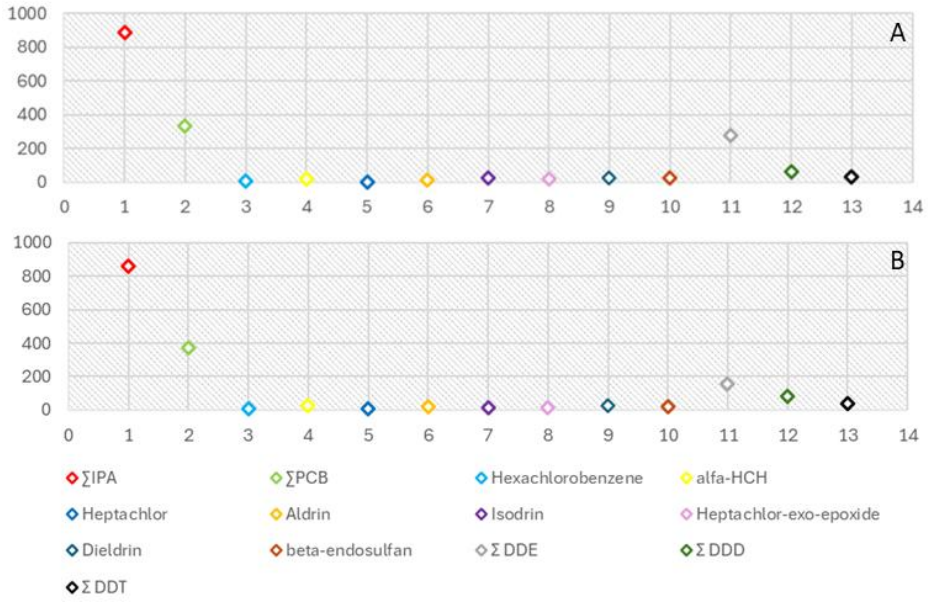

Figure 4.3.9.1. Organic compounds detected in water at R1 by SPMD passive samplers. A) Inside mesocosm B) outside mesocosm.

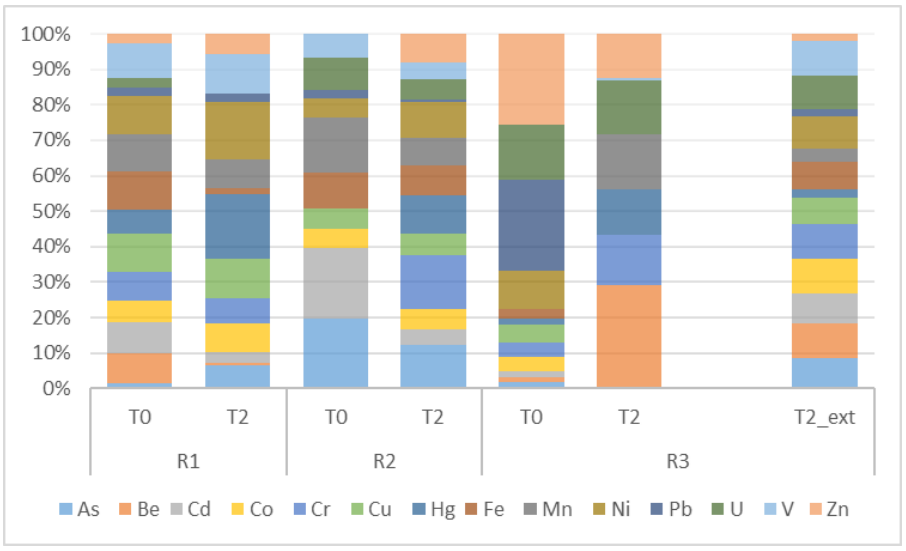

Figure 4.3.9.2. Percentage distribution of metals in the surface sediments sampled in the three experimental areas of the Grado lagoons at the two sampling times.

4.3.10 Ecotoxicological assessment

The integrated results of the ecotoxicological test battery, expressed as TBI (see Materials and Methods), showed for seawaters (Figure 4.3.10.2 **A**) an absence or negligible toxicity at T0, which then slightly increased at T2 moderately at R1, more markedly at R2, and sharply at R3.Sediment elutriates (Figure 4.3.10.2 **B**), on the other hand, showed slight toxicity already at T0. This toxicity increased at T2 for R1, unexpectedly decreased slightly for R2, and was high at T0 for R3, decreasing only marginally at T2. Considering the results of both matrices together (Figure 4.3.10.2**C**), which provide a single integrated toxicity value, R1 exhibited moderate toxicity that did not change after the enclosure period. R2 showed high initial toxicity that decreased over time. Finally, R3 had the highest toxicity value, which decreased slightly at T2 but remained within the same "High toxicity" category.

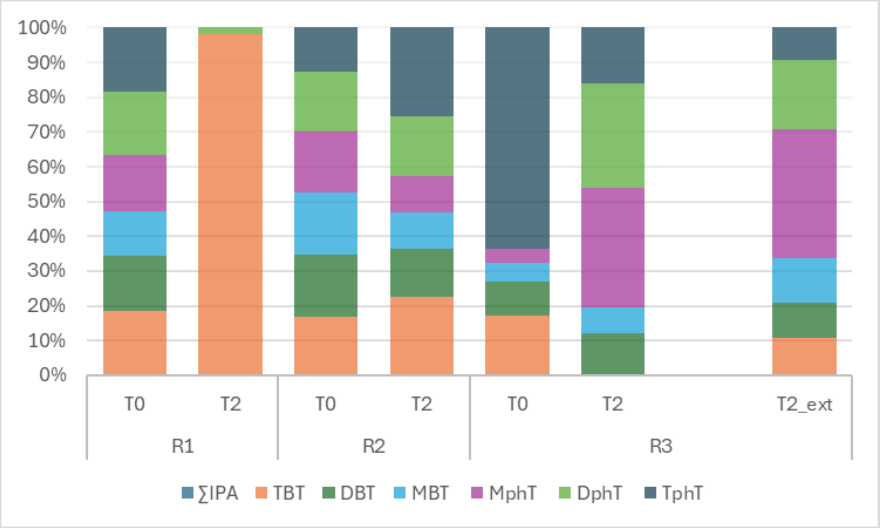

Figure 4.3.10.1 Percentage distribution of measured organic compounds in the sediments sampled in the three experimental areas of the Grado lagoons at the two sampling times.

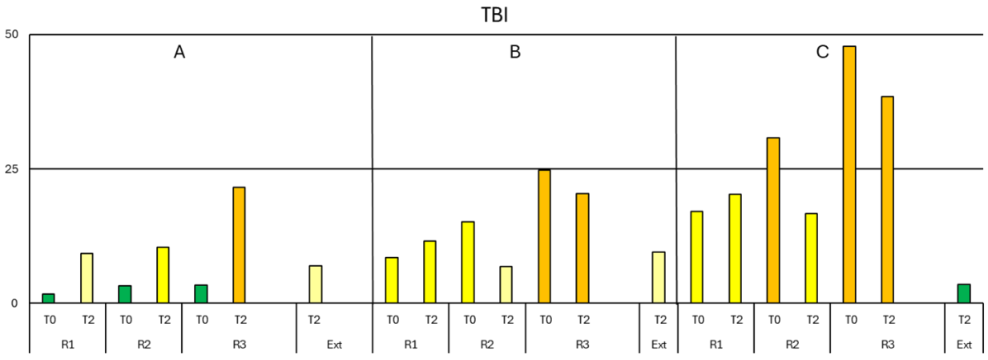

Figure 4.3.10.2 Integrated results of the ecotoxicological test battery as TBI (see Materials and Methods) for the three areas (R1, R2, R3) at experimental times (T0 and T2), for seawaters **(A)**, sediment elutriates **(B)** and considering results of both matrices **(C)**.

4.4 Discussion

The patchy distribution of *Cymodocea nodosa* in the study area led to conditions of oxygen supersaturation and prevented the establishment of proper hypoxia during the experimental period. Moreover, adverse meteorological conditions with strong north-eastern winds occurred after the second sampling, disrupting water stratification and inducing a thorough mixing of lagoon waters. However, despite hypoxic conditions did not establish, a significant decline in dissolved oxygen was still obtained in mesocosms compared to external controls, at both experimental times, triggering shifts in structural physical-chemical and biological variables, and in the main biological processes.

After 4 days, besides oxygen, also the total phytoplankton biomass significantly decreased (-37.6 ± 5.9% vs control), and the senescent cells likely settled towards the bottom accumulating in surface sediments. Indeed, TN and TOC increased at T_1 by +20.1 ± 10.6% and +11.1 ± 5.5%, respectively, compared to external conditions. This input of fresh organic matter in sediments stimulated both pelagic and benthic degradation processes. In fact, at T_1 HCP increased both in the water column (+27.2 ± 21.4% compared to external) and particularly in the sediments (+45.3 ± 26.2% internally compared to external values). This high microbial activity in both matrices was a proxy of a strong microbial remineralization. Notably, at T_1 ammonium increased by ca. 2.5x and silicates by +65.3 ± 44.2% compared to the external control. This high nutrient availability, also following the organic matter deposition from the water column, triggered MPB biomass proliferation (+86.5 ± 22.6% vs control). However, the autotrophic pathway in surface sediments was mostly directed towards the increase of microalgal biomass rather than to the benthic photosynthetic activity. Indeed, both GPP and NPP displayed significantly lower rates compared to those estimated externally, highlighting the importance of seawater renewal in supporting benthic phototrophic processes.

After 10 days, the trophic state inside the enclosures completely shifted towards heterotrophy. TOC and TN contents were very similar to the external conditions, and very low phytoplankton biomass could not either relevantly uptake inorganic nutrients or provide fresh organic material. This, in turn, slowed down microbial remineralization rates in the water (-23.7 ± 28.8% vs control) and sediments (-18.2 ± 64.1%) resulting in an excess of non-uptaken inorganic nutrients: phosphates increased by ca. 5x, ammonium by ca. 2.5x, and silicates by +65.3 ± 44.2%, compared to external conditions. Consequently, also the photosynthetic activity was significantly lower than outside both in the water (-21.8 ± 13.9% vs control), and in surface sediments. Only MPB took advantage of these conditions, increasing its biomass up to +87.2 ± 73.3% compared to outside, confirming remarkable resistance of the benthic diatom community to unfavourable and anoxic conditions (Larson and Sundbäck, 2008).

Generally, the induced confinement led to higher benthic respiration, reduced production and, consequently, to overall heterotrophic conditions while in natural conditions autotrophic conditions persisted at both experimental times.

Finally, PCA analysis confirmed a shift from initial natural, well-oxygenated conditions, towards a pelagic autotrophic peak after 4 days, and a dominance of all heterotrophic processes at the end of the experiment, with mass and energy fluxes shifting from the water column to sediments. Even a moderate oxygen decrease (–48.1 ± 7.3%) triggered cascading effects on biological and biogeochemical processes, leading to an imbalance in the benthic-pelagic coupling of the lagoon ecosystem.

Water samples for metal analyses were collected at three spatial replicates (R1-R3) at T0 around the mesocosms before starting the experiment. For logistic reasons, the time necessary to complete the sampling for the analyses of all physical-chemical and biological variables at each spatial replicate was around one hour, therefore it took approximately three hours to conclude the water sampling at T0. The concentration of prevalent metals differed greatly among the three replicates (R1-R3), and this depended on the speed at which environmental conditions change in the lagoon. In particular, the great variability in the occurrence of metals among replicates was clearly due to tide conditions: incoming vs outcoming tide rapidly change the chemical features of the lagoon water, and the contaminants it contains. As a consequence, Zn was the most represented metal in R2 but less abundant in R1 and R3. Similarly, also the distribution pattern of other metals markedly differed among the three spatial replicates.

At the end of the experiment (T2), water samples for metal analyses were collected from three distinct mesocosms, and from one external point to compare the results obtained in the enclosures with those from the natural environment. Two replicates (R2 and R3) were very alike: both displayed a similar distribution pattern of metals, and Zn was the most represented element in both mesocosms. The replicate R1, however, greatly differed from the other replicates. These mesocosms are quite large, each enclosing 1 m2 of the lagoon bed, and therefore the conditions that are established inside can vary greatly. They, in fact, represent and mirror the ecological spatial variability of the lagoon ecosystem and, to some extent, these differences among replicates were expected.

Interestingly, the distribution pattern of metals and the dominance of the same elements, which was obtained in R3 at the beginning of the experiment, was very similar to that observed externally after 10 days, at the end of the experiment. Even though several days have passed between the two sampling events, similar tide conditions occurred at the moment of sampling and therefore it is likely that comparable water masses with similar contaminant contents, were collected.

Regarding the results obtained using passive samplers, those placed inside and outside the mesocosms did not return a very dissimilar picture in terms of the distribution pattern of metals. However, they evidenced an enrichment of some metals, especially of Hg, inside the mesocosms. This suggests that the stagnation and water stratification, induced by the enclosure, already cause the transfer of Hg from sediments to the water column, even without having reached proper hypoxic conditions. This finding may have important implications for the lagoon ecosystem functioning, especially in its most confined areas where water stagnation is common in summer and autumn.

On the other hand, SPMD passive samplers showed only slight differences in the concentration of the considered organic compounds between inside and outside, suggesting that the altered conditions inside the mesocosms were anyway too mild to trigger any noticeable effect on their mobility.

Regarding the distribution of metals in surface sediments, the greatly diverse results obtained from the three spatial replicates at T0 indicate the very patchy distribution of metals in a small spatial area around the mesocosms. This is also evidenced from the results of ecotoxicological assays, and it is supported by the varying grain-size composition obtained around the mesocosm. It is also in line with previous results on metal distribution in the Grado lagoon and in the Gulf of Trieste, where the highest metal concentrations, especially Hg, were found to be associated with coarse sediments due to the occurrence of cinnabar (HgS) particles of mining origin (Biester et al., 2000). This makes it more difficult to extrapolate any possible effects induced by water stagnation from those linked to the intrinsic natural variability of these sediments.

Ecotoxicological evaluations also showed clear differences among the three replicates. For the sediment matrices at T0, toxicity tended to decrease over the experimental period. This could be due to the mobilization of contaminants—such as Hg in R2 or Zn in R3—from the sediment to the water, likely linked to enclosure effects (Figure 4.3.10.2 A, B).

Taking into account the measured organic compounds, the decrease in sediment toxicity can similarly be explained by the degradation of some compounds over time inside the mesocosms. This is clearly evident in R3, where the high concentration of TPhT measured at T0 was substantially reduced, accompanied by a concurrent increase in MPhT and DPhT. TBT was also reduced, with a slight increase in DBT and MBT.

In R1, the increased toxicity observed over the experimental period is consistent with the marked increase in Hg in the water and of TBT in the sediment sampled inside the mesocosms. This is probably due to changes in redox conditions that can mobilize organotins from porewater into the particulate phase, increasing measured sediment concentrations.

That desorbed TBT could re-adsorb onto fine particles or newly settled sediment, giving the illusion of an “increase” in surface sediment concentration.

4.5 Conclusions

The experimental set-up with mesocosms allowed observation of ecosystem responses to multiple stressors in a near-future scenario, revealing short-term resilience. Nevertheless, the modifications in the benthic-pelagic coupling suggest that prolonged or recurrent water stagnation could lead to dystrophic events already at the beginning of summer. Overall, these findings provide evidence on the vulnerability, yet adaptive capacity of coastal lagoons exposed to multiple stressors, and highlight the enclosure set-up as a powerful tool to understand complex ecosystem responses under global change.

5 Case study Panarea vents: Integrated approaches to evaluate the effects of environmental degradation on the persistence of habitat structural species such as *Posidonia oceanica*

5.1 Introduction

The global ocean is undergoing profound transformations driven by anthropogenic climate change and escalating chemical pollution. Increasing atmospheric CO_2 concentrations are causing ocean warming and acidification, with major consequences for seawater chemistry and marine biodiversity (IPCC, 2023). These stressors disrupt fundamental physiological processes, including calcification, photosynthesis, and nutrient uptake, thereby inducing large-scale shifts in ecosystem structure and function (Gattuso et al., 2015).

Concurrently, contamination by trace metals (e.g., mercury, arsenic) and sulfide compounds derived from industrial, agricultural, and urban effluents exerts additional pressure on marine systems. These toxicants accumulate in sediments and biota, impairing metabolic activity and reducing organisms resilience to environmental fluctuations (El-Sharkawy, 2024). In coastal ecosystems, the interaction between climate-related stressors and chemical pollutants often results in synergistic or antagonistic effects, amplifying ecological instability and leading to complex, non-linear responses (Nardi et al., 2020).

Within this framework, *Posidonia oceanica* meadows represent key yet highly vulnerable habitats in the Mediterranean Sea. Indeed, as photosynthetic and habitat-forming organisms, seagrasses can create local refugia from unfavorable or toxic conditions associated with global change, owing to their high carbon sequestration capacity and the structural complexity of the microhabitats they form (Falkenberg et al., 2021). Moreover, they provide essential ecological, physical, and socioeconomic services, including primary production, habitat provision, nursery functions for commercially valuable species, coastal protection, and carbon storage (Vassallo et al., 2013). Despite their recognized importance, ongoing environmental degradation and the emergence of new abiotic stressors (e.g., warming, acidification, and contamination) threaten both the persistence of these habitats and their ability to sustain surrounding biodiversity and ecosystem functioning. Evidence from natural CO_2-vent systems suggests that elevated CO_2 concentrations can enhance photosynthesis and carbon assimilation in *P. oceanica*. However, these potential benefits may be counterbalanced by increased sulfide intrusion or trace metal toxicity under warmer and more acidic conditions (Signa et al., 2024; Relitti et al., 2024).

Despite these insights, knowledge of the cumulative and long-term effects of climate change and pollution on *P. oceanica* functionality remains limited, particularly when evaluated through an integrated chemical and ecotoxicological perspective. In this context, the aim of the present study is to investigate the combined effects of global change drivers (warming and acidification), chemical contamination (sulfides and trace metals) and ecotoxicological characterization on *P. oceanica* meadows. The ultimate goal is to elucidate the extent to which this key species can act as biological stress mitigator, maintaining stable morphology and phenology, and to contribute to a deeper understanding of how forthcoming changes may trigger the decline of essential habitats and, consequently, the loss of critical ecosystem services on which human well-being depends.

5.2 Materials and methods

Coastal volcanic areas share several features with projected global climate change scenarios in marine systems (e.g., elevated temperature and CO_2 levels, resulting in reduced pH and high concentrations of toxic compounds such as sulfides and trace metals) (Dahms et al., 2018). These environments therefore represent valuable natural laboratories for investigating short- and long-term biological and ecological responses at different hierarchical levels of organization (species, communities, and ecosystems). Within this framework, two sampling campaigns (September 2024 and May 2025) were conducted in the fumarolic

field of Panarea island (Aeolian archipelago), one of the largest shallow hydrothermal systems in the Mediterranean.

5.2.1 Study area

The submarine hydrothermal system surrounding Panarea Island consists of an almost circular volcanic platform bounded by a shelf break at depths of approximately 120-130 m (Romagnoli et al., 2012). This system hosts numerous active vent sites characterized by vigorous discharge of CO_2-dominated (83.6-98.4 vol%) gases with low H_2S content (0.4-4 vol%) and very low concentrations of other gases such as H_2, He, and CH_4 (Esposito et al., 2006; Tassi et al., 2009; Voltattorni et al., 2009; Espa et al., 2010; Caramanna et al., 2011), as well as thermal fluids reaching temperatures of up to 140 °C (Italiano, 2009). In November 2002, the hydrothermal system experienced a sudden intensification of venting activity (Caracausi et al., 2005), attributed to the injection of magmatic fluids into the deep geothermal reservoir. This event triggered a low-energy submarine explosion that led to the near-complete eradication of marine life within the affected area, with evident impacts also on *Posidonia oceanica* meadows and associated fauna up to 50 m from the event's epicenter. Recolonization of the affected area by the seagrass began only two years after the gas burst (Andaloro et al., 2008). Subsequent ecological investigations revealed that *P. oceanica* meadows in the Panarea area display distinctive morphological and functional traits, such as reduced shoot size, the absence of a seasonal growth cycle, and a depauperate epiphytic community (Vizzini et al., 2010; Gambi et al., 2023). These features make the Panarea hydrothermal system an exceptional natural laboratory for studying the responses of this key seagrass species to climate-related stressors and environmental degradation.

Building on several years of research conducted by OGS in the area, two representative shallow hydrothermal sites (Hot-Cold and Campo21; Figure 5.2.1.1a) were selected based on their different physico-chemical characteristics and depth. In addition, three control sites were identified along the southern coast of Salina Island, two at 12 m depth (Tre Pietre and Punta Megna) and one at 21 m depth (Lingua). These control locations were chosen to match the Panarea sites in terms of depth, meadow structure, sediment grain size, and hydrodynamic exposure, while being unaffected by hydrothermal emissions (Figure 5.2.1.1 b).

The **Hot-Cold** site, located at depths between 10 and 12 m, displays a mosaic-like seafloor morphology where *P. oceanica* forms patchy meadows rooted in matte substrates interspersed with coarse sand deposits. This site is notable for pronounced thermal heterogeneity: some zones remain at ambient temperature, whereas others are influenced by hot fluid emissions that warm the sediments to as much as 60 °C. The warmer patches are commonly identified by the presence of yellowish bacterial mats, indicative of ongoing hydrothermal activity (Karuza et al., 2012).

The **Campo21** site, adjacent to a tectonic fault, is characterized by a rocky seabed and a rocky wall rising from 22 m to 15-16 m depth. Due to the presence of hydrogen sulfide in the emitted gases, the area is densely colonized by sulfur-oxidizing microbial biofilms (Maugeri et al., 2009). The benthic environment supports high macrophyte diversity, including extensive stands of both *P. oceanica* and *Cymodocea nodosa*, occurring near the emissions at 21 m as well as on the upper platform at 16 m, providing an ideal setting for investigating interactions between habitat-forming species and chemically dynamic conditions (Gaglioti & Gambi, 2018).

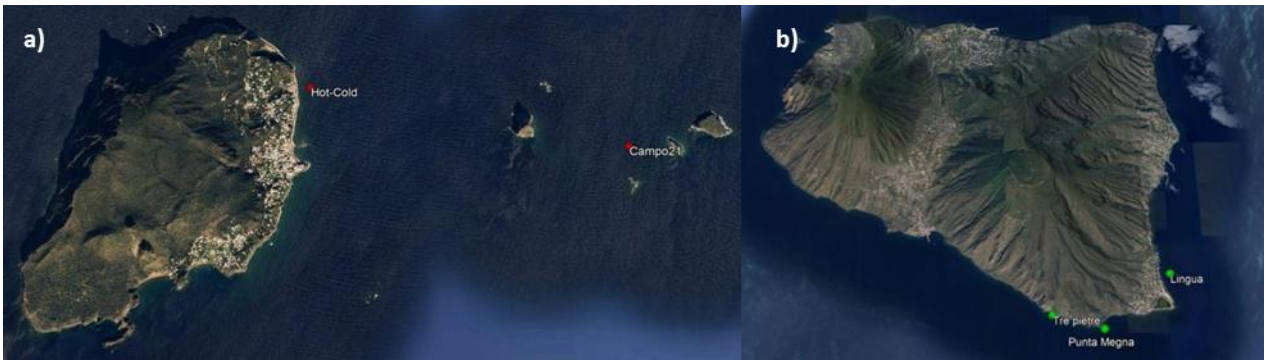

Figure 5.2.1.1. Sampling sites in a) Panarea and b) Salina islands

5.2.1 Sample collection

Seawater, sediments and *P. oceanica* shoots were collected to evaluate the occurrence, the extent and the potential impact of the stressors. Passive samplers were also deployed to estimate bioavailable metals.

5.2.1.1 Seawater

✓ *Water column characterization*

Hobo probes were deployed for real-time continuous data of temperatures and pH in the two impacted sites of Panarea and in the three control sites of Salina Island. Two probes per site, approximately 5 m apart, were placed on the first day of the sampling cruise and recovered the last day.

CTD profiles (SBE 19plus V2 SeaCAT) were performed at each sampling site to characterize the vertical water column structure in terms of temperature, salinity, dissolved oxygen and pH.

✓ *Carbonate system*

Discrete water samples were collected with Niskin bottles, as close to the seafloor as possible at three different stations in each site, for total alkalinity (TA), spectrophotometric pHT and nutrients analyses to assess the changes in the carbonate system. For pH and TA determinations, 250-mL borosilicate glass bottles were filled with seawater, poisoned with 100 µL of saturated mercuric chloride (HgCl2) to halt biological activity, sealed with glass stoppers and stored in the dark at 4˚C until analysis. Samples for dissolved inorganic nutrients (nitrite, NO_2, nitrate, NO_3, ammonium, NH_4, phosphate PO_4, and silicic acid, H_4SiO_4) determination were filtered on 0.7 µm pore size glassfibre filters (Whatman GF/F) and stored frozen (-20˚C) in polyethylene vials until laboratory analysis.

✓ *Bioavailable metals*

The freely dissolved, time-weighted average concentrations of trace metals in the water of the shallower target sites were measured using passive samplers deployed throughout the period of the planned sampling activities. More specifically, one set of n. 18/24 DGT (almost 4 for each class of elements: trace metals, As, Hg) passive samplers were deployed at each of the shallower sites (Hot-Cold in Panarea island and Punta Megna in Salina Island) along the water column at a maximum depth of 5 m from the surface. Temperature was measured and sediment (50 ml) and water samples (100 ml) for metal and ecotoxicological analyses were collected when the DGTs were placed and then also when they were recovered one week after.

5.2.1.2 Interstitial water

Samples of interstitial water were collected as close as possible to the seagrass and in non-vegetated bottom in Hot-Cold and Campo21_21m sites in Panarea and Punta Megna site in Salina to assess the chemical composition. Samples were collected using a 1 m long stainless-steel tube (0.5 cm in diameter) inserted in the submarine sediments down to several tens of cm. Water was pumped from the tube and transferred to a plastic 100 cc syringe through a three-way Teflon valve by a scuba diver and finally stored in HDPE bottles. In the lab, alkalinity was analyzed by acidimetric titration (AT) using an automatic burette filled with 0.01 M HCl and methyl-orange as an indicator. Temperature (◦C) was measured directly in the sediment using the customized underwater probe 100K NTC, while pH and redox potential (Eh) were determined using a Lange sension portable meter.

5.2.1.3 Sediments

At each station, surface sediment adjacent to seagrass meadows was collected by SCUBA divers in triplicate using a PVC container.

5.2.1.4 Posidonia oceanica

At each station, shoot density was recorded by SCUBA divers (six replicates) using a quadrat metal frame (40 x 40 cm) (Buia et al. 2004). Moreover, fifteen orthotropic (vertical) shoots of *Posidonia oceanica* were randomly collected at each station by carefully detaching them from the plagiotropic (horizontal) rhizomes at their insertion point.

5.2.2 Laboratory analyses and data elaboration

The collected samples were analyzed in laboratories of the research team (ENEA, OGS ECCSEL NatLab Italy of Panarea island, UNIPA), based on the competences and skills of each partner.

5.2.2.1 Seawater

- ✓ *Carbonate system*

Analyses of pH and TA were carried out using a Cary 100 Scan UV–visible spectrophotometer and a Mettler Toledo G20 equipped with a LAUDA L100, respectively, following the laboratory procedures described by Dickson et al. (2007). The analytical precision for pH was estimated to be ±0.002 pH_T units. The accuracy and precision of the TA measurements on CRM were determined to be better than ±2.0 mmol kg^{-1}. TA values were calculated using the Alkalinity Calculator spreadsheet developed by Currie et al. (2024), based on Standard Operating Procedure 3b of Dickson et al. (2007). As for nutrients, samples were defrosted and analysed colorimetrically using a segmented flow QUAATRO Seal Analytical AutoAnalyzer according to Hansen & Koroleff (1999). The detection limits for the method were 0.01 µM, 0.02 µM, 0.03 µM, 0.01 µM, and 0.01 µMfor NO_2, NO_3, NH_4, PO_4, and H_4SiO_4, respectively. All the analyses were performed by OGS part at the laboratories in Trieste and part at the ECCSEL-ERIC NatLab Italy in Panarea. All resulting data were processed using the CO_2SYS 3.0 Excel implementation (Pierrot et al., 2021) to calculate additional parameters, including Total Dissolved Inorganic Carbon (DIC or CT) and partial pressure of CO_2 (pCO_2), necessary to assess changes in the carbonate system.

- ✓ *Bioavailable metals*

Immediately after the retrieval from seawater, DGTs were rinsed with Milli-Q water and stored at 4°C; successively, in laboratory, metals and As were eluted from the binding gel of the device in 1 ml of 2M H NO_3. The elution extracts were diluted with Milli-Q water and trace metal analysis was carried out by ICP-MS (Agilent 7800). A blank resin was always considered. DGT performance was evaluated according to the method used by Zhang and Davison (1995). The concentrations of metals and As measured by DGT, in three replicates, were calculated using equations and parameters provided by Davison (2016). Analysis of total mercury concentrations in DGT units was performed using AMA 254 mercury analyser: the chelating resin was removed from the device and directly analysed without further preparations. A blank resin was analysed in the same conditions, and its mercury content was always subtracted to the mercury concentrations measured for the samples.

The measurements of metal element concentrations in seawater samples were performed using ICP-MS (Agilent 7800) equipped with a UHMI (Ultra High Matrix Introduction) system, for the analysis of complex matrices characterized by high salt content, an Ar humidifier and with both a He and a HeHe collision cell, to suppress any interferences. External calibration standard solutions were prepared by appropriately diluting a 10 µg mL-1 multi-element standard solution (Environmental Calibration Standard solution, from Agilent Technologies) in a salt matrix consisting of 3.5% NaCl (99.99 SuprapurR, Merck) in H2O MilliQ and 1% di HNO3 (TraceSelectTM Ultra, Fluka), to simulate "artificial" seawater. A Rh solution was used as an internal standard to compensate for any variations in instrument efficiency that could influence the measurements during analysis.

Quality data was evaluated analysing, in the same analytical conditions used for seawater samples, the following certified reference materials: CASS-5, CASS-6 - Nearshore Seawater Certified Reference Materials for Trace Metals and other Constituents, and ERMCA403 seawater (element content).

5.2.2.2 Interstitial water

The main cations (Ca2+, Mg2+, Na+, K+) and anions (Cl-, SO42-, Br-, F-, NO3-) were determined by ion chromatography (IC) in the laboratories of the Dept. of Earth Sciences of the University of Firenze, using Metrohm 861 Compact IC and Metrohm 761 Advanced Compact IC chromatographs, respectively. Ammonium (NH4+) was analyzed by molecular spectrophotometry (MSP, Nessler Method) using a HACH DR2010 instrument. The analytical errors for AT, IC, and MSP were below 5%.

5.2.2.3 Sediment

✓ *Trace element analysis*

The analytical determination of trace elements (Arsenic, As; Cadmium, Cd; Chromium, Cr; Copper, Cu; Iron, Fe; Lead, Pb; Mercury, Hg; Manganese, Mn; Nickel, Ni; Vanadium, V; Zinc, Zn) in freeze-dried powdered sediment samples was conducted using the USEPA 6010C/2007 'Inductively Coupled Plasma-Atomic Emission Spectrometry' protocol, with samples analysed using an ICP-OES (Optima 8000, PerkinElmer) equipped with an autosampler. Samples were previously subjected to mineralisation by mixing samples with HNO_3, H_2O_2 and Milli-Q distilled water in a closed microwave system (CEM, Model MARS). For As and Hg, a hydride generator was used alongside ICP-OES and the samples were treated with a reducing solution containing $NaBH_4$ and NaOH. Analytical control was performed by mineralising certified reference materials (CRMs) "Marine sediment" (NIST-2702, National Institute of Standards and Technology). The recovery ranged from 84 to 101%. The detection limit was calculated as three times the standard deviation of the blanks ($n > 20$) and was 0.003 mg kg^{-1} dry weight (dw) for all trace elements. All results are expressed in mg kg^{-1} dw.

✓ *Isotopic and elemental analyses*

Freeze-dried powdered sediment samples were analysed for carbon and nitrogen stable isotopes ($\delta^{13}C$ and $\delta^{15}N$ ‰) using a Thermo Delta Plus XP isotope ratio mass spectrometer (IRMS) connected to a Thermo Flash EA 1112 elemental analyser. The isotopic values were expressed in δ notation (parts per million) relative

to the international standards Pee Dee Belemnite for $\delta^{13}C$ and atmospheric N_2 for $\delta^{15}N$, according to the formula: $\delta_X = [(R_{sample}/R_{standard}) - 1 \times 10^3$, where X is the mass of the stable isotope (13 for C and 15 for N) and R is the corresponding $^{13}C/^{12}C$ or $^{15}N/^{14}N$ ratio. The analytical precision, based on the standard deviation of replicates of internal standard analyses (IAEA-CH-6 for $\delta^{13}C$ and IAEA-NO-3 for $\delta^{15}N$), was 0.1‰ for $\delta^{13}C$ and 0.2 ‰ for $\delta^{15}N$. At the same time, total carbon (C %), total organic carbon (TOC %) and nitrogen (N %) in sediment samples were analysed using method VII.1, 'Determination of total or organic carbon and total nitrogen with an elemental analyser, as reported in Ministerial Decree 13/09/1999 (GURI, 1999). The detection limits of the elemental analyser used were respectively 0.01% for C_{org} and 0.005% for NT. For TOC% only, the samples were first subjected to acid attack with HCl and then dried at 50°C.

5.2.2.4 Ecotoxicological characterization

✓ *Samples preparation*

Toxicity tests, in triplicate, were carried out on seawater and sediment elutriates. For the preparation of sediment elutriate, Artificial SeaWater (ASW) (ASTM 1994) was added to the sediment in the ratio 4:1 (volume/dry weight) and placed in a shaker for 1 h at room temperature. Then, the mixture was centrifuged at 3,000 rpm (1,000×g) for 20 min and filtered (Ø 0.45 µm). For aqueous samples, a bioassay battery, consisting of three different species representing different trophic levels, algae *Dunaliella tertiolecta*, bacteria *Vibrio fischeri*, and crustacean *Artemia salina*, was chosen.

i. *D. tertiolecta* test

The chronic test was carried out according to ISO 10253. The culture medium for algal growth was prepared according to ISO protocol. A screening with the undiluted (whole) sample was performed. An algal suspension at a concentration of 1×10^6 cells/mL was prepared. Then, an aliquot of algal suspension was added to each replicate to reach the final concentration of 1×10^4 cells/mL. Culture medium has been utilized as negative control (six replicates). The test flasks were placed in a thermostatic chamber at 20 °C with a light source in the 7,000– 8,000-lux range for 72 h. The cell density of each sample was measured after 72 h by the Burker chamber. The effect percentage for each sample was calculated with respect to the control.

ii. *A. salina test*

Cysts were hatched by using the procedure described in APAT IRSA-CNR (2003). The encysted organisms were first hydrated in a volume of ASW for 1 h at 25 °C at 3,000–4,000 lx. Then, the cysts were incubated for 24 h in the dark at the same temperature. Acute toxicity test (96 h) was conducted according to APAT-IRSA (2003). Ten nauplii were transferred in a beaker with 40 mL of sample. Each sample was tested in triplicate. The negative control consisted of six replicates of artificial seawater. The treatments were incubated at 25 °C with a light regime of 14:10 h light/dark. No food was provided during the exposure. Every 24 h, the number of live individuals was recorded. The effect percentage for each sample was calculated with respect to the control.

iii. *Aliivibrio fischeri test*

Aliivibrio fischeri luminescence inhibition test was carried out using whole (undiluted) seawater and elutriate samples as a screening assessment. Each sample was mixed with the bacterial suspension and incubated according to the biolight toxy procedure. A negative control consisting of diluent (2% NaCl) was included in each test run. Luminescence was measured after 15 and 30 minutes of exposure using the Biolight toxy, following the manufacturer's instructions. Results were expressed as the percentage of luminescence inhibition relative to the control.

iv. *Toxicity test Battery Index (TBI)*

For each sample, the results of the different tests were integrated using the TBI (Manzo et al., 2014). The TBI was calculated also for seawater and elutriate samples separately. The effects on the chosen endpoints were expressed as percentage and classified. To calculate the TBI, the percentage of the effect (%E) on each endpoint was corrected to obtain the Score test Endpoint (SEi) using the following formula: SEi = %E (M x S) SCF where SCF (statistical correction factor) is the Students t-test between sample and control. The

values of 0, 1, 2, 3, and 4 were attributed to SCF, corresponding to no differences ($p > 0.05$), biostimulation ($p < 0.05$), high biostimulation ($p < 0.01$), toxicity ($p < 0.05$), and high toxicity ($p < 0.01$), respectively; matrix (M) based on the ecological relevance of the matrices and on the level of sample manipulation equal to 2 for elutriate; severity (S) referred to the degree of effect that the bioassay endpoints measure. Mortality and bioluminescence inhibition are considered the most severe endpoints followed by algal growth and fertilization equal to 4 for algal growth, 3 for fertilization, and 5 for mortality and bioluminescence. SEi is expressed in a 0–100 scale relative to test battery utilized as follows: %SEi = SEi (%Em) / (SE max) where % Em is the maximum effect percentage observed corresponding to the maximum MS obtained, and SE max is the maximum Score test Endpoint calculated. TBI is calculated according to the following formula: %TBI = (∑%Sei /N) where N is the number of endpoints. The ecotoxicological risk is defined as follows: absent (TBI ≤5%), low (5 < tbi <10%), moderate (10% <20%), high (20% <50%), very high (tbi>50%).

5.2.2.5 Posidonia oceanica

In the laboratory, *Posidonia oceanica* samples were thoroughly rinsed with distilled water to remove any extraneous material. Phenological and lepidochronological analyses were carried out on the same *P. oceanica* shoots following the approach described by Pergent (1987). First, leaf blades were then gently detached from the rhizomes, starting from the outermost (oldest) leaf and proceeding toward the innermost (youngest). Leaves were then numbered sequentially and classified according to the presence/absence of the leaf base and leaf blade length into adult (base present), intermediate (base absent, leaf blade > 5 cm), and juvenile (base absent, leaf blade < 5 cm) leaves (Giraud, 1977). After that, leaf biometric measurements (see "*Phenological analysis*" section for more details) were carried out. Adult leaves were gently scraped using a ceramic blade to collect the associated epiphytes that were freeze-dried, weighed for biomass measurement and finely ground prior to further analysis. Then, *P. oceanica* scales were gently removed from the rhizomes starting from the oldest portion of the rhizome, following their natural distichous and alternate insertion order. The scales were then arranged on a bench maintaining the order of removal and subject to lepidochronological measurements (see "*Lepidochronological analysis*" section for more details). After that, rhizome portions and both intact and non-intact scales were weighed to estimate their relative biomass. Scales were then finely ground prior to further analysis.

✓ *Phenological analysis*

Biometric measurements of *P. oceanica* leaves were taken manually using a ruler and a digital caliper (Reyes et al., 1995). For each leaf, the following parameters were measured:

i. Length of the leaf base (adult leaves only);
ii. Length of the leaf blade (from ligula to apex), including any brown (non-photosynthetic) tissue;
iii. Maximum leaf width at the central portion of the blade;
iv. Apex condition (0 = intact; 1 = eroded).

From the phenological dataset, the following parameters derived were calculated:

i. Surface area (leaf blade length x width) / shoot;
ii. Percentage of brown tissue (brown tissue length/leaf blade length) / shoot;
iii. Coefficient A (percentage of adult and intermediate leaves with eroded apices) / shoot.

✓ *Lepidochronological analysis*

To identify the annual growth cycle of the *P. oceanica* shoots, the thinnest scales were cut 10 mm from their insertion point on the rhizome, and their thickness was measured under a stereomicroscope. The portion of rhizome between two consecutive thinnest scales, corresponding to a lepidochronological year, was measured for length (mm), and maximum and minimum width (mm) using a caliper. The corresponding scales were counted and, when intact, their length (mm) was also recorded.

By considering only the rhizome sections that had completed a full annual cycle, thus excluding the youngest and oldest portions, the following parameters were derived:

i. Yearly rhizome growth rate;
ii. Number of scales produced per year;
iii. Rhizome primary production;
iv. Mean shoot age.

✓ *Trace element analysis*

Analysis of trace elements (As, Cd, Cr, Cu, Fe, Pb, Hg, Mn, Ni, V, Zn) in *P. oceanica* samples was performed as described in Section 5.2.3.3 for sediment samples. The only difference lies in the analytical control, which in this case was performed by mineralising the "*Lagarosiphon major* BCR-060" CRM from the Institute for Reference Materials and Measurements.

✓ *Isotopic and elemental analyses*

Stable carbon and nitrogen isotope and elemental analysis were performed on *P. oceanica* leaf and root samples as described in Section 5.2.3.3 for sediment samples. Freeze-dried *P. oceanica* samples were also analyzed for $\delta^{34}S$ and S% using a ThermoFisher IRMS (Delta V ADVANTAGE) coupled with an elemental analyzer (ThermoFisher Flash 2000) and interfaced via a Conflo IV for the management of dilution and reference gases. Results are given in the δ notation as per mil deviation from the international standard (Vienna-Canyon Diablo Troilite V-CDT) as follows: $\delta^{34}S = [(^{34}S/^{32}S \text{ sample})/(^{34}S/^{32}S \text{ standard}) - 1] \times 10^3$. The analytical precision, based on the standard deviation of replicates of internal standards (IAEA-SO-6, IAEA-S-1, NBS127) was ± 0.2‰.

For total sulphur content (S %), the analytical procedure was verified using a standard reference material (recovery between 94 and 102%) supplied by the United States Geological Survey: Marine Sediment, MAG-1 (0.39%) and Cody Shale, SCo-1 (0.059%). Calibration was performed by analysing sulfanilamide (S = 18.6%).

5.2.3 Statistical analyses

Principal Component Analysis (PCA) was used to visualise distances among stations in the two seasons considered and their relationships with trace elements both in surface sediment and in *P. oceanica* leaves and roots.

For each compartment (Sediment, Leaves and Roots) a Multiple Pollutant Index (MPI) defined by Usero et al. (2005), was created considering only non-essential trace elements (As, Cd, Cr, Hg, Pb) and using the following formula:

$$MPI = (\prod_{i=1}^{n} Cf_i)^{1/n}$$

Where Cf_i is the concentration of each trace element.

Partial least squares (PLS) regression multivariate analysis was used to assess the influence of different types of factors on *Posidonia oceanica* metrics (Density, Surface area, Brown tissue, Epiphyte biomass, Leaf Number, Coefficient A). The explanatory variables considered are namely water pH (pHT), MPI for sediment (MPI S), *P. oceanica* leaves (MPI L) and roots (MPI R), sulfur stable isotope ratio in leaves ($\delta^{34}S$ L) and roots ($\delta^{34}S$ R). M. The leave-one-out cross-validation was used for each model. The best number of PLS components was chosen based on the best trade-off between lower RMSE and lower model complexity. Jack-Knifing method was used to compute confidence interval for testing if the coefficients are statistically different from zero. PLS models were computed using the pls R package (Liland et al., 2024). A p-value < 0.05 was considered significant. All the analyses were performed using the R (4.2.2) statistical software.

5.3 Results

5.3.1 Seawater

✓ *Water column characterization*

The HOBO probes used for continuous pH monitoring revealed a marked fluctuation during the ten-day survey conducted in September 2024, with the lowest peak of 6.8 ± 0.48 recorded in Hot site. In contrast, the Cold site proved to be the least acidified and the most stable among the impacted areas (Figure 5.3.1.1 a). In May 2025, the overall pH range (from 7.96 ± 0.14 measured at Campo21_21m to 7.40 ± 0.40 at Campo21_16m) was narrower than that observed in September, and the trend recorded over the ten-day period showed less variability across all impacted sites (Figure 5.3.1.1 b).

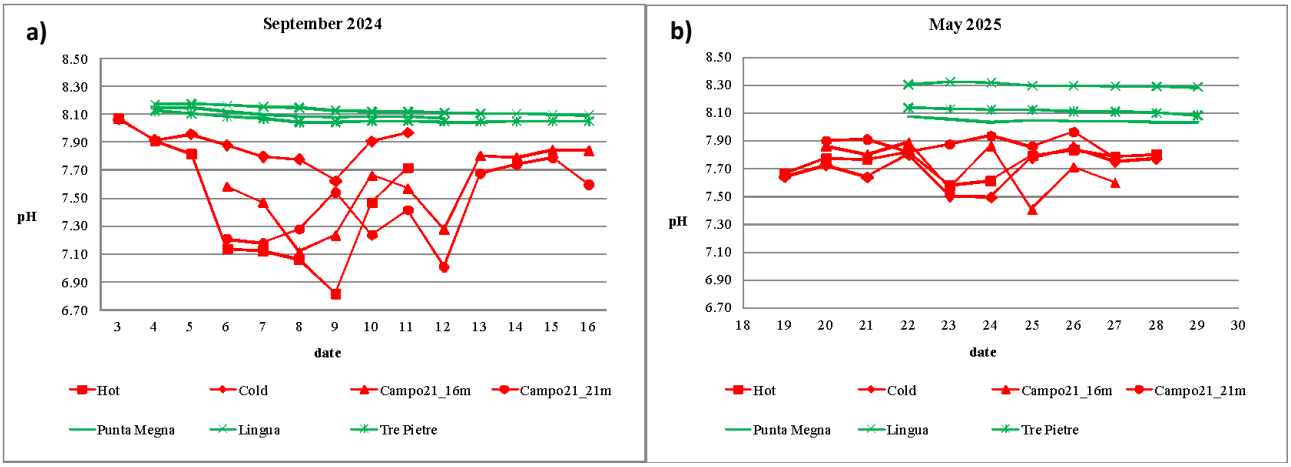

Figure 5.3.1.1. Average daily pH values measured by HOBO probes deployed at the sampling sites in Panarea and Salina islands during a) the September 2024 and b) the May 2025 sampling campaigns.

The physico-chemical characterization of the water column showed no anomalies in temperature, salinity, or dissolved oxygen, all of which displayed profiles typical of the sampling season (September 2024 and May 2025) across all sites. In contrast, the pH profiles measured in May 2025 at the impacted sites of Panarea exhibited differences compared with those of the control sites, as illustrated in Figure 5.3.1.2 and Figure 5.3.1.3. Data recorded by the pH sensor of the CTD probe deployed at the Hot-Cold site indicated that Hot showed values ranging from 6.91 to 7.42 within the first two meters (corresponding to the thermocline), followed by a gradual increase up to 7.71 at 10 m depth (Figure 5.3.1.2 a). Cold, on the other hand, displayed an almost linear profile down to 9.5 m, after which a slight decrease was observed (Figure 5.3.1.2 b).

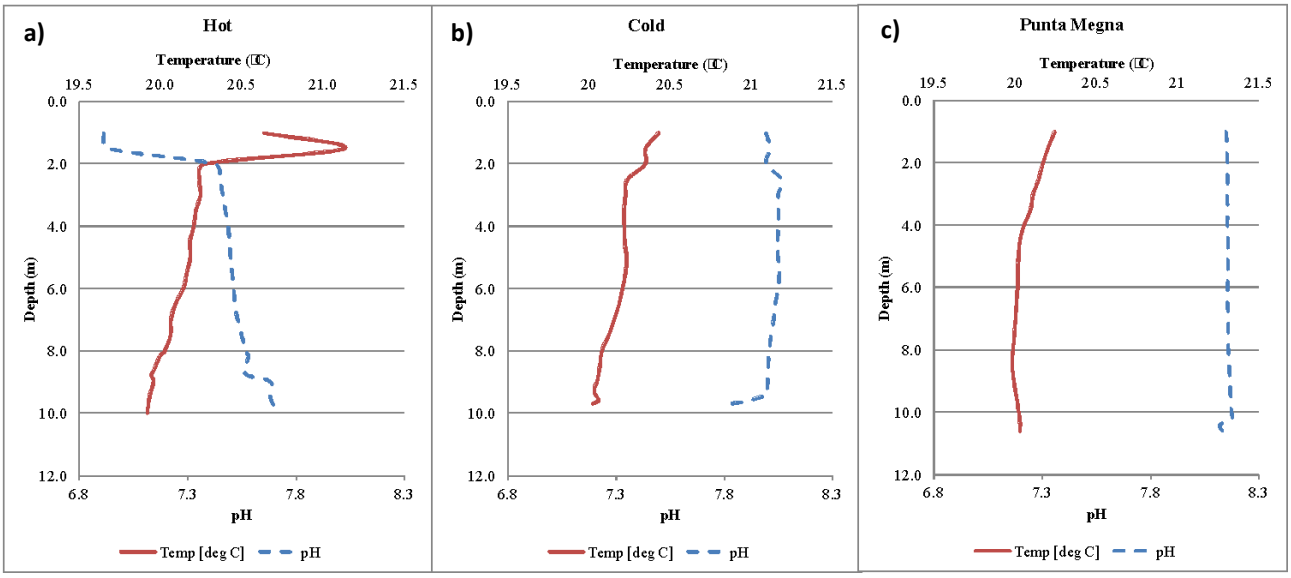

Figure 5.3.1.2. pH and temperature profiles measured by CTD probe deployed at: a-b) Hot-Cold site in Panarea and c) the control in Salina Island during the May 2025 sampling campaigns.

For Campo21_16m, the pH profile in May 2025 showed values exceeding 8.0 near the surface and then decreasing progressively with depth. A pronounced drop is observed around 10-12 m, where pH falls below 7.0, reaching its minimum in the deeper layers of the profile (Figure 5.3.1.3 a).

The vertical profiles recorded at the control stations, Punta Megna and Tre Pietre (Figure 5.3.1.2 c and Figure 5.3.1.3 b respectively), in Salina Island indicate a typical early summer stratification with a limited pH variability along the water column.

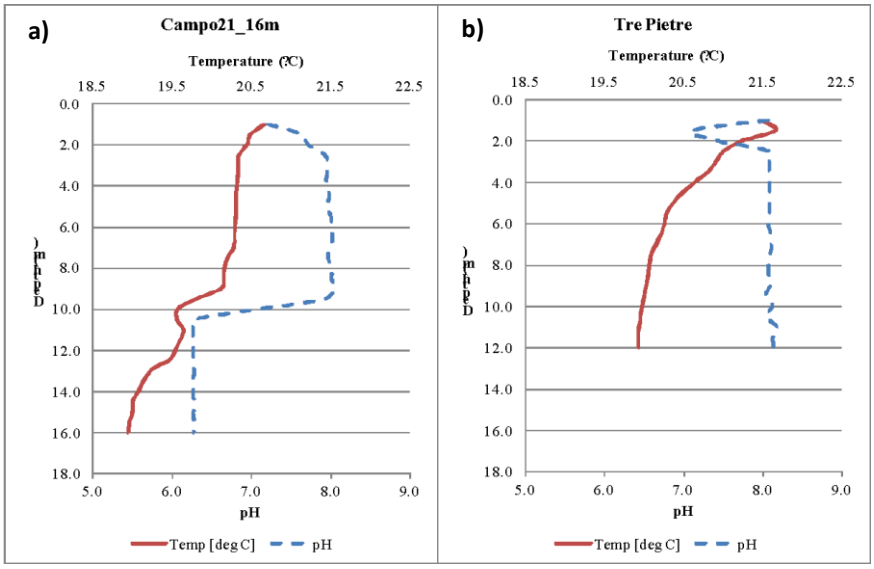

Figure 5.3.1.3. pH and temperature profiles measured by CTD probe deployed at: a) Campo21_16m site in Panarea and c) the control in Salina Island during the May 2025 sampling campaigns.

✓ *Carbonate system*

The results obtained measuring pH_T in the water samples collected by Niskin bottles showed that average pH values recorded in May 2025 were generally lower than those measured in September 2024 and that in both the campaigns the pH_T at *in situ* temperature resulted to be lower in the impacted than in control sites, except for Cold in September with $pH_T = 8.01$ (Table 5.3.1.1). The most acidified site was Campo 21_16m with pH_T September = 7.88 and pH_T May = 7.30.

Table 5.3.1.1. Average pH values measured by spectrophotometer for each sampling sites during the September 2024 and the May 2025 sampling campaigns.

Area	Site	Depth (m)	pH_T	
			September 2024	May 2025
Panarea	Hot	11	7.93	7.79
Panarea	Cold	11	8.01	7.71
Panarea	Campo 21_16m	16	7.88	7.30
Panarea	Campo 21_21m	21	7.96	7.32
Salina	Punta Megna	12	8.02	7.95
Salina	Tre Pietre	12	8.04	7.94
Salina	Lingua	20	8.07	7.97

Regarding the other carbonate system parameters calculated for September 2024 (Table 5.3.1.2), TA showed similar values at the Panarea and Salina sites, ranging from 2514.51 µmol kg^{-1}, the minimum recorded at the Lingua control site, to 2562.75 µmol kg^{-1}, the maximum measured at Cold impacted site. The lowest saturation states of ΩCa and ΩAr were both recorded at Campo21_16m, with values of 4.2 and 2.8, respectively. For dissolved inorganic nutrients, silicate ($Si(OH)_4$) was generally the most abundant across all sites, showing the highest concentration (2.565 µmol L^{-1}) at Hot. Nitrate (NO_3) followed as the second most represented nutrient, with a maximum value of 1.787 µmol L^{-1} also measured at Hot. Ammonia (NH_4) concentrations reached a maximum of 0.111 µmol L^{-1} at the Cold site. Nitrite (NO_2) concentrations were generally between 0.01 and 0.02 µmol L^{-1}, while phosphate remained below the detection limit at all sites except Campo21_21m (Table 5.3.1.2).

Table 5.3.1.2. Average values of carbonate system parameters and dissolved inorganic nutrients measured in each sampling sites during the September 2024 sampling campaign

Area	Site	Depth (m)	Total Alcalinity (µmol/kg)	pCO2 (matm)	ΩCa	ΩAr	NO2 (µmoli/L)	NO3 (µmoli/L)	PO4 (µmoli/L)	NH4 (µmoli/L)	Si(OH)4 (µmoli/L)
Panarea	Hot	11	2,559.29	595.1	4.9	3.3	0.010	1.787	< 0.01	0.104	2.565
Panarea	Cold	11	2,562.75	483.2	5.6	3.7	< 0.01	1.294	< 0.01	0.111	1.718
Panarea	Campo 21_16m	16	2,537.34	711.4	4.2	2.8	0.018	1.217	< 0.01	0.088	0.958
Panarea	Campo 21_21m	21	2,532.84	542.3	4.5	2.9	0.016	< 0.02	0.015	0.059	0.930
Salina	Punta Megna	12	2,561.53	458.3	5.6	3.7	0.019	0.247	< 0.01	0.101	1.775
Salina	Tre Pietre	12	2,535.49	429.2	5.8	3.8	< 0.01	0.163	< 0.01	0.100	0.881
Salina	Lingua	20	2,514.51	399.8	5.4	3.5	< 0.01	0.108	< 0.01	0.146	0.893

✓ *Bioavailable metals*

Trace metal concentrations measured in seawater samples, collected in September 2024 and in May 2025 sampling campaigns, in the three sites of Panarea island (Hot /Cold, Bottaro cratere, Lisca Nera, in 2024 and Panarelli, in 2025) and in one site in Salina (Grottazza/Punta Megna) are shown in Table 5.3.1.3 and Table 5.3.1.4. Seawater samples were collected at the moment of the DGT deployment. It can be noticed that there were no significant differences in the metal concentration values between the different sanpling sites for September 2024 sampling campaign. Most of the elements showed concentration values below the corresponding detection limits. Differences between the concentration values measured in seawaters are observed for Mn and Fe. Mn contents in seawater samples were in the range of 0.368 μgL^{-1} (lower concentration value measured in Grottazza/Punta Megna) and 3.54 μgL^{-1} (higher concentration measured in water sample measured in HotCold site). Fe showed the higher concentration (7.48 μgL^{-1}) in seawater sampled in Salina site (Grottazza/Punta Megan), while in the samples collected in the remaining sites, its concentrations were below the detection limit of 1.00 $\mu g\ L^{-1}$ or at this value.

Table 5.3.1.3. Chemical characterization of seawater samples (values in μgL^{-1}) of each sampling site obtained during DGT deployment in September 2024 sampling campaign

		V	Cr	Mn	Fe	Co	Ni	Cu	Zn	As	Mo	Cd	Pb	U
							(μgL^{-1})							
							September 2024							
Panarea	**Hot Cold**	1.66	< 0.100	3.54	1.00	< 0.025	< 0.100	< 0.100	0.924	1.40	12.0	< 0.010	< 0.100	4.07
Panarea	**Bottaro cratere**	1.71	< 0.100	0.479	< 1.00	< 0.025	< 0.100	< 0.100	< 0.500	1.46	12.1	< 0.010	< 0.100	4.19
Panarea	**Lisca Nera**	1.68	0.100	0.853	< 1.00	< 0.025	< 0.100	< 0.100	< 0.500	1.42	12.0	< 0.010	< 0.100	4.16
Salina	**Grottazza /Punta Megna**	1.74	< 0.100	0.368	7.48	< 0.025	< 0.100	< 0.100	< 0.500	1.46	11.9	< 0.010	0.139	4.13

A greater variability in trace metal concentration values measured in the seawaters sampled in the different sampling sites was observed for the sampling campaign in May 2025. The seawater sample collected at the Hot-Cold site showed high concentrations of Mn (11.5 μgL^{-1}) and Fe (7.46 μgL^{-1}), compared to the corresponding concentrations measured for both in the other sites. At Punta Megna site, higher concentrations of Fe (8.18 μgL^{-1}) and Zn (26.6 μgL^{-1}) were observed than those determined for these two elements in the other sites. The concentrations of Ni and Cu measured in seawater samples did not differ significantly between the different sites: for Ni, values ranged between 0.179 μgL^{-1} (measured in Bottaro cratere) and 0.272 $\mu g\ L^{-1}$ (measured in Panarelli) and for Cu, between 0.125 μgL^{-1} (in Bottaro cratere) and 0.430 μgL^{-1} (in Punta Megna site). As, Mo, V concentrations did not differ significatively both between sites and sampling campaigns. Moreover, differently from the results obtained in September 2024 sampling campaign, Pb concentration values in seawater samples collected in May 2025, were above the detection limit of this metal in each sampling site, with values that ranged from 0.190 $\mu g\ L^{-1}$, measured in Bottaro crater, to 3.70 $\mu g\ L^{-1}$, determined in Punta Megna.

Table 5.3.1.4. Chemical characterization of seawater samples (values in μgL^{-1}) of each sampling site obtained during DGT deployment in May 2025 sampling campaign

		V	Cr	Mn	Fe	Co	Ni	Cu	Zn	As	Mo	Cd	Pb	U
							(μgL^{-1})							
							May 2025							
Panarea	**Hot Cold**	1.60	< 0.100	11.5	7.46	0.033	0.254	0.331	4.43	1.67	11.0	< 0.010	1.03	3.09
Panarea	**Bottaro cratere**	1.74	< 0.100	4.79	2.45	0.028	0.179	0.125	2.23	1.75	11.0	< 0.010	0.190	3.03
Panarea	**Panarelli**	1.77	< 0.100	0.476	1.96	0.027	0.272	0.386	5.33	1.80	11.1	< 0.010	1.26	3.07
Salina	**Punta Megna**	1.78	< 0.100	0.906	8.18	0.029	0.249	0.430	26.6	1.76	11.2	< 0.010	3.70	3.03

Time-weighted average concentrations of the labile/bioavailable fraction of metals in seawater samples, determined using DGTat the shallower investigated sites during the two sampling campaigns (September 2024 and May 2025) are shown in Table 5.3.1.5 and Table 5.3.1.6. In general, for most metal species, the calculated C_{DGT} values were lower than or close to the total concentration (C) values of these metals measured directly in the seawater samples. For some metal ions, in particular nickel and copper, at all the sites analyzed in the 2024 sampling campaign and at some points in the 2025 campaign, and under certain sea conditions, the concentrations obtained with the DGT were higher than those measured directly in the corresponding seawater samples. This is likely due to the accumulation of bioavailable and mobile complexes , during the exposure of the passive sampler of these elements (nickel, copper and in some cases also manganese and zinc) in the DGT resin gel. As consequence, higher concentration values were obtained than the "total" values measured for these ions in the seawater sample taken at the same sites of DGT deployment. Finally, use of DGTs allows us to obtain data and information for all those elements (particularly mercury, whose concentration was not measured in the seawater sample) whose total concentrations were so low as to be below the corresponding instrumental detection limits.

Table 5.3.1.5. Concentrations of DGT labile metals (values in μgL^{-1} and, for Hg, in ng L^{-1}) obtained during 7-days deployments at each sampling site in September 2024 sampling campaign

		C_{DGT} V	C_{DGT} Cr	C_{DGT} Mn	C_{DGT} Fe	C_{DGT} Co	C_{DGT} Ni	C_{DGT} Cu	C_{DGT} Zn	C_{DGT} As	C_{DGT} Cd	C_{DGT} Pb	C_{DGT} Hg
							(μgL^{-1})						ngL^{-1}
							September 2024						
Panarea	**Hot Cold**	0.174	< 0.010	1.62	1.04	0.022	0.118	0.350	0.734	0.335	0.008	0.025	11.2
Panarea	**Bottaro cratere**	1.27	< 0.010	1.29	0.365	0.024	0.135	0.277	0.612	0.718	0.009	0.045	8.72
Panarea	**Panarea - Lisca Nera**	2.04	< 0.010	1.00	0.277	0.013	0.144	0.292	0.548	1.13	0.008	0.067	29.4
Salina	**Grottazza /Punta Megna**	0.218	< 0.010	2.79	0.436	0.014	0.137	0.421	1.42	0.435	0.007	0.111	11.8

Table 5.3.1.6. Concentrations of DGT labile metals (values in μgL^{-1} and, for Hg, in ng L^{-1}) obtained during 7-days deployments at each sampling site in May 2025 sampling campaign

		C_{DGT} V	C_{DGT} Cr	C_{DGT} Mn	C_{DGT} Fe	C_{DGT} Co	C_{DGT} Ni	C_{DGT} Cu	C_{DGT} Zn	C_{DGT} As	C_{DGT} Cd	C_{DGT} Pb	C_{DGT} Hg
		(μgL^{-1})											ngL^{-1}
		May 2025											
Panarea	**Hot Cold**	0.078	0.028	2.39	1.67	0.007	0.203	0.453	0.500	0.181	0.005	0.016	3.17
Panarea	**Bottaro cratere**	0.026	0.033	0.839	0.536	0.008	0.310	0.312	0.981	0.182	0.006	0.064	0.96
Panarea	**Panarelli**	0.129	0.023	0.283	0.206	0.009	0.215	0.114	1.06	0.223	0.006	0.053	3.26
Salina	**Grottazza**	0.036	0.025	0.503	4.19	0.007	0.230	0.161	2.09	0.228	0.007	0.151	4.06

5.3.2 Interstitial water

Interstitial water chemistry differed between Panarea and Salina (Table 5.3.2.1). Sediment temperatures at Panarea reached 41.0°C in September 2024 and 54.0°C in May 2025 at the Hot site. At Salina, temperatures remained within 20.4-26.4°C during both sampling periods. Redox potential showed substantial spatial variability. In May 2025, Panarea recorded the lowest Eh values, down to -221 and -234 mV at the Campo21_21m sites. Salina values ranged from -70.2 to -8.4 mV. Ammonium concentrations in September 2024 ranged from 1.0 to 6.4 mg L^{-1} at Panarea and 2.2 to 3.5 mg L^{-1} at Salina. In May 2025, concentrations at Panarea ranged from 1.2 to 4.8 mg L^{-1}, while at Salina they ranged from 1.5 to 1.9 mg L^{-1}. Nitrate concentrations increased markedly at Salina in September 2024, reaching 330.6 mg L^{-1} at the vegetated site. During the same period, Panarea values ranged from 2.3 to 3.5 mg L^{-1}. In May 2025, nitrate concentrations ranged from 3.3 to 12.0 mg L^{-1} at Panarea and 3.3 to 21.0 mg L^{-1} at Salina. Bicarbonate concentrations in September 2024 ranged from 82.4 to 103.7 mg L^{-1} at Panarea and 0.0-173.9 mg L^{-1} at Salina. In May 2025, Panarea concentrations increased to 98.0-141.0 mg L^{-1}, while Salina recorded 0.0 mg L^{-1} at both sites. Major ions (Na^+, Mg^{2+}, Ca^{2+}, Cl^-, Br^-, and SO_4^{2-}) showed similar concentrations between Panarea and Salina across both sampling periods, with no consistent differences detected. The presence of *P. oceanica* (veg.) influenced several chemical parameters. At Panarea, vegetated sites showed higher Eh values and lower ammonium concentrations than adjacent unvegetated sites. At Salina, vegetated sites displayed lower Eh than unvegetated ones. The strongest vegetation-related difference occurred at Salina in September 2024, when the vegetated site showed the highest nitrate concentration recorded.

Table 5.3.2.1. Chemical characterization of interstitial water samples collected in vegetated (veg: light grey) and unvegetated (unveg: white) sediments in Hot-Cold, Campo21_21m and Punta Megna sites during the two sampling campaigns.

Area	Site	Sediment temp (°C)	pH	Eh (mV)	NH_4^+	HCO_3^-	Na^+	K^+	Mg^{2+}	Ca^{2+} (mg/L)	F^-	Cl^-	Br^-	NO_3^-	$(SO_4)^{2-}$
September 2024															
Panarea	Hot	41.0			3.3	82.4	13,137.7	385.8	1,313.2	440.7	2.3	20,620.1	72.7	2.3	2,960.6
Panarea	Cold	28.3			1.0	103.7	13,303.3	398.0	1,383.4	420.6	2.4	22,352.9	74.3	3.4	3,144.0
Panarea	Campo21_21m veg	25.7			3.9	0.0	13,491.7	363.6	1,355.7	415.4	2.0	22,302.2	75.8	3.5	3,099.1
Panarea	Campo21_21m unveg	25.7			6.4	6.1	14,697.1	352.4	1,264.7	375.6	1.9	22,670.2	77.2	2.3	3,297.2
Salina	Punta Megna veg	26.4			2.2	0.0	14,439.9	415.8	1,321.0	460.1	1.2	22,250.6	80.4	330.6	3,086.9
Salina	Punta Megna unveg	26.4			3.5	173.9	15,151.9	367.5	1,362.8	472.3	3.1	26,639.8	73.3	2.7	2,986.0
May 2025															
Panarea	Hot	54.0	6.55	13	2.1	115.0	13,588.0	344.0	1,215.0	351.0	2.5	22,896.0	76.0	12.0	2,888.0
Panarea	Cold	27.3	5.7	41.2	1.2	98.0	13,985.0	391.0	1,375.0	387.0	2.5	22,663.0	71.0	6.5	3,254.0
Panarea	Campo21_21m veg	19.3	5.5	-221	3.5	33.0	13,551.0	347.0	1,321.0	351.0	2.2	23,045.0	78.0	3.3	3,055.0
Panarea	Campo21_21m unveg	18.6	6.4	-234	4.8	141.0	14,885.0	411.0	1,180.0	366.0	1.8	23,152.0	79.0	6.9	3,369.0
Salina	Punta Megna veg	20.9	7.13	-70.2	1.5	0.0	14,674.0	405.0	1,225.0	385.0	1.5	23,544.0	78.0	21.0	3,185.0
Salina	Punta Megna unveg	20.4	6.8	-8.4	1.9	0.0	14,896.0	415.0	1,452.0	520.0	1.9	24,855.0	80.0	3.3	3,384.0

5.3.3 Sediment

✓ *Trace element analysis*

Overall, trace element concentrations in the surface sediments collected in September 2024 and May 2025 from the study areas, including both the vent area in Panarea, with 4 sites (Hot, Cold, Campo21_16m and Campo21_21m), and the control area in Salina Islands with 3 sites (Tre Pietre, Punta Megna e Lingua) exhibited markedly different patterns across elements (Figure 5.3.3.1).

One trend, consisting in generally higher concentrations at the vent area compared with the control area, was evident for Cr and Hg, although with a certain degree of variability across sites, e.g. Cr concentrations peaked in Lingua than the other control areas, and Hg was the only element showing significantly higher concentration in Campo21 sites than the other vent areas (Figure 5.3.3.1, Table 5.3.3.1). All the other trace elements showed, in contrast, significantly higher concentrations at the Hot and Cold sites than at both the Campo21 sites. The latter sites, in turn, displayed almost always comparable concentrations to each other and broadly similar to those measured at Salina, only for As and Ni. Differently, Hot and Cold sites were generally similar to Salina sites for Cd, Cu, Fe, Pb, V and Zn, although the Lingua site showed in some cases significantly higher concentrations than at the other control areas (Figure 5.3.3.1, Table 5.3.3.1). A slightly different pattern emerged for Mn, whose concentrations were consistently higher at Salina than at Panarea, with the following trend: Salina > Hot and Cold > Campo-21 (Figure 5.3.3.1, Table 5.3.3.1).

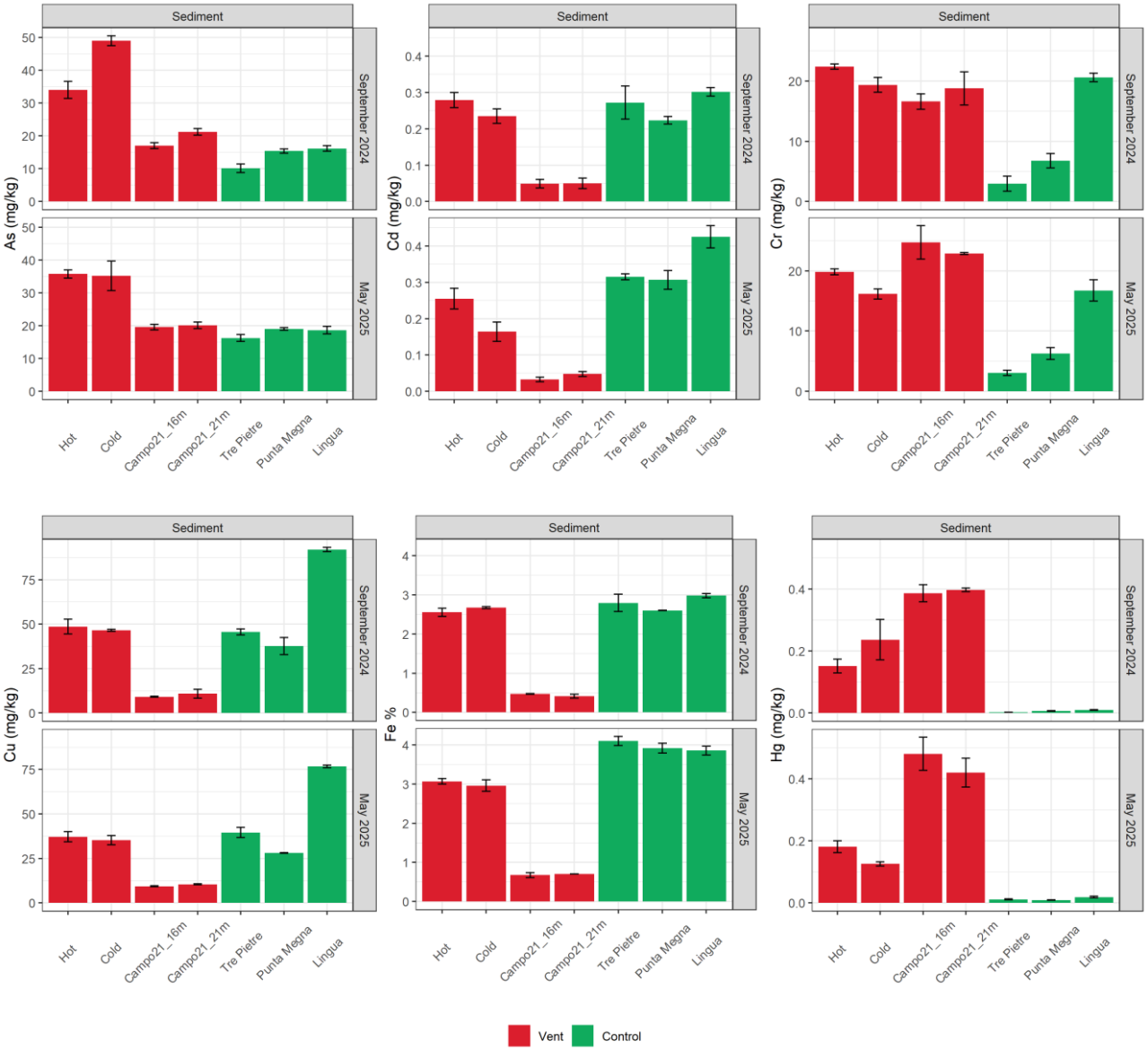

Figure 5.3.3.1 Mean (± SD) concentration of trace elements in surface sediment across the study sites and seasons.

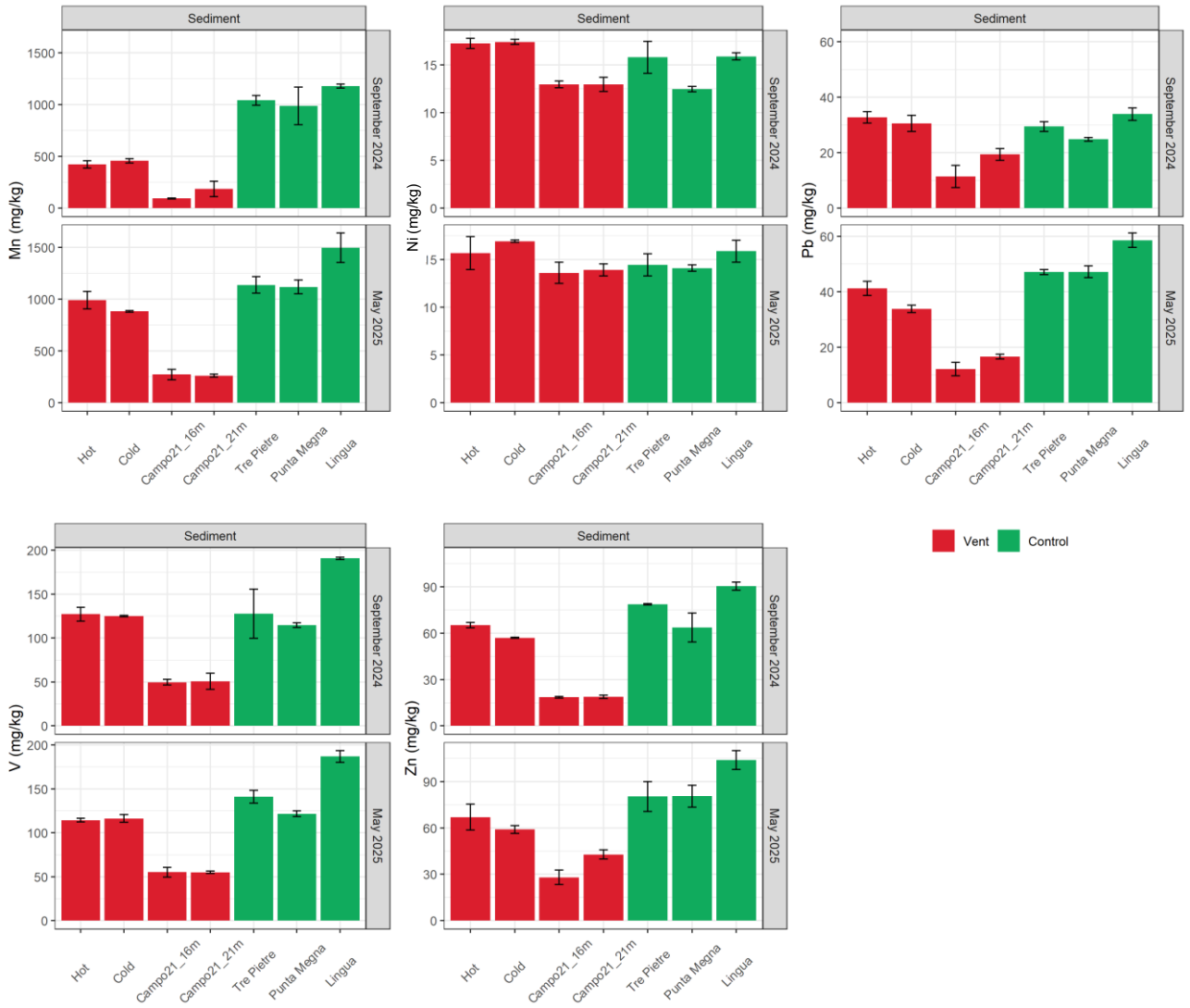

Fig. 5.3.3.1 (continued)

Table 5.3.3.1. Univariate PERMANOVA results for trace element concentrations in surface sediment across the study sites and seasons. Significant values are indicated in red.

a) Main test		As		Cd		Cr		Cu		Fe		Hg	
Source of variation	df	Pseudo-F	p	Pseudo-F	p	Pseudo-F	p	Pseudo-F	p	Pseudo-F	p	Pseudo-F	p
Season (Se)	1	0.1	0.828	2.7	0.115	0.2	0.674	39.7	0.001	166.1	0.001	0.3	0.598
Sites (St)	6	81.4	0.001	62.6	0.001	57.8	0.001	241.5	0.001	334.8	0.001	86.8	0.001
Se x St	6	7.5	0.001	4.7	0.004	4.9	0.002	3.2	0.017	11.7	0.001	2.4	0.039
Residuals	28												

b) Pairwise tests	As		Cd		Cr		Cu		Fe		Hg	
Between sites within seasons	S24	M25	S24	M25	S24	M25	S24	M25	S24	M25	S24	M25
	p	p	p	p	p	p	p	p	p	p	p	p
Hot, Cold	0.010	0.909	0.184	0.08	0.068	0.024	0.65	0.645	0.331	0.562	0.279	0.052
Hot, Campo21_16m	0.003	0.001	0.001	0.003	0.011	0.169	0.001	0.002	0.001	0.001	0.001	0.009
Hot, Campo21_21m	0.006	0.003	0.002	0.004	0.305	0.007	0.002	0.001	0.001	0.001	0.002	0.011
Hot, Tre Pietre	0.002	0.001	0.896	0.116	0.002	0.001	0.524	0.592	0.381	0.004	0.005	0.001
Hot, Punta Megna	0.003	0.001	0.078	0.258	0.001	0.001	0.154	0.035	0.702	0.006	0.007	0.002
Hot, Lingua	0.006	0.002	0.37	0.015	0.074	0.177	0.002	0.001	0.023	0.004	0.006	0.002
Cold, Campo21_16m	0.001	0.028	0.003	0.014	0.172	0.05	0.001	0.006	0.001	0.001	0.097	0.003
Cold, Campo21_21m	0.001	0.037	0.002	0.013	0.868	0.003	0.001	0.001	0.001	0.001	0.072	0.003
Cold, Tre Pietre	0.001	0.018	0.498	0.007	0.001	0.001	0.595	0.319	0.649	0.005	0.029	0.001
Cold, Punta Megna	0.001	0.032	0.623	0.017	0.004	0.002	0.122	0.04	0.058	0.007	0.032	0.001
Cold, Lingua	0.001	0.021	0.045	0.003	0.419	0.774	0.001	0.001	0.004	0.01	0.031	0.001
Campo21_16m, Campo21_21m	0.042	0.686	0.976	0.174	0.505	0.554	0.511	0.048	0.31	0.702	0.725	0.42
Campo21_16m, Tre Pietre	0.016	0.064	0.008	0.001	0.006	0.003	0.001	0.002	0.002	0.001	0.001	0.003
Campo21_16m, Punta Megna	0.206	0.613	0.001	0.001	0.005	0.003	0.006	0.001	0.001	0.001	0.001	0.002
Campo21_16m, Lingua	0.531	0.541	0.002	0.001	0.055	0.065	0.001	0.001	0.001	0.002	0.001	0.002
Campo21_21m, Tre Pietre	0.005	0.055	0.006	0.001	0.007	0.001	0.001	0.001	0.002	0.001	0.001	0.002
Campo21_21m, Punta Megna	0.016	0.357	0.001	0.001	0.017	0.002	0.003	0.001	0.001	0.001	0.001	0.003
Campo21_21m, Lingua	0.012	0.414	0.001	0.001	0.537	0.02	0.001	0.001	0.001	0.001	0.001	0.002
Tre Pietre, Punta Megna	0.014	0.063	0.36	0.768	0.09	0.036	0.194	0.013	0.465	0.342	0.017	0.199
Tre Pietre, Lingua	0.013	0.181	0.565	0.025	0.001	0.001	0.001	0.001	0.463	0.188	0.01	0.061
Punta Megna, Lingua	0.497	0.758	0.01	0.047	0.002	0.007	0.001	0.001	0.004	0.768	0.126	0.021

Between seasons within sites	cfr	p	cfr	p	cfr	p	cfr	p	cfr	p	cfr	p
Hot	S24 = M25	0.572	S24 = M25	0.544	**S24 < M25**	0.017	S24 = M25	0.076	**S24 < M25**	0.017	S24 = M25	0.369
Cold	**M25 < S24**	0.039	S24 = M25	0.088	S24 = M25	0.096	**M25 < S24**	0.008	S24 = M25	0.135	S24 = M25	0.173
Campo21_16m	S24 = M25	0.098	S24 = M25	0.289	S24 = M25	0.059	S24 = M25	0.738	**S24 < M25**	0.038	S24 = M25	0.199
Campo21_21m	S24 = M25	0.474	S24 = M25	0.891	S24 = M25	0.219	S24 = M25	0.868	**S24 < M25**	0.001	S24 = M25	0.629
Tre Pietre	**S24 < M25**	0.024	S24 = M25	0.424	S24 = M25	0.941	S24 = M25	0.129	**S24 < M25**	0.004	**S24 < M25**	0.003
Punta Megna	**S24 < M25**	0.012	**S24 < M25**	0.048	S24 = M25	0.782	S24 = M25	0.121	**S24 < M25**	0.002	S24 = M25	0.131
Lingua	S24 = M25	0.150	**S24 < M25**	0.019	S24 = M25	0.124	**M25 < S24**	0.002	**S24 < M25**	0.005	**S24 < M25**	0.034

Table 5.3.3.1 (continued)

a) Main test		Mn		Pb		Ni		V		Zn	
Source of variation	df	Pseudo-F	p	Pseudo-F	p	Pseudo-F	p	Pseudo-F	p	Pseudo-F	p
Season (Se)	1	38.2	0.001	80.2	0.001	0.0	0.954	0.0	0.903	12.4	0.005
Sites (St)	6	64.5	0.001	59.9	0.001	6.5	0.002	57.4	0.001	50.0	0.001
Se x St	6	2.9	0.027	12.2	0.001	0.9	0.536	0.6	0.775	1.4	0.273
Residuals	28										

b) Pairwise tests	Mn		Pb		Ni	V	Zn
Between sites within seasons	S24	M25	S24	M25	*Between sites across seasons*		
	p	p	p	p	p	p	p
Hot, Cold	0.445	0.26	0.595	0.054	0.536	0.981	0.117
Hot, Campo21_16m	0.002	0.002	0.008	0.002	0.023	0.001	0.002
Hot, Campo21_21m	0.045	0.002	0.012	0.001	0.029	0.006	0.004
Hot, Tre Pietre	0.001	0.27	0.281	0.097	0.372	0.488	0.065
Hot, Punta Megna	0.026	0.301	0.022	0.152	0.023	0.623	0.411
Hot, Lingua	0.001	0.042	0.734	0.014	0.6	0.003	0.003
Cold, Campo21_16m	0.001	0.001	0.019	0.001	0.007	0.003	0.006
Cold, Campo21_21m	0.026	0.001	0.045	0.001	0.003	0.005	0.002
Cold, Tre Pietre	0.001	0.035	0.767	0.001	0.084	0.468	0.008
Cold, Punta Megna	0.052	0.031	0.104	0.009	0.004	0.406	0.035
Cold, Lingua	0.001	0.013	0.41	0.003	0.067	0.002	0.002
Campo21_16m, Campo21_21m	0.286	0.868	0.165	0.154	0.859	0.939	0.031
Campo21_16m, Tre Pietre	0.001	0.001	0.013	0.001	0.164	0.003	0.001
Campo21_16m, Punta Megna	0.008	0.002	0.034	0.001	0.989	0.001	0.003

Campo21_16m, Lingua	0.001	0.001	0.005	0.003	0.017	0.006	0.002
Campo21_21m, Tre Pietre	0.001	0.001	0.026	0.001	0.192	0.002	0.003
Campo21_21m, Punta Megna	0.014	0.002	0.092	0.001	0.786	0.005	0.004
Campo21_21m, Lingua	0.001	0.001	0.008	0.001	0.013	0.006	0.004
Tre Pietre, Punta Megna	0.798	0.856	0.069	0.966	0.138	0.352	0.36
Tre Pietre, Lingua	0.059	0.099	0.197	0.011	0.545	0.019	0.012
Punta Megna, Lingua	0.346	0.078	0.016	0.03	0.007	0.003	0.007

Between seasons within sites	**cfr**	**p**	**cfr**	**p**
Hot	**S24 < M25**	0.005	S24 = M25	0.057
Cold	**S24 < M25**	0.001	S24 = M25	0.388
Campo21_16m	**S24 < M25**	0.029	S24 = M25	0.881
Campo21_21m	S24 = M25	0.362	S24 = M25	0.301
Tre Pietre	S24 = M25	0.340	**S24 < M25**	0.002
Punta Megna	S24 = M25	0.532	**S24 < M25**	0.002
Lingua	S24 = M25	0.104	**S24 < M25**	0.003

Between seasons across sites	
cfr	**p**
S24 < M25	0.003

The Principal Component Analysis (PCA) performed on the full trace-element dataset confirmed the spatial patterns previously described. The first two components (PC1 and PC2) captured the main gradients in element concentrations in both seasons, clearly separating the vent sites from the control ones (Figure 5.3.3.2). This pattern is consistent with the multivariate differences detected by the PERMANOVA (Table 5.3.3.2). In both seasons, PC1 was mainly driven by Hg, which showed the highest values at the Campo21 vent sites, and from Mn, Cd, Cu, Fe, Pb, V and Zn at the control area, especially driven by the Lingua site. PC2 reflected a secondary gradient associated with As, Ni and Cr, along which Panarea Hot and Cold sites separated from the other Panarea sites and from all the Salina sites, confirming its comparatively higher concentrations for these elements (Figure 5.3.3.2).

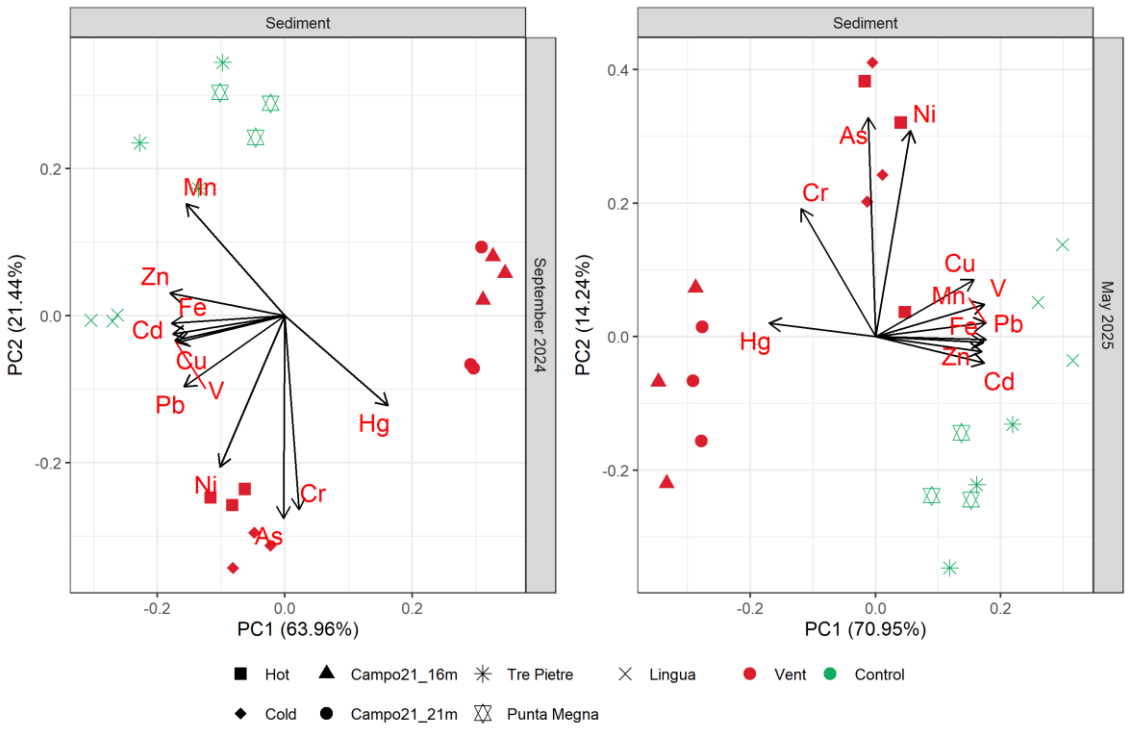

Figure 5.3.3.2. Principal Component Analysis (PCA) of trace element concentration in surface sediment across the study sites and seasons.

Table 5.3.3.2. Multivariate PERMANOVA results for all trace element concentrations in surface sediment across the study sites and seasons. Significant values are indicated in red.

a) Main test			
Source of variation	**df**	**Pseudo-F**	**p**
Season (Se)	1	11.3	0.001
Site (St)	6	46.4	0.001
Se x St	6	28.6	0.001
Residuals	28		

b) Pairwise tests					
1) Between sites within seasons	**S24**	**M25**	***2) Between seasons within sites***	**cfr**	**p**
	p	**p**			
Hot, Cold	0.024	0.277	**Hot**	S24 = M25	0.116

Hot, Campo21_16m	0.001	0.002
Hot, Campo21_21m	0.003	0.003
Hot, Tre Pietre	0.010	0.019
Hot, Punta Megna	0.002	0.024
Hot, Lingua	0.001	0.008
Cold, Campo21_16m	0.002	0.005
Cold, Campo21_21m	0.001	0.001
Cold, Tre Pietre	0.004	0.003
Cold, Punta Megna	0.001	0.005
Cold, Lingua	0.001	0.004
Campo21_16m, Campo21_21m	0.374	0.527
Campo21_16m, Tre Pietre	0.003	0.001
Campo21_16m, Punta Megna	0.001	0.001
Campo21_16m, Lingua	0.001	0.001
Campo21_21m, Tre Pietre	0.003	0.001
Campo21_21m, Punta Megna	0.002	0.001
Campo21_21m, Lingua	0.001	0.001
Tre Pietre, Punta Megna	0.121	0.456
Tre Pietre, Lingua	0.009	0.012
Punta Megna, Lingua	0.002	0.007

Cold	S24 ≠ M25	0.013
Campo21_16m	S24 = M25	0.132
Campo21_21m	S24 = M25	0.114
Tre Pietre	S24 = M25	0.155
Punta Megna	S24 ≠ M25	0.009
Lingua	S24 ≠ M25	0.018

Comparing trace element concentrations in sediments with the concentration thresholds established by the Italian Ministerial Decrees DM 172/2015, DM 173/2016 and subsequent amendments (GURI, 2015; GURI, 2016) revealed that As exceeded both L1 and L2 limits (**Errore. L'origine riferimento non è stata trovata.**), namely the concentration below which sediments are considered to pose low or high, respectively, probability of toxic effects or bioaccumulation at both areas and seasons. Exceedances of the L2 threshold also occurred consistently at the Hot and Cold sites, and occasionally at Campo21. Cd sporadically exceeded the L1 limit across areas, with a marked and consistent exceedance at Salina in May 2025. Cr and Ni never exceeded either L1 or L2. Cu exceeded L1 at the Hot and Cold sites and at Tre Pietre, and reached its highest value at Lingua, where it surpassed the L2 limit in both seasons. Hg exceeded the L1 threshold only at Campo21 in both sampling periods. Pb showed a pattern broadly similar to Cu, exceeding the L1 limit at the Hot and Cold sites and at Salina, although without ever surpassing L2. Finally, Zn slightly exceeded its L1 threshold only at Lingua in May 2025. For Mn and V, no regulatory reference thresholds for sediments are currently provided by the applicable legislation (**Errore. L'origine riferimento non è stata trovata.**.3).

Table 5.3.3.3. Threshold concentrations for trace elements in marine sediments according to Italian regulations (GURI, 2015, 2016). In bolt the thresholds that exceeded in this study.

Trace element	DM 172/2015 Tab.2A,3A,3B (mg/kg d.w.)	DM 173/2016 Tab.2.5-L1 (mg/kg d.w.)	DM 173/2016 Tab.2.5-L2 (mg/kg d.w.)
As	**12.0**	**12.0**	**20.0**
Cd	**0.3**	**0.3**	0.8
Cr	50.0	50.0	150.0
Cu	-	**40.0**	**52.0**
Hg	**0.3**	**0.3**	0.8
Ni	-	30.0	75.0
Pb	**30.0**	**30.0**	70.0
Zn	-	100.0	150.0

✓ *Isotopic and elemental composition*

$\delta^{13}C$ values were overall comparable across all vent sites compared to control areas, where significantly more depleted and enriched values were recorded at Tre Pietre and Lingua respectively (Figure 5.3.3.3, Table 5.3.3.3). $\delta^{15}N$ showed no detectable signal and is not presented graphically. Total nitrogen (N%) and total and organic carbon (C%, TOC%) displayed overall higher concentrations at the vent area, particularly at Campo21 sites, compared to both Hot-Cold and Salina sites, except for Lingua where comparable (N%) or even higher values (C%) were found. C/N and Corg/N ratios were consistently lower at Hot site compared to all the other ones, while Campo21_21m displayed the highest value across the vent area and Lingua across the other Salina sites (Figure 5.3.3.3, Table 5.3.3.4).

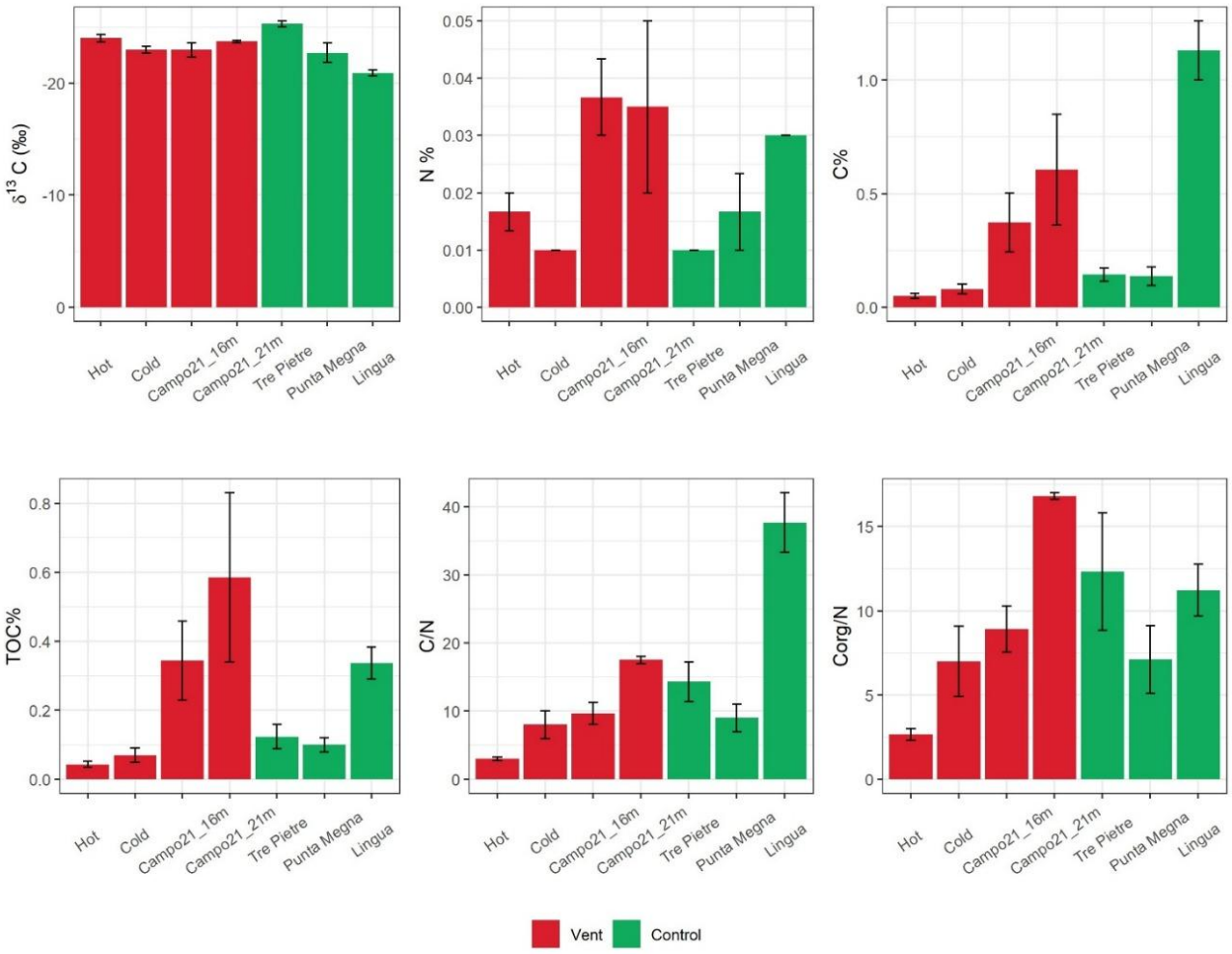

Figure 5.3.3.3. Mean (± SD) of carbon isotopic composition ($\delta^{13}C$), elemental concentrations (total nitrogen, N; total carbon, C; total organic carbon, TOC) and elemental ratios (C/N and C_{org}/N) in surface sediments across the study sites in September 2024.

Table 5.3.3.4. Univariate PERMANOVA results for carbon isotopic composition ($\delta^{13}C$), elemental concentrations (total nitrogen, N; total carbon, C; total organic carbon, TOC) and elemental ratios (C/N and C_{org}/N) in surface sediment across the study sites in September 2024. Significant values are indicated in red.

a) Main test		$\delta^{13}C$		N		C		TOC		C/N		Corg/N	
Source of variation	**df**	**Pseudo-F**	**p**	**Pseudo-F**	**p**	**Pseudo-F**	**p**	**Pseudo-F**	**p**	**Pseudo-F**	**p**	**Pseudo-F**	**p**
Site (St)	6	7.9	0.004	4.6	0.012	17.2	0.002	5.6	0.009	21.7	0.002	4.5	0.013
Residuals	13												

b) Pairwise tests	$\delta^{13}C$	N	C	TOC	C/N	Corg/N
Between sites	**p**	**p**	**p**	**p**	**p**	**p**
Hot, Cold	0.080	0.122	0.272	0.299	0.072	0.007
Hot, Campo21_16m	0.205	0.039	0.034	0.049	0.114	0.012
Hot, Campo21_21m	0.521	0.047	0.043	0.033	0.001	0.001
Hot, Tre Pietre	0.036	0.111	0.737	0.085	0.021	0.038
Hot, Punta Megna	0.244	0.561	0.113	0.060	0.043	0.023
Hot, Lingua	0.004	0.019	0.001	0.003	0.002	0.005
Cold, Campo21_16m	1.000	0.022	0.023	0.038	0.586	0.515
Cold, Campo21_21m	0.171	0.030	0.012	0.031	0.047	0.035
Cold, Tre Pietre	0.005	1.000	0.155	0.254	0.161	0.271
Cold, Punta Megna	0.763	0.369	0.283	0.387	0.738	0.971
Cold, Lingua	0.012	0.032	0.002	0.005	0.007	0.173
Campo21_16m, Campo21_21m	0.433	0.909	0.418	0.374	0.038	0.021
Campo21_16m, Tre Pietre	0.036	0.016	0.012	0.047	0.236	0.413
Campo21_16m, Punta Megna	0.828	0.008	0.014	0.036	0.815	0.502
Campo21_16m, Lingua	0.033	0.373	0.535	0.962	0.007	0.306
Campo21_21m, Tre Pietre	0.022	0.031	0.014	0.022	0.456	0.406
Campo21_21m, Punta Megna	0.453	0.007	0.012	0.019	0.038	0.031
Campo21_21m, Lingua	0.007	0.672	0.066	0.278	0.038	0.061
Tre Pietre, Punta Megna	0.050	0.362	0.897	0.579	0.213	0.233
Tre Pietre, Lingua	0.002	0.034	0.004	0.023	0.012	0.782
Punta Megna, Lingua	0.116	0.122	0.002	0.013	0.004	0.160

Consistently, the cross-plot of Corg/Ntot versus $\delta^{13}C$ shown in Figure 5.3.3.4 indicates that $\delta^{13}C$ values at the vent area were more homogeneous than Corg/Ntot, which instead spanned a wider range and displayed a clear gradient from the Hot to Campo 21_21m site. In contrast, at the Control area, both Corg/Ntot and $\delta^{13}C$ values exhibited a rather pronounced spatial gradient. However, almost none of the values overlapped with those reported in the literature for *P. oceanica*, whereas most values instead showed partial overlap with the $\delta^{13}C$ and Corg/Ntot ranges reported for bacteria, marine algae, and particulate and dissolved organic carbon (POC and DOC) mainly derived from phytoplankton, zooplankton, and detrital material (Lamb et al., 2006), suggesting a variable contribution of all these sources according to the sites.

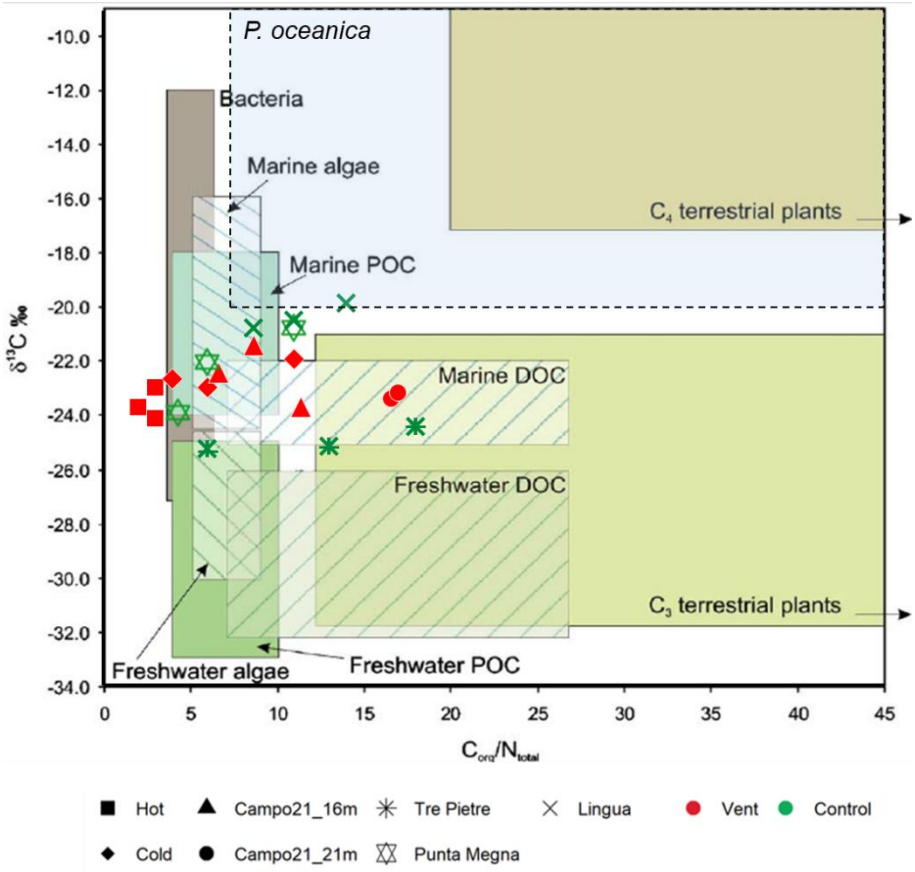

Figure 5.3.3.4. $\delta^{13}C$ *vs.* C_{org}/N ratios of in surface sediments across the study sites superimposed to the published $\delta^{13}C$ *vs.* C_{org}/N ranges for organic inputs to coastal environments (from Lamb et al., 2006)

5.3.4 *Posidonia oceanica*

✓ *Density, epiphyte biomass and phenological analysis*

As regards *Posidonia oceanica*, no significant seasonal differences in shoot density were detected, whereas seasonal variability emerged when considering epiphyte biomass. A clear spatial gradient in shoot density was also evident across the control sites, but not across vent sites, where shoot density was overall lower than compared to the control sites (Figure 5.3.4.1, Table 5.3.4.1). Epiphyte biomass exhibited marked

spatial variability, especially during the May 2025 survey. In this period, the highest epiphyte biomass was recorded at the Cold and Tre Pietre sites at the Vent and Control areas respectively (Figure 5.3.4.1, Table 5.3.4.1).

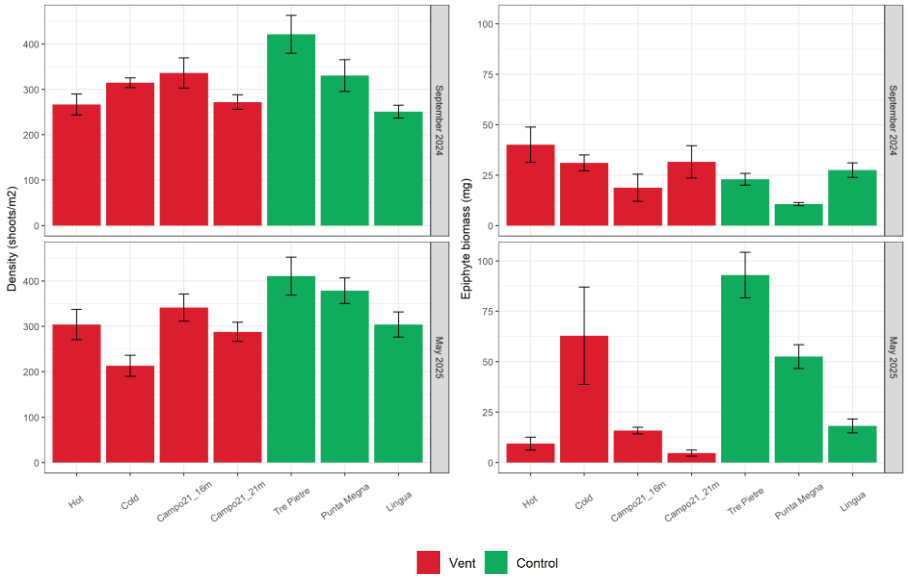

Figure 5.3.4.1. Mean (± SD) *P. oceanica* shoot density and epiphyte biomass across the study sites and seasons.

Table 5.3.4.1. Univariate PERMANOVA results for *P. oceanica* epiphyte biomass and shoot density across the study sites and seasons. Significant values are indicated in red.

a) Main test		Epiphyte biomass		Shoot density	
Source of variation	**df**	**Pseudo-F**	**p**	**Pseudo-F**	**p**
Season (Se)	1	5.40	0.023	0.20	0.658
Site (St)	6	6.59	0.004	7.36	0.001
Se x St	6	9.92	0.001	1.68	0.191
Residuals	28				

b) Pairwise tests	Epiphyte biomass		Shoot density
Between sites within seasons	**S24**	**M25**	***Between sites across seasons***
	p	**p**	**p**
Hot, Cold	0.412	0.096	0.405
Hot, Campo21_16m	0.141	0.118	0.136
Hot, Campo21_21m	0.572	0.288	0.853
Hot, Tre Pietre	0.144	0.003	0.014
Hot, Punta Megna	0.033	0.001	0.052
Hot, Lingua	0.263	0.143	0.773
Cold, Campo21_16m	0.199	0.129	0.028
Cold, Campo21_21m	0.967	0.06	0.441
Cold, Tre Pietre	0.178	0.317	0.004
Cold, Punta Megna	0.008	0.677	0.010

Cold, Lingua	0.54	0.132	0.496
Campo21_16m, Campo21_21m	0.313	0.011	0.060
Campo21_16m, Tre Pietre	0.592	0.003	0.068
Campo21_16m, Punta Megna	0.327	0.007	0.584
Campo21_16m, Lingua	0.316	0.592	0.046
Campo21_21m, Tre Pietre	0.389	0.002	0.006
Campo21_21m, Punta Megna	0.084	0.005	0.023
Campo21_21m, Lingua	0.712	0.026	0.930
Tre Pietre, Punta Megna	0.016	0.029	0.130
Tre Pietre, Lingua	0.368	0.004	0.010
Punta Megna, Lingua	0.013	0.001	0.023

Between seasons within sites	**cfr**	**p**
Hot	**M25 < S24**	0.032
Cold	S24 = M25	0.261
Campo21_16m	S24 = M25	0.688
Campo21_21m	S24 = M25	0.058
Tre Pietre	**S24 < M25**	0.004
Punta Megna	**S24 < M25**	0.004
Lingua	S24 = M25	0.121

Analyses of *P. oceanica* phenological traits highlighted contrasting spatial and seasonal patterns. Leaf production and the percentage of leaves with eroded apex (Coefficient A) showed significant differences both among sites and between seasons, while leaf surface area and the percentage of brown tissue were mainly influenced by seasonality rather than spatial variability (Table 5.3.4.2). In more detail, all variables but Surface Area were significantly lower in May 2025 compared to September 2024. Moreover, no marked spatial variability was found for leaf number, despite the lowest values being observed at the Lingua control site (Figure 5.3.4.2. Mean (± SD) *P. oceanica* leaf number, surface area, brown tissue/shoot percentage, and coefficient A across the study sites and seasons

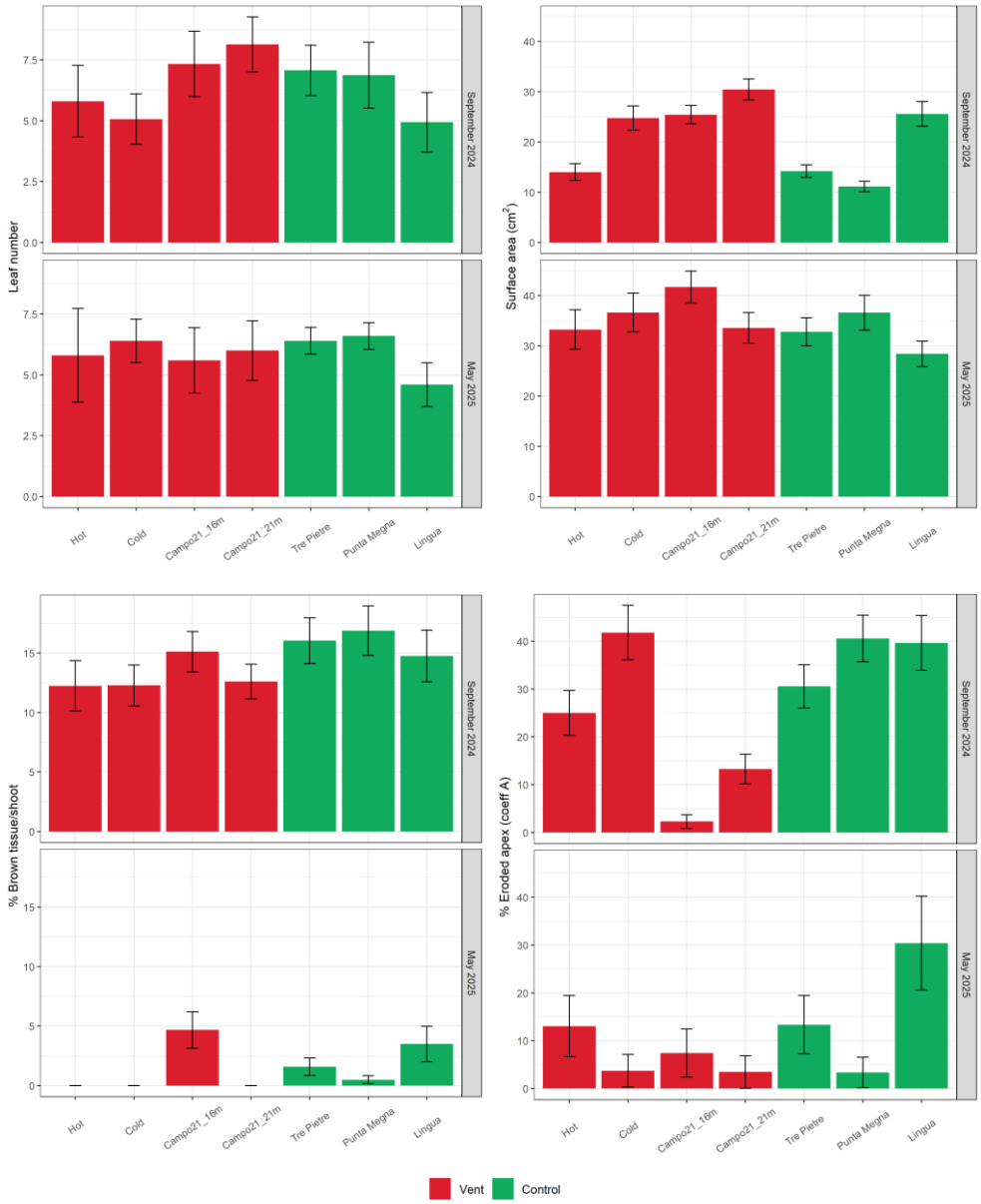

Figure 5.3.4.2. Mean (± SD) *P. oceanica* leaf number, surface area, brown tissue/shoot percentage, and coefficient A across the study sites and seasons

Table 5.3.4.2. Univariate PERMANOVA results for *P. oceanica* leaf number, Coefficient A, surface area and brown tissue % across the study sites and seasons. Significant values are indicated in red.

a) Main test		**Leaf number**		**Coefficient A**		**Surface area**		**% brown tissue**	
Source of variation	**df**	**Pseudo-F**	**p**	**Pseudo-F**	**p**	**Pseudo-F**	**p**	**Pseudo-F**	**p**
Season (Se)	1	17.18	0.001	12.83	0.002	45.12	0.001	216.74	0.001
Site (St)	6	3.50	0.01	3.62	0.007	2.38	0.064	1.97	0.112
Se x St	6	2.00	0.108	2.21	0.091	1.95	0.092	0.78	0.554
Residuals	28								

b) Pairwise tests	Leaf number	Coefficient A	Surface area	% brown tissue
Between sites across seasons	**p**	**p**		
Hot, Cold	0.972	0.556		
Hot, Campo21_16m	0.161	0.032		
Hot, Campo21_21m	0.067	0.042		
Hot, Tre Pietre	0.148	0.633		
Hot, Punta Megna	0.196	0.720		
Hot, Lingua	0.146	0.145		
Cold, Campo21_16m	0.175	0.018		
Cold, Campo21_21m	0.077	0.004		
Cold, Tre Pietre	0.190	0.920		
Cold, Punta Megna	0.192	0.722		
Cold, Lingua	0.159	0.155		
Campo21_16m, Campo21_21m	0.477	0.794		
Campo21_16m, Tre Pietre	0.851	0.089		
Campo21_16m, Punta Megna	0.974	0.023		
Campo21_16m, Lingua	0.001	0.008		
Campo21_21m, Tre Pietre	0.635	0.068		
Campo21_21m, Punta Megna	0.513	0.003		
Campo21_21m, Lingua	0.004	0.006		
Tre Pietre, Punta Megna	0.885	0.757		
Tre Pietre, Lingua	0.004	0.298		
Punta Megna, Lingua	0.005	0.133		

Between seasons across sites	**cfr**	**p**	**cfr**	**p**	**cfr**	**p**	**cfr**	**p**
	M25 < S24	0.001	**M25 < S24**	0.001	**S24 < M25**	0.001	**M25 < S24**	0.001

✓ *Lepidochronological analysis*

Lepidochronological analysis of orthotropic rhizomes, integrating data from both sampling seasons, provided historical information on growth dynamics and leaf production across the study areas. When considering pooled data, area-specific growth strategies in scale production emerged (Figure 5.3.4.3). Cold and Campo21_16m site were characterised by the higher and lower scale number produced over time, despite coupled with marked interannual variability, whereas Hot and Campo21_21m sites were respectively characterised by an increase and a decrease in scale production over time. At the control area, all sites displayed a more stable pattern over time, with minimal fluctuations in Punta Megna.

When rhizome primary production was examined using pooled data, values across all sites ranged overall between 0 and 0.3 g dw rhizome^{-1} (Figure 5.3.4.4). Despite this relatively narrow range, a clear temporal pattern emerged. At vent sites, rhizome primary production showed a marked decrease in recent years, particularly from around 2020 onwards, whereas a similar decline was observed at control areas but was less pronounced. In contrast, mean rhizome growth rate exhibited a different pattern (Figure 5.3.4.5). Overall, growth rates were characterised by higher variability at vent sites than at control areas. However, the temporal trend revealed a more pronounced decrease in growth rate at control sites, whereas vent areas showed a comparatively weaker decline through time. This pattern contrasts with that observed for rhizome primary production, suggesting a differential response of growth-related parameters to local environmental conditions.

Shoot age showed clear differences between vent and control sites (Figure 5.3.4.6). Overall, vent areas (Hot, Cold and Campo21 at both depths) were characterised by lower mean shoot age and relatively limited variability, indicating a generally younger and more homogeneous population structure. In contrast, control

sites exhibited higher shoot age values and greater variability, with Punta Megna and Lingua showing the highest and lowest mean shoot age respectively. This pattern suggests a more mature and heterogeneous meadow structure at control areas compared to vent-impacted areas.

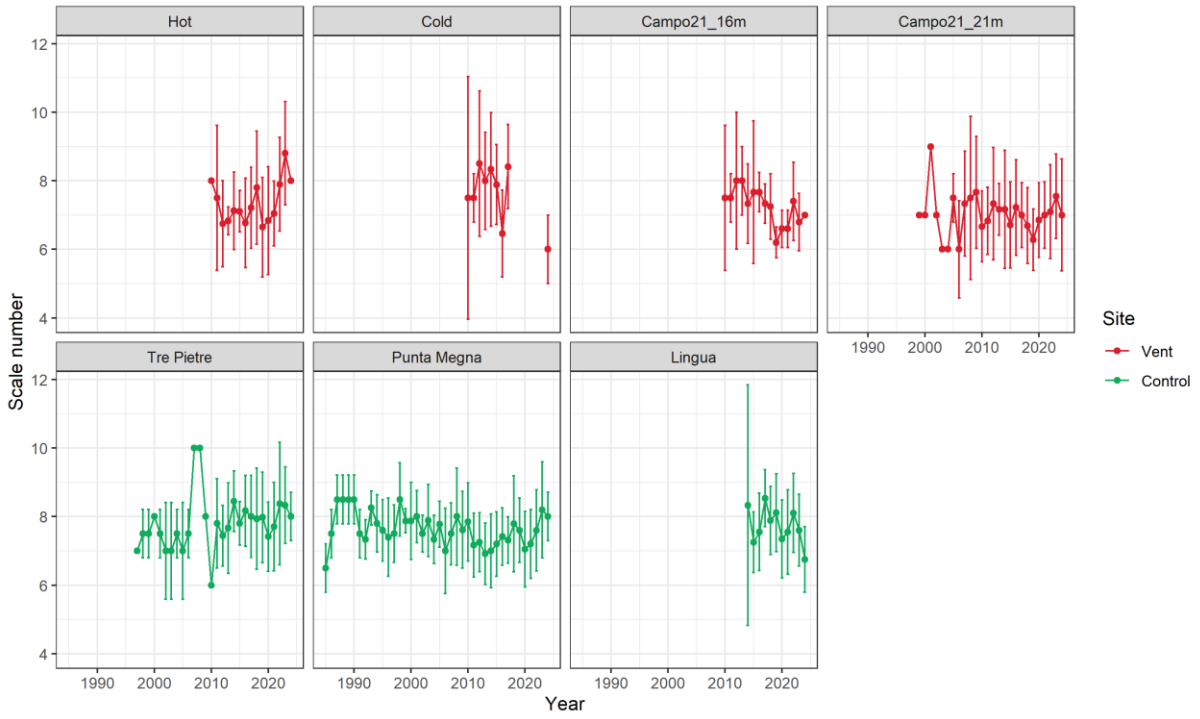

Figure 5.3.4.3. Mean (±SD) *P. oceanica* scale number across the study sites pooling the two seasons.

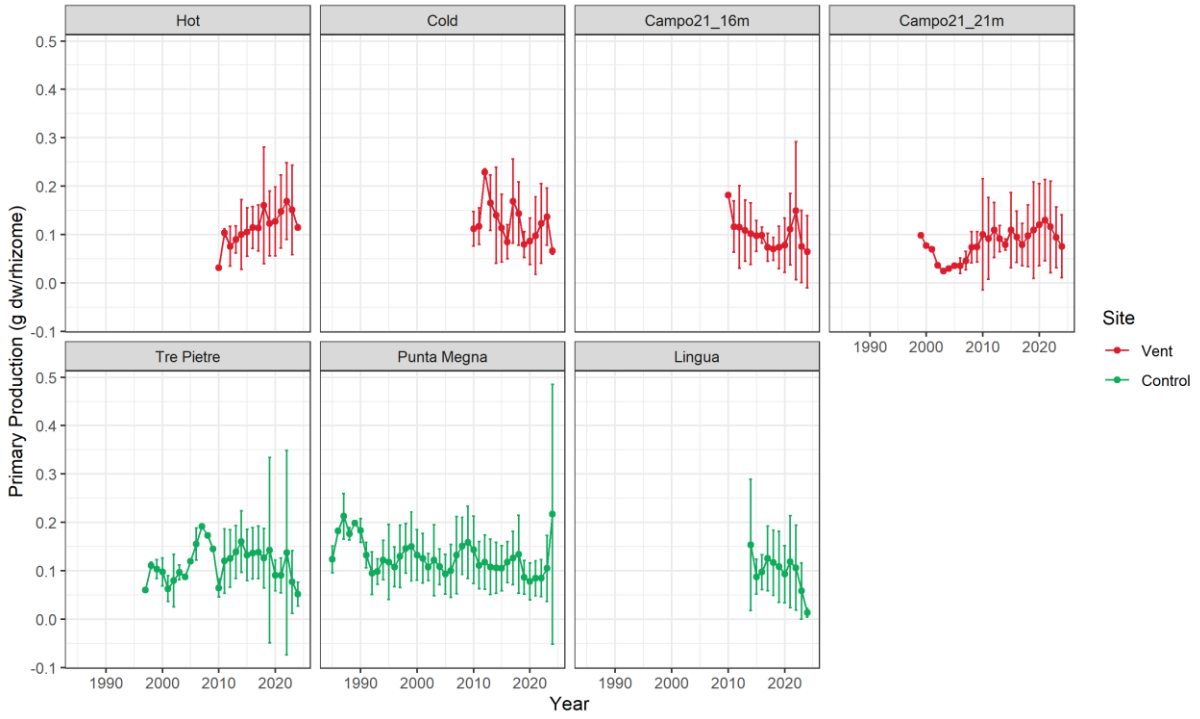

Figure 5.3.4.4. Mean (±SD) *P. oceanica* rhizome primary production across the study sites pooling the two seasons.

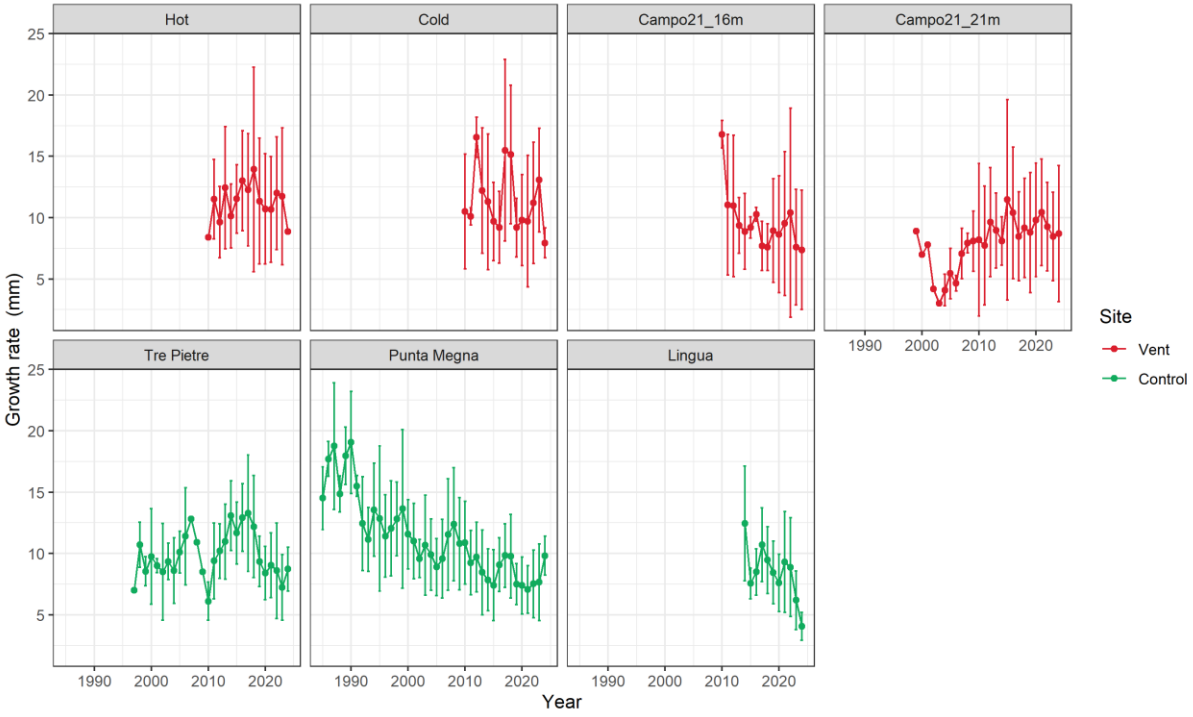

Figure 5.3.4.5. Mean (±SD) *P. oceanica* annual shoot growth rate across the study sites pooling the two seasons.

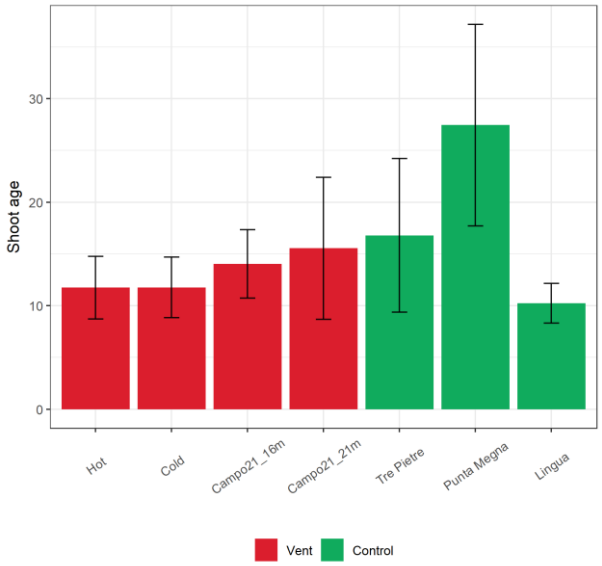

Figure 5.3.4.6. Mean (±SD) shoot age (years) across the study sites pooling the two seasons.

✓ *Trace element analysis*

Overall, trace element concentrations in *P. oceanica* leaves and roots collected in September 2024 and May 2025 showed significant spatial and seasonal patterns across elements (Figure 5.3.4.7, Table 5.3.4.4). In general, concentrations were higher in roots than in leaves, highlighting the role of belowground tissues as the main accumulation compartment.

A common pattern among several elements (including As, Fe, Hg, Mn, Pb and V) consisted of seasonally consistent higher concentrations at vent sites compared to control sites, particularly in root tissues. Within the vent area, Hot and Cold sites generally exhibited higher values than the Campo21 sites, while Campo21 concentrations were often comparable to those measured at the Salina sites. In contrast, elements such as Cr and Cu showed limited spatial variability, with overall comparable concentrations between vent and control areas and between tissues. A different pattern emerged for Ni and Zn, whose concentrations were generally higher at control sites than at vent sites, especially in leaves, reflecting a pattern different from that observed for most other elements. Seasonal variability was overall less marked than spatial variability. However, higher concentrations were generally recorded in September 2024 compared to May 2025 for several elements, particularly at vent sites, whereas control areas showed more stable values between seasons.

Figure 5.3.4.7. Mean (± SD) concentration of trace elements in *P. oceanica* leaves and roots from across the study sites and seasons.

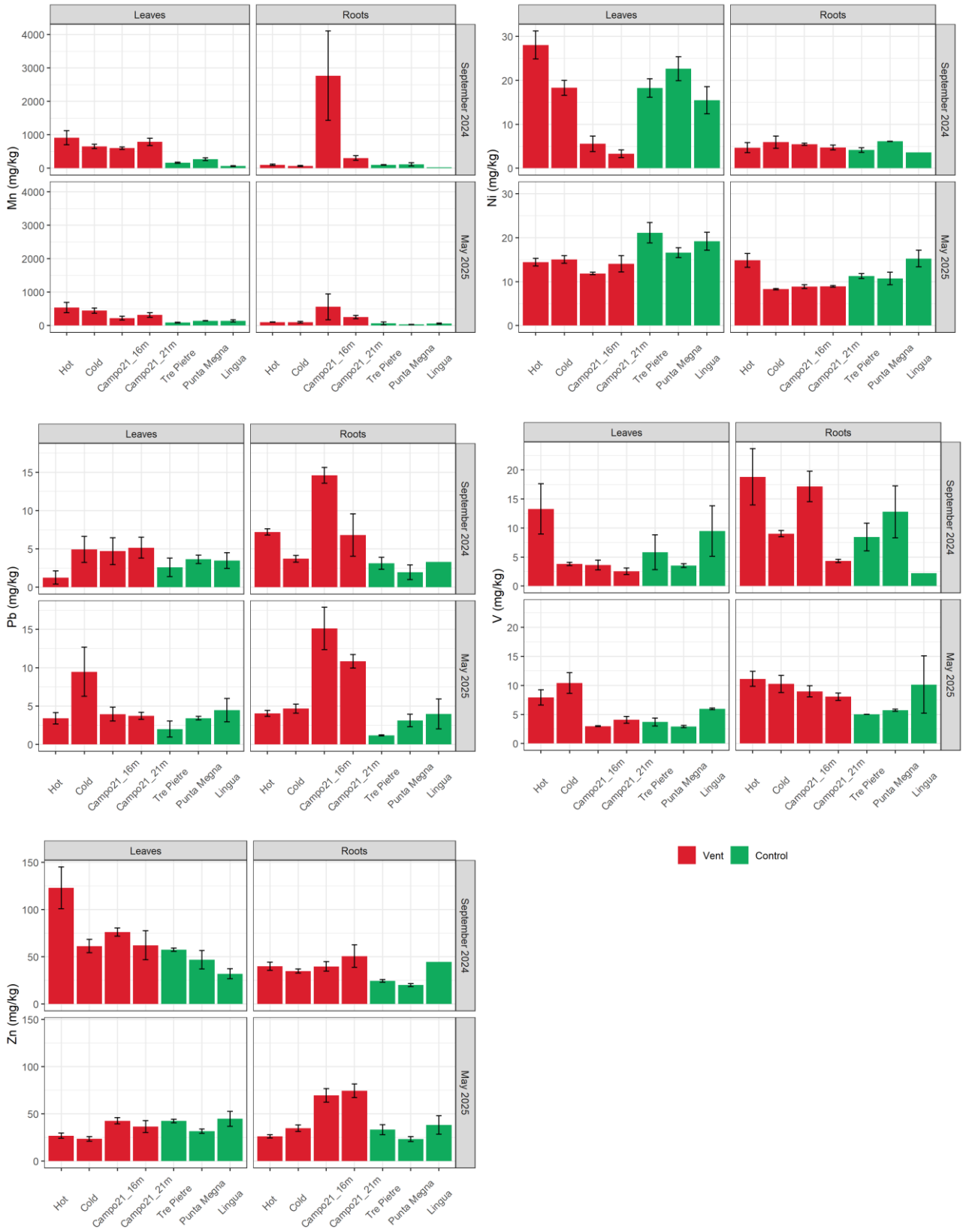

Figure 5.3.4.7 (continued)

Table 5.3.4.3. Univariate PERMANOVA results for trace element concentration in *P. oceanica* leaves from across the study sites and seasons. Significant values are indicated in red.

a) Main test		As		Cd		Cu		Fe		Hg		Mn	
Source of variation	**df**	**Pseudo-F**	**p**	**Pseudo-F**	**p**	**Pseudo-F**	**p**	**Pseudo-F**	**p**	**Pseudo-F**	**p**	**Pseudo-F**	**p**
Season (Se)	1	0.4	0.552	9.8	0.005	39.1	0.001	3.3	0.046	4.6	0.048	23.3	0.001
Site (St)	6	9.1	0.002	1.8	0.132	8.7	0.001	30.9	0.001	45.8	0.001	15.6	0.001
Se x St	6	3.3	0.002	8.5	0.001	19.5	0.001	4.2	0.001	3.8	0.008	2.5	0.039
Residuals	28												

b) Pairwise tests	As		Cd		Cu		Fe		Hg		Mn	
1) Between sites within seasons	**S24**	**M25**	**S24**	**M25**	**S24**	**M25**	**S24**	**M25**	**S24**	**M25**	**S24**	**M25**
	p	**p**	**p**	**p**	**p**	**p**	**p**	**p**	**p**	**p**	**p**	**p**
Hot, Cold	0.076	0.129	0.361	0.310	0.361	0.106	0.022	0.002	0.725	0.211	0.292	0.610
Hot, Campo21_16m	0.074	0.272	0.159	0.090	0.159	0.115	0.019	0.001	0.002	0.018	0.210	0.120
Hot, Campo21_21m	0.055	0.043	0.305	0.005	0.305	0.049	0.021	0.001	0.002	0.019	0.653	0.045
Hot, Tre Pietre	0.045	0.073	0.661	0.018	0.661	0.109	0.017	0.001	0.008	0.012	0.024	0.062
Hot, Punta Megna	0.052	0.181	0.008	0.055	0.008	0.056	0.016	0.001	0.002	0.079	0.050	0.261
Hot, Lingua	0.054	0.357	0.015	0.020	0.015	0.009	0.017	0.002	0.001	0.160	0.016	0.067
Cold, Campo21_16m	0.872	0.880	0.993	0.908	0.993	0.648	0.011	0.006	0.002	0.001	0.529	0.086
Cold, Campo21_21m	0.054	0.923	0.196	0.244	0.196	0.951	0.010	0.003	0.002	0.008	0.357	0.291
Cold, Tre Pietre	0.007	0.008	0.283	0.018	0.283	0.407	0.063	0.013	0.001	0.002	0.003	0.005
Cold, Punta Megna	0.004	0.034	0.070	0.071	0.070	0.601	0.005	0.003	0.001	0.001	0.009	0.022
Cold, Lingua	0.985	0.465	0.054	0.045	0.054	0.034	0.008	0.011	0.001	0.031	0.005	0.029
Campo21_16m, Campo21_21m	0.159	0.849	0.078	0.210	0.078	0.632	1.000	1.000	0.552	0.222	0.168	0.330
Campo21_16m, Tre Pietre	0.031	0.217	0.160	0.008	0.160	0.336	0.368	0.370	0.122	0.546	0.001	0.092
Campo21_16m, Punta Megna	0.043	0.289	0.005	0.036	0.005	0.975	1.000	1.000	0.051	0.116	0.002	0.298
Campo21_16m, Lingua	0.937	0.709	0.007	0.043	0.007	0.165	1.000	0.379	0.078	0.196	0.002	0.303
Campo21_21m, Tre Pietre	0.069	0.167	0.673	0.065	0.673	0.051	0.374	0.368	0.059	0.357	0.006	0.035
Campo21_21m, Punta Megna	0.066	0.224	0.132	0.463	0.132	0.544	1.000	1.000	0.142	0.075	0.012	0.069

Campo21_21m, Lingua	0.521	0.518	0.128	0.170	0.128	0.020	1.000	0.374	0.280	0.730	0.004	0.083
Tre Pietre, Punta Megna	0.470	0.486	0.120	0.140	0.120	0.186	0.383	0.372	0.001	0.090	0.067	0.026
Tre Pietre, Lingua	0.213	0.055	0.081	0.816	0.081	0.012	0.352	1.000	0.005	0.280	0.009	0.215
Punta Megna, Lingua	0.276	0.096	0.915	0.333	0.915	0.090	1.000	0.361	0.515	0.087	0.008	0.936

2) Between seasons within sites	**cfr**	**p**	**cfr**	**p**	**cfr**	**p**	**cfr**	**p**	**cfr**	**p**	**cfr**	**p**
Hot	S24 = M25	0.158	S24 = M25	0.059	S24 = M25	0.104	**M25 < S24**	0.001	S24 = M25	0.288	S24 = M25	0.206
Cold	S24 = M25	0.063	S24 = M25	0.272	**M25 < S24**	0.026	S24 = M25	0.120	S24 = M25	0.504	S24 = M25	0.114
Campo21_16m	S24 = M25	0.453	S24 = M25	0.075	**S24 < M25**	0.019	S24 = M25	0.222	S24 = M25	0.216	**M25 < S24**	0.004
Campo21_21m	S24 = M25	0.172	**S24 < M25**	0.042	S24 = M25	0.119	S24 = M25	1.000	**S24 < M25**	0.009	**M25 < S24**	0.031
Tre Pietre	S24 = M25	0.288	**S24 < M25**	0.004	**S24 < M25**	0.025	S24 = M25	1.000	S24 = M25	0.453	**M25 < S24**	0.028
Punta Megna	S24 = M25	0.182	S24 = M25	0.198	**S24 < M25**	0.002	S24 = M25	1.000	S24 = M25	0.071	**M25 < S24**	0.027
Lingua	S24 = M25	0.206	**S24 < M25**	0.010	**S24 < M25**	0.001	S24 = M25	0.388	**S24 < M25**	0.046	S24 = M25	0.100

Table. 5.3.4.3 continued

a) Main test		**Ni**		**Zn**		**Pb**		**V**		**Cr**	
Source of variation	**df**	**Pseudo-F**	**p**	**Pseudo-F**	**p**	**Pseudo-F**	**p**	**Pseudo-F**	**p**	**Pseudo-F**	**p**
Season (Se)	1	0.0	0.938	42.2	0.001	0.8	0.396	0.3	0.591	9.2	0.003
Site (St)	6	14.1	0.001	4.5	0.004	2.9	0.027	4.2	0.003	1.8	0.116
Se x St	6	8.9	0.001	7.5	0.001	1.2	0.361	2.0	0.095	1.1	0.404
Residuals	28										

b) Pairwise tests	**Ni**		**Zn**		**Pb**	**V**	**Cr**	
1) Between sites within seasons	**S24**	**M25**	**S24**	**M25**	***3) Between sites across seasons***		***4) Between seasons across sites***	
	p	**p**	**p**	**p**	**p**	**p**	**cfr**	**p**
Hot, Cold	0.047	0.626	0.054	0.438	0.039	0.191	**M25 < S24**	0.008
Hot, Campo21_16m	0.004	0.044	0.105	0.014	0.122	0.01		
Hot, Campo21_21m	0.002	0.054	0.091	0.01	0.948	0.059		

Hot, Tre Pietre	0.063	0.197	0.052	0.252	0.103	0.013
Hot, Punta Megna	0.274	0.842	0.029	0.226	0.045	0.015
Hot, Lingua	0.035	0.103	0.017	0.088	0.179	0.367
Cold, Campo21_16m	0.005	0.032	0.168	0.014	0.218	0.004
Cold, Campo21_21m	0.001	0.624	0.963	0.124	0.196	0.005
Cold, Tre Pietre	0.989	0.079	0.607	0.006	0.036	0.253
Cold, Punta Megna	0.254	0.351	0.295	0.076	0.103	0.002
Cold, Lingua	0.449	0.134	0.03	0.053	0.159	0.818
Campo21_16m, Campo21_21m	0.303	0.299	0.461	0.441	0.925	0.968
Campo21_16m, Tre Pietre	0.008	0.022	0.017	0.962	0.127	0.436
Campo21_16m, Punta Megna	0.01	0.024	0.058	0.049	0.473	0.899
Campo21_16m, Lingua	0.053	0.021	0.007	0.804	0.812	0.053
Campo21_21m, Tre Pietre	0.004	0.061	0.775	0.444	0.072	0.46
Campo21_21m, Punta Megna	0.003	0.305	0.422	0.516	0.3	0.85
Campo21_21m, Lingua	0.019	0.136	0.137	0.476	0.711	0.047
Tre Pietre, Punta Megna	0.235	0.168	0.348	0.027	0.16	0.447
Tre Pietre, Lingua	0.51	0.552	0.015	0.785	0.204	0.333
Punta Megna, Lingua	0.174	0.324	0.26	0.181	0.672	0.038

2) Between seasons within sites	**cfr**	**p**	**cfr**	**p**
Hot	**S24 < M25**	0.014	**M25 < S24**	0.005
Cold	S24 = M25	0.178	**M25 < S24**	0.006
Campo21_16m	**S24 < M25**	0.025	**M25 < S24**	0.005
Campo21_21m	S24 = M25	0.412	**M25 < S24**	0.008
Tre Pietre	S24 = M25	0.119	S24 = M25	0.2
Punta Megna	**M25 < S24**	0.008	S24 = M25	0.168
Lingua	S24 = M25	0.368	S24 = M25	0.232

Table 5.3.4.4. Univariate PERMANOVA results for trace element concentration in *P. oceanica* roots from across the study sites and seasons. Significant values are indicated in red

a) Main test		Cr		Cu		Hg		Ni		Zn	
Source of variation	**df**	**Pseudo-F**	**p**	**Pseudo-F**	**p**	**Pseudo-F**	**p**	**Pseudo-F**	**p**	**Pseudo-F**	**p**
Season (Se)	1	9.8	0.006	0.2	0.716	72.1	0.001	103.0	0.001	4.0	0.062
Site (St)	6	6.0	0.001	5.8	0.002	101.8	0.001	2.2	0.078	12.4	0.001
Se x St	6	5.1	0.004	2.9	0.027	12.3	0.001	4.6	0.001	3.9	0.004
Residuals	28										

b) Pairwise tests	Cr		Cu		Hg		Ni		Zn	
1) Between sites within seasons	**S24**	**M25**	**S24**	**M25**	**S24**	**M25**	**S24**	**M25**	**S24**	**M25**
	p	**p**	**p**	**p**	**p**	**p**	**p**	**p**	**p**	**p**
Hot, Cold	0.847	0.020	0.954	0.001	0.907	0.005	0.527	0.017	0.352	0.113
Hot, Campo21_16m	0.511	0.071	0.526	0.060	0.013	0.001	0.532	0.023	0.956	0.003
Hot, Campo21_21m	0.248	0.017	0.684	0.142	0.016	0.001	0.981	0.028	0.401	0.005
Hot, Tre Pietre	0.237	0.195	0.519	0.673	0.006	0.001	0.668	0.186	0.028	0.221
Hot, Punta Megna	0.930	0.033	0.867	0.717	0.033	0.001	0.368	0.131	0.042	0.412
Hot, Lingua	0.660	0.022	0.296	0.613	0.077	0.001	0.678	0.890	0.659	0.265
Cold, Campo21_16m	0.578	0.226	0.199	0.291	0.002	0.001	0.754	0.241	0.408	0.012
Cold, Campo21_21m	0.131	0.059	0.433	0.010	0.010	0.001	0.584	0.058	0.190	0.008
Cold, Tre Pietre	0.084	0.017	0.296	0.007	0.001	0.003	0.283	0.007	0.020	0.815
Cold, Punta Megna	0.715	0.379	0.461	0.003	0.008	0.001	0.941	0.168	0.016	0.067
Cold, Lingua	0.465	0.706	0.028	0.011	0.039	0.002	0.501	0.022	0.145	0.743
Campo21_16m, Campo21_21m	0.140	0.109	0.200	0.147	0.032	0.043	0.281	0.942	0.431	0.674
Campo21_16m, Tre Pietre	0.085	0.433	0.107	0.093	0.005	0.032	0.112	0.039	0.042	0.029
Campo21_16m, Punta Megna	0.438	0.599	0.473	0.043	0.041	0.010	0.109	0.282	0.055	0.006
Campo21_16m, Lingua	0.425	0.181	0.060	0.109	0.056	0.089	0.066	0.034	0.674	0.069
Campo21_21m, Tre Pietre	0.515	0.010	0.939	0.176	0.673	0.004	0.545	0.015	0.061	0.025
Campo21_21m, Punta Megna	0.047	0.186	0.376	0.143	0.962	0.020	0.124	0.284	0.127	0.006
Campo21_21m, Lingua	0.310	0.171	0.379	0.513	0.499	0.471	0.464	0.028	0.800	0.041
Tre Pietre, Punta Megna	0.059	0.176	0.273	0.919	0.764	0.928	0.071	0.801	0.159	0.131

Tre Pietre, Lingua	0.603	0.024	0.201	0.524	0.133	0.482	0.666	0.209	0.027	0.737
Punta Megna, Lingua	0.277	0.332	0.088	0.470	0.564	0.332	0.014	0.141	0.090	0.190

Table 5.3.4.4 continued

2) Between seasons within sites	**cfr**	**p**	**cfr**	**p**	**cfr**	**p**	**cfr**	**p**	**cfr**	**p**
Hot	**S24 < M25**	0.035	S24 = M25	0.277	**S24 < M25**	0.033	**S24 < M25**	0.011	**M25 < S24**	0.05
Cold	S24 = M25	0.267	**S24 < M25**	0.005	**S24 < M25**	0.004	S24 = M25	0.187	S24 = M25	0.975
Campo21_16m	S24 = M25	0.755	S24 = M25	0.868	**S24 < M25**	0.032	**S24 < M25**	0.001	**S24 < M25**	0.032
Campo21_21m	S24 = M25	0.933	S24 = M25	0.977	**S24 < M25**	0.002	**S24 < M25**	0.007	S24 = M25	0.171
Tre Pietre	**S24 < M25**	0.014	S24 = M25	0.344	**S24 < M25**	0.033	**S24 < M25**	0.003	S24 = M25	0.139
Punta Megna	S24 = M25	0.718	**M25 < S24**	0.032	S24 = M25	0.162	S24 = M25	0.09	S24 = M25	0.47
Lingua	S24 = M25	0.926	S24 = M25	0.214	S24 = M25	0.231	S24 = M25	0.087	S24 = M25	0.783

a) Main test		**As**		**Fe**		**Mn**		**Pb**		**V**		**Cd**	
Source of variation	**df**	**Pseudo-F**	**p**	**Pseudo-F**	**p**	**Pseudo-F**	**p**	**Pseudo-F**	**p**	**Pseudo-F**	**p**	**Pseudo-F**	**p**
Season (Se)	1	0.0	0.874	0.4	0.557	1.8	0.196	0.2	0.683	1.6	0.221	4.0	0.056
Site (St)	6	14.1	0.001	8.8	0.001	4.0	0.04	23.5	0.001	3.3	0.023	3.7	0.039
Se x St	6	1.3	0.271	1.6	0.183	2.0	0.089	1.5	0.24	2.3	0.069	1.2	0.266
Residuals	28												

b) Pairwise tests	**As**	**Fe**	**Mn**	**Pb**	**V**	**Cd**
1) Between sites across seasons	**p**	**p**	**p**	**p**	**p**	**p**
Hot, Cold	0.871	0.585	0.242	0.024	0.055	0.281
Hot, Campo21_16m	0.043	0.003	0.037	0.004	0.548	0.004
Hot, Campo21_21m	0.016	0.003	0.003	0.023	0.017	0.007
Hot, Tre Pietre	0.004	0.001	0.326	0.004	0.032	0.015
Hot, Punta Megna	0.009	0.002	0.175	0.007	0.116	0.059

Hot, Lingua	0.052	0.008	0.010	0.236	0.115	0.030
Cold, Campo21_16m	0.002	0.011	0.024	0.005	0.067	0.035
Cold, Campo21_21m	0.002	0.020	0.005	0.012	0.012	0.075
Cold, Tre Pietre	0.001	0.023	0.975	0.014	0.118	0.067
Cold, Punta Megna	0.001	0.031	0.685	0.055	0.829	0.126
Cold, Lingua	0.003	0.155	0.102	0.673	0.388	0.178
Campo21_16m, Campo21_21m	0.050	0.003	0.106	0.027	0.009	0.354
Campo21_16m, Tre Pietre	0.007	0.126	0.044	0.003	0.024	0.272
Campo21_16m, Punta Megna	0.022	0.050	0.055	0.003	0.116	0.117
Campo21_16m, Lingua	0.126	0.126	0.192	0.004	0.136	0.471
Campo21_21m, Tre Pietre	0.008	0.006	0.003	0.005	0.777	0.720
Campo21_21m, Punta Megna	0.183	0.033	0.003	0.002	0.121	0.254
Campo21_21m, Lingua	0.364	0.118	0.004	0.055	0.999	0.920
Tre Pietre, Punta Megna	0.124	0.070	0.753	0.690	0.295	0.344
Tre Pietre, Lingua	0.002	0.165	0.153	0.420	0.909	0.807
Punta Megna, Lingua	0.127	0.919	0.292	0.523	0.521	0.343

The Principal Component Analysis (PCA) performed on the trace element concentrations measured in *P. oceanica* leaves and roots confirmed the spatial patterns previously described by the univariate analyses (Figure 5.3.4.8, Table 5.3.4.5). In both seasons, the first two principal components (PC1 and PC2) explained a substantial proportion of the total variance and clearly separated vent sites from control sites, in agreement with the multivariate differences detected by the PERMANOVA (Table 5.3.4.5).

In both tissues and seasons, PC1 primarily captured the vent–control gradient, reflecting overall higher trace-element concentrations at vent sites compared to controls. This axis 1 was mainly driven by As, Hg, Fe, V and Zn, whose loadings were consistently associated with vent areas, particularly Hot and Cold, confirming the accumulation patterns previously observed in both sediments and plant tissues. Control sites generally clustered on the oppoarea side of vent sites along PC1, reflecting generally lower and more homogeneous concentrations. PC2 represented a secondary gradient, associated mainly with Pb, Ni and Cr, and highlighted differences within the vent area. Along this axis, Hot and Cold sites were clearly separated from the Campo21 sites, indicating higher concentrations of these elements at the former, consistent with the spatial patterns described for both sediments and *P. oceanica* tissues. This separation was more pronounced in roots than in leaves, further supporting the role of belowground tissues as the main compartment for trace element accumulation. Seasonal differences were comparatively less marked than spatial ones, with a broadly similar ordination structure in September 2024 and May 2025. This indicates that spatial variability between vent and control areas represents the dominant source of variation in trace element composition, while seasonal effects play a secondary role.

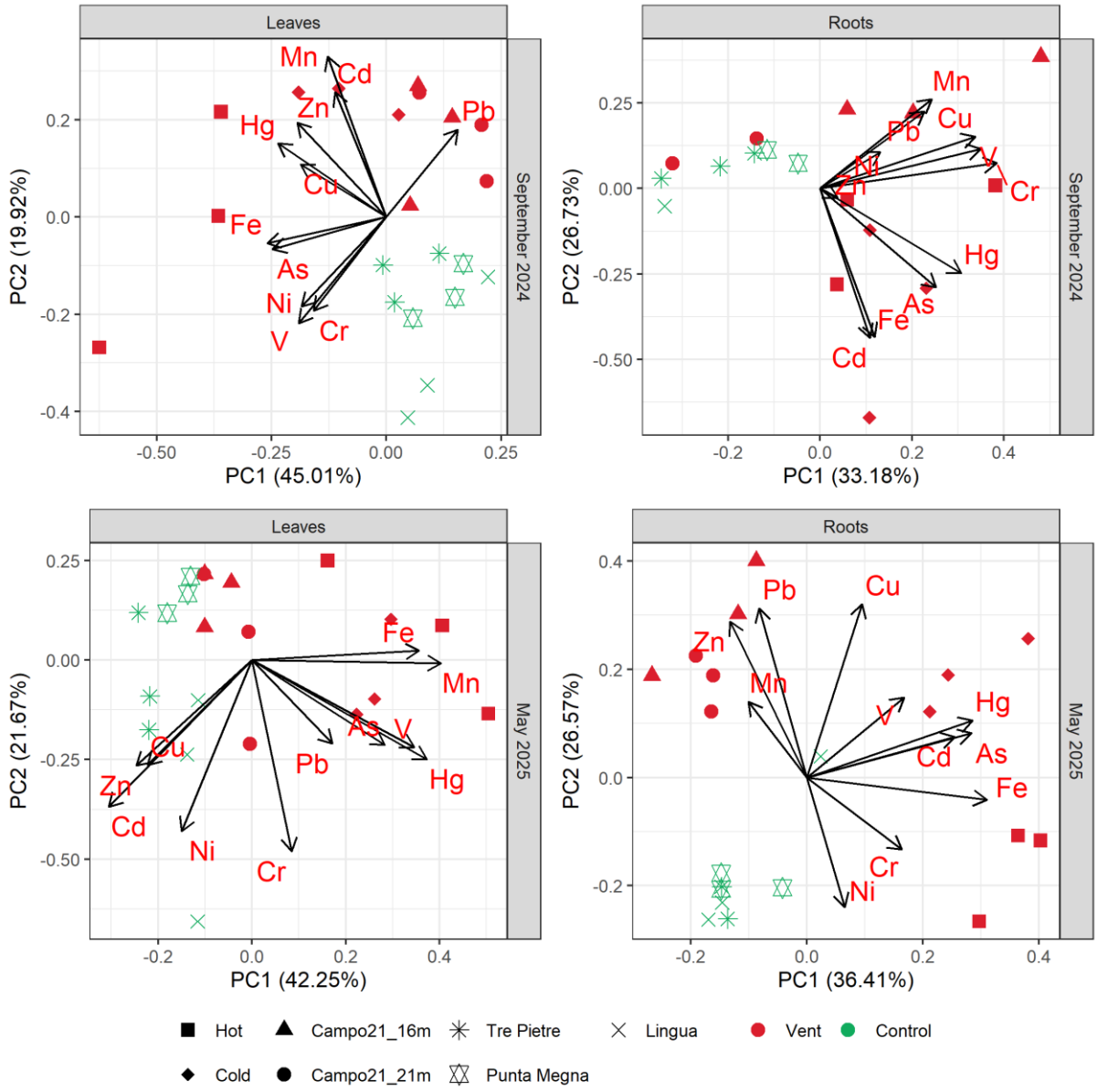

Figure 5.3.4.8. Principal Component Analysis (PCA) of trace element concentrations in *P. oceanica* leaves and roots across the study sites and seasons.

Table 5.3.4.5. Multivariate PERMANOVA results for all trace element concentrations in *P. oceanica* leaves and roots across the study sites and seasons. Significant values are indicated in red.

a) Main test		**Leaves**		**Roots**	
Source of variation	**df**	**Pseudo-F**	**p**	**Pseudo-F**	**p**
Season (Se)	1	90.18	0.001	8.03	0.001
Site (St)	6	75.41	0.001	7.98	0.001
Se x St	6	41.05	0.001	2.55	0.001
Residuals	28				

b) Pairwise tests	**Leaves**		**Roots**	
Between sites within seasons	**S24**	**M25**	**S24**	**M25**
	p	**p**	**p**	**p**
Hot, Cold	0.03	0.083	0.243	0.003

Hot, Campo21_16m	0.019	0.024	0.098	0.008
Hot, Campo21_21m	0.023	0.013	0.119	0.002
Hot, Tre Pietre	0.016	0.005	0.054	0.027
Hot, Punta Megna	0.015	0.039	0.189	0.005
Hot, Lingua	0.018	0.02	0.241	0.017
Cold, Campo21_16m	0.022	0.03	0.052	0.005
Cold, Campo21_21m	0.015	0.06	0.107	0.002
Cold, Tre Pietre	0.042	0.013	0.053	0.002
Cold, Punta Megna	0.014	0.02	0.159	0.001
Cold, Lingua	0.016	0.042	0.328	0.012
Campo21_16m, Campo21_21m	0.175	0.408	0.12	0.16
Campo21_16m, Tre Pietre	0.063	0.02	0.033	0.036
Campo21_16m, Punta Megna	0.016	0.077	0.083	0.019
Campo21_16m, Lingua	0.029	0.052	0.177	0.025
Campo21_21m, Tre Pietre	0.016	0.05	0.17	0.007
Campo21_21m, Punta Megna	0.013	0.127	0.132	0.007
Campo21_21m, Lingua	0.024	0.179	0.423	0.031
Tre Pietre, Punta Megna	0.284	0.106	0.282	0.225
Tre Pietre, Lingua	0.299	0.105	0.184	0.315
Punta Megna, Lingua	0.17	0.048	0.193	0.291

b) Pairwise tests	Leaves		Roots	
Between seasons within sites	**cfr**	**p**	**cfr**	**p**
Hot	S24 ≠ M25	0.037	S24 ≠ M25	0.024
Cold	S24 = M25	0.078	S24 = M25	0.144
Campo21_16m	S24 ≠ M25	0.027	S24 = M25	0.128
Campo21_21m	S24 = M25	0.141	S24 = M25	0.095
Tre Pietre	S24 ≠ M25	0.016	S24 ≠ M25	0.025
Punta Megna	S24 ≠ M25	0.014	S24 = M25	0.058
Lingua	S24 ≠ M25	0.019	S24 = M25	0.284

The heat-map representation of bioaccumulation (BAF) and biotranslocation (BTF) factors illustrates clear element-, site- and season-dependent patterns in *P. oceanica* accumulation of trace elements in roots from sediment and associated translocation to leaves (Table 5.3.4.6). In this study, BAF was calculated as the ratio between trace element concentrations in roots and sediments (roots/sediments), reflecting the capacity of belowground tissues to accumulate elements from the surrounding sediment. BTF was calculated as the ratio between concentrations in leaves and roots (leaves/roots), providing an estimate of internal translocation from belowground to aboveground tissues.

BAF values indicated moderate to high accumulation for selected elements, particularly Cd, Cu, Hg, Mn and Zn, with the highest values generally observed at vent-impacted sites, especially Campo21 (both depths). This pattern was consistent across seasons, although slightly higher BAF values were often recorded in September 2024 compared to May 2025. In contrast, Cr, Fe, Ni, Pb and V consistently showed low BAF values across all sites and seasons, indicating limited sediment-to-root accumulation.

BTF values displayed greater heterogeneity than BAF, highlighting marked spatial variability in element translocation to the above-ground plant tissues. Elevated BTF values were mainly associated with Mn, Ni and Zn, followed by Cr and Cd. This was particularly evident at vent sites during September 2024, suggesting enhanced root-to-leaf transfer under vent-influenced conditions. In May 2025, BTF values were generally lower and more homogeneous, although relatively high translocation of Mn persisted at some sites.

Table 5.3.4.6. Bioaccumulation (BAF) and biotranslocation (BTF) factor values for trace elements across the study sites and seasons, displayed as a heat map. Colour intensity reflects the magnitude of BAF and BTF values, with higher values indicating stronger bioaccumulation and translocation potential.

a) BAF	As	Cd	Cr	Cu	Fe	Hg	Mn	Ni	Pb	V	Zn
September 24											
Hot	0.7	5.7	0.1	0.7	0.2	1.1	0.3	0.3	0.2	0.2	0.6
Cold	0.7	12.6	0.2	0.7	0.5	0.7	0.1	0.3	0.1	0.1	0.6
Campo21_16m	1.0	13.1	0.2	4.3	0.2	0.2	28.2	0.4	1.8	0.3	2.1
Campo21_21m	0.2	16.9	0.1	3.5	0.1	0.1	2.9	0.3	0.3	0.1	2.7
Tre Pietre	0.5	3.1	0.9	0.6	0.0	11.4	0.1	0.3	0.1	0.1	0.3
Punta Megna	0.2	4.6	0.5	1.1	0.1	4.3	0.1	0.5	0.1	0.1	0.4
Lingua	0.9	3.0	0.1	0.1	0.1	1.9	0.0	0.2	0.1	0.0	0.5
May 25											
Hot	1.0	4.2	0.6	0.6	0.4	1.2	0.1	1.0	0.1	0.1	0.4
Cold	0.8	7.7	0.1	1.3	0.3	2.4	0.1	0.5	0.1	0.1	0.6
Campo21_16m	0.7	18.3	0.2	4.1	0.1	0.2	1.7	0.7	1.4	0.2	2.7
Campo21_21m	0.6	16.2	0.1	2.7	0.1	0.2	1.0	0.6	0.7	0.1	1.8
Tre Pietre	0.1	1.9	2.0	0.5	0.0	3.9	0.1	0.7	0.0	0.0	0.4
Punta Megna	0.4	1.9	0.6	0.8	0.1	5.3	0.0	0.8	0.1	0.0	0.3
Lingua	0.3	1.1	0.1	0.3	0.1	3.3	0.0	1.0	0.1	0.1	0.4

b) BTF	As	Cd	Cr	Cu	Fe	Hg	Mn	Ni	Pb	V	Zn
September 24											
Hot	0.6	0.5	2.2	0.6	0.5	0.6	10.3	6.9	0.2	0.7	3.2
Cold	0.0	0.4	1.1	0.7	0.0	0.6	10.9	3.5	1.3	0.4	1.8
Campo21_16m	0.1	1.7	0.9	0.2	0.1	0.4	0.3	1.0	0.3	0.2	2.0
Campo21_21m	0.3	0.9	1.1	0.3	0.4	0.5	2.4	0.6	1.2	0.5	1.0
Tre Pietre	0.2	0.9	2.3	0.5	0.2	0.8	1.7	4.7	1.0	0.8	2.4
Punta Megna	0.2	0.4	1.1	0.3	0.1	0.4	3.2	4.1	2.3	0.3	2.5
Lingua	0.0	0.4	1.3	0.7	0.1	0.6	3.1	2.6	1.7	1.5	0.8
May 25											
Hot	0.1	0.6	0.2	0.6	0.1	0.3	5.2	1.0	0.9	0.7	1.0
Cold	0.1	0.6	0.9	0.4	0.0	0.3	4.9	1.8	2.0	1.0	0.7
Campo21_16m	0.2	1.5	0.4	0.5	0.1	0.3	1.3	1.3	0.3	0.3	0.6
Campo21_21m	0.2	1.2	1.8	0.7	0.2	0.6	1.4	1.6	0.3	0.5	0.5
Tre Pietre	0.5	1.7	0.3	0.8	0.2	0.6	2.3	1.8	0.8	0.7	1.3
Punta Megna	0.2	1.7	0.5	0.8	0.1	0.5	4.8	1.6	1.2	0.5	1.4
Lingua	0.6	2.3	1.7	1.0	0.0	0.7	2.7	1.3	2.2	0.9	1.5

✓ *Isotopic and elemental composition*

In *P. oceanica* leaf tissues, $\delta^{13}C$, N% and C/N values in September 2024 showed a clear spatial structuring between vent and control areas (Figure 5.3.4.9, Table 5.3.4.7). Overall, $\delta^{13}C$ values at vent sites were rather heterogeneous and slightly more depleted compared to control areas, which displayed a lower variability. Among vent sites, Campo21_16m exhibited the more depleted $\delta^{13}C$ values than the other vent and control

sites, whereas Lingua showed the most enriched signatures. On the other hands, $\delta^{15}N$ did not show a detectable signal and is therefore not presented.

Total nitrogen (N%) concentrations and C/N ratio showed a specular pattern, being the former generally lower at the Campo21 sites than at the Hot-Cold and control ones, while C/N ratios were characterized by lower values at the Hot-Cold and control sites than at both the Campo21 ones. On the other hand, total carbon (C%) concentrations were markedly homogeneous across all sites.

Turning to rhizome scales, the temporal evolution of $\delta^{13}C$ values revealed contrasting trends between control and some vent sites (Figure 5.3.4.10). Across the entire time series, that spanned between 2015 and 2024, control sites showed relatively stable $\delta^{13}C$ values, displaying limited interannual variability. In contrast, both Campo21 vent sites exhibited markedly more depleted $\delta^{13}C$ signatures and a substantially higher temporal variability, whereas Hot-Cold sites showed a diverging pattern: Hot site values overlapped to control sites, and Cold site showed a marked decreasing pattern over time. Intriguingly, at Campo21 and Cold sites, $\delta^{13}C$ values showed a clear shift towards more negative values from about 2019 to 2021, followed by persistently depleted signatures in subsequent years. This pattern was consistent across the different vent sites, although the magnitude of the depletion varied among them. No comparable temporal trend was observed at Hot and control sites, which maintained more enriched and stable $\delta^{13}C$ values throughout the study period.

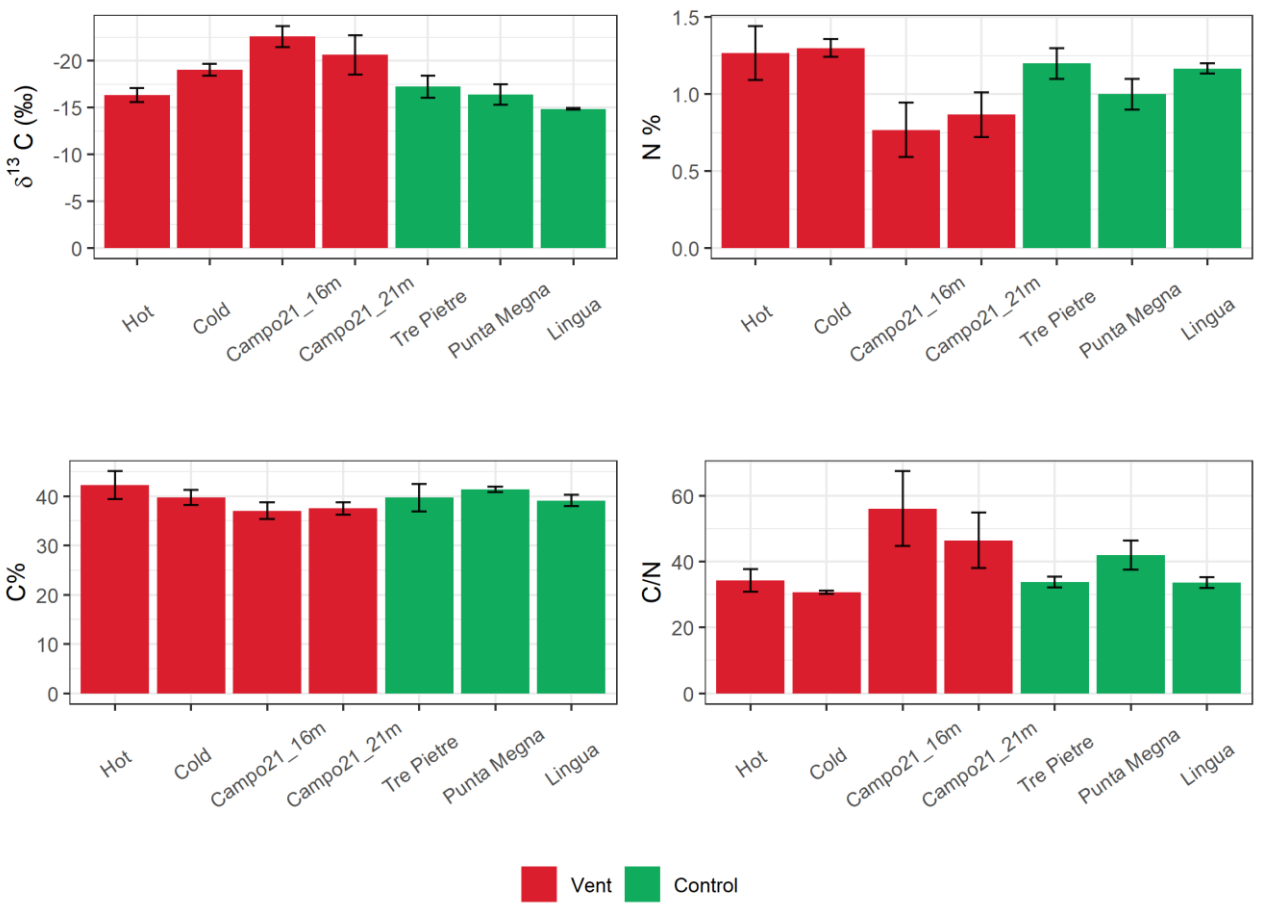

Figure 5.3.4.9. Mean (± SD) carbon isotopic composition ($\delta^{13}C$), elemental concentrations (total nitrogen, N; total carbon, C; total organic carbon, TOC) and elemental ratios (C/N) in *P. oceanica* leaves across the study sites in September 2024.

Table 5.3.4.7. Univariate PERMANOVA results for carbon isotopic composition ($\delta^{13}C$), elemental concentrations (total nitrogen, N and total carbon, C) and elemental ratio (C/N) in *P. oceanica* leaves the study sites in September 2024. Significant values are indicated in red

a) Main test		$\delta^{13}C$		N		C/N		C	
Source of variation	**df**	**Pseudo-F**	**p**	**Pseudo-F**	**p**	**Pseudo-F**	**p**	**Pseudo-F**	**p**
Site (St)	6	5.7	0.006	2.9	0.048	2.5	0.049	1.0	0.429
Residuals	14								

b) Pairwise tests	$\delta^{13}C$	N	C/N
Between sites	**p**	**p**	**p**
Hot, Cold	0.063	0.830	0.365
Hot, Campo21_16m	0.008	0.014	0.037
Hot, Campo21_21m	0.136	0.047	0.029
Hot, Tre Pietre	0.557	0.725	0.893
Hot, Punta Megna	0.963	0.257	0.249
Hot, Lingua	0.131	0.614	0.862
Cold, Campo21_16m	0.048	0.044	0.023
Cold, Campo21_21m	0.530	0.033	0.035
Cold, Tre Pietre	0.269	0.436	0.156
Cold, Punta Megna	0.101	0.084	0.064
Cold, Lingua	0.002	0.161	0.168
Campo21_16m, Campo21_21m	0.466	0.584	0.548
Campo21_16m, Tre Pietre	0.039	0.004	0.018
Campo21_16m, Punta Megna	0.025	0.257	0.306
Campo21_16m, Lingua	0.008	0.084	0.134
Campo21_21m, Tre Pietre	0.225	0.171	0.232
Campo21_21m, Punta Megna	0.157	0.485	0.645
Campo21_21m, Lingua	0.044	0.138	0.193
Tre Pietre, Punta Megna	0.661	0.327	0.164
Tre Pietre, Lingua	0.137	0.906	0.932
Punta Megna, Lingua	0.219	0.236	0.147

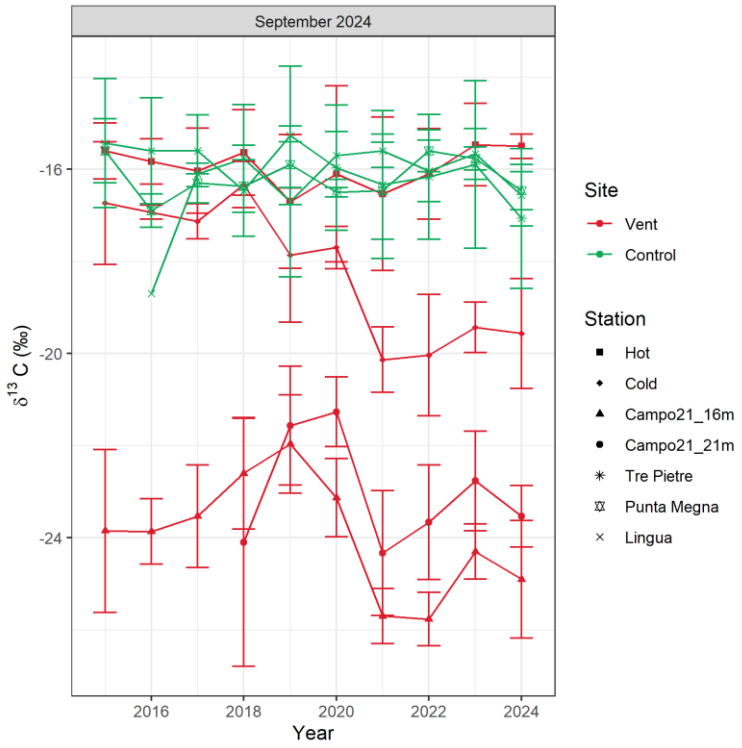

Figure 5.3.4.10. Mean (±SD) annual *P. oceanica* carbon isotopic composition ($\delta^{13}C$) of rhizome scales across the study sites in September 2024.

Lastly, sulfur isotopic composition ($\delta^{34}S$) and elemental content (S%) in *P. oceanica* leaves and roots showed clear tissue- and area-dependent patterns across the study seasons (Figure 5.3.4.11, Table 5.3.4.8).

Overall, $\delta^{34}S$ values were consistently higher in leaves than in roots, indicating a differential incorporation of sulfur between above- and belowground tissues. Furthermore, vent sites generally exhibited lower and more variable values compared to control sites, particularly in root tissues. Within the vent area, Campo21 sites showed the lowest $\delta^{34}S$ values especially in roots, while Hot and Cold displayed intermediate signatures. Control sites were characterized by higher and more homogeneous $\delta^{34}S$ values in leaves, with limited differences among sites, while Punta Megna showed significant lowest values in roots. Seasonal variability was moderate, with slightly higher and more homogeneous $\delta^{34}S$ values observed in September 2024 compared to May 2025, especially in leaves. Sulfur content (S%) also differed between tissues and sites, while seasonal differences were less marked. In both seasons and tissues, S% values were generally higher at vent sites than at control sites.

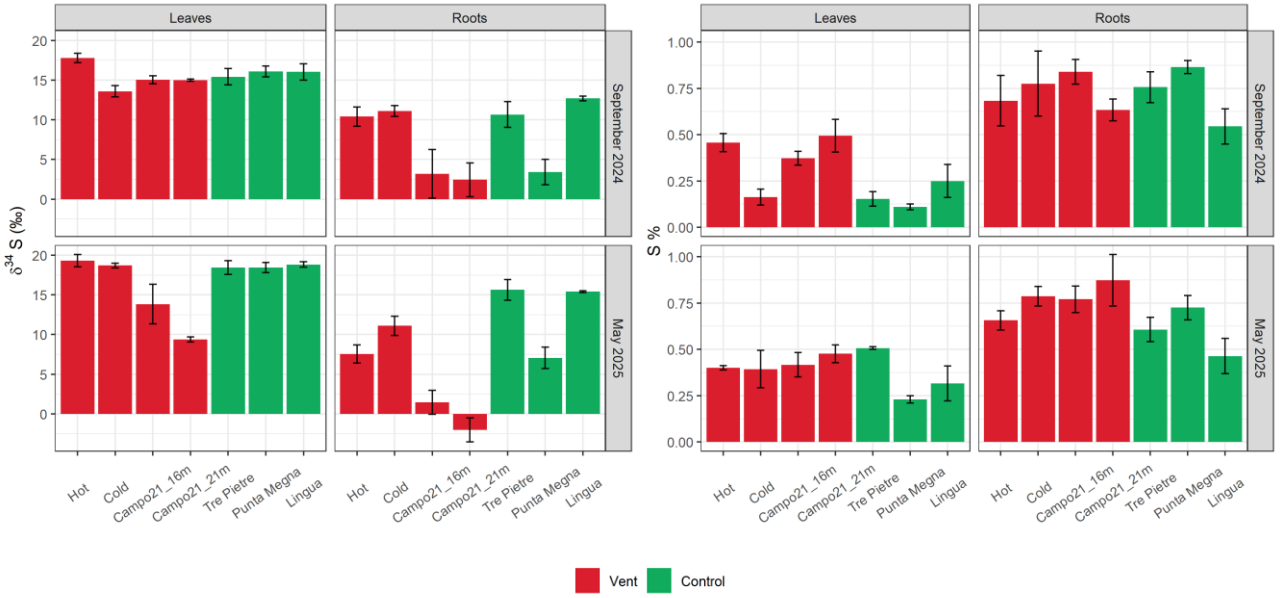

Figure 5.3.4.11. Mean (± SD) sulphur isotopic composition ($\delta^{34}S$) and elemental concentration (total sulphur S) in *P. oceanica* leaves and roots across the study sites and seasons.

Table 5.3.4.8. Univariate PERMANOVA results for sulphur isotopic composition ($\delta^{34}S$) and elemental concentration (total sulphur, S) in *P. oceanica* leaves and roots across the study sites and seasons. Significant values are indicated in red

		$\delta^{34}S$				S%			
a) Main test		**Leaves**		**Roots**		**Leaves**		**Roots**	
Source of variation	**df**	**Pseudo-F**	**p**	**Pseudo-F**	**p**	**Pseudo-F**	**p**	**Pseudo-F**	**p**
Season (Se)	1	5.19	0.032	0.13	0.714	11.14	0.007	0.39	0.545
Site (St)	6	10.79	0.001	22.53	0.001	6.44	0.002	2.45	0.048
Se x St	6	7.20	0.001	2.45	0.041	2.94	0.033	1.10	0.405
Residuals	28								

b) Pairwise tests	**Leaves**		**Roots**		**Leaves**		**Roots**
1) Between sites within seasons	**S24**	**M25**	**S24**	**M25**	**S24**	**M25**	**2) Between sites across seasons**
	p	**p**	**p**	**p**	**p**	**p**	**p**
Hot, Cold	0.014	0.84	0.726	0.029	0.007	0.945	0.309
Hot, Campo21_16m	0.001	0.003	0.008	0.027	0.23	0.833	0.173
Hot, Campo21_21m	0.002	0.004	0.035	0.008	0.724	0.202	0.463
Hot, Tre Pietre	0.896	0.116	0.883	0.011	0.013	0.418	0.888
Hot, Punta Megna	0.078	0.258	0.035	0.816	0.003	0.004	0.284
Hot, Lingua	0.37	0.158	0.211	0.003	0.023	0.002	0.145
Cold, Campo21_16m	0.003	0.014	0.023	0.008	0.017	0.839	0.77
Cold, Campo21_21m	0.002	0.013	0.046	0.002	0.029	0.525	0.799
Cold, Tre Pietre	0.048	0.756	0.858	0.047	0.857	0.878	0.291
Cold, Punta Megna	0.026	0.176	0.039	0.011	0.311	0.003	0.874

Cold, Lingua	0.045	0.343	0.164	0.024	0.395	0.016	0.023
Campo21_16m, Campo21_21m	0.976	0.004	0.043	0.175	0.265	0.509	0.576
Campo21_16m, Tre Pietre	0.128	0.001	0.015	0.002	0.019	0.254	0.125
Campo21_16m, Punta Megna	0.145	0.001	0.971	0.015	0.004	0.058	0.886
Campo21_16m, Lingua	0.256	0.001	0.025	0.001	0.264	0.424	0.008
Campo21_21m, Tre Pietre	0.645	0.001	0.038	0.002	0.018	0.576	0.471
Campo21_21m, Punta Megna	0.671	0.001	0.767	0.022	0.011	0.012	0.685
Campo21_21m, Lingua	0.341	0.001	0.033	0.002	0.014	0.021	0.059
Tre Pietre, Punta Megna	0.36	0.768	0.018	0.021	0.365	0.001	0.168
Tre Pietre, Lingua	0.565	0.250	0.404	0.882	0.395	0.012	0.037
Punta Megna, Lingua	0.996	0.476	0.042	0.004	0.196	0.404	0.024

b) Pairwise tests	**Leaves**		**Roots**		**Leaves**	
Between seasons within sites	**cfr**	**p**	**cfr**	**p**	**cfr**	**p**
Hot	S24 = M25	0.192	S24 = M25	0.153	S24 = M25	0.339
Cold	**M25 < S24**	0.004	S24 = M25	1.000	S24 = M25	0.099
Campo21_16m	S24 = M25	0.658	S24 = M25	0.647	S24 = M25	0.578
Campo21_21m	**S24 < M25**	0.001	S24 = M25	0.160	S24 = M25	0.891
Tre Pietre	S24 = M25	0.078	S24 = M25	0.081	**M25 < S24**	0.001
Punta Megna	S24 = M25	0.080	S24 = M25	0.217	**M25 < S24**	0.014
Lingua	S24 = M25	0.060	**M25 < S24**	0.003	S24 = M25	0.660

✓ Response of *Posidonia oceanica* to abiotic drivers

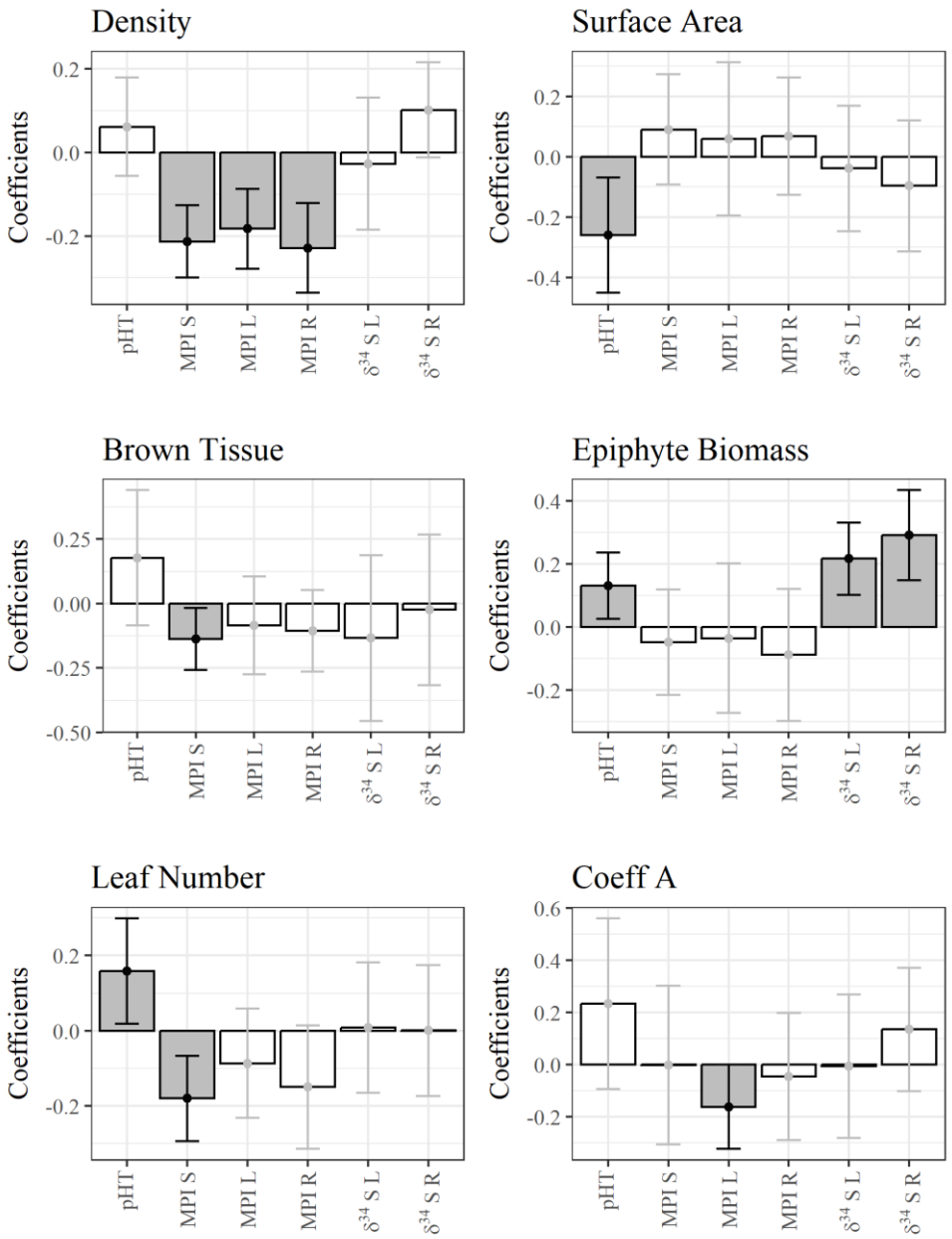

Figure 5.3.4.12. PLS regression models

All Partial least squares (PLS) regression multivariate models indicated that several explanatory variables significantly influenced *P. oceanica* (Figure 5.3.4.12). pH_T had a significant negative effect on surface area, while positively affecting epiphyte biomass and leaf number. The Sediment Multiple Pollutant Index (MPI S) created considering only non-essential trace elements (As, Cd, Cr, Hg, Pb), showed significant negative effects on *P. oceanica* shoot density, brown tissue, and leaf number. Leaf MPI (MPI L) negatively affected shoot density and coefficient A, whereas Root MPI (MPI R) exhibited a negative effect only on shoot density. Finally, $\delta^{34}S$ of both leaves and roots had a positive effect on epiphyte biomass only.

5.4 Discussion

5.4.1 Seawater

The characterization of the water column revealed substantial spatial and temporal variability associated with hydrothermal activity at Panarea, while the Salina sites exhibited stable conditions typical of non-vent Mediterranean coastal environments. Continuous pH monitoring during the September 2024 deployment showed pronounced fluctuations, most notably the extreme minimum of 6.8 ± 0.48 recorded in the Hot site, highlighting the dynamic nature of shallow CO_2 venting, where degassing intensity may vary on hourly to diel timescales. Such extreme short-term depressions are consistent with episodic CO_2 pulses previously described for Panarea (Saidi et al., 2023), as well as for other Mediterranean volcanic CO_2 seeps where vent turbulence and hydrothermal plume oscillations generate rapid pH shifts (Karuza et al., 2012; Price et al., 2017). In contrast, the Cold site displayed the least acidified and most stable pH signal among the impacted areas, consistent with earlier observations that distinct vent subzones at Panarea can sustain different geochemical signatures and degassing dynamics (Price et al., 2017). The narrower pH range and reduced variability observed during the May 2025 deployment, ranging from 7.96 ± 0.14 at Campo21_21m to 7.40 ± 0.40 at Campo21_16m, likely reflect seasonal changes in water-column stratification and hydrothermal plume dispersal. Similar seasonal modulation of CO_2 vent expression has been documented in Mediterranean shallow-water systems, where late-spring mixing and less pronounced vertical gradients tend to dampen chemical fluctuations (Saidi et al., 2023). Despite these seasonal differences, both campaigns consistently identified the shallow, CO_2-enriched vent sectors as the most acidified zones. Vertical CTD profiles provide additional insight into the spatial structure of acidification. Temperature, salinity, and dissolved oxygen were typical of their respective seasons, consistent with previous findings that hydrothermal influence at Panarea is highly localized for thermal and redox parameters, but extensive for pH and carbonate chemistry (Karuza et al., 2012; Price et al., 2017). During May 2025, the profile at the Hot site showed strong near-surface acidification (6.91-7.42 within the first two meters), followed by progressive attenuation with depth. This pattern reflects intense shallow degassing and subsequent dilution across the pycnocline, a mechanism previously described by Saidi et al. (2023). Conversely, the Cold site displayed an almost linear pH decrease down to 9.5 m, consistent with weaker and more diffuse vent influence and in agreement with the lesser temporal variability revealed by HOBO time series. The pH structure at Campo21_16m differed markedly, with pH values exceeding 8.0 near the surface and declining sharply below the thermocline, reaching <7.0 at 10-12 m. This deepening of the acidification signal is consistent with the downward transport of dense, CO_2-rich hydrothermal fluids, a process also reported in previous characterizations of this sector (Price et al., 2017). The strong vertical gradient and the depth of the minimum suggest a plume-driven accumulation of high-CO_2 waters whose extent likely varies with currents and vent flux intensity. By contrast, the Salina control sites (Punta Megna and Tre Pietre) showed typical early-summer stratification with minimal pH variation along the water column, reflecting stable, non-hydrothermal conditions. These reference profiles reinforce the strong geochemical contrast between the Panarea vents and surrounding waters, confirming that the observed chemical patterns are driven by localized hydrothermal CO_2 emissions rather than basin-wide seasonal variability. Overall, the combination of continuous pH monitoring and vertical profiling demonstrates that acidification at Panarea is both spatially heterogeneous and temporally dynamic.

The physicochemical patterns observed across the hydrothermal sites of Panarea (Hot-Cold and Campo21) and the control sites at Salina further highlight the strong influence of volcanic CO_2 emissions on seawater carbonate chemistry and nutrient dynamics, with clear implications for *P. oceanica* meadow functioning. The significantly lower pHT values recorded in May 2025 compared to September 2024, together with consistently lower pHT in impacted relative to control sites, confirm that CO_2 venting exerts a persistent acidifying effect. The exception of Cold in September (pHT = 8.01) underscores the inherent variability of vent systems where, as previously stated, degassing intensity, stratification, and local hydrodynamics may temporarily dampen or enhance acidification. Among all stations, Campo21_16m exhibited the strongest acidification (pHT = 7.88 in September; 7.30 in May), suggesting a higher or more sustained CO_2 flux. These values fall within the range reported for other Mediterranean volcanic seeps, reinforcing the role of Campo21 as a relevant natural analogue for future ocean acidification. Total alkalinity (TA) was remarkably similar between Panarea and Salina, indicating that hydrothermal systems predominantly increase dissolved inorganic carbon (DIC) without reducing TA, thereby generating strong pH decreases

without affecting buffering capacity (Karuza et al., 2012). This supports the interpretation that the low pHT observed at Panarea is primarily driven by CO_2-rich hydrothermal fluids. The lowest saturation states of ΩCa and ΩAr at Campo21_16m indicate reduced thermodynamic potential for calcium carbonate precipitation. This agrees with previous analyses documenting conditions unfavorable for carbonate formation near Panarea vents (Karuza et al., 2012; Price et al., 2017). Reduced carbonate saturation can constrain calcifying organisms and alter epiphytic communities associated with *P. oceanica*, with potential consequences for meadow structure and sediment stability. Nutrient distribution patterns also reflect hydrothermal influence. Silicate was consistently the most abundant nutrient and reached its maximum at Hot, consistent with silica-rich hydrothermal inputs described for Mediterranean shallow vents. Nitrate also peaked at Hot, likely due to enhanced regeneration or localized upwelling driven by vent turbulence. Ammonia, highest at Cold, may reflect reductive processes or sedimentary mineralization associated with venting. Nitrite remained low and phosphate was generally below detection, indicating phosphorus limitation across the system except at Campo21_21m. Saidi et al. (2023) demonstrated that Panarea venting alters nutrient availability and stimulates microbial enzymatic activity, influencing biogeochemical pathways. The combined nutrient patterns indicate fine-scale heterogeneity that may affect productivity and microbial dynamics within *P. oceanica* meadows.

Together, the observed decreases in pHT, reduced carbonate saturation, and altered nutrient regimes are fully consistent with previous work on Panarea's shallow-water hydrothermal fields. These results confirm that Panarea represents a dynamic natural analogue for ocean acidification, where hydrothermal CO_2 emissions and associated geochemical processes create environmental conditions that closely resemble future acidified oceans.

5.4.2 Interstitial water

The interstitial water chemistry revealed marked contrasts between the hydrothermal sites of Panarea and the non-vent environments of Salina, reflecting the strong influence of volcanic inputs on sediment geochemistry. Sediment temperatures at Panarea reached extremely high values (41°C in September 2024 and up to 54°C in May 2025 at the Hot site), consistent with direct hydrothermal heating. Similar high sediment temperatures have been reported for shallow vents in Panarea and other Mediterranean volcanic systems, where conductive and advective heat fluxes create steep thermal gradients within only a few centimeters of the sediment surface (Price et al., 2017; Monecke et al., 2012). In contrast, Salina exhibited temperatures within the expected seasonal range for Mediterranean seagrass meadows (20-27°C), highlighting the absence of geothermal influence.

Redox potential (Eh) showed strong spatial variability, with Panarea exhibiting the lowest values in May 2025 (down to -221 and -234 mV at Campo21_21m). Such reducing conditions are characteristic of CO_2-rich hydrothermal sediments, where high organic matter degradation, sulfide accumulation, and metal-rich fluids contribute to redox depletion (Di Bella et al., 2022; German & Von Damm, 2006). The substantially higher Eh values measured at Salina (-70 to -8.4 mV) are typical of well-oxygenated *Posidonia oceanica* sediments, where rhizome oxygen leakage and active bioturbation help maintain less reducing conditions (Mateo et al., 2006).

Ammonium concentrations were consistently higher at Panarea than at Salina in both seasons, reflecting enhanced remineralization and possibly ammonium-rich hydrothermal pore fluids. The comparatively lower ammonium levels at vegetated sites in Panarea suggest that *P. oceanica* may partially modulate sediment biogeochemistry, likely through oxygen release from roots and rhizomes and enhanced uptake by plant–microbe consortia, a process observed in other seagrass ecosystems subjected to reducing conditions (Marbà et al., 2006). Nitrate patterns differed strikingly between islands. Salina showed exceptionally high nitrate concentrations in September 2024 (up to 330.6 mg L^{-1} at the vegetated site), far exceeding typical values for Mediterranean sediments. In contrast, Panarea nitrate concentrations were much lower across both campaigns, consistent with suppressed nitrification in hydrothermal sediments dominated by reducing and ammonium-rich conditions (Di Bella et al., 2022). Bicarbonate concentrations showed considerable variability between islands and seasons, with generally higher values at Panarea, particularly in May 2025 (98-141 mg L^{-1}). This enrichment is consistent with dissolution of CO_2-rich fluids into interstitial waters, as documented in previous studies showing that hydrothermal CO_2 contributes substantially to DIC accumulation in both pore waters and the overlying water column (Karuza et al., 2012; Hall-Spencer et al.,

2008). The near-zero bicarbonate concentrations recorded at Salina in May 2025 likely reflect methodological or detection-limit constraints, but the overall trends support the interpretation that hydrothermal CO_2 strongly shapes carbonate chemistry at Panarea. In contrast to the strong differences detected for redox parameters, nutrients, and bicarbonate, major ions (Na^+, Mg^{2+}, Ca^{2+}, Cl^-, Br^-, SO_4^{2-}) showed no consistent differences between islands or seasons. This is expected for shallow hydrothermal systems where fluids are dominated by magmatic CO_2 rather than by high-temperature endmember fluids that cause major deviations in ionic composition (Price et al., 2017; Italiano & Nuccio, 1991).

The presence of *P. oceanica* had a notable influence on interstitial chemistry at both islands, although the direction and magnitude differed by site. At Panarea, vegetated sediments showed higher Eh and lower ammonium than unvegetated ones, consistent with the oxygenating effect of seagrass roots and their capacity to limit anaerobic processes. At Salina, however, vegetated sites exhibited lower Eh than unvegetated ones, possibly reflecting higher sediment organic content and enhanced microbial decomposition beneath dense canopies, a pattern frequently observed in healthy *P. oceanica* meadows (Mateo et al., 2006).

Overall, interstitial water chemistry clearly distinguishes hydrothermal from non-hydrothermal sediments, with Panarea characterized by elevated temperatures, reducing conditions, enhanced ammonium, suppressed nitrate, and elevated bicarbonate. These patterns align with previous geochemical studies of Mediterranean volcanic CO_2 vents (Karuza et al., 2012; Price et al., 2017; Di Bella et al., 2022) and reinforce the role of Panarea as a natural laboratory for studying the sedimentary consequences of long-term acidification.

5.4.3 Sediment

The distribution and concentration of trace elements in surface sediments from the Panarea hydrothermal area reflected the complex interaction between localized hydrothermal inputs and environmental and sedimentary processes, suggesting the coexistence of multiple controlling processes. The low pH driven by CO_2 emissions may enhance metal solubility and sediment–water exchanges, while elevated temperatures and reducing porewaters associated with sulfide emissions promote selective metal immobilization (German & Von Damm, 2006; Pichler, 2024).

Hg and Cr showed higher concentrations overall at vent sites, consistent with hydrothermal fluids acting as natural sources of volatile and element-rich compounds in shallow vent systems (Dando et al., 1999; Vizzini et al., 2013). This interpretation agrees with previous investigations conducted in the Panarea hydrothermal field, which documented significant trace element enrichment in sediments and biota following intense degassing episodes (Renzi et al., 2011, Andaloro et al., 2012). More recent studies have confirmed that hydrothermal fluids and associated porewaters at Panarea may contain extremely elevated Hg concentrations, with strong spatial heterogeneity linked to vent intensity and temperature (Pichler, 2024). The particularly high Hg concentrations observed at the Campo21 sites likely reflect efficient trapping under reducing and sulfide-rich sediment conditions, where precipitation of mercury sulfide minerals can lead to localized accumulation (Pichler, 2024). In contrast, As enrichment at Hot and Cold sites is consistent with stronger direct exposure to hydrothermal fluxes, as arsenic is commonly associated with magmatic degassing and high-temperature water–rock interactions (German & Von Damm, 2006; Price et al., 2013). Most other trace elements (Cd, Cu, Pb, V and Zn) and Fe were generally higher at Hot and Cold than at Campo21, while Campo21 sediments were often comparable to those at Salina. This suggests that their distribution is not controlled by hydrothermal inputs alone but is also influenced by sedimentary factors such as grain size and organic matter content (Signa et al., 2017). Mn displayed a distinct behaviour, with consistently higher concentrations at Salina and progressive decrease toward vent sites. Because Mn is highly sensitive to redox conditions and becomes mobilized under reducing environments, this pattern likely reflects dissolution and diffusion from sulfide-rich hydrothermal sediments (Canfield et al., 2005).

Multivariate analyses corroborate these interpretations: PCA and PERMANOVA clearly separated vent from control sites and further distinguished subzones within the vent field, confirming that spatial variability is the dominant source of variation and that hydrothermal systems should not be treated as geochemically uniform environments.

From a regulatory perspective, frequent exceedances of Italian sediment quality thresholds (GURI 2015; 2016) were observed for As and Hg at several vent sites, indicating a potential risk of bioaccumulation in biota. More localized exceedances for Cu and Pb suggest that both vent and some control sediments may act as long-term reservoirs of trace element enrichment. Although Cr and Ni remained below regulatory limits, the absence of thresholds for Mn and V prevents a complete risk assessment for these redox-sensitive elements.

Sediment elemental and isotopic composition further supports the interpretation of a hydrothermally influenced but spatially heterogeneous environment. Higher total and organic carbon and nitrogen contents at vent sites, particularly at Campo21, indicate enhanced organic matter accumulation relative to most control areas. $\delta^{13}C$ values were comparatively homogeneous and more depleted across vent sites, whereas both $\delta^{13}C$ and Corg/N ratios displayed clearer spatial gradients at control areas, suggesting that organic matter at Panarea results from the mixing of multiple sources. Indeed, the combined $\delta^{13}C$ *vs.* Corg/N signatures indicate that sediment organic matter does not primarily derive from *P. oceanica*, as most values fall outside the typical isotopic and elemental ranges reported for seagrass material. Instead, they overlap with values characteristic of bacteria, marine algae and plankton-derived particulate and dissolved organic carbon (Lamb et al., 2006), pointing to a mixed contribution of microbial and marine sources. In vent areas, enhanced microbial activity and altered carbon cycling driven by CO_2 enrichment may blur isotopic distinctions between primary producers and detrital pools, generating relatively homogeneous $\delta^{13}C$ signatures across impacted sites. Comparable isotopic homogenization has been described for Panarea and other shallow CO_2 vent systems (Andolina et al., 2025). The absence of a detectable $\delta^{15}N$ signal could indicate rapid nitrogen cycling under strongly reducing sediment conditions.

5.4.4 Posidonia oceanica

The structural and functional responses of *Posidonia oceanica* meadows at Panarea reflect the persistent influence of hydrothermal stressors on plant performance. Vent sites were characterized by consistently lower shoot density and younger shoot age compared to controls, indicating a simplified and more homogeneous population structure. Such patterns are consistent with chronic environmental stress limiting long-term shoot survival, as previously observed in disturbed or extreme environments where *P. oceanica* meadows shift toward faster turnover and reduced structural complexity (Vizzini et al., 2010; Gambi et al., 2023).

Seasonal and spatial variability in phenological traits suggests that vent exposure affects leaf dynamics and tissue condition despite a certain spatial and metric-dependent variability. The lower Coefficient A (eroded leaf apices) at vent sites indicates reduced herbivory, contrasting with controls. This suppressed herbivory at Panarea likely reflects toxic effects of hydrothermal co-stressors (H_2S, trace metals) on herbivore communities. However, elevated Coefficient A at some vent sites suggests that physical or chemical stress can also impair leaf integrity directly, as previously documented by Signa et al. (2024) for *P. oceanica* under combined low pH and sulfide exposure from other Panarea areas. These contrasting patterns highlight the complexity of plant-herbivore interactions in multi-stressor hydrothermal systems. Similarly, the pronounced spatial variability and seasonal variability in epiphyte biomass, particularly at vent areas, also indicates that hydrothermal conditions indirectly modulate meadow functioning by altering epiphytic communities and plant–epiphyte interactions.

Lepidochronological reconstructions reveal that vent meadows are characterized by highly variable growth trajectories and recent declines in rhizome primary production, especially after 2020, suggesting unstable growth conditions. The coexistence of decreasing and fluctuating production and growth rates may indicate a shift in carbon allocation strategies under chronic stress. Comparable patterns of altered growth dynamics and resilience trade-offs have been described in *P. oceanica* meadows subjected to disturbance due to environmental extremes (Noé et al., 2020; Gambi et al., 2023).

Trace element analyses demonstrate that vent conditions strongly influence metal accumulation in *P. oceanica*, with roots acting as the primary sink. Elevated concentrations of As, Cd, Cr, Hg, Fe, Mn, Pb and V in vent plants mirror the geochemical enrichment of surrounding sediments and confirm the tight coupling between sediment chemistry and plant uptake (Vizzini et al., 2013; Signa et al., 2024b). High bioconcentration

factors for Cd, Cu, Hg and Mn, particularly at Campo21, indicate an efficient capacity of belowground tissues to accumulate sediment-derived elements, while heterogeneous translocation to leaves suggests element-specific regulation of internal transport. Such compartmentalization is consistent with the role of seagrasses as partial biogeochemical buffers that can sequester contaminants in belowground tissues (Vizzini et al., 2010, Signa et al., 2024b).

Isotopic signatures provide additional insight into physiological functioning under vent influence. More depleted and temporally variable $\delta^{13}C$ values in vent rhizomes, especially at Campo21, indicate long-term modifications in carbon acquisition consistent with persistent exposure to CO_2-enriched waters. Similar isotopic shifts have been documented in seagrasses growing near volcanic vents, where elevated dissolved CO_2 alters carbon assimilation pathways and growth efficiency (Noè et al., 2020, Vizzini et al., 2010). Moreover, lower and more variable $\delta^{34}S$ values in vent tissues, together with higher sulfur content, further reflect the incorporation of hydrothermal sulfur and exposure to sulfide-rich sediments. This pattern supports the interpretation that vent meadows operate under altered redox and sulfur cycling regimes that influence both below- and above-ground tissues.

5.4.5 Integration of abiotic and biotic

Partial Least Squares (PLS) regression models integrating seawater pH, trace element concentrations in sediments and plant tissues (leaves and roots), and sulfur isotopic composition ($\delta^{34}S$) in below- and aboveground compartments revealed multiple pathways through which hydrothermal conditions influence *Posidonia oceanica* performance.

Shoot density, leaf number, and brown tissue percentage exhibited significant negative associations with trace element indices in sediments (MPI_S) while only shoot density also with trace element indices in leaves, and roots (MPI_L, MPI_R), confirming that metal bioavailability and accumulation constrain meadow structure and foliar dynamics independently of pH effects. These patterns are consistent with toxicity-driven reductions in photosynthetic capacity and carbon allocation to new tissue production (Prange and Dennison, 2000; Marbà et al., 2007). The lack of—or contrasting—pH associations with these metrics differ markedly from Signa et al. (2024b) at a different Panarea vent area (Bottaro), where low pH increased leaf number and brown tissue while reducing leaf size. This discrepancy likely reflects area-specific differences in trace metal contamination: the dominant negative effects of MPI_S in our study suggest that metal toxicity—not characterized by Signa et al. (2024)—may override or modulate pH-driven compensatory responses (accelerated turnover, premature senescence) observed at less trace element-impacted areas. The negative relationship between leaf surface area and seawater pH—implying larger leaves under lower pH—also contrasts with ocean acidification studies where chronic low pH typically and sulfur exposure reduces *P. oceanica* leaf size (Gambi et al., 2023). This counterintuitive pattern may reflect transient CO_2 fertilization effects that temporarily enhance leaf growth before chronic stress impacts prevail (Repolho et al., 2017), or confounding effects of spatial variability in trace metal contamination and unmeasured co-stressors (*e.g.* H_2S, light availability) that may obscure the true pH-leaf size relationship.

Epiphyte biomass showed positive associations with pH and $\delta^{34}S$ in both leaves and roots, suggesting that acidification and altered sulfur cycling—particularly low pH and the incorporation of hydrothermally derived, ^{34}S-depleted sulfur—may modulate epiphytic community structure. Particularly, the reduction in epiphyte biomass near the vents is consistent with the classic response of calcifying epibionts to ocean acidification (Hall-Spencer et al. 2008, Nogueira et al. 2017).

5.5 Conclusions

The integrated analysis of seawater chemistry, interstitial processes, sediment geochemistry and *Posidonia oceanica* responses shows that the Panarea hydrothermal system functions as a tightly coupled multi-compartment environment in which CO_2-driven acidification, redox dynamics and metal enrichment interact across spatial scales. Hydrothermal emissions generate highly heterogeneous and temporally dynamic water-column conditions, characterized by persistent acidification, reduced carbonate saturation

and altered nutrient regimes. These signals extend to sediments, where elevated temperatures and reducing porewaters modify elemental cycling and trace metal distributions, producing geochemical patterns that differ substantially from non-vent Mediterranean environments.

Sediment records captured the long-term imprint of hydrothermal forcing and highlight the coexistence of multiple geochemical controls, confirming that vent systems should be considered spatially structured environments rather than uniform settings. These sedimentary conditions are reflected in the biology of *P. oceanica*, whose meadows display signatures of chronic hydrothermal influence, including reduced structural complexity, altered growth dynamics, enhanced metal accumulation and modified isotopic composition. Multivariate modelling further indicates that these responses arise from the combined action of acidification, metal exposure and altered sulfur cycling, rather than from single stressors acting in isolation.

Together, these findings indicate that *P. oceanica* can persist under sustained exposure to combined chemical stressors, but that hydrothermal conditions may constrain long-term meadow stability and ecosystem functioning. The observed coupling between environmental chemistry and plant performance supports the need for integrated assessments that simultaneously consider water-column, sedimentary and biological processes when evaluating the impacts of global change drivers on seagrass ecosystems.

Within the broader framework of this project, Panarea provides a valuable natural setting for examining how warming, acidification and contamination interact to influence the functionality of a key Mediterranean habitat. The results contribute to improving our understanding of the capacity of *P. oceanica* meadows to act as biological buffers under multi-stressor conditions and provide a reference baseline for assessing future changes in coastal ecosystem structure and functioning.

6 Understanding polymer fate in the context of climate change: A chemical, physical and biological study in the natural hydrothermal laboratory of the Aeolian Archipelago

6.1 Introduction

In coastal regions, physical, chemical, and biological pressures co-occur, creating a multistressor framework that challenges ecosystem resilience and biodiversity maintenance (Gunderson et al., 2016). Among the most pervasive pressures are plastic pollution, anthropogenic disturbance and climate-driven changes such as ocean warming and acidification, whose interactions frequently produce non-linear and sometimes synergistic ecological responses (Crain et al., 2008; Côté et al., 2016). Plastic contamination represents a major threat in marine environments, where macro- and microplastics accumulate in seawater, sediments and organisms, altering physiological processes, community structure and biogeochemical functioning (Thushari & Senevirathna, 2020; Law 2017). In semi-enclosed basins such as the Mediterranean Sea, high population density and intense maritime traffic further enhance plastic persistence and fragmentation, increasing the likelihood of ingestion and entanglement events and intensifying the exposure of benthic and pelagic communities. Plastics also act as vectors of chemical contaminants and microorganisms, influencing pollutant dynamics, biofilm development and microbial colonization patterns (Zettler et al., 2013; Amelia et al., 2021). At the same time, anthropogenic activities, including shipping, fisheries, aquaculture, urbanization and tourism, intensify nutrient and contaminant inputs, degrade habitats and reduce the recovery capacity of ecosystems from disturbance events (Halpern et al., 2015). Ocean acidification adds another major stressor, altering carbonate chemistry and impacting calcification, metabolism and ecological interactions across multiple trophic levels (Orr et al., 2005; Doney et al., 2009; Figuerola et al., 2021). When acting simultaneously with plastic pollution or local pressures, acidification can accelerate polymer degradation, alter leachate chemistry and modulate biological responses, thereby amplifying the ecological consequences of plastic exposure (Vuong 2023; Dayananda et al., 2025).

Within this context, the present study evaluates the colonization, degradation and ecotoxicological response behavior of two conventional polymers (PE, PP) and two biodegradable polymers (PLA, Mater-Bi) (Figure 6.2.1.1), deployed for up to six months at different sites characterized by contrasting environmental conditions of acidification, hydrothermal activity, and human impact (Figure 6.2.1.2).

6.2 Materials and methods

6.2.1 Study area

The Aeolian Archipelago, located in the central Tyrrhenian Sea off the northeastern coast of Sicily, is a complex of seven volcanic islands that represents a natural laboratory for studying interactions between geochemical and biological processes. The area is characterized by strong environmental gradients driven by natural volcanic CO_2 emissions, which generate spatial variation in pH, temperature, and water chemistry. In addition, the archipelago experiences variable levels of anthropogenic pressure linked to tourism, maritime traffic, and coastal settlements (Boatta et al., 2013; Carapezza et al., 2011).

At six selected sites, - three on the island of Vulcano and three on the island of Lipari (Figure 6.2.1.2, Table 6.2.1.1) - chosen for their differing environmental conditions (pH and temperature) and varying intensities of anthropogenic activity, stainless steel containers (Figure 6.2.1.3) were deployed in September 2024, each containing four different types of polymers. To avoid contamination, microplastics have been cut from virgin sterilized macrocontainers of the same polymer and inserted into each macrocontainer (Figure 6.2.1.1). Depending on the type of analysis, macrocontainers with microplastics were collected after 3 (t1) or 6 (t2) months of placement to conduct (i) biological assessments of macrofouling and microfouling communities developed on polymer surfaces (the plastisphere); (ii) physical degradation analyses of the plastic materials; and (iii) ecotoxicological assays to evaluate potential hazards of the exposed

microplastics. In addition, biochemical and nutritional analyses were performed on *Oblada melanurus* to investigate metabolic, protein, and lipid responses to environmental stressors. Furthermore, at each sampling site, samples for chemical characterization of the area were collected at the time of cylinder deployment.

Figure 6.2.1.1. Macrocontainers recovered at Baia di Levante after three months of deployment

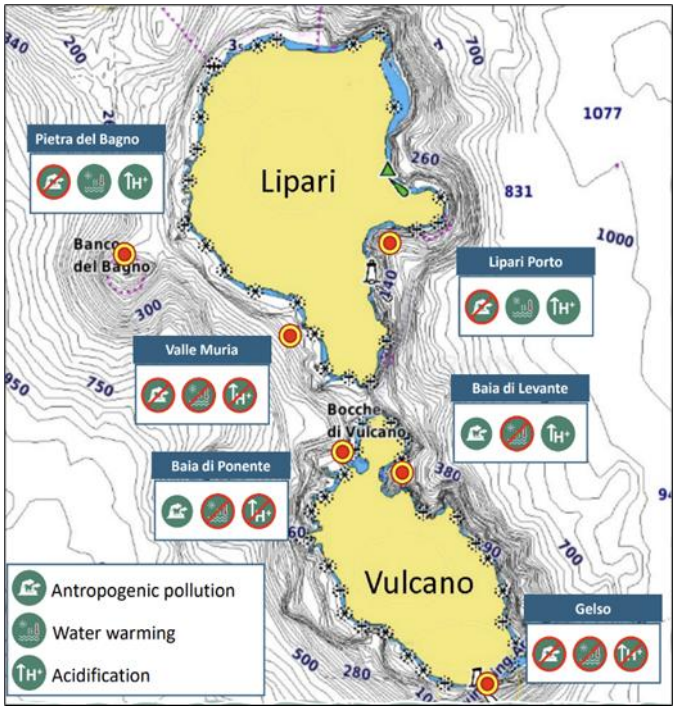

Figure 6.2.1.2. Maps of the study sites (red dots) showing the main environmental stressors in each location

Table 6.2.1.1. Coordinated and depths of study sites

ISLAND	SITE	COORDINATES		DEPTH (m)
Vulcano	Baia di Levante	38.419379 N	14.961983 E	3-4

Vulcano	Baia di Ponente	38.419220 N	14.952530 E	3-4
Vulcano – Gelso	Spiaggia Punta dell'Asino	38.368827 N	14.994507 E	3-4
Lipari	Porto	38.474828 N	14.956564 E	3-4
Lipari	Spiaggia Valle Muria	38.458923 N	14.932375 E	3-4
Lipari	Pietra del Bagno	38.475117 N	14.896807 E	12

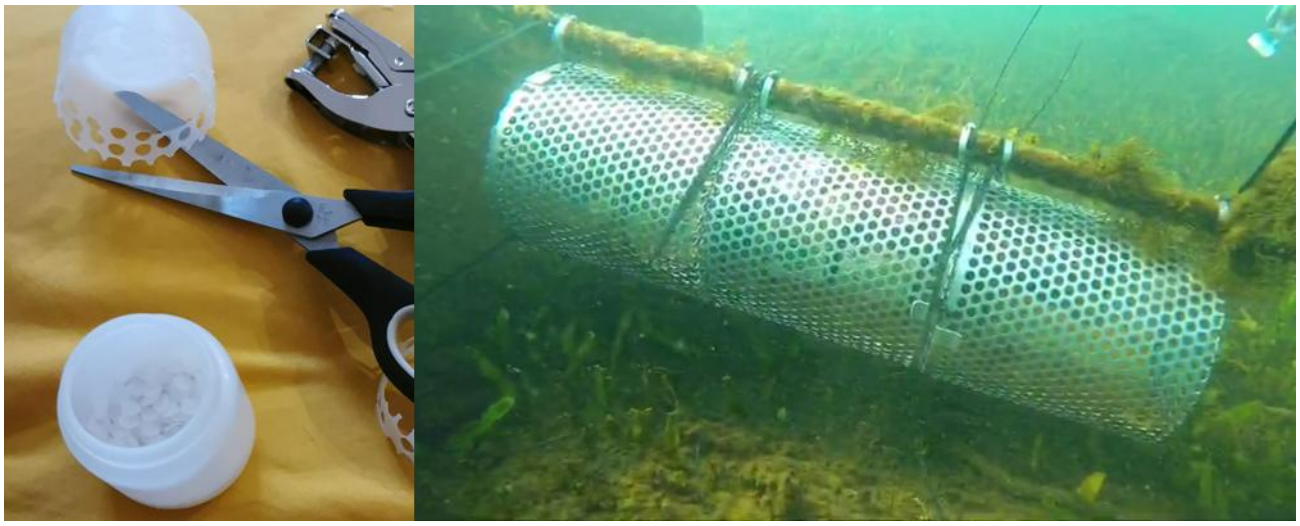

Figure 6.2.1.3. Left: Microplastics of the same polymer types cut for PE; Right: Cylinders deployed in Baia di Levante

6.2.2 Chemical characterization of study sites

Samples for all chemical analyses (sediments, seawater, DGTs, and SPMDs) were collected at t0 of the experimental.

6.2.2.1 Sediments

✓ *Polycyclic Aromatic Hydrocarbons (PAHs)*

At each study area, approximately 2.5 g of sample were weighed and extracted after addition of surrogate standards (deuterated PAHs) using an Accelerated Solvent Extractor (ASE 200, Dionex) with hexane:acetone (1:1) at 120°C and 1500 psi for two extraction cycles. The extract was washed with water to remove acetone, and the hexane phase (dried over sodium sulfate) was concentrated to a few mL with a rotary evaporator after adding 1 mL of iso-octane (EPA 3545a). The hexane fraction was purified on a silica gel column (Merck 60, 70–230 mesh, activated at 250°C for 16 h) and eluted in two fractions: F1: 10 mL hexane and F2: 30 mL hexane:dichloromethane (2:1). F2, containing PAHs, was reduced to 0.5 mL and spiked with p-terphenyl as an injection standard (EPA 3630 cleanup). Analyses were performed by GC-MS (Agilent 7890a/5975c) with a 5% phenyl-methylsiloxane capillary column (EPA 8270D). Detection used quadrupole MS with EI at 70 eV and SIM mode. Helium (N55) was used as carrier gas. Peak identification was based on retention times and mass isotope ratios. Response factors were checked regularly with calibration mixtures. Quantification followed an internal standard calibration curve. Detection limit was 0.1 µg/kg per compound.

✓ *Trace elements*

Sediment aliquots (except for Hg analysis) were oven-dried at 40°C, sieved to 2 mm, and finely ground. Trace metals were determined after microwave-assisted acid digestion (HNO_3, HF, H_2O_2). Excess HF was removed by evaporation to near dryness, followed by re-dissolution in 1% HNO_3. Analyses were conducted using ICP-MS (Agilent 7800). Calibration standards were prepared from a 10 µg/mL multielement solution. An internal standard mix (Bi, Ge, In, Li^6, Sc, Tb, Y) was used to correct matrix effects. Analytical quality was checked using blanks and certified reference materials PACS-3 and MESS-4 (NRCC). For Hg, samples were air-dried and analyzed directly using an AMA-254 Hg analyzer, with PACS-3 and MESS-4 used for quality control.

6.2.2.2 Seawater

✓ *Nutrients*

Water samples for dissolved inorganic nutrients determination (nitrite, NO2, nitrate, NO3, ammonium, NH4, phosphate PO4, and silicic acid, H4SiO4) were collected with Niskin bottles, filtered on 0.7 µm pore size glass-fibre filters (Whatman GF/F) and stored frozen (−20 °C) in polyethylene vials until laboratory analysis. Samples were defrosted and analysed colorimetrically using a segmented flow QUAATRO Seal Analytical AutoAnalyzer according to Hansen and Koroleff. The detection limits for the method were 0.01 µM, 0.02 µM, 0.03 µM, 0.01 µM, and 0.01 µM for NO2, NO3, NH4, PO4, and H4SiO4, respectively.

✓ *Trace elements*

During the sampling, seawater samples were filtered using a 0.45 µm membrane filter (Millex HA, Merck) and acidified with ultrapure 1% HNO3. Then, measurements of trace elements were performed using Agilent 7800 ICP-MS, equipped with a UHMI (Ultra High Matrix Introduction) system for the analysis of complex matrices with high salt content and, in order to suppress interferences, in He and, for As and Fe, HeHe mode. A 0.1 mg L-1 of Rh solution was used as an internal standard to compensate for any variations in instrument efficiency that could influence the measurements during analysis. The standard solutions used for the calibration curves were prepared by appropriately diluting a 10 g L-1 multi-element standard solution - Environmental Calibration Standard solution, from Agilent Technologies - in a salt matrix consisting of 3.5% NaCl (99.99 Suprapur, Merck) in H2O MilliQ and 1% di HNO3 (TraceSelectTM Ultra, Fluka), to simulate "artificial" seawater. Quality measurements were evaluated by analyzing the following certified reference materials: CASS-5, CASS-6-Nearshore Seawater Certified Reference Materials for Trace Metals and other Constituents, and ERMCA403 seawater (element content).

6.2.2.3 Semi-Permeable Membrane Devices for Polycyclic Aromatic Hydrocarbons (SPMD)

SPDM were deployed in seawater for a maximum period of 24 days (Figure 6.2.2.1). For PAH determination, membranes were extracted twice for 24 h each with 200 mL n-hexane containing surrogate standards (deuterated PAHs). Combined extracts were dried over anhydrous sodium sulfate and concentrated by rotary evaporation. Clean-up used a silica gel column (Merck 60, 70–230 mesh, activated at 250°C for 16 h), eluting: F1: 10 mL hexane; F2: 30 mL hexane:dichloromethane (2:1). F2 was reduced to 0.5 mL and spiked with p-terphenyl (EPA 3630). Analyses were performed by GC-MS (Agilent 7890a/5975c) with a 5% phenyl-methylsiloxane column, EI 70 eV, SIM mode, helium carrier gas. Peak identification was based on retention times and isotopic ratios. Quantification was via internal standard calibration. Detection limit was 0.1 µg/kg per PAH.

6.2.2.4 Diffusive Gradient in Thin films (DGT) for metal measurements

The DGTs were immersed in seawater for up to 7 days (Figure 6.2.2.2). Immediately after the passive samplers withdrawn from the sea, the devices were rinsed thoroughly with Milli-Q water. Successively, in laboratory, the metals (As, Cd, Cr, Co, Cu, Fe, Pb, Mn, Ni, V And Zn) were eluted from the binding gel in 1 ml of 2M HNO3 for 24h. The obtained extracts were diluted with Milli-Q water and trace metal analysis was carried

out by using ICP-MS (Agilent 7800). A blank resin was always considered. DGT performance was evaluated according to the method used by Zhang and Davison (Zhang and Davison, 1995). The concentrations of metals measured by DGT, in three replicates, were calculated using equations and parameters provided by Davison (2016). Analysis of total mercury concentrations in DGT units was performed using AMA 254 mercury analyzer: the chelating resin was removed from the device and directly analyzed without further preparations. A blank resin was analyzed in the same conditions, and its mercury content was always subtracted to the mercury quantity measured for the samples. The concentrations of mercury measured by DGT, in three replicates, were then calculated using equations and parameters provided by Davison (2016).

Figure 6.2.2.1. SPMD before their deployment in seawater

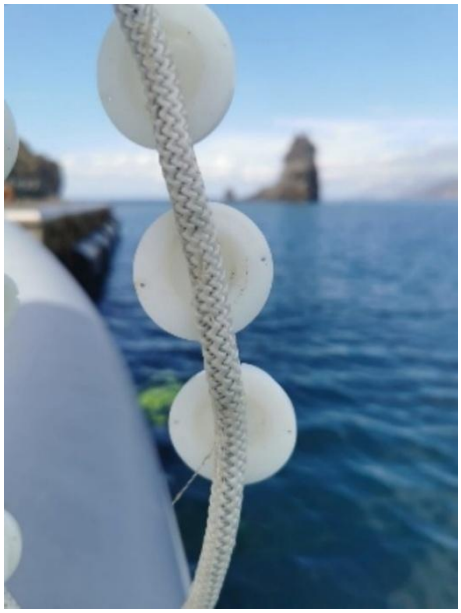

Figure 6.2.2.2. Preparation of DGT before their deployment in seawater

6.2.3 Laboratory analyses

6.2.3.1 Biological

After 3 months of deployment, the macro-containers containing microplastics were retrieved for biological analyses, as described below.

✓ *Microfouling*

For microbiological analyses, microbial communities from the surrounding seawater (T0) and those forming the plastisphere (T1, after 3 months) were compared. Seawater was collected and filtered in situ at the start of the experiment, while microfouling biofilms developing on the microplastics were analyzed after three months of exposure. Microbial communities were characterized through DNA metabarcoding targeting the 16S rRNA gene, both in seawater (T1, T*f*; 3 L filtered on 0.2 µm membranes) and on plastic fragments (T*f*; 5 fragments). DNA extraction from filters and plastics was performed using the DNeasy PowerWater Kit (Qiagen) with slight modifications to increase DNA yield (Celussi et al., 2018). DNA was quantified using a Qubit fluorometer (Thermo Fisher Scientific). The V4–V5 region of the 16S rRNA gene was amplified with primers 515-Y and 926R (Parada et al., 2016). Libraries were prepared following the 16S Metagenomic Sequencing Library Preparation protocol and sequenced on an Illumina NovaSeq 6000 platform (2 × 250 bp) at the Institute of Applied Genomics (IGA), Udine (Italy). Raw reads were inspected with FastQC and MultiQC, and primers were trimmed using cutadapt (v. 4.5). Sequences were quality-filtered and denoised using DADA2 (v. 1.32.0) in R (v. 4.4.1) with the pseudo-pooling method. Chimeras were removed using the consensus approach. Error learning parameters were adjusted to account for NovaSeq binned quality scores. Taxonomy was assigned to amplicon sequence variants (ASVs) using the sklearn naïve Bayes classifier against the SILVA 138.2 99% database (7 taxonomic levels) within QIIME2 (v. 2024.2). ASVs affiliated with Eukarya, mitochondria, chloroplasts, or with frequency < 2 were removed. Community patterns were investigated through PERMANOVA (4999 permutations; adonis function) on normalized ASV tables, and by non-metric multidimensional scaling (NMDS) based on Bray–Curtis dissimilarity using the vegan R package (Oksanen et al., 2019).

✓ *Macrofouling*

Macro-containers were retrieved with care to preserve encrusting organisms, which were fixed in 80% ethanol. In the laboratory, samples were examined under a stereomicroscope and macrofouling taxa were identified to the lowest possible taxonomic level.

6.2.3.2 Physical

FT-IR analyses were carried on microplastics after 3 and 6 months with LUMOS II (Bruker Optik GmbH) equipped with a single reflection Diamond ATR cell. The spectra were recorded with 256 scans in the mid infrared range (400–4000 cm−1) at a resolution of 4 cm−1.

6.2.3.3 Ecotoxicological

Ecotoxicological analyses were performed on plastic leachates collected from each site after 3 and 6 months of exposure, according to the following procedure. For the preparation of plastic leachates, plastic pellets were mixed with Artificial SeaWater (ASW) (ASTM 1994) at a ratio of 1:10 (pellet dry weight/volume) and subjected to continuous agitation for 24 h at room temperature. After agitation, the mixture was filtered (Ø 0.45 µm) to obtain the aqueous leachate. Toxicity evaluation of the leachates was conducted using two bioassays representing different trophic levels: the microalga *Dunaliella tertiolecta* and the bioluminescent bacterium *Aliivibrio fischeri*. Tests were performed using leachates at a concentration equivalent to 75 mg L^{-1} of plastic. (i) *D. tertiolecta* test: The chronic test was carried out according to ISO 10253. The culture medium for algal growth was prepared according to ISO protocol. A screening with the undiluted (whole)

sample was performed. An algal suspension at a concentration of 1×106 cells/mL was prepared. Then, an aliquot of algal suspension was added to each replicate to reach the final concentration of 1×104 cells/mL. Culture medium has been utilized as negative control (six replicates). The test flasks were placed in a thermostatic chamber at 20 °C with a light source in the 7,000– 8,000-lux range for 72 h. The cell density of each sample was measured after 72 h by the Burker chamber. The effect percentage for each sample was calculated with respect to the control. (ii) *A. fischeri test*: *A. fischeri* luminescence inhibition test was carried out using whole (undiluted) seawater and elutriate samples as a screening assessment. Each sample was mixed with the bacterial suspension and incubated according to the Biolight toxy procedure. A negative control consisting of diluent (2% NaCl) was included in each test run. Luminescence was measured after 15 and 30 minutes of exposure using the Biolight toxy, following the manufacturer's instructions. Results were expressed as the percentage of luminescence inhibition relative to the control.

6.2.3.4 Nutritional composition

To assess whether anthropogenic pressure could influence total protein content, total lipids, fatty acid profiles, and mineral element composition in *Oblada melanurus*, ten specimens were collected at two sites: Lipari Porto and Spiaggia Punta dell'Asino. All samples were analyzed to determine total protein content using the Kjeldahl method, total lipids using the Folch extraction method, and fatty acid composition by gas chromatography coupled with a flame ionization detector (GC-FID). The mineral element profile was quantified using inductively coupled plasma mass spectrometry (ICP-MS).

6.3 Results

6.3.1 Chemical characterization of study sites

6.3.1.1 Sediments

- ✓ *Polycyclic Aromatic Hydrocarbons (PAHs)*

The concentration of PAHs in sediments showed clear spatial variability across the study area, reflecting differences in contamination sources and local environmental conditions (Fig. 6.3.1.1). Overall, Baia di Levante exhibited the highest levels of PAHs (∑PAHs 646.01 ng/g), followed by Valle Muria (∑PAHs 609.14 ng/g) and Spiaggia Punta dell'Asino (∑PAHs 429.08 ng/g). Benzo[ghi]fluoranthene, followed by fluorene and dibenzothiophene, were the most abundant contaminants, showing their highest values in Valle Muria (148.24 ng/g), Baia di Levante (241.78 ng/g), and Spiaggia Punta dell'Asino (66.28 ng/g), respectively.

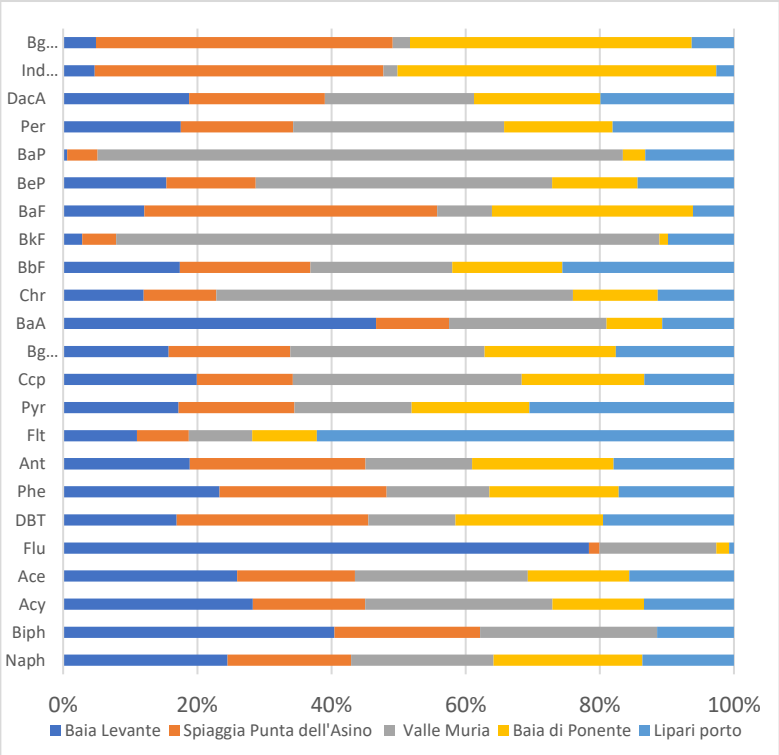

Figure 6.3.1.1: Relative abundance (%) of PAHs in sediments at the different sampling sites.

✓ *Trace elements*

Spiaggia Punta dell'Asino, followed by Baia di Levante and Valle Muria, resulted as the most metal-enriched sites (Fig. 6.3.1.1). Fe (57,941 mg/kg) was the most abundant trace metal, followed by Mn (1,269 mg/kg) and V (308 mg/kg), all recorded at Spiaggia Punta dell'Asino. In Valle Muria, the highest values were recorded for V (245 mg/kg), Mn (1,228 mg/kg) and Fe (50,766 mg/kg). Baia di Ponente showed the lowest trace element concentrations. Toxic elements (Cd, Pb, Hg) were generally low at all sites, with Cd values ranging from 0.123 mg/kg (Baia di Ponente) to 0.196 mg/kg (Baia di Levante), Pb from 7.98 mg/kg (Spiaggia Punta dell'Asino) to 24.0 mg/kg (Lipari Porto), and Hg always very low, ranging from 0.002 mg/kg (Baia di Ponente and Lipari Porto) to 0.232 mg/kg (Valle Muria).

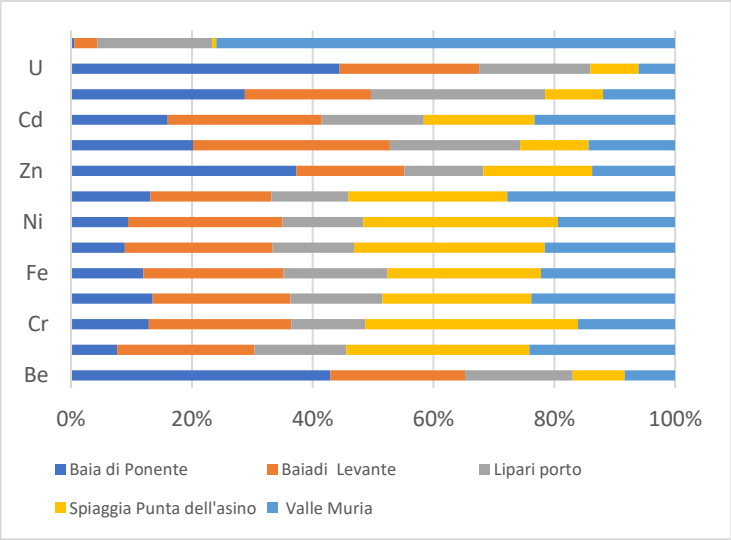

Figure 6.3.1.1: Relative abundance (%) of trace elements in sediments at the different sampling sites

6.3.1.2 Seawater

✓ *Nutrients*

Nutrient concentrations showed spatial variability (Figure 6.3.1.1). Pietra del Bagno showed the high values of nutrients in particular of silicic acid (36.3 µmol L^{-1}), more than ten times higher than any other site, ammonium (0.47 µmol L^{-1}), nitrite (0.067 µmol L^{-1}) and nitrate (0.066 µmol L^{-1}). Phosphate values were under limit of detection in all sites except for Pietra del Bagno (0,034 µmol L^{-1}) and Valle Muria (0,084 µmol L^{-1}).

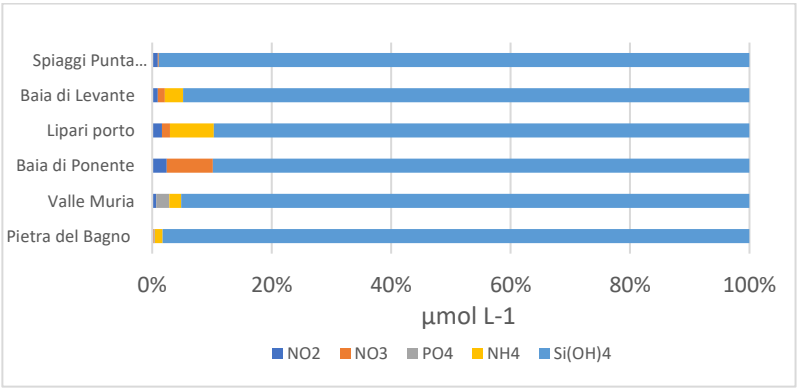

Figure 6.3.1.1. Relative abundance (%) of nutrients in seawater at the different sampling sites

✓ *Trace elements*

The concentrations of trace elements measured in seawater samples did not show significant differences among the sampling sites (Figure 6.3.1.2). For each element, the values observed across locations were relatively similar and comparable. At the Lipari Porto site, however, seawater exhibited slightly higher concentrations of Zn (17.4 µg/L) and Ni (0.113 µg/L) compared to the other areas. In the same site, Cu also showed an elevated concentration (0.412 µg/L), higher than those measured elsewhere, except for the Baia di Ponente area, where Cu reached 0.475 µg/L. In all sites Cd were recorded under detection limit (< 0,010 µg/L).

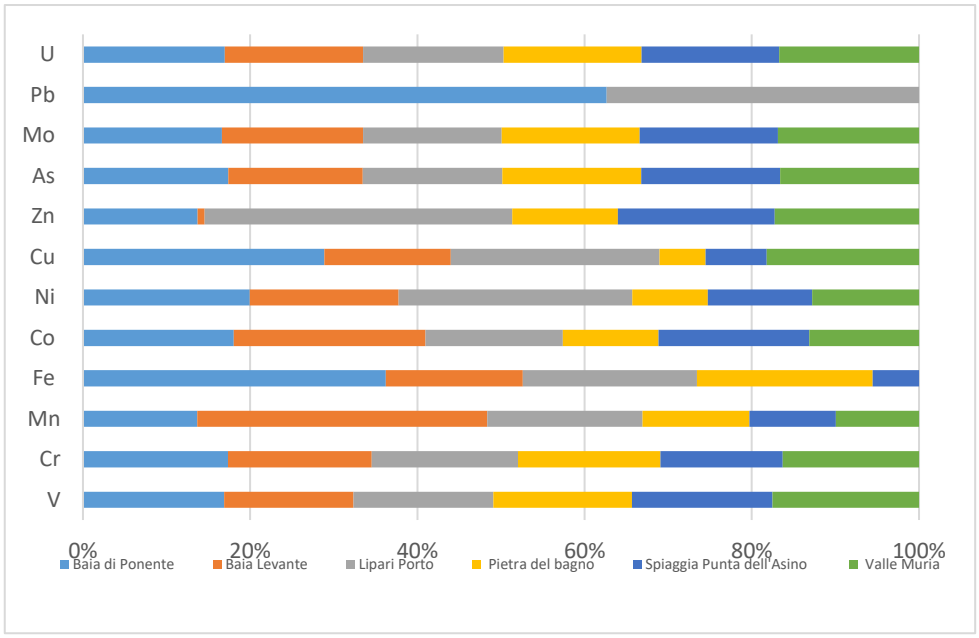

Figure 6.3.1.2. Relative abundance (%) of trace elements in is seawater at the different sampling sites

6.3.1.3 SPMD

The highest levels of PAHs were detected at Pietra del Bagno, where naphthalene reached 1469.69 ng/L and biphenyl 1135.79 ng/L (Figure 6.3.1.3). Similarly, elevated values were observed at Valle Muria (naphthalene 1323.77 ng/L, biphenyl 1276.18 ng/L) and at Baia Levante (naphthalene 1251.21 ng/L, biphenyl 1081.52 ng/L). The most abundant compound is benzo(k)fluoranthene, which shows the highest values at all sites (up to 4327.39 ng/L at Pietra del Bagno), followed by naphthalene (up to 1469.69 ng/L) and biphenyl (up to 1276.18 ng/L), both with higher values at Valle Muria.

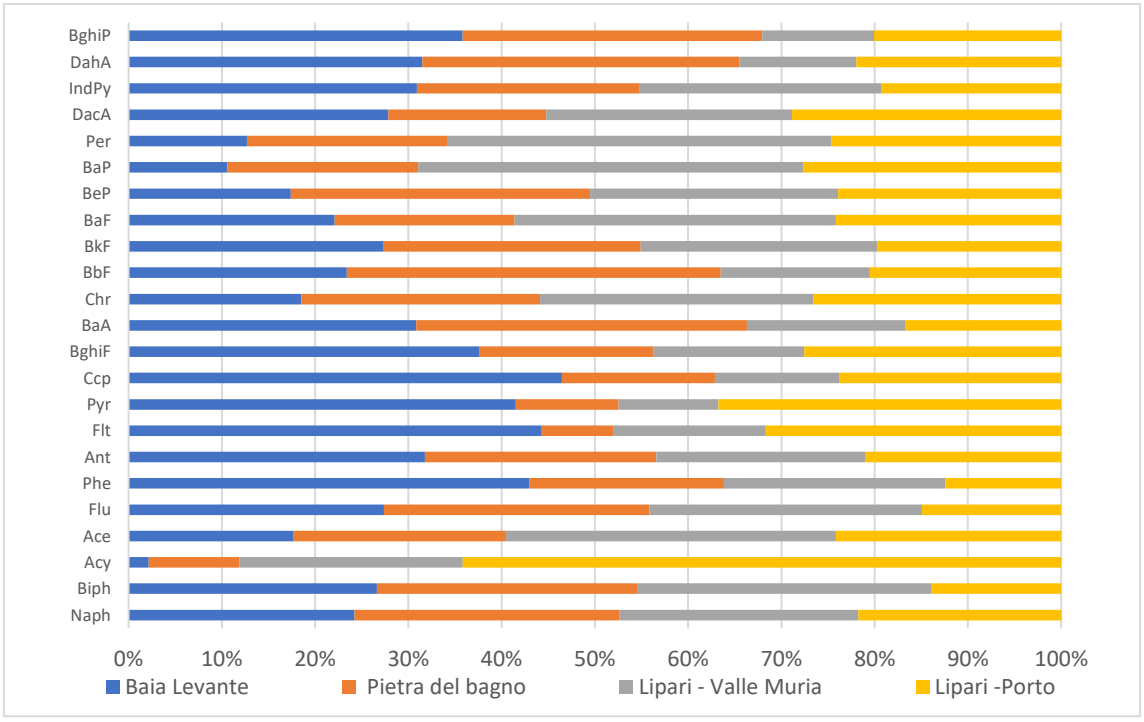

Figure 6.3.1.3. Relative abundance (%) of PAHs absorbed by SPMD at the different sampling sites

6.3.1.4 DGT

The concentration values of the elements obtained using passive samplers were generally consistent with the direct measurements of the same elements in seawater (Figure 6.3.1.2, Figure 6.3.1.4). The most abundant element was Zn, with the highest value recorded at Lipari Porto (10.2 µg/L), followed by Valle Muria (9.96 µg/L). Overall, the highest metal values were recorded at Pietra del Bagno, with elevated concentrations of Fe (10.5 µg/L) and Mn (7.72 µg/L). Hg showed its highest values at Valle Muria (2.10 ng/L), Pietra del Bagno (2.05 ng/L), and Baia di Levante (1.61 ng/L).

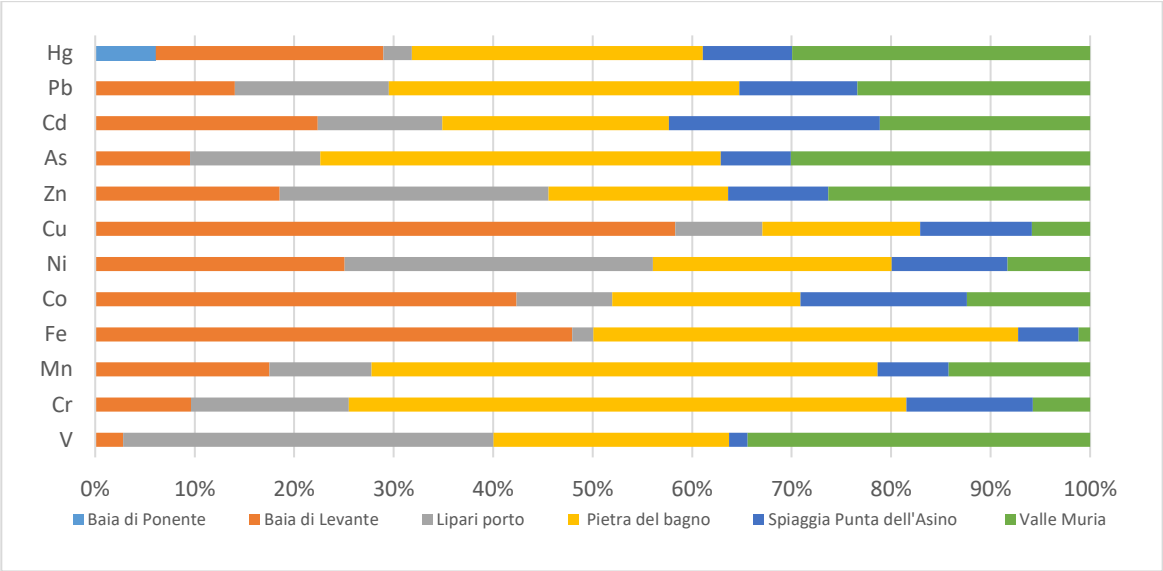

Figure 6.3.1.4, Relative abundance (%) of trace elements absorbed by DGT at the different sampling sites

6.3.2 Biological

✓ *Microfouling*

For the 36 samples, a total of 35,510,200 raw sequences were generated, with an average of 986,394 ± 486,577 sequences. After the denoising procedure, 26,066,808 were retained with an average of 724,078 ± 394,206 sequences per sample. For the final dataset, 23,668,030 sequences were retained with an average of 657,445 ± 366,305 sequences per sample, and corresponding to 77,102 ASVs, with an average of 8,272 ± 3,220 per sample. The taxonomic composition of plastic samples differed significantly ($p < 0.001$) from that of seawater, as determined by PERMANOVA. (Pelagibacterales) Clade Ia and Synechococcus and were the most abundant taxa at the genus level in seawater. Levante site showed a higher proportion (~12% vs ~0.5% at the other sites, on average) of the chemolithoautotrophic, sulfur-oxidizing bacterium on the contrary, plastic pieces were characterized by the presence of particle-associated bacteria, such as members of the Chitinophagales order, the Saprospiraceae family and the *Woeseia* genus (Figure 6.3.2.1)

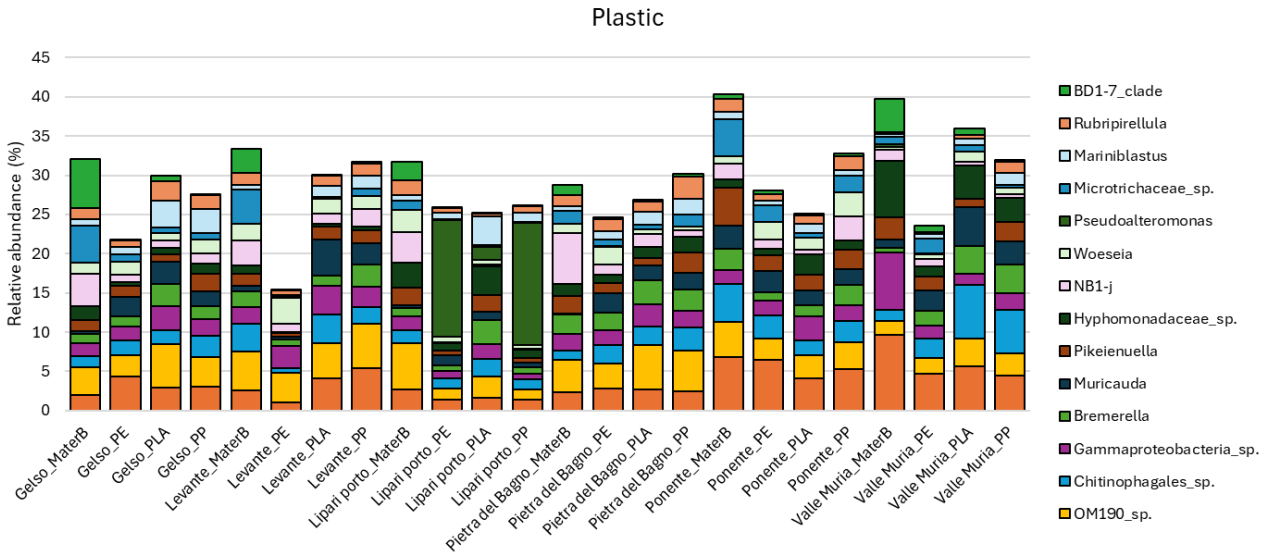

Figure 6.3.2.1. Taxonomic composition of plastic-associated prokaryotic communities at the genus level. The 15 most abundant taxa on average are shown.

Lipari porto PLA and PP samples showed a higher proportion (~15% vs ~0.1% in the other samples, on average) of *Pseudoalteromonas*. MaterB-associated communities presented a higher proportion (~3% vs ~0.3% in the other samples, on average) of the (Spongiibacteraceae) BD1-7_clade (Figure 6.3.2.1). Focusing on plastic samples, NMDS showed that samples were mainly grouped by site (Figure 6.3.2.2). This was confirmed by PERMANOVA, which indicated that both sampling site and plastic type had a significant effect ($p < 0.001$) on prokaryotic community structure. The highest proportion of variance explained was by site (35%), which was greater than that explained by plastic type (16%).

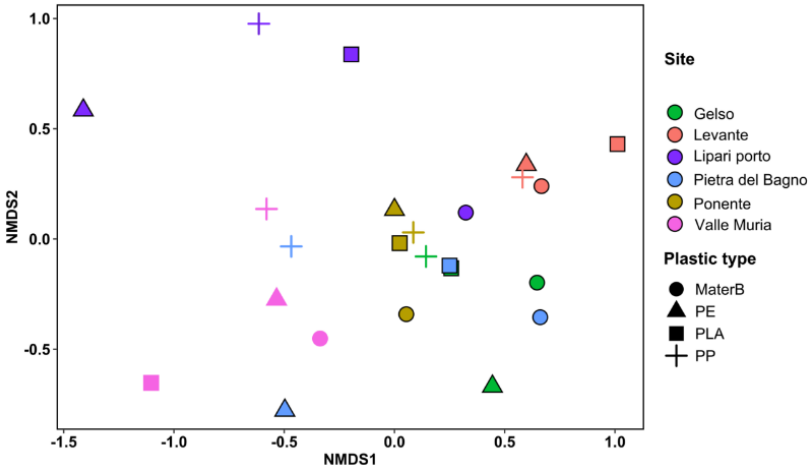

Figure 6.3.2.2. NMDS plot (stress = 0.16) showing Bray–Curtis dissimilarity in community composition. Samples are colored by site and type.

✓ *Macrofouling*

A total of 93 macrofouling specimens were recorded. Polychaetes represented the dominant taxonomic group (59.3% of the total assemblage). The lowest values of abundance (N) and Shannon diversity (H′) were observed at Baia di Levante and at Lipari Porto (Figure 6.3.2.3). The cryptogenic polychaete *Simplaria pseudomilitaris* (Thiriot-Quievreux, 1965) was the most abundant species (30 specimens), while

Neodexiospira pseudocorrugata (Bush, 1905) was the most frequent. The non-indigenous bivalve Pinctada radiata (Leach, 1814) occurred at all sites except the control site Valle Muria, and was found exclusively on biodegradable plastics, 90% on Mater-bi, both inside and outside the containers, with an average shell length of 8.6 ± 4.7 mm. Overall, Mater-bi was the most colonized polymer, hosting 40.7% of the total macrofaunal assemblage (Figure 6.3.2.4). These findings confirm the role of plastics as substrates for the recruitment and growth of non- indigenous species.

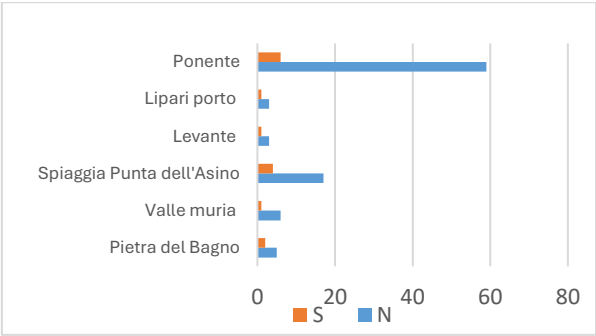

Figure 6.3.2.3. Biodiversity indices of macrofouling at the sampling sites

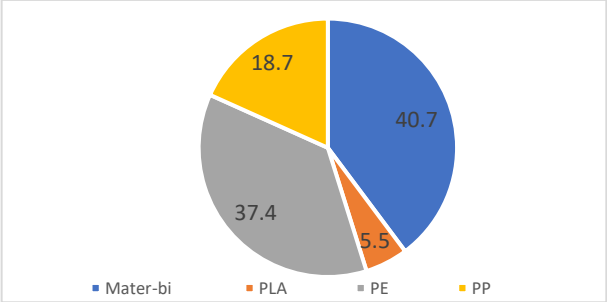

Figure 6.3.2.4. Fouling percentages on different plastic polymers

6.3.3 Physical

The FTIR results obtained for the samples collected at t1 and t2 were used to assess chemical modifications associated with biodegradation over time. The infrared spectra of each sample were compared with that of the pristine material to identify variations in the main bands corresponding to characteristic functional groups. Overall, no site-specific and no pronounced degradation phenomena were observed in the samples (Figure 6.3.3.1). Among the tested materials, the Mater-Bi samples appeared to be the most degraded. After only 3 months, the loss of the stearamide additive was evident from the disappearance of the peaks at 2926 cm^{-1} and 2855 cm^{-1} (C–H stretching) and at 1650 cm^{-1} (C=O stretching) (Al-Mutairi et al., 2024). In addition, the intensity of the band at 1720 cm^{-1}, attributed to the C=O stretching vibrations of ester groups in PBAT, increased progressively with exposure time. For PP and HDPE, aging was indicated by the formation of oxygenated groups, primarily by the appearance of a band centered at approximately 3340 cm^{-1} after the first sampling, and by new bands around 1650 cm^{-1} and in the 1300–1000 cm^{-1} region after the second sampling, consistent with the formation of hydroxyl groups. Other studies on the weathering of conventional polymers in seawater have similarly attributed new bands in the 3000–3500 cm^{-1} and 1500–1750 cm^{-1} regions to hydroxyl and carboxyl groups formed during oxidative photodegradation. In contrast, PLA showed no clear signs of chemical change.

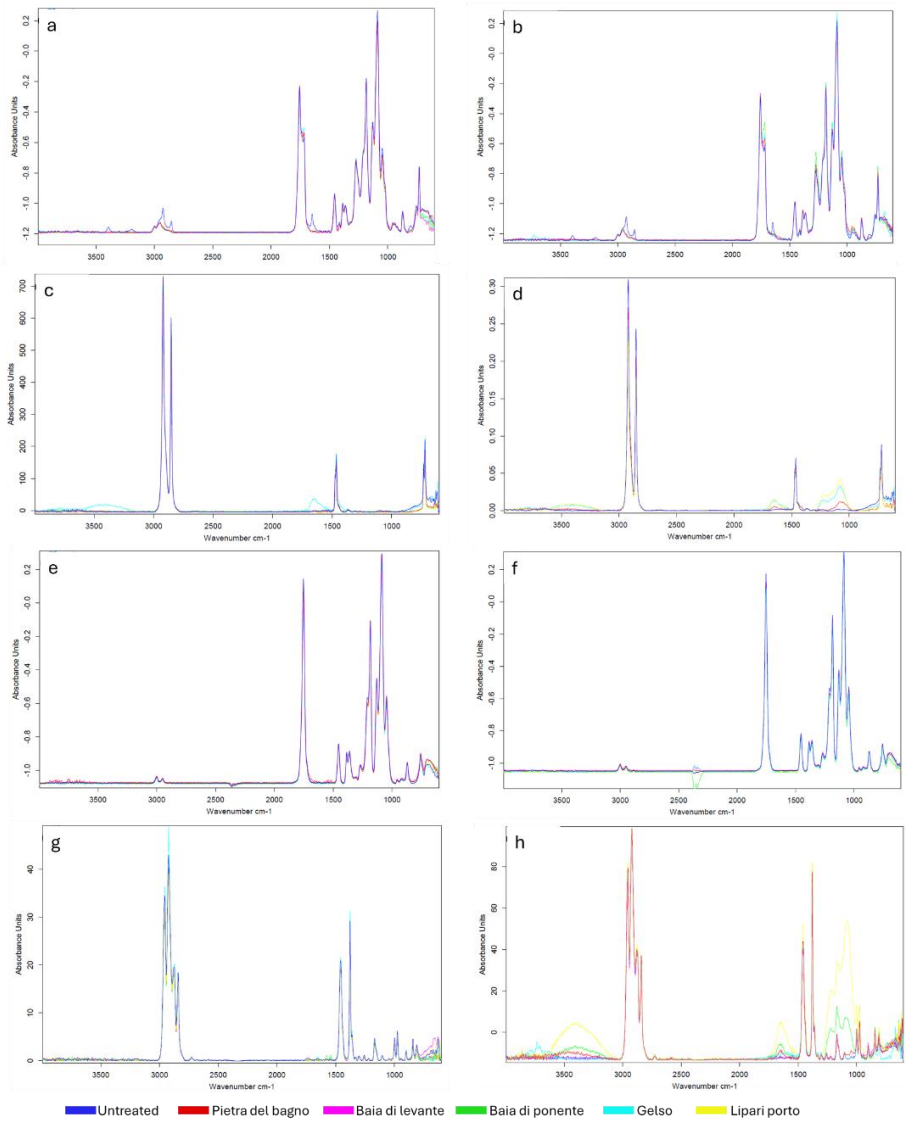

Figure 6.3.3.1. FT-IR spectra of the analyzed samples: Mater-Bi samples at t1 (a) and t2 (b); HDPE at t1 (c) and t2 (d); PLA samples at t1 (e) and t2 (f); PP at t1 (g) and t2 (h).

6.3.4 Ecotoxicological

The ecotoxicological responses of plastic leachates varied across the different sites and exposure times (3 and 6 months), suggesting that both polymer type and local environmental conditions influenced toxicity. After 3 months, all polymers induced moderate effects (40–60%) on *D. tertiolecta* and *A. fischeri*, with polyethylene (PE) and polylactic acid (PLA) showing consistently higher toxicity in all sites. Mater-bi generally exhibited lower effects (<50%), particularly in low-stress environments such as Spiaggia Punta dell'Asino and Baia di Ponente (Figure 6.3.4.1, Figure 6.3.4.2).

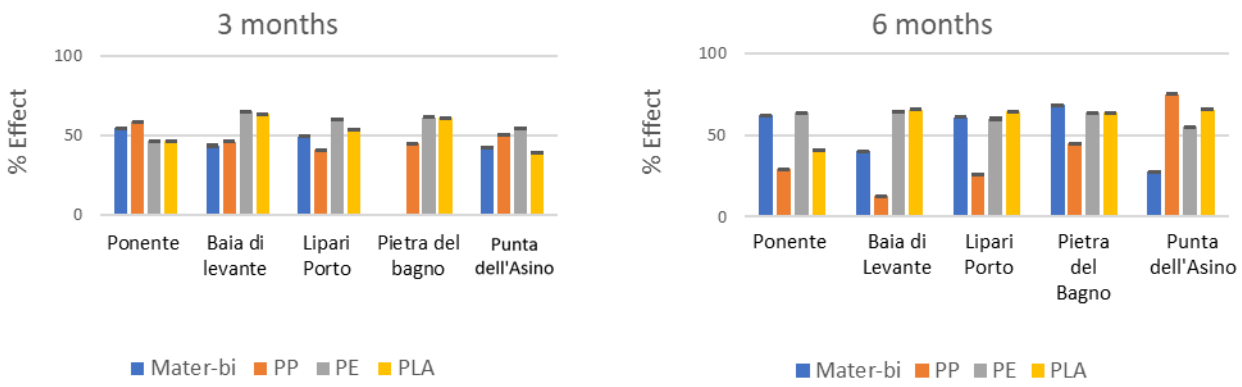

Figure 6.3.4.1. Toxicity (% effect) of plastic leachates collected after 3 and 6 months of in situ exposure on microalgae *D. tertiolecta*

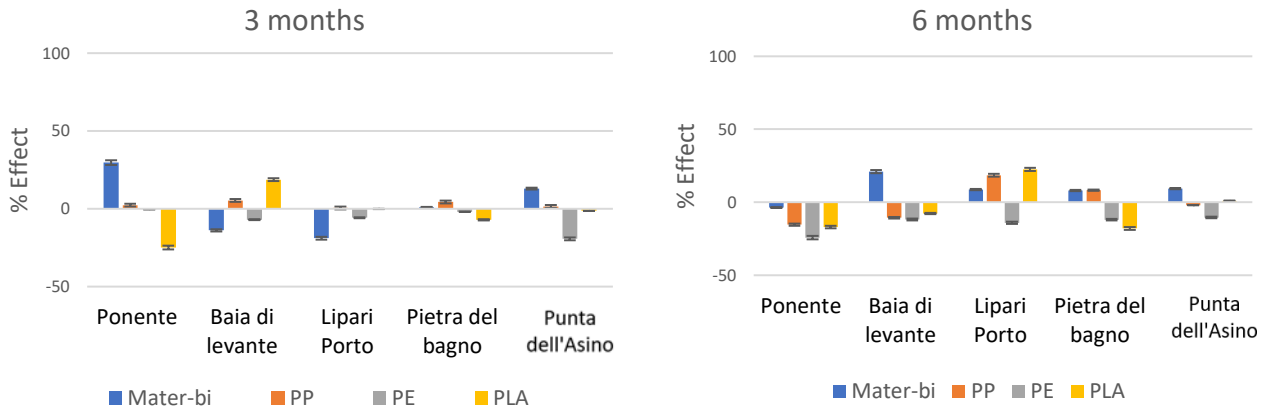

Figure 6.3.4.2. Toxicity (% effect) of plastic leachates collected after 3 and 6 months of in situ exposure on bacteria *A. fischeri*

After 6 months, the effects became more pronounced and site dependent. In sites characterized by natural or anthropogenic stressors, particularly Baia di Levante (acidification and anthropization) and Pietra del Bagno (temperature/acidification), toxicity of bio-based (Mater-bi, PLA) and conventional plastics (PP, PE) increased. For instance, PE and PLA leachates exceeded 60% effect in Pietra del Bagno, while Mater-bi increased markedly at Baia di Levante, indicating that environmental stress may accelerate polymer degradation and release of soluble toxic compounds. The two bioassays showed distinct sensitivity patterns to plastic leachates. *D. tertiolecta* generally exhibited stronger inhibition than *A. fischeri*, particularly for PE and PLA after 3 and 6 months of exposure. This suggests that algal cells, due to their photosynthetic metabolism and larger surface area, may be more susceptible to compounds affecting membrane integrity, nutrient uptake, and photosynthetic pathways. In contrast, *A. fischeri* responses were more variable and appeared less affected at early exposure times but became more pronounced after 6 months, especially at sites subjected to environmental stressors (e.g., Baia di Levante and Pietra del Bagno). This delayed rise in bacterial toxicity suggests that prolonged degradation may release compounds that interfere with bacterial luminescence systems, such as surfactants or oxidative by-products. Overall, algae respond more readily to early polymer degradation products, while bacteria are more sensitive to later-stage leachates enriched in reactive or soluble compounds.

6.3.5 Nutritional composition

A total of 10 specimens of *Oblada melanurus* were analyzed, of which 8 caught in Lipari Porto (LIP_) and 2 in Spiaggia Punta dell'Asino (GEL_). Protein content ranged between 20.3 and 22.3 g/100 g in specimens from Lipari Porto and between 19.5 and 19.9 g/100 g in those from Gelso. Also, lipid concentrations showed a limited site-related pattern. Fish from Lipari displayed total lipid values between 1.99 and 2.51 g/100 g, while individuals from Spiaggia Punta dell'Asino exhibited markedly higher levels, ranging from 3.10 to 3.32 g/100 g (Figure 6.3.5.1).

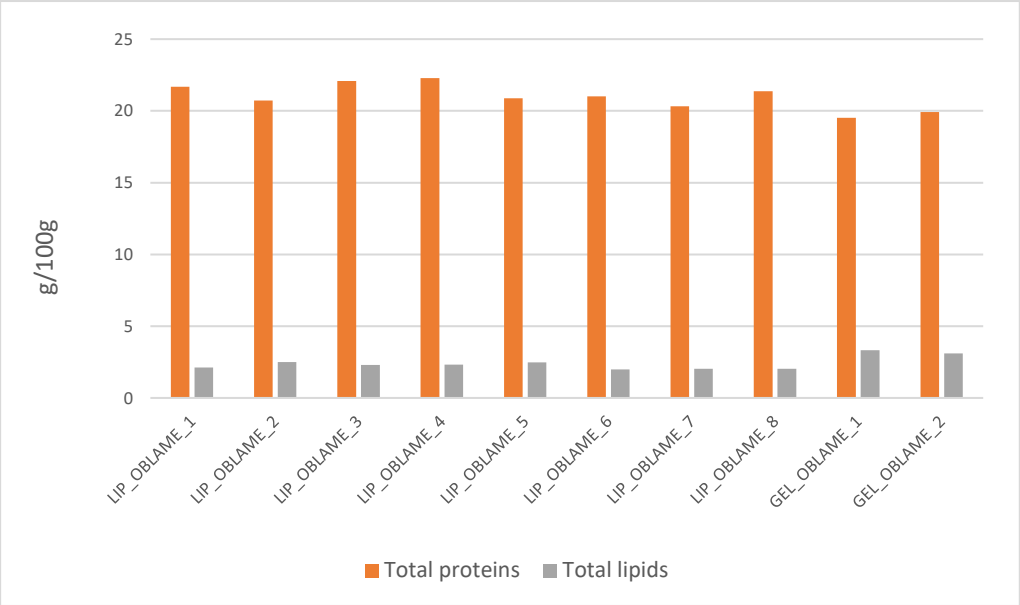

Figure 6.3.5.1. Abundances of total proteins and lipids (g/100) in *O. melanurus* collected in Lipari Porto (LIP_) and Spiaggia Punta dell'Asino (GEL_)

The fatty acid profile of *O. melanurus* showed site-related variability, particularly in the distribution of monounsaturated (MUFA) and polyunsaturated fatty acids (PUFA). Saturated fatty acids (SFA) represented the dominant fraction in both sites, ranging from 36.0 to 46.5 g/100 g FA in Lipari samples and from 33.6 to 42.4 g/100 g FA in Spiaggia Punta dell'Asino specimens. Palmitic acid (C16:0) and stearic acid (C18:0) were the most abundant SFA across all individuals. MUFA levels were generally higher in Spiaggia Punta dell'Asino fish, reaching up to 42.9 g/100 g FA, compared to 23.5–29.5 g/100 g FA in specimens from Lipari. This difference was mainly driven by elevated oleic acid (C18:1 n-9), which reached 31.5 g/100 g FA in Spiaggia Punta dell'Asino compared to 16.9–23.3 g/100 g FA in Lipari. The higher MUFA content in Spiaggia Punta dell'Asino individuals is consistent with their greater total lipid content, suggesting enhanced energy storage (Figure 6.3.5.2).

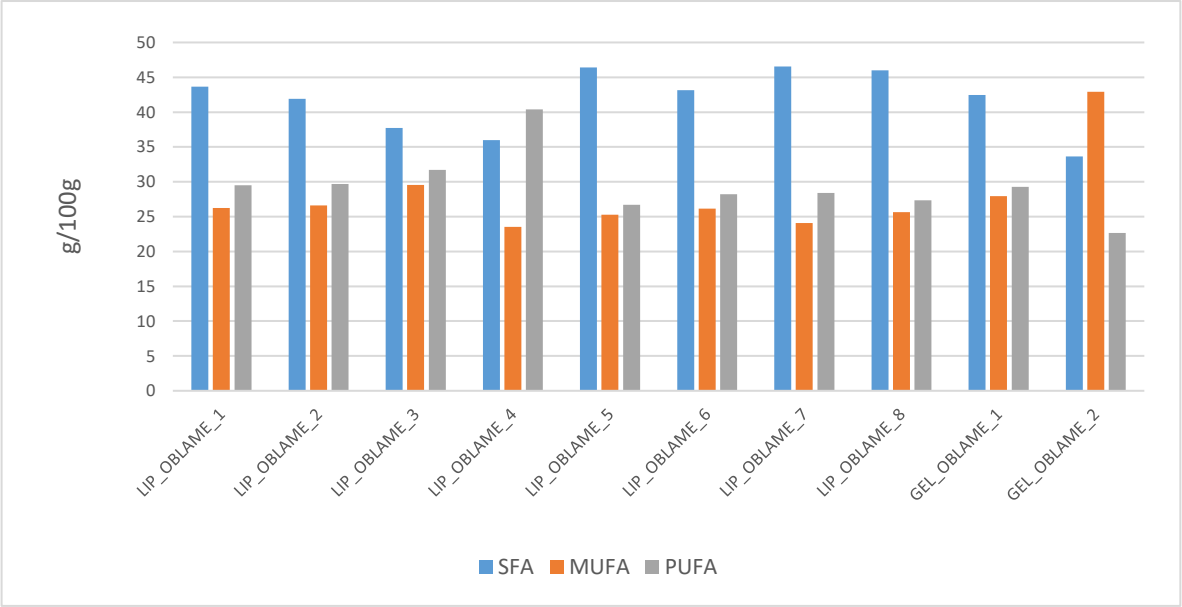

Figure 6.3.5.2. Abundances of fatty acids (g/100) in *O. melanurus* collected at Lipari Porto (LIP_) and Spiaggia Punta dell'Asino (GEL_)

PUFA levels were more variable but followed an opposite pattern. Lipari samples showed higher PUFA proportions (up to 40.4 g/100 g FA), largely due to elevated levels of docosahexaenoic acid (C22:6 n-3, DHA), which ranged between 15.7 and 23.5 g/100 g FA. In contrast, PUFA values in Spiaggia Punta dell'Asino fish were lower (22.7–29.3 g/100 g FA), with correspondingly reduced DHA and eicosapentaenoic acid (C20:5 n-3, EPA). The mineral composition of *O. melanurus* showed consistent patterns between specimens collected at Lipari Porto and Gelso, with moderate site-related differences in both macro- and trace elements. Macroelements (Ca, K, Na, Mg, P) were generally higher in Lipari individuals. Calcium (Ca) ranged from 434.7 to 458.9 mg/kg in Lipari samples and from 379.9 to 407.7 mg/kg in Spiaggia Punta dell'Asino fish (Figure 6.3.5.3).

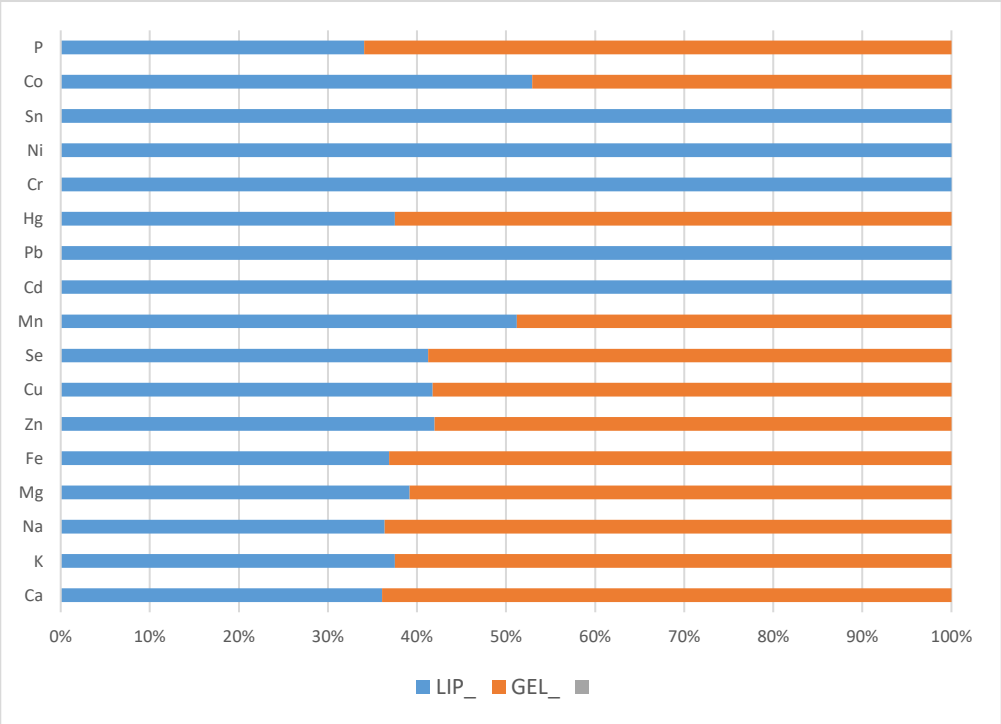

Figure 6.3.5.3. Average concentrations of mineral elements (mg/kg) in *O. melanurus* collected at Lipari Porto (LIP_) and Spiaggia Punta dell'Asino (GEL_)

Sodium (Na) was the most abundant element, ranging between 505.97 and 436.29 in Lipari and 403.19 and 419.99 in Spiaggia Punta dell'Asino. Potassium (K), the most abundant mineral, varied between 4100 and 4900 mg/kg in Lipari specimens, while values in Spiaggia Punta dell'Asino ranged from 3447 to 3965 mg/kg. Among trace elements, Fe, Zn and Cu showed a consistent reduction in Spiaggia Punta dell'Asino specimens. Iron (Fe) ranged from 31.6 to 36.7 mg/kg in Lipari fish, compared to 28.3–29.0 mg/kg in Gelso. Zinc (Zn) followed the same pattern, with values between 15.7 and 19.3 mg/kg in Lipari and 10.6–13.0 mg/kg in Spiaggia Punta dell'Asino. Copper (Cu) levels were also lower at Spiaggia Punta dell'Asino (4.6–5.5 mg/kg) compared to Lipari (6.4–8.5 mg/kg). Selenium (Se) concentrations were low but detectable in all samples (0.12–0.21 mg/kg), with slightly higher values in Lipari specimens. Manganese (Mn) was also consistently higher in Lipari (0.12–0.20 mg/kg) than in Spiaggia Punta dell'Asino (0.07–0.08 mg/kg). Toxic elements (Pb, Cd, Hg, As) were either below the limit of quantification (LOQ) or present at very low concentrations in all samples. Lead (Pb) and Cadmium (Cd) were detected sporadically at trace levels (≤0.02 mg/kg), whereas Arsenic (As) remained below LOQ in all fish. Sb was not detected in any sample. Mercury (Hg) was measurable in most specimens but always at minimal concentrations (0.01–0.02 mg/kg), well below thresholds of concern. Phosphorus (P) showed the highest values among elements, ranging from 2016 to 2072 mg/kg in Lipari samples and slightly lower values (1954–1990 mg/kg) in Spiaggia Punta dell'Asino fish.

6.4 Discussion

6.4.1 Chemical

The spatial variability of PAHs in sediments, with highest ∑PAHs at Baia di Levante followed by Valle Muria and Spiaggia Punta dell'Asino, is coherent with a mixed influence of volcanic inputs and localized anthropogenic pressure (Culotta et al., 2007). Similar PAH levels and patterns were previously reported for Vulcano Island muds and nearby coastal sediments, where both hydrothermal emissions and human activities contribute to contamination (Culotta et al., 2007). The dominance of benzo[ghi]fluoranthene, fluorene and dibenzothiophene at the most impacted sites is consistent with observations from other areas

of the Aeolian arc (Kozak et al., 2017). Trace-element patterns in sediments, with Spiaggia Punta dell'Asino and Valle Muria showing the highest Fe, Mn and V levels, reflect the strong imprint of the volcanic origin of the study areas (Andaloro et al., 2012), even though no vents or acidification were never observed in either area. The comparatively lower metal concentrations at Baia di Ponente are in line with a weaker volcanic and anthropogenic influence. Toxic metals (Cd, Pb, Hg) remained low at all sites and comparable to or below ranges reported for other central Mediterranean sediments, indicating limited anthropogenic metal enrichment relative to the strong natural geochemical background (Andaloro et al., 2012). Nutrient distributions showed a clear spatial signal, with Pietra del Bagno characterized by markedly elevated silicic acid and relatively higher inorganic nitrogen compared to the other sites. This pattern is consistent with observations of nutrient-enriched waters associated with remineralization and local up-welling in the southern Tyrrhenian and around volcanic structures of the Aeolian sector (Spagnoli et al., 2023). Trace elements in seawater were relatively homogeneous among sites, with only slightly elevated Zn and Ni at Lipari Porto, consistent with localized harbour and vessel-related inputs as described for other Mediterranean coastal areas (Zhang & Davison, 2015). SPMD data revealed that the highest dissolved and bioavailable PAH concentrations occurred at Pietra del Bagno, followed by Valle Muria and Baia di Levante, with benzo(k)fluoranthene, naphthalene and biphenyl as the most abundant compounds. This pattern reflects findings from other Western Mediterranean coastal sites, where SPMDs have shown strong sensitivity to gradients in PAH contamination associated with maritime traffic and confined embayments. (Alvarez et al., 2013). DGT results for trace metals were generally consistent with direct seawater measurements, indicating that the labile and bioavailable fractions of Zn, Fe, Mn and Hg closely follow total dissolved patterns. This agreement is in line with previous applications of DGT in Mediterranean coastal waters, where DGT has been shown to provide robust, integrative estimates of metal availability under varying hydrodynamic and contamination regimes (Zhang & Davison, 2015). The elevated Zn at Lipari Porto and Valle Muria, as well as higher Fe and Mn at Pietra del Bagno, reflect the combined influence of volcanic geochemistry, coastal morphology and local anthropogenic pressures already highlighted in regional hydrothermal and tectonic studies of the Aeolian Archipelago (Andaloro et al., 2012).

6.4.2 Biological

The high sequencing depth and the large number of ASVs observed across samples highlight the strong microbial diversity associated with both seawater and plastic substrates. The clear compositional separation between seawater and plastic-associated communities, confirmed by PERMANOVA, is consistent with previous studies showing that biofilms developing on plastics form distinct ecological niches compared to surrounding water (Cao et al. 2014; Saidi et al. 2023). In seawater, the dominance of Pelagibacterales (Clade Ia) and Synechococcus reflects typical oligotrophic Mediterranean profiles. The unusually high abundance of sulfur-oxidizing Thiomicrorhabdus at Baia di Levante aligns with its known occurrence in hydrothermal and gas-vent systems, where reduced sulfur compounds fuel chemolithoautotrophic growth (Cao et al. 2014; Saidi et al. 2023). The presence of this genus confirms the strong geochemical imprint of local CO_2-rich emissions on microbial assemblages. Plastic substrates instead supported typical particle-attached taxa, including Chitinophagales, Saprospiraceae, and the benthic-associated genus Woeseia, a pattern frequently described in plastisphere communities worldwide. The enrichment of Pseudoalteromonas, up to 15% in PP and PLA from Lipari Porto, is notable because this genus includes hydrocarbon-degrading and biofilm-forming strains favored in ports and polluted coasts (Zettler et al. 2013; Lv et al. 2024). Biodegradable polymers showed specific microbial signatures: Mater-bi pieces hosted elevated proportions of the BD1-7 clade (Spongiibacteraceae), a taxon recently linked to colonization and degradation of bioplastics in marine waters (de Vogel et al. 2024). This suggests an early microbial response to bio-based polymer components, potentially accelerating surface modification and fouling. NMDS analysis showed that site explained more variance (35%) than polymer type (16%), indicating that local environmental conditions—such as acidification at Baia di Levante, anthropogenic pollution at Lipari Porto, and low-impact conditions at Spiaggia Punta dell'Asino play a stronger role than the substrate itself in shaping prokaryotic assemblages. Similar patterns have been reported in Mediterranean plastisphere studies, where temperature, pH, and local pollution are primary drivers of community structure. Regarding the macrofouling, the community assemblage, with polychaetes representing the dominant group is agrees with previous observations in

Mediterranean fouling systems, where polychaetes are among the first colonizers of artificial substrates and often dominate early successional stages (D'Alessandro et al., 2018). The lowest abundances and diversity values at Baia di Levante and Lipari Porto are consistent with known negative effects of acidification and anthropogenic pressure on calcifying and soft-bodied benthic fauna (Ries et al, 2009). The presence of the cryptogenic species *S. pseudomilitaris* and *N. pseudocorrugata*, confirms that opportunistic polychaetes thrive on newly available substrates. Mater-bi emerged as the most colonized polymer, hosting also the almost totality of the non-indigenous bivalve *P. radiata*. This high colonization should be due to a mix of features such as its fast degradation in seawater or faster biofilm formation if compared to conventional polymer (Dussud et al., 2018).

6.4.3 Physical

The FTIR results provide insight into the early stages of polymer degradation under the environmental conditions of the Aeolian Archipelago. Despite the environmental variability across sites, no pronounced site-specific degradation patterns were detected, suggesting that a 3–6-month immersion period is generally insufficient to induce strong chemical alteration under natural conditions. Nevertheless, some material-dependent differences clearly emerged. Among all polymers, Mater-Bi showed the clearest signs of early degradation, mainly through additive loss. After only 3 months, FTIR spectra displayed the disappearance of bands at 2926 cm^{-1} and 2855 cm^{-1} (C–H stretching) and at 1650 cm^{-1} (C=O stretching), indicating leaching of stearamide. Similar patterns of additive depletion in starch-based and biodegradable blends exposed to seawater have been reported in recent work, where substantial modifications occurred even before backbone degradation (Al-Mutairi et al., 2024). The progressive increase in the PBAT-related ester band at 1720 cm^{-1} is consistent with reports showing that PBAT undergoes surface oxidation and chain scission during early weathering (Hejna et al., 2023). For PP and HDPE, early signs of oxidative aging were evident through the appearance of oxygen-bearing functional groups, including a broad band around 3340 cm^{-1} (hydroxyl groups) and emerging carbonyl and C–O stretching bands near 1650 cm^{-1} and 1300–1000 cm^{-1}. These changes align with established weathering pathways where UV exposure, oxygen diffusion and biofilm activity promote surface oxidation before any measurable mass loss (La Mantia et al., 2023; Rouillon et al., 2016). Similar spectral features associated with photodegradation, particularly carbonyl and hydroxyl bands, have been widely reported in marine-aging experiments on polyolefins. In contrast, PLA did not show evident chemical transformation, in agreement with previous findings showing that PLA is relatively resistant to short-term degradation in seawater due to its slow hydrolysis rate at natural temperatures and limited UV-induced oxidation (Feijoo et al., 2025; Nazareth et al., 2019). PLA tends to degrade appreciably only under industrial composting conditions or over much longer periods in the environment.

6.4.4 Ecotoxicological

The ecotoxicological responses of plastic leachates revealed strong site- and time-dependent patterns, indicating that both polymer composition and local environmental stressors play a central role in determining toxicity. After 3 months, all polymers produced moderate inhibition in both *D. tertiolecta* and *A. fischeri*, with PE and PLA consistently inducing the strongest effects. This finding aligns with previous studies showing that polyolefins and polyesters tend to release more bioactive compounds during early weathering, including oxidized additives and low-molecular-weight oligomers (Rummel et al., 2022; Maday et al. 2025). After 6 months, toxicity increased substantially, especially at sites under strong natural or anthropogenic stress, such as Baia di Levante and Pietra del Bagno. Elevated acidity, hydrothermal inputs, and local anthropogenic pressures likely accelerated the degradation of both conventional and bioplastics. The sharp increase in Mater-Bi toxicity at Baia di Levante supports the idea that environmental stress acts as a catalyst for polymer fragmentation, increasing the release of compounds that were not present at earlier stages (Campani et al. 2020). The two bioassays provided complementary insights: *D. tertiolecta* showed a higher sensitivity throughout the experiment, particularly toward PE and PLA. This heightened vulnerability likely reflects the sensitivity of photosynthetic organisms to leachates affecting membrane integrity, chloroplasts, and oxidative balance, as previously reported for microalgae exposed to

plastic-derived chemicals (Schiavo et al. 2021). In contrast, *A. fischeri* responses were limited at 3 months but intensified after 6 months, especially in the more stressed sites. This behavior is typical of bacteria whose luminescence is inhibited primarily by later-stage degradation products, including surfactants, oxidized hydrocarbons, and acidic compounds (Klein et al. 2021). The delayed response suggests that aging plastics progressively release more bacteriotoxic substances as their polymer matrix becomes more oxidized (Rummel et al., 2022).

Overall, the results indicate that algae are early responders to polymer degradation products, while bacteria are more sensitive to late-stage leachates enriched in reactive or soluble compounds.

6.4.5 Nutritional composition

The biochemical and elemental analyses of *O. melanurus* revealed clear site-related differences between individuals collected at Lipari Porto and Spiaggia Punta dell'Asino, despite the limited number of specimens. Such variability aligns with findings from Mediterranean sparids, whose biochemical composition reflects local environmental conditions, trophic resources, and metabolic constraints (Yuvka et al., 2025). Protein content remained relatively stable across sites, ranging between 20.3 and 22.3 g/100 g in fish from Lipari Porto and between 19.5 and 19.9 g/100 g in those from Spiaggia Punta dell'Asino. This limited variability suggests similar trophic positioning and metabolic requirements, consistent with observations of wild Mediterranean sparids experiencing moderate environmental gradients (Duarte et al. 2022). Also, lipid concentrations showed a low spatial pattern. The slightly higher lipid reserves in Spiaggia Punta dell'Asino fish may be linked to greater food availability, lower environmental stress, or reduced metabolic expenditure, all of which can enhance energy storage in coastal fish populations (Laurent et al., 2025). Fatty acid profiles also showed site-related differences. Saturated fatty acids (SFA) dominated in both sites, with palmitic (C16:0) and stearic acid (C18:0) as the main contributors, a pattern widely reported for Mediterranean teleosts (Özogul et al. 2009). Monounsaturated fatty acids (MUFA) were higher in fish from Spiaggia Punta dell'Asino, driven mainly by oleic acid (C18:1 n-9). This trend mirrors the elevated total lipid content and likely reflects dietary differences or more favourable metabolic conditions in Spiaggia Punta dell'Asino. Conversely, polyunsaturated fatty acids (PUFA) were higher in Lipari specimens, largely due to elevated DHA and EPA. Such enrichment is typically associated with diets richer in pelagic prey and may reflect different food-web structures and metabolic demands in more anthropized harbour conditions (Özogul et al. 2009). The mineral composition showed consistent patterns between sites, but with notable differences. Macroelements (Ca, K, Na, Mg, P) were generally higher in fish from Lipari Porto. Such enrichment may result from greater exposure to dissolved minerals in port environments or differences in diet and osmoregulatory activity (Prabhu et al. 2015). Sodium and potassium were the dominant elements in both sites, reflecting their essential roles in ionic regulation. Phosphorus was also abundant, with slightly higher concentrations in Lipari individuals, possibly linked to dietary intake (Prabhu et al. 2015).

Trace elements showed a consistent reduction in fish from Spiaggia Punta dell'Asino compared to Lipari Porto. Iron, zinc and copper were all higher in Lipari specimens, a trend commonly associated with harbour-related contamination from maritime traffic, antifouling paints, and coastal runoff (Chouba et al, 2024). Elements such as selenium and manganese also followed this pattern, although with lower absolute variability. Despite these differences, toxic metals (Pb, Cd, Hg, As) remained extremely low at both sites, in agreement with previous studies indicating negligible biomagnification of these contaminants in low-trophic-level Mediterranean fish (Renieri et al., 2014). Mercury levels (0.01–0.02 mg/kg) were well within background concentrations reported for coastal species across the Mediterranean basin (Evers et al., 2024). Overall, fish from Spiaggia Punta dell'Asino showed biochemical features indicative of better nutritional status (higher lipids and MUFA), while those from Lipari Porto exhibited higher PUFA and trace elements, possibly reflecting differences in trophic dynamics, environmental quality and exposure to harbour-related contaminants. Toxic metals remained negligible, suggesting limited ecological risk for *O. melanurus* in both sites.

6.5 Conclusions

The results of this study show that, among all the polymers tested, Mater-Bi was the most sensitive to environmental stress, exhibiting clear chemical and physical transformations even after short-term exposure. The acidified and hydrothermal-influenced conditions, typical of the Aeolian Archipelago, produced the first signs of additive loss, surface oxidation, and structural modification, accompanied by a marked increase in leachate toxicity. These results indicate that bioplastics, despite being designed to degrade more rapidly, can release reactive and potentially harmful compounds during the early stages of environmental change. This challenges the common assumption that biodegradability inherently reduces ecological impact, highlighting that bioplastic degradation in natural marine conditions may not equate to reduced ecological risk. However, further studies are needed to better understand this important topic. Environmental variability has played a central role in shaping both the chemical behavior of polymers and the biological responses of surrounding communities. For all materials, sites characterized by natural stressors (acidification, hydrothermal inputs) or anthropogenic pressures (port activity, local pollution) accelerated degradation processes and amplified toxicity, confirming that the environmental context is a dominant modulator of polymer aging and associated risks. Chemical and ecotoxicological analyses also showed that biological communities responded consistently to local environmental gradients, reinforcing the close link between polymer behavior, contaminant availability, and ecosystem functioning. Overall, the evidence demonstrates the importance of evaluating polymer performance in realistic, multi-stress scenarios representative of Mediterranean coastal ecosystems. Further research should address long-term degradation dynamics, the evolution of leachate toxicity with prolonged exposure, and the interactive effects of multiple natural and anthropogenic stressors on marine organisms and habitats. Such efforts are crucial to inform material design, regulatory policies, and waste management strategies aimed at reducing plastic-related risks in vulnerable semi-enclosed basins such as the Mediterranean Sea.

7 General Conclusions

Across the coastal, transitional, and hydrothermal vent systems examined in this deliverable, the findings converge on a critical insight: environmental stressors - whether oxygen depletion, acidification, sulfide, metal enrichment, or emerging chemical contaminants - pose significant threats to ecosystem functioning. In the Grado-Marano Lagoon, even moderate oxygen decreases triggered cascading effects that disrupted benthic-pelagic coupling and shifted metabolism from autotrophic to heterotrophic, while mobilizing mercury from sediments to the water column. At Panarea's hydrothermal vents, CO_2-driven acidification combined with elevated trace elements impairs *Posidonia oceanica* performance, with metal toxicity overriding pH-driven responses and causing meadow structural simplification. At Lipari and Vulcano vents, spatial heterogeneity in contamination drives distinct ecotoxicological conditions, where environmental stress accelerates polymer degradation and toxicity release.

These results demonstrate that ecosystem degradation operates through interconnected chemical, biological, and ecological pathways. Multiple environmental stressors do not act in isolation but interact synergistically, weakening resilience and recovery capacity. The integration of chemical analysis, biological assessment, ecotoxicological testing, and ecological measurement through multidisciplinary approaches has revealed mechanistic pathways and site-specific vulnerabilities that individual disciplines cannot access. Accordingly, sustainable management of coastal and marine environments requires governance frameworks and decision-making processes that are informed by interdisciplinary science and are capable of translating scientific evidence into adaptive policies, regulatory tools, and targeted management actions for vulnerable habitats.

8 References

Acquavita, A., Aleffi, I. F., Benci, C., Bettoso, N., Crevatin, E., Milani, L., Tamberlich, F., Toniatti, L., Barbieri, P., Licen, S., & Mattassi, G. (2015). Annual characterization of the nutrients and trophic state in a Mediterranean coastal lagoon: The Marano and Grado Lagoon (northern Adriatic Sea). Regional Studies in Marine Science, 2, 132–144. https://doi.org/10.1016/j.rsma.2015.08.017.

Acquavita, A., Bettoso, N., Blasutto, O., Pittaluga, F., & Orlandi, C. (2024). Seasonal and interannual variability of the trophic state in the Marano and Grado Lagoon (Adriatic Sea, Italy) during the 2011–2021 period. Environments, 11(7), 152. https://doi.org/10.3390/environments11070152.

Al-Mutairi, N. H., Al-Kawaz, A. E., Abd Al-Hussain, M., Kadhim, B. J., Al-Kawaz, Y., Layla, A. Y., & Hadi, S. F. (2024). Tribological and rheological behavior of polypropylene blended with different types of slipping additives. Jurnal Tribologi, 42(January 2025), 71–84.

Alvarez, D. A. (2013). Development of semipermeable membrane devices (SPMDs) and polar organic chemical integrative samplers (POCIS) for environmental monitoring. Environmental toxicology and chemistry, **32**(10), 2179-2181. https://doi.org/10.1002/etc.2339.

Amelia, T. S. M., Khalik, W. M. A. W. M., Ong, M. C., Shao, Y. T., Pan, H. J., & Bhubalan, K. (2021). Marine microplastics as vectors of major ocean pollutants and its hazards to the marine ecosystem and humans. Progress in earth and planetary science, **8**(1), 12. https://doi.org/10.1186/s40645-020-00405-4.

Andaloro, F., Romeo, T., Ancora, S., & Italiano, F. (2008). La biodiversità marina in aree vulcaniche. Effetti dell'idrotermalismo sulle specie ittiche nell'area eoliana. In: P. Coiro, G.F. Russo (Ed.), I quaderni di uomo e natura n. 3; Il Fuoco dal Mare, vulcanesimo e ambienti sottomarini, 4, 69-79.

Andaloro, F., Romeo, T., Renzi, M., Guerranti, C., Perra, G., Consoli, P., ... & Focardi, S. E. (2012). Alteration of potential harmful elements levels in sediments and biota from the central Mediterranean Sea (Aeolian Archipelago) following an episode of intense volcanic activity. Environmental Monitoring and Assessment, 184(7), 4035-4047. https://doi.org/10.1007/s10661-011-2242-0.

Andolina, C., Cilluffo, G., Zammuto, V., Signa, G., Papale, M., Giudice, A. L., ... & Vizzini, S. (2025). Extreme abiotics drive sediment biocomplexity along pH gradients in a shallow submarine volcanic vent. Marine Pollution Bulletin, 211, 117470. https://doi.org/10.1016/j.marpolbul.2024.117470.

APAT IRSA-CNR. (2003). Metodi analitici per le acque. Manuali e Linee guida. 29/2003. Vol. Terzo. Sezione 8000: metodi ecotossicologici.

ARPA FVG (2020). Monitoring of transitional and coastal marine waters in the Friuli Venezia Giulia Region (Italian Legislative Decree 152/2006): Ecological and chemical status for the 2017–2019 period. Regional Agency for Environmental Protection of Friuli Venezia Giulia. Available at: https://www.arpa.fvg.it.

ARPA FVG (2023). Ecological and chemical status of transitional and coastal marine waters in Friuli Venezia Giulia (Italian Legislative Decree 152/06 and subsequent amendments): 2020–2022 monitoring period – Report CWTW_2020–22. Regional Agency for Environmental Protection of Friuli Venezia Giulia. Available at: https://www.arpa.fvg.it.

ASTM (1994). Standard guide for designing biological tests with sediments. In: Annual book of ASTM standards water and environmental technology, E1525-02. ASTM Philadelphia.

Baldassarre, L., Natali, V., De Pascale, F., Vezzi, A., Banchi, E., Bazzaro, M., Relitti, F., Tagliapietra, D., & Cibic, T. (2023). The impact of MOSE (Experimental Electromechanical Module) flood barriers on microphytobenthic community of the Venice Lagoon. Microorganisms, 11(4), 936. https://doi.org/10.3390/microorganisms11040936.

Bellino, A., Mangano, M. C., Baldantoni, D., Russell, B. D., Mannino, A. M., Mazzola, A., Vizzini, S., & Sarà, G. (2019). Seasonal patterns of biodiversity in Mediterranean coastal lagoons. Diversity and Distributions, 25(7), 1153–1166. https://doi.org/10.1111/ddi.12942.

Béné, C., Phillips, M., & Allison, E. H. (2011). The forgotten service: Food as an ecosystem service from estuarine and coastal zones. In E. Wolanski & D. S. McLusky (Eds.), Ecological economics of estuaries and coasts (Vol. 12, pp. 147–180). Treatise on Estuarine and Coastal Science. Elsevier. https://doi.org/10.1016/B978-0-12-374711-2.01208-0.

Bettoso, N., Pittaluga, F., Predonzani, S., Zanello, A., & Acquavita, A. (2023). Mercury levels in sediment, water and selected organisms collected in a coastal contaminated environment: The Marano and Grado Lagoon (Northern Adriatic Sea, Italy). Applied Sciences, 13(5), 3064. https://doi.org/10.3390/app13053064

Bhatnagar, S., Cowley, E.S., Kopf, S.H. et al. Microbial community dynamics and coexistence in a sulfide-driven phototrophic bloom. Environmental Microbiome 15, 3 (2020). https://doi.org/10.1186/s40793-019-0348-0.

Boatta, F., D'Alessandro, W., Gagliano, A. L., Liotta, M., Milazzo, M., Rodolfo-Metalpa, R., ... & Parello, F. (2013). Geochemical survey of Levante Bay, Vulcano Island (Italy), a natural laboratory for the study of ocean acidification. Marine Pollution Bulletin, 73(2), 485-494. https://doi.org/10.1016/j.marpolbul.2013.01.029.

Breder, R. (1987). Distribution of heavy metals in Ligurian and Tyrrhenian coastal waters. Science of The Total Environment, 60, 197-212. https://doi.org/10.1016/0048-9697(87)90416-5.

Campani, T., Baini, M., Giannetti, M., & Fossi, M. C. (2020). Early degradation of bioplastics in coastal waters. Science of the Total Environment, 720, 137540.

Canfield, D. E., Kristensen, E., & Thamdrup, B. (2005). The sulfur cycle. In Advances in Marine Biology (Vol. 48, pp. 313-381). Academic Press. https://doi.org/10.1016/S0065-2881(05)48009-8.

Cao, H., Wang, Y., Lee, O. O., Zeng, X., Shao, Z., & Qian, P. Y. (2014). Microbial sulfur cycle in two hydrothermal chimneys on the Southwest Indian Ridge. MBio, 5(1), 10-1128. https://doi.org/10.1128/mbio.00980-13

Caracausi, A., Ditta, M., Italiano, F., Longo, M., Nuccio, P.M., Paonita, A., & Rizzo, A. (2005). Changes in fluid geochemistry and physico-chemical conditions of geothermal systems caused by magmatic input: The recent abrupt outgassing off the island of Panarea (Aeolian Islands, Italy). Geochimica et Cosmochimica Acta, 69(12), 3045-3059. https://doi.org/10.1016/j.gca.2005.02.011.

Caramanna, G., Voltattorni, N., & Maroto-Valer, M.M. (2011). Is Panarea Island (Italy) a valid cost-effective natural laboratory for the development of detection and monitoring techniques for submarine CO2 seepage? Greenhouse Gases: Science and Technology 1(3), 200-210. https://doi.org/10.1002/ghg.28

Carapezza, M. L., Barberi, F., Ranaldi, M., Ricci, T., Tarchini, L., Barrancos, J., ... & Gattuso, A. (2011). Diffuse CO2 soil degassing and CO2 and H2S concentrations in air and related hazards at Vulcano Island (Aeolian arc, Italy). Journal of Volcanology and Geothermal Research, 207(3-4), 130-144. https://doi.org/10.1016/j.jvolgeores.2011.06.010.

Celussi, M., Quero, G. M., Zoccarato, L., Franzo, A., Corinaldesi, C., Rastelli, E., ... & Luna, G. M. (2018). Planktonic prokaryote and protist communities in a submarine canyon system in the Ligurian Sea (NW Mediterranean). Progress in Oceanography, 168, 210-221. https://doi.org/10.1016/j.pocean.2018.10.002.

Chamas, A., Moon, H., Zheng, J., Qiu, Y., Tabassum, T., Jang, J. H., ... & Suh, S. (2020). Degradation rates of plastics in the environment. ACS Sustainable Chemistry & Engineering, 8(9), 3494-3511. https://doi.org/10.1021/acssuschemeng.9b06635.

Chouba, C., Pringault, O., Domeau, A., Delpoux, S., Causse, L., Marie, M., ... & Montigny, C. (2024). Added value of water column spatiotemporal monitoring to assess variability of trace metal elements and organotin compounds in Mediterranean harbours. Journal of Marine Science and Engineering, 12(3), 399. https://doi.org/10.3390/jmse12030399.

Cibic, T., & Blasutto, O. (2011). Living marine benthic diatoms as indicators of nutrient enrichment: A case study in the Gulf of Trieste. In J. C. Compton (Ed.), Diatoms: Ecology and life cycle (pp. 169–184). Nova Science Publishers. https://hdl.handle.net/20.500.14083/3560.

Cibic, T., & Virgilio, D. (2010). Different fixatives and chloridric acid concentrations in microphytobenthic primary production estimates using radiolabeled carbon: their use and misuse. Limnology and Oceanography: Methods, 8(9), 453-461. https://hdl.handle.net/20.500.14083/3457.

Cibic, T., & Virgilio, D. (2011) In situ primary production measurements as an analytical support to remote sensing—an experimental approach to standardize the ^{14}C incorporation technique. INTECH OpenAccess Publisher. https://doi.org/10.5772/17175.

Cibic, T., Baldassarre, L., Cerino, F., Comici, C., Fornasaro, D., Kralj, M., & Giani, M. (2022a). Benthic and pelagic contributions to Primary Production: Experimental insights from the Gulf of Trieste (Northern Adriatic Sea). Frontiers in Marine Science, 9, 877935. https://doi.org/10.3389/fmars.2022.877935.

Cibic, T., Blasutto, O., Burba, N., Fonda Umani, S. (2008). Microphytobenthic primary production as ^{14}C uptake in sublittoral sediments of the Gulf of Trieste (northern Adriatic Sea): methodological aspects and data analyses. Estuarine, Coastal and Shelf Science, 77, 113–122. https://hdl.handle.net/20.500.14083/2789.

Cibic, T., Blasutto, O., Falconi, C., & Fonda Umani, S. (2007a). Microphytobenthic biomass, species composition and nutrient availability in sublittoral sediments of the Gulf of Trieste (northern Adriatic Sea). Estuarine, Coastal and Shelf Science, 75(1–2), 50–62. https://doi.org/10.1016/j.ecss.2007.01.020.

Cibic, T., Franzo, A., Celussi, M., Fabbro, C., & De Negro, P. (2012b). Benthic ecosystem functioning in hydrocarbon and heavy-metal contaminated sediments of an Adriatic lagoon. Marine Ecology Progress Series, 458, 69–87. https://doi.org/10.3354/meps09741.

Cibic, T., Orlando-Bonaca, M., & Rubino, F. (2022). Editorial: New perspectives in benthic–pelagic coupling in marine and transitional coastal areas. Frontiers in Marine Science, 9, 1009078. https://doi.org/10.3389/fmars.2022.1009078.

Cingano, P., Vuerich, M., Petruzzellis, F., Orzan, L., Trotta, G., Casolo, V., Asquini, E., Bacaro, G., & Boscutti, F. (2024). Seagrasses on the move: Tracing the multi-decadal species distribution trends in lagoon meadows using Landsat imagery. Estuarine, Coastal and Shelf Science, 299, 108998. https://doi.org/10.1016/j.ecoinf.2024.102685.

Côté, I. M., Darling, E. S., & Brown, C. J. (2016). Interactions among ecosystem stressors and their importance in conservation. Proceedings of the Royal Society B: Biological Sciences, 283(1824), 20152592. https://doi.org/10.1098/rspb.2015.2592.

Crain, C. M., Kroeker, K., & Halpern, B. S. (2008). Interactive and cumulative effects of multiple human stressors in marine systems. Ecology letters, 11(12), 1304-1315. https://doi.org/10.1111/j.1461-0248.2008.01253.x.

Culotta, L., Gianguzza, A., Mannino, M. R., & Orecchio, S. (2007). Polycyclic aromatic hydrocarbons (pah) in Vulcano Island (aeolian archipelago) mud utilized for therapeutic purpose. Polycyclic Aromatic Compounds, 27(4), 281-294. https://doi.org/10.1080/10406630701476023.

Currie, K., Sabine, C., Lowder, K., Hassoun, A. E. R., García-Ibáñez, M. I., Meléndez, M., & Schoo, K. (2024). Determining Total Alkalinity. In K. Lowder, S. Chu, R. Easley, R. Spaulding, B. Peterson, K. Grabb, & A. Reed (Eds.), Practical Best Practices, version 1 (1st ed.).

D'Alessandro, M., Esposito, V., Porporato, E. M., Berto, D., Renzi, M., Giacobbe, S., ... & Romeo, T. (2018). Relationships between plastic litter and chemical pollutants on benthic biodiversity. Environmental Pollution, 242, 1546-1556. https://doi.org/10.1016/j.envpol.2018.08.002.

Dahms, H. U., Schizas, N. V., James, R. A., Wang, L., & Hwang, J. S. (2018). Marine hydrothermal vents as templates for global change scenarios. Hydrobiologia, 818(1), 1-10. https://doi.org/10.1007/s10750-018-3598-8.

Dando, P. R., Stüben, D., & Varnavas, S. P. (1999). Hydrothermalism in the Mediterranean Sea. Progress in Oceanography, 44(1-3), 333-367. https://doi.org/10.1016/S0079-6611(99)00032-4.

Davison, W. (2016). Diffusive gradients in thin-films for environmental measurements. Cambridge University Press. https://doi.org/10.1017/CBO9781316442654.

Dayananda, N. R., Wijesinghe, J., Botheju, S. M., Perera, W. P. R. T., & Liyanage, J. A. (2025). Ocean Warming, Acidification, Plastic Pollution, and Water Quality Deterioration: A Multifaceted Crisis Unveiled. Coastal and Marine Pollution: Source to Sink, Mitigation and Management, 111-138. https://doi.org/10.1002/9781394237029.ch6Digital Object Identifier (DOI)

de Vogel, F. A., Goudriaan, M., Zettler, E. R., Niemann, H., Eich, A., Weber, M., ... & Amaral-Zettler, L. A. (2024). Biodegradable plastics in Mediterranean coastal environments feature contrasting microbial succession. Science of the Total Environment, 928, 172288. https://doi.org/10.1016/j.scitotenv.2024.172288.

Di Bella, L., Conte, A. M., Conti, A., Esposito, V., Gaglioti, M., Ingrassia, M., De Vittor, C., & Bigi, S. (2022). Potential resilience of benthic foraminifers to acidification in Posidonia oceanica meadows at the Panarea vent system. Geosciences, 12(5), 184. https://doi.org/10.3390/geosciences12050184.

Dickson, A. G., Sabine, C. L., & Christian, J. R. (2007). Guide to best practices for ocean CO2 Measurements, Vol. 3. Sidney. Canada: PICES Special Publication.

Dizdarevič, T. (2001). The influence of mercury production in Idrija mine on the environment in the Idrija region and over a broad area. RMZ–Materials and Geoenvironment, 48, 56–64.

Doney, S. C., Fabry, V. J., Feely, R. A., & Kleypas, J. A. (2009). Ocean acidification: the other CO2 problem. Annual review of marine science, 1(1), 169-192. https://doi.org/10.1146/annurev.marine.010908.163834.

Duarte, A. M., Silva, F., Mendes, S., Pinto, F. R., Barroso, S., Silva, E., ... & Gil, M. M. (2022). Seasonal study of the nutritional composition of unexploited and low commercial value fish species from the Portuguese coast. Food Science & Nutrition, 10(10), 3368-3379. https://doi.org/10.1002/fsn3.2937.

Dussud, C., Hudec, C., George, M., Fabre, P., Higgs, P., Bruzaud, S., ... & Ghiglione, J. F. (2018). Colonization of non-biodegradable and biodegradable plastics by marine microorganisms. Frontiers in microbiology, 9, 1571. https://doi.org/10.3389/fmicb.2018.01571.

Dwivedi, A. K., Mallawaarachchi, I., & Alvarado, L. A. (2017). Analysis of small sample size studies using nonparametric bootstrap test with pooled resampling method. Statistics in Medicine, 36(23), 3639–3656. https://doi.org/10.1002/sim.7263.

Edler, L. (1979). Recommendations on methods for marine biological studies in the Baltic Sea: Phytoplankton and chlorophyll. Baltic Marine Biologists Publication, 5, 1–38.

El-Sharkawy, M., Alotaibi, M. O., Li, J., Du, D., & Mahmoud, E. (2025). Heavy metal pollution in coastal environments: Ecological implications and management strategies: A review. Sustainability, 17(2), 701. https://doi.org/10.3390/su17020701.

Espa, S., Caramanna, G., & Bouché, V. (2010). Field study and laboratory experiments of bubble plumes in shallow seas as analogues of sub-seabed CO2 leakages. Applied Geochemistry, 25(5), 696-704. https://doi.org/10.1016/j.apgeochem.2010.02.002.

Esposito, A., Giordano, G., & Anzidei, M. (2006). The 2002-2003 submarine gas eruption at Panarea volcano, Aeolian Islands, Italy: volcanology of the seafloor and implications for the hazard scenario. Marine Geology, 227 (1-2), 119-134. https://doi.org/10.1016/j.margeo.2005.11.007.

Evers, D. C., Ackerman, J. T., Åkerblom, S., Bally, D., Basu, N., Bishop, K., ... & Wu, P. (2024). Global mercury concentrations in biota: their use as a basis for a global biomonitoring framework. Ecotoxicology, 33(4), 325-396. https://doi.org/10.1007/s10646-024-02747-x.

Falkenberg, L. J., Scanes, E., Ducker, J., & Ross, P. M. (2021). Biotic habitats as refugia under ocean acidification. Conservation Physiology, 9(1), coab077. https://doi.org/10.1093/conphys/coab077.

Feijoo, P., Marín, A., Sánchez-Safont, E., Tena-Medialdea, J., García-March, J. R., Gámez-Pérez, J., & Cabedo, L. (2025). Marine degradation of plastics in Western Mediterranean Sea: Comparison between biodegradable and conventional polymers. Polymer Degradation and Stability, 234(January). https://doi.org/10.1016/j.polymdegradstab.2025.111222

Ferrarin, C., Cucco, A., Umgiesser, G., Bellafiore, D., & Amos, C. L. (2010). Modelling fluxes of water and sediment between Venice Lagoon and the sea. Continental Shelf Research, 30(8), 904–914. https://doi.org/10.1016/j.csr.2009.08.014.

Figuerola, B., Hancock, A. M., Bax, N., Cummings, V. J., Downey, R., Griffiths, H. J., ... & Stark, J. S. (2021). A review and meta-analysis of potential impacts of ocean acidification on marine calcifiers from the Southern Ocean. Frontiers in Marine Science, 8, 584445. https://doi.org/10.3389/fmars.2021.584445.

Franzo, A., Cibic, T., Del Negro, P., & De Vittor, C. (2015). Spatial distribution of microphytobenthos, meiofauna and macrofauna in the northwestern Adriatic Sea: A synoptic study. Advances in Oceanography and Limnology, 6(1-2), 58–75. https://doi.org/10.4081/aiol.2015.5470.

Gaglioti, M., & Gambi, M. C. (2018). The natural laboratory of the CO2 vents off Panarea (Aeolian Islands, Italy): a special ecological setting and a further stepping stone for some alien macrophytes. Not. SIBM, 74, 111-117.

Gambi, M. C., Esposito, V., & Marín-Guirao, L. (2023). Posidonia bonsai: Dwarf Posidonia oceanica shoots associated to hydrothemal vent systems (Panarea Island, Italy). Aquatic Botany, 185, 103611. https://doi.org/10.1016/j.aquabot.2022.103611.

Gargas, E. (1975). A manual for phytoplankton primary production studies in the Baltic. Baltic Marine Biologists Publication, 2, 1–88.

Gattuso, J. P., Magnan, A., Billé, R., Cheung, W. W., Howes, E. L., Joos, F., Bopp, L., Cooley, S. R., Eakin, C. M., Hoegh-Guldberg, O., Kelly, R. P., Pörtner, H.-O., Rogers, A. D., Baxter, J. M., Laffoley, D., Osborn, D., Rankovic, A., Rochette, J., Sumaila, U. R., Treyer, S., & Turley, C. (2015). Contrasting futures for ocean and society from different anthropogenic CO2 emissions scenarios. Science, 349(6243), aac4722. https://doi.org/10.1126/science.aac4722.

Geppi, E., Riera, R., Colodro, I., & Pérez-Ruzafa, Á. (2023). Small but key to nature conservation: Small packed communities in a small lagoon from a biodiversity hotspot. Science of The Total Environment, 906, 167601. https://doi.org/10.1016/j.ecss.2023.108546.

German, C. R., & Von Damm, K. L. (2006). Hydrothermal processes. In H. Elderfield (Ed.), Treatise on geochemistry, 6, 181-222. https://doi.org/10.1016/B0-08-043751-6/06109-0.

Giraud G. 1977. Contribution à la description et à la phénologie quantitative des herbiers à *Posidonia oceanica* (L.) Delile. Thèse doctorat 3eme cycle, univ. Aix-Marseille II, France:150 pp.

Gissi, E., Manea, E., Mazaris, A. D., Fraschetti, S., Almpanidou, V., Bevilacqua, S., Coll, M., Guarnieri, G., Lloret-Lloret, E., Pascual, M., Petza, D., Rilov, G., Schonwald, M., Stelzenmüller, V., & Katsanevakis, S. (2021). A review of the combined effects of climate change and other local human stressors on the marine environment. Science of The Total Environment, 755 (Pt 2), 142564. https://doi.org/10.1016/j.scitotenv.2020.142564.

Glibert, P. M., Cai, W.-J., Hall, E. R., Li, M., Main, K. L., Rose, K. A., Testa, J. M., & Vidyarathna, N. K. (2022). Stressing over the complexities of multiple stressors in marine and estuarine systems. Research, 2022, 9787258. https://doi.org/10.34133/2022/9787258.

Gunderson, A. R., Armstrong, E. J., & Stillman, J. H. (2016). Multiple Stressors in a Changing World: The Need for an Improved Perspective on Physiological Responses to the Dynamic Marine Environment. Annual Review of Marine Science, 8, 357–378. https://doi.org/10.1146/annurev-marine-122414-033953.

GURI (1999). Ministry of Agricultural and Forestry Policies. "Approval of the official methods of chemical soil analysis." Ministerial Decree of 13 September 1999. Official Gazette of the Italian Republic, General Series No. 248, 21 October 1999.

GURI (2015). Ministry of the Environment and Protection of Land and Sea. Ministerial Decree No. 172/2015: Environmental quality standards for marine sediments.". Official Gazette of the Italian Republic, General Series No. 208 of 8 September 2015.

GURI (2016). Ministry of the Environment and Protection of Land and Sea. "Ministerial Decree No. 173/2016: Technical criteria for the management and classification of dredged marine sediments." Official Gazette of the Italian Republic, General Series No. 208 of 6 September 2016.

Hall-Spencer, J. M., and others. 2008. Volcanic carbon dioxide vents show ecosystem effects of ocean acidification. Nature 454: 96–99. https://doi.org/10.1038/nature07051

Hall-Spencer, J. M., Rodolfo-Metalpa, R., Martin, S., Ransome, E., Fine, M., Turner, S. M., Rowley, S. J., Tedesco, D., & Buia, M. C. (2008). Volcanic carbon dioxide vents show ecosystem effects of ocean acidification. Nature, 454(7200), 96–99. https://doi.org/10.1038/nature07051.

Halpern, B. S., Frazier, M., Potapenko, J., Casey, K. S., Koenig, K., Longo, C., ... & Walbridge, S. (2015). Spatial and temporal changes in cumulative human impacts on the world's ocean. Nature communications, 6(1), 7615. https://doi.org/10.1038/ncomms8615.

Hansen, H. P., & Koroleff, F. (1999). Determination of nutrients. In K. Grasshoff, K. Kremling, & M. Ehrhardt (Eds.), Methods of seawater analysis (3rd ed., pp. 159–228). Wiley-VCH. https://doi.org/10.1002/9783527613984.ch10.

Hejna, A., Kosmela, P., Mysiukiewicz, O., & Barczewski, M. (2023). Insights into Seawater Biodegradation of Sustainable Mater-Bi/Poly(ε-caprolactone)-Based Biocomposites Filled with Diisocyanate-Modified Cellulose Particles. Environments - MDPI, 10(5). https://doi.org/10.3390/environments10050090.

Hillebrand, H., Dürselen, C.-D., Kirschtel, D., Pollingher, U., & Zohary, T. (1999). Biovolume calculation for pelagic and benthic microalgae. Journal of Phycology, 35(2), 403–424. https://doi.org/10.1046/j.1529-8817.1999.3520403.x.

Holmer, M., Duarte, C. M., Boschker, H. T. S., & Barrón, C. (2004). Carbon cycling and bacterial carbon sources in pristine and impacted Mediterranean seagrass sediments. Aquatic Microbial Ecology, 36(3), 227-237. https://doi.org/10.3354/ame036227.

IPCC (2023). Sixth Assessment Report (AR6): Climate Change 2023 – Synthesis Report. Intergovernmental Panel on Climate Change.

ISO 10253:2024. International Organization for Standardization (ISO). Water quality — Marine algal growth inhibition test with *Skeletonema* sp. and *Phaeodactylum tricornutum*. Geneva: ISO; 2024.

Italiano, F. (2009). Hydrothermal fluids vented at shallow depths at the Aeolian islands: relationships with volcanic and geothermal systems. In 1st International Workshop Research in Shallow Marine and Fresh Water Systems (p. 55).

Italiano, F., & Nuccio, P. M. (1991). Geochemical investigations at Panarea. Journal of Volcanology and Geothermal Research, 46(1-2), 125–141. https://doi.org/10.1016/0377-0273(91)90079-F.

Karuza, A., Celussi, M., Cibic, T., Del Negro, P. & De Vittor, C. (2012). Virioplankton and bacterioplankton in a shallow CO_2-dominated hydrothermal vent (Panarea island, Tyrrhenian sea). Estuarine, Coastal and Shelf Science 97, 10-18. https://doi.org/10.1016/j.ecss.2011.10.027.

Kennish, M. J. (2015). Coastal lagoons. In M. J. Kennish (Ed.), Encyclopedia of Estuaries (pp. 140–143). Springer. https://doi.org/10.1007/978-94-017-8801-4_47.

Kirchman, D., K'Nees, E., & Hodson, R. (1985). Leucine incorporation and its potential as a measure of protein synthesis by bacteria in natural aquatic systems. Applied and Environmental Microbiology, 49(3), 599–607. https://doi.org/10.1128/aem.49.3.599-607.1985.

Klein, K., Hof, D., Dombrowski, A., Schweyen, P., Dierkes, G., Ternes, T., ... & Oehlmann, J. (2021). Enhanced in vitro toxicity of plastic leachates after UV irradiation. Water Research, 199, 117203. https://doi.org/10.1016/j.watres.2021.117203.

Knoppers, B. (1994). Aquatic primary production in coastal lagoons. In B. Kjerfve (Ed.), Coastal Lagoon Processes (Vol. 60, pp. 243–286). Elsevier Oceanography Series. Elsevier.

Kozak, K., Ruman, M., Kosek, K., Karasiński, G., Stachnik, Ł., & Polkowska, Ż. (2017). Impact of volcanic eruptions on the occurrence of PAHs compounds in the aquatic ecosystem of the southern part of West Spitsbergen (Hornsund Fjord, Svalbard). Water, 9(1), 42. https://doi.org/10.3390/w9010042.

La Mantia, F. P., Scaffaro, R., Baiamonte, M., Ceraulo, M., & Mistretta, M. C. (2023). Comparison of the Recycling Behavior of a Polypropylene Sample Aged in Air and in Marine Water. Polymers, 15(9). https://doi.org/10.3390/polym15092173.

Lamb, A. L., Wilson, G. P., & Leng, M. J. (2006). A review of coastal palaeoclimate and relative sea-level reconstructions using $\delta^{13}C$ and C/N ratios in organic material. Earth-Science Reviews, 75(1–4), 29–57. https://doi.org/10.1016/j.earscirev.2005.10.003.

Larson, F., & Sundbäck, K. (2008). Role of microphytobenthos in recovery of functions in a shallow-water sediment system after hypoxic events. Marine Ecology Progress Series, 357, 1–16. https://doi.org/10.3354/meps07426.

Laurent, J., Le Grand, F., Bideau, A., Le Berre, I., Le Floch, S., Pichereau, V., & Laroche, J. (2025). Fatty acid analysis in an estuarine fish species to assess the health status of hydrosystems impacted by eutrophication

and multistressors. Estuarine, Coastal and Shelf Science, 319, 109279. https://doi.org/10.1016/j.ecss.2025.109279

Law, K. L. (2017). Plastics in the marine environment. Annual review of marine science, 9(1), 205-229. https://doi.org/10.1146/annurev-marine-010816-060409

Ligorini, V., Crayol, E., Huneau, F., Garel, E., Malet, N., Garrido, M., Simon, L., Cecchi, P., & Pasqualini, V. (2023). Small Mediterranean coastal Lagoons Under Threat: Hydro-ecological Disturbances and Local Anthropogenic Pressures (Size Matters). Estuaries and Coasts, 46(8), 2220-2243. https://doi.org/10.1007/s12237-023-01182-1.

Liland, K.H., Mevik, B.-H., & Wehrens, R. (2024). pls: Partial Least Squares and Principal Component Regression (R package version 2.8-5). CRAN. https://CRAN.R-project.org/package=pls

Lorenzen, C. J., & Jeffrey, S. W. (1980). Determination of chlorophyll in seawater: Report of intercalibration tests sponsored by SCOR and carried out in September–October 1978. UNESCO Technical Papers in Marine Science, 35, 1–20.

Lv, S., Wang, Q., Li, Y., Gu, L., Hu, R., Chen, Z., & Shao, Z. (2024). Biodegradation of polystyrene (PS) and polypropylene (PP) by deep-sea psychrophilic bacteria of *Pseudoalteromonas* in accompany with simultaneous release of microplastics and nanoplastics. Science of The Total Environment, 948, 174857. https://doi.org/10.1016/j.scitotenv.2024.174857.

Macreadie, P. I., Fourqurean, J. W., & Kelleway, J. J. (2021). Blue carbon as a natural climate solution. Nature Reviews Earth & Environment, 1(12), 732–745. https://doi.org/10.1038/s43017-021-00224-1.

Maday, S. D., Handley, K. M., Northcott, G., Kingsbury, J. M., Smith, D., Pantos, O., & Lear, G. (2025). Plastic leachates alter the composition of marine microbial communities, not functional potential for plastic degradation. FEMS Microbiology Ecology, 101(9), fiaf087. https://doi.org/10.1093/femsec/fiaf087.

Manzo, S., De Nicola, F., Picione, F. D. L., Maisto, G., & Alfani, A. (2008). Assessment of the effects of soil PAH accumulation by a battery of ecotoxicological tests. Chemosphere, 71(10), 1937-1944. https://doi.org/10.1016/j.chemosphere.2007.12.026.

Manzo, S., Schiavo, S., Aleksi, P., & Tabaku, A. (2014). Application of a toxicity test battery integrated index for a first screening of the ecotoxicological threat posed by ports and harbors in the southern Adriatic Sea (Italy). Environmental monitoring and assessment, 186(11), 7127-7139. https://doi.org/10.1007/s10661-014-3915-2.

Marbà, N., Holmer, M., Gacia, E., & Barron, C. (2006). Seagrass beds and coastal biogeochemistry. In: Larkum, A. W. D., Orth, R. J., & Duarte, C. M., editors. Seagrasses: biology, ecology, and conservation. Dordrecht, The Netherlands: Springer; 2006. pp. 135–57. https://doi.org/10.1007/978-1-4020-2983-7_6.

Martínez-Megías, C., & Rico, A. (2022). Biodiversity impacts by multiple anthropogenic stressors in Mediterranean coastal wetlands. Science of The Total Environment, 807, 151712. https://doi.org/10.1016/j.scitotenv.2021.151712.

Mateo, M.A., Cebrian, J., Dunton, K., & Mutchler, T. (2006). Carbon flux in seagrass ecosystems. Seagrasses: Biology, Ecology and Conservation. Springer-Verlag, Berlin/Heidelberg, 159-192. https://doi.org/10.1007/978-1-4020-2983-7_7.

Maugeri, T. L, Lentini, V., Gugliandolo, C., Italiano, F., Cousin S., & Stackebrandt E. (2009). Microbial communities at two shallow hydrothermal vents off Panarea Island (Eolian Islands, Italy). Extremophiles, 13(1), 199-212. https://doi.org/10.1007/s00792-008-0210-6.

Menden-Deuer, S., & Lessard, E. J. (2000). Carbon to volume relationships for dinoflagellates, diatoms, and other protist plankton. Limnology and Oceanography, 45(3), 569–579. https://doi.org/10.4319/lo.2000.45.3.0569.

Mitsch, W. J., & Gosselink, J. G. (2015). Wetlands (5th ed.). John Wiley & Sons.

Monecke, T., Petersen, S., Hannington, M. D., Anzidei, M., Esposito, A., Giordano, G., Garbe-Schönberg, D., Augustin, N., Melchert, B., & Hocking, M. (2012). Explosion craters associated with shallow submarine gas venting off Panarea island, Italy. Bulletin of volcanology, 74(9), 1937-1944. https://doi.org/10.1007/s00445-012-0651-8.

Moya, A., Tambutté, S., Bertucci, A., Tambutté, E., Lotto, S., Vullo, D., Supuran, C. T., Allemand, D., & Zoccola, D. (2014). Carbonic anhydrase in the scleractinian coral Stylophora pistillata: Characterization, localization, and role in biomineralization. Journal of Biological Chemistry, 283(37), 25475–25484. https://doi.org/10.1074/jbc.M804726200.

Nardi, A. (2020). Interactive effects of pollutants and climate change in marine ecosystems. PhD thesis.

National Research Council Canada. (2007). PACS-2: Marine sediment certified reference material for trace metals and other constituents. Ottawa, Ontario: National Research Council Canada, Institute for National Measurement Standards.

Nazareth, M., Marques, M. R. C., Leite, M. C. A., & Castro, Í. B. (2019). Commercial plastics claiming biodegradable status: Is this also accurate for marine environments? Journal of Hazardous Materials, 366(September 2018), 714–722. https://doi.org/10.1016/j.jhazmat.2018.12.052

Newton, A., Brito, A. C., Icely, J. D., Derolez, V., Clara, I., Angus, S., Schernewski, G., Inácio, M., Lillebø, A. I., Béjaoui, B., et al. (2018). Assessing, quantifying and valuing the ecosystem services of coastal lagoons. Journal of Nature Conservation, 44, 50–65. https://doi.org/10.1016/j.jnc.2018.02.009.

Nielsen, E. S. (1952). The use of radioactive carbon (^{14}C) for measuring organic production in the sea. Journal du Conseil, 18(2), 117–140. https://doi.org/10.1093/icesjms/18.2.117.

Nieuwenhuize, J., Maas, Y. E. M., & Middelburg, J. J. (1994). Rapid analysis of organic carbon and nitrogen in particulate materials. Marine Chemistry, 45(3), 217–224. https://doi.org/10.1016/0304-4203(94)90005-1.

Noè, S., Bellavia, C., Calvo, S., Mazzola, A., Pirrotta, M., Sciandra, M., ... & Tomasello, A. (2020). Resilience of the seagrass *Posidonia oceanica* following pulse-type disturbance. Marine Environmental Research, 159, 105011. https://doi.org/10.1016/j.marenvres.2020.105011.

Nogueira, P., M. C. Gambi, S. Vizzini, G. Califano, A. M. Tavares, R. Santos, and B. Martínez-Crego. 2017. Altered epiphyte community and sea urchin diet in *Posidonia oceanica* meadows in the vicinity of volcanic CO2 vents. Marine Environmental Research. 127: 102–111. https://doi.org/10.1016/j.marenvres.2017.04.002

Oksanen, J. (2015). Vegan: community ecology package. R package version, 2, 3.

Orr, J. C., Fabry, V. J., Aumont, O., Bopp, L., Doney, S. C., Feely, R. A., ... & Yool, A. (2005). Anthropogenic ocean acidification over the twenty-first century and its impact on calcifying organisms. Nature, 437(7059), 681-686. https://doi.org/10.1038/nature04095.

Ostrowski, A., Connolly, R. M., & Sievers, M. (2021). Evaluating multiple stressor research in coastal wetlands: A systematic review. Science of The Total Environment, 789, 147966. https://doi.org/10.1016/j.marenvres.2020.105239.

Özogul, Y., Özogul, F. H., Çi˙ çek, E., Polat, A., & Kuley, E. (2009). Fat content and fatty acid compositions of 34 marine water fish species from the Mediterranean Sea. International journal of food sciences and nutrition, 60(6), 464-475. https://doi.org/10.1080/09637480701838175.

Pella, E., & Colombo, B. (1973). Study of carbon, hydrogen and nitrogen determination by combustion–gas chromatography. Mikrochimica Acta, 61(1), 697–719. https://doi.org/10.1007/BF01218130.

Pergent G., 1987. Recherches lépidocronologiques chez *Posidonia oceanica* (Potamogetonaceae). Fluctuations des paramètres anatomiques et morphologiques des écailles des rhizomes. Thèse Doctor. Océanol., Univ. Aix-Marseille II, 1-853.

Pichler, T. (2024). Environmental inventory of mercury (Hg) for the marine shallow water hydrothermal system at Panarea, Italy. Science of The Total Environment, 911, 168575. https://doi.org/10.1016/j.scitotenv.2023.168575.

Pierrot, D., Epitalon, J.-M., Orr, J.C., Lewis, E., & Wallace, D.W.R., (2021). MS Excel program developed for CO2 system calculations – version 3.0, GitHub repository, https://github.com/dpierrot/co2sys_xl.

Pittaluga, F., Aleffi, I. F., Bettoso, N., Blasutto, O., Celio, M., Codarin, A., Cumani, F., Faresi, L., Guiatti, D., Orlandi, C., Zanello, A., & Acquavita, A. (2022). The SHAPE Project: An innovative approach to understanding seasonal and diel dissolved oxygen dynamics in the Marano and Grado Lagoon (Adriatic Sea) under the WFD/2000/60/CE. Agenzia Regionale per la Protezione dell'Ambiente (Arpa FVG).

Prabhu, P. A. J. (2015). Minerals in fish: does the source matter? (Doctoral dissertation, Wageningen University and Research).

Prange, J. A., & Dennison, W. C. (2000). Physiological responses of five seagrass species to trace metals. Marine Pollution Bulletin, 41(7-12), 327-336. https://doi.org/10.1016/S0025-326X(00)00126-0.

Price, R. E., et al. (2017). Geochemistry of vent fluids from three shallow vents off Panarea Island. PANGAEA Dataset. https://doi.org/10.1594/PANGAEA.873672

Price, R. E., Savov, I., Planer-Friedrich, B., Bühring, S. I., Amend, J., & Pichler, T. (2013). Processes influencing extreme As enrichment in shallow-sea hydrothermal fluids of Milos Island, Greece. Chemical Geology, 348, 15-26. https://doi.org/10.1016/j.chemgeo.2012.06.007.

Relitti, F., Ogrinc, N., Esposito, V., Gambi, M. C., Potočnik, D., Giani, M., & De Vittor, C. (2023). You are what you eat: stable isotope signature of the seagrass *Posidonia oceanica* in Panarea hydrothermal vents. Biologia Marina Mediterranea, 28(1), 5-8. Retrieved from https://www.biologiamarinamediterranea.it/index.php/metis/article/view/143

Renieri, E. A., Alegakis, A. K., Kiriakakis, M., Vinceti, M., Ozcagli, E., Wilks, M. F., & Tsatsakis, A. M. (2014). Cd, Pb and Hg biomonitoring in fish of the Mediterranean region and risk estimations on fish consumption. Toxics, 2(3), 417-442. https://doi.org/10.3390/toxics2030417.

Renzi, M., Romeo, T., Guerranti, C., Perra, G., Italiano, F., Focardi, S. E., ... & Andaloro, F. (2011). Temporal trends and matrix-dependent behaviors of trace elements closed to a geothermal hot-spot source (Aeolian Archipelago, Italy). Procedia Earth and Planetary Science, 4, 10-28. https://doi.org/10.1016/j.proeps.2011.11.003.

Repolho, T., Duarte, B., Dionísio, G., Paula, J. R., Lopes, A. R., Rosa, I. C., ... & Rosa, R. (2017). Seagrass ecophysiological performance under ocean warming and acidification. Scientific Reports, 7(1), 41443. https://doi.org/10.1038/srep41443.

Revsbech, N. P. (2005). Analysis of microbial communities with electrochemical microsensors and microscale biosensors. Methods in Enzymology, 397, 147–166. https://doi.org/10.1016/S0076-6879(05)97009-2.

Revsbech, N. P., & Jørgensen, B. B. (1989). Microelectrodes: Their use in microbial ecology. Advances in Microbial Ecology, 11, 293–352. https://doi.org/10.1007/978-1-4757-0611-6_7.

Reyes J., Sanson M., Afonso-Carrillo J. 1995. Leaf phenology, growth and production of the seagrass Cymodocea nodosa at El Medano (South of Tenerife, Canary Islands). Botanica Marina, 38: 457-465. https://doi.org/10.1515/BOTM.1995.38.1-6.457.

Ries, J. B., Cohen, A. L., & McCorkle, D. C. (2009). Marine calcifiers exhibit mixed responses to CO2-induced Ocean acidification. Geology, 37(12), 1131-1134. https://doi.org/10.1130/G30210A.1.

Romagnoli, C., Bortoluzzi, G., Bosman, A., Casalbore, D., Chiocci, F., D'Oriano, F., Gamberi, F., Ligi, M., & Marani, M. (2012). Bathy-morphological setting of the Aeolian Arc. In: Lucchi, F., Peccerillo, A., Keller, J., Tranne, C., & Rossi, P., editors. Geology of the Aeolian Islands (Italy). Geological Society of London, Memoirs; Vol. 37, pp. 27-36. https://doi.org/10.1144/M37.4.

Rouillon, C., Bussiere, P. O., Desnoux, E., Collin, S., Vial, C., Therias, S., & Gardette, J. L. (2016). Is carbonyl index a quantitative probe to monitor polypropylene photodegradation? Polymer Degradation and Stability, 128, 200–208. https://doi.org/10.1016/j.polymdegradstab.2015.12.011.

Rummel, C. D., Schäfer, H., Jahnke, A., Arp, H. P. H., & Schmitt-Jansen, M. (2022). Effects of leachates from UV-weathered microplastic on the microalgae *Scenedesmus vacuolatus*. Analytical and bioanalytical chemistry, 414(4), 1469-1479. https://doi.org/10.1007/s00216-021-03798-3.

Saidi, A., Banchi, E., Fonti, V., Manna, V., De Vittor, C., Giani, M., Malfatti, F., & Celussi, M. (2023). Microbial dynamics in shallow CO_2 seeps system off Panarea Island (Italy). Marine Biology, 170(8), 97. https://doi.org/10.1007/s00227-023-04247-8

Schiavo, S., Oliviero, M., Chiavarini, S., Dumontet, S., & Manzo, S. (2021). Polyethylene, Polystyrene, and Polypropylene leachate impact upon marine microalgae *Dunaliella tertiolecta*. Journal of Toxicology and Environmental Health, Part A, 84(6), 249-260. https://doi.org/10.1080/15287394.2020.1860173.

Signa, G., Mazzola, A., Di Leonardo, R., & Vizzini, S. (2017). Element-specific behaviour and sediment properties modulate transfer and bioaccumulation of trace elements in a highly-contaminated area (Augusta Bay, Central Mediterranean Sea). Chemosphere, 187, 230-239. https://doi.org/10.1016/j.chemosphere.2017.08.099.

Signa, G., Sciutteri, V., Tomasello, A., Costa, A., Casabianca, S., Cilluffo, G., Andolina, C., & Vizzini S. (2024). Combined exposure to CO_2 and H_2S significantly reduces the performance of the Mediterranean seagrass Posidonia oceanica: Evidence from a volcanic vent. Limnology and Oceanography Letters, 9(4), 461-468. https://doi.org/10.1002/lol2.10368.

Signa, G., Tomasello, A., Cilluffo, G., Tramati, C. D., Mazzola, A., Calvo, S., & Vizzini, S. (2024b). Does transplanted Posidonia oceanica act as a sink or source of trace elements? Ecological implications for restoring polluted coastal areas. Journal of Environmental Management, 359, 121008. https://doi.org/10.1016/j.jenvman.2024.121008.

Simon, M., & Azam, F. (1989). Protein content and protein synthesis rates of planktonic marine bacteria. Marine Ecology Progress Series, 51, 201–213. https://doi.org/10.3354/meps051201.

Smith, D. C., & Azam, F. (1992). A simple, economical method for measuring bacterial protein synthesis rates in seawater using ^{3}H-leucine. Marine Microbial Food Webs, 6(2), 107–114. https://api.semanticscholar.org/CorpusID:89585101.

Spagnoli, F., & Ravaioli, M. (2023). Dissolved fluxes of nutrients and carbon at the sediment-water interface in the Adriatic Sea: review of early data and methods from the Italian National Research Council (CNR). Advances in Oceanography and Limnology, 14(1). https://doi.org/10.4081/aiol.2023.11094.

Tassi, F., Capaccioni, B., Caramanna, G., Cinti, D., Montegrossi, G., Pizzino, L., & Vaselli, O. (2009). Low-pH waters discharging from submarine vents at Panarea Island after the 2002 gas blast: Origin and implications for volcanic surveillance. Applied Geochemistry, 24(2), 246–254. https://doi.org/10.1016/j.apgeochem.2008.11.015.

Throndsen, J. (1978). Preservation and Storage. In A. Sournia (Ed.), Phytoplankton Manual (UNESCO Monographs on Oceanographic Methodology, Vol. 6, pp. 69-74). UNESCO.

Thushari, G. G. N., & Senevirathna, J. D. M. (2020). Plastic pollution in the marine environment. Heliyon, 6(8). https://doi.org/10.1016/j.heliyon.2020.e04709.

Toffolo, M. M., Grilli, F., Prandi, C., Goffredo, S., & Marini, M. (2022). Extreme flooding events in coastal lagoons: Seawater parameters and rainfall over a six-year period in the Mar Menor (SE Spain). Journal of Marine Science and Engineering, 10(10), 1521. https://doi.org/10.3390/jmse10101521.

Usero, J., Morillo, J., & Gracia, I. (2005). Heavy metal concentrations in molluscs from the Atlantic coast of southern Spain. Chemosphere, 59(8), 1175-1181. https://doi.org/10.1016/j.chemosphere.2004.11.089.

Utermöhl, H. (1958). Zur Vervollkommnung der quantitativen Phytoplankton-Methodik. Mitteilungen der Internationalen Vereinigung für Theoretische und Angewandte Limnologie, 9, 1–38. https://doi.org/10.1080/05384680.1958.11904091.

Uwadiae, R. E., Chidolue, A., & Fakpor, A. M. (2025). Carbon Sequestration Capacity of the Lagos Lagoon: Examining the Potentials of a Typical Nigerian Coastal Ecosystem for Climate Change Mitigation. Transylvanian Review of Systematical and Ecological Research, 26(2), 1–16. https://doi.org/10.2478/trser-2024-0007.

van Duyl, F. C., & Kop, A. J. (1994). Bacterial production in North Sea sediments: Clues to seasonal and spatial variations. Marine Biology, 120(3), 323–337. https://doi.org/10.1007/BF00349694

Vassallo, P., Paoli, C., Rovere, A., Montefalcone, M., Morri C., & Bianchi, C. N. (2013). The value of the seagrass Posidonia oceanica: A natural capital assessment. Marine Pollution Bulletin, 75(1-2), 157-167. https://doi.org/10.1016/j.marpolbul.2013.07.044.

Vizzini, S., Di Leonardo, R., Costa, V., Tramati, C. D., Luzzu, F., & Mazzola, A. (2013). Trace element bias in the use of CO2 vents as analogues for low pH environments: Implications for contamination levels in acidified oceans. Estuarine, Coastal and Shelf Science, 134, 19-30. https://doi.org/10.1016/j.ecss.2013.09.015.

Vizzini, S., Tomasello, A., Maida, G. D., Pirrotta, M., Mazzola, A., & Calvo, S. (2010). Effect of explosive shallow hydrothermal vents on $\delta^{13}C$ and growth performance in the seagrass *Posidonia oceanica*. Journal of Ecology, 98(6), 1284-1291. https://doi.org/10.1111/j.1365-2745.2010.01730.x

Voltattorni, N., Caramanna, G., Cinti, D., Galli, G., Pizzino, L., & Quattrocchi, F. (2006). Study of natural CO2 emissions in different Italian geological scenarios. In Advances in the Geological Storage of Carbon Dioxide: International Approaches to Reduce Anthropogenic Greenhouse Gas Emissions (pp. 175-190). Dordrecht: Springer Netherlands. https://doi.org/10.1007/1-4020-4471-2_15.

Vuong, H. (2023). Marine plastic pollution: a review of the scientific evidence, current policies, and potential solutions. World Maritime University Dissertation.

Wentworth, C. K. (1922). A scale of grade and class terms for clastic sediments. The Journal of Geology, 30(5), 377–392. https://doi.org/10.1086/622910.

Yuvka, İ., Kosker, A. R., Durmus, M., Ucar, Y., & Ozogul, Y. (2025). Seasonal changes in the elemental composition of five valuable fish species (sparidae) from Bozcaada, North Aegean Sea: a health risk and nutritional benefit assessment. Foods, 14(2), 324. https://doi.org/10.3390/foods14020324.

Zettler, E. R., Mincer, T. J., & Amaral-Zettler, L. A. (2013). Life in the "plastisphere": microbial communities on plastic marine debris. Environmental science & technology, 47(13), 7137-7146. https://doi.org/10.1021/es401288x.

Zhang, H. and Davison, W. (1995) Performance Characteristics of Diffusion Gradients in Thin Films for the *in situ* Measurement of Trace Metals in Aqueous Solution. Analytical Chemistry, 67, 3391-3400. http://dx.doi.org/10.1021/ac00115a005.

Zhang, H., & Davison, W. (2015). Use of diffusive gradients in thin-films for studies of chemical speciation and bioavailability. Environmental Chemistry, 12(2), 85-101. https://doi.org/10.1071/EN14105.

Zingone, A., Montresor, M., & Marino, D. (1990). Morphological variability of *Chaetoceros socialis* Lauder (Bacillariophyceae), with a critical revision of the species concept. Phycologia, 29(4), 345–355. 10.1111/j.1529-8817.2007.00430.x.

9 Acknowledgements

We sincerely thank all those who provided valuable support during the experimental activities in the Grado-Marano Lagoon, including Rocco Auriemma, Mauro Celussi, Alessandra Davanzo, Tommaso Diociaiuti, Simona Iannucci, Federica Nasi, and Lisa Sandri.

10 Supplementary Material

Table 10.S1 Results of the bootstrap resampling test of biotic and abiotic variables measured in mesocosms at experimental times T_1 and T_2. For each variable, mean, minimum, and maximum values inside and outside the mesocosms are reported. The *Significant* column indicates whether differences between inside and outside were significant.

Experimental time	Variable	Mean	Min	Max	External	Significant
T1	BP	-16.4	-17.9	-14.7	43.7	Yes
T1	C/N	-0.710	-1.21	-0.0900	10.3	Yes
T1	CRs	-1.01	-2.16	0.864	-10.4	No
T1	Chl *a*	-0.0700	-0.19	0.0800	1.64	No
T1	Clay	1.24	-1.59	3.3	11.5	No
T1	Coccolithopores	-0.0167	-0.09	0.04	0.09	No
T1	Diatoms	-12.5	-15.2	-9.28	29.0	Yes
T1	Dinoflagellates	-1.23	-3.87	3.07	6.77	No
T1	Flagellates	-2.68	-4.51	-1.07	7.85	Yes
T1	GPPw	-0.93	-2.88	1.19	14.1	No
T1	GPPs	-6.94	-9.28	-4.21	14.0	Yes
T1	HCPw	1.97	0.130	4.05	7.25	Yes
T1	HCPs	1.01	0.0300	1.55	2.23	Yes
T1	MPB	40.7	26.2	63.3	47.0	Yes
T1	$N\text{-}NH_4$	4.27	2.6	7.2	1.73	Yes
T1	$N\text{-}NO_2$	-0.0833	-0.11	-0.07	0.32	Yes
T1	$N\text{-}NO_3$	-2.72	-2.87	-2.54	5.04	Yes
T1	NPPs	-7.94	-11.0	-3.35	3.61	Yes
T1	$O_2(\%)$	-27.0	-44.6	-17.4	124.0	Yes
T1	$P\text{-}PO_4$	0.0	0.0	0.0	0.01	No
T1	Salinity	-2.01	-2.08	-1.95	27.7	Yes
T1	Sand	-1.40	-8.3	6.7	58.0	No
T1	$Si\text{-}Si(OH)_4$	6.28	1.79	14.4	9.61	Yes
T1	Silt	0.163	-5.11	5.0	30.5	No
T1	TC	-0.247	-1.08	0.190	67	No
T1	TN	0.377	0.100	0.55	1.89	Yes
T1	TOC	1.84	0.690	2.56	16.6	Yes
T1	Temperature	0.0933	-0.110	0.260	26.6	No
T1	pH	-0.123	-0.190	-0.0600	8.37	Yes
T2	BP	1.22	-1.56	2.74	5.44	No
T2	C/N	-0.0133	-0.780	1.22	10.5	No
T2	CRs	1.85	-1.30	4.54	-9.50	No
T2	Chl *a*	-0.0533	-0.11	0.0300	0.79	No
T2	Clay	-0.233	-3.3	3.3	18.5	No
T2	Coccolithopores	-0.04	-0.04	-0.04	0.04	Yes
T2	Diatoms	2.92	1.11	4.48	1.93	Yes
T2	Dinoflagellates	-0.623	-1.31	0.41	1.52	No
T2	Flagellates	-1.03	-1.32	-0.74	1.95	Yes
T2	GPPw	-1.46	-2.24	-0.78	6.7	Yes
T2	GPPs	-9.43	-11.0	-6.41	14.6	Yes

T2	HCPw	-2.92	-5.99	-0.92	12.3	Yes
T2	HCPs	-0.787	-2.36	1.82	4.33	No
T2	MPB	63.0	-0.730	177.0	72.2	No
T2	$N\text{-}NH_4$	4.41	3.53	5.52	1.68	Yes
T2	$N\text{-}NO_2$	0.0467	0.0	0.14	0.16	No
T2	$N\text{-}NO_3$	-0.0200	-0.2	0.0900	1.3	No
T2	NPPs	-7.58	-8.55	-6.48	5.09	Yes
T2	$O_2(\%)$	-32.2	-34.9	-29.1	139.0	Yes
T2	$P\text{-}PO_4$	0.0533	0.01	0.13	0.01	Yes
T2	Salinity	1.72	1.59	1.87	25.2	Yes
T2	Sand	3.1	-6.9	13.0	36.3	No
T2	$Si\text{-}Si(OH)_4$	6.77	4.57	10.9	10.3	Yes
T2	Silt	-2.87	-9.7	3.60	45.2	No
T2	TC	-0.0267	-1.35	1.72	67.0	No
T2	TN	0.0100	-0.52	0.44	1.93	No
T2	TOC	-0.180	-3.15	2.4	17.3	No
T2	Temperature	-0.283	-0.450	-0.0500	27.6	Yes
T2	pH	-0.130	-0.150	-0.100	8.47	Yes

Table 10.S2 Results of the Tukey HSD test for multiple comparisons among experimental times (T_0, T_1, T_2) for all considered variables. For each variable, the. columns *T1–T0 diff*, *T2–T0 diff*, and *T2–T1 diff* report the mean differences between times, followed by the p-value in parentheses. The *Significance* column indicates the level of significance (multiple comparisons): *** p < 0.001 (extremely significant), ** 0.001 ≤ p < 0.01 (highly significant), * 0.01 ≤ p < 0.05 (significant), ns p ≥ 0.05 (not significant).

Variable	T1–T0 diff (p)	Significant	T2–T0 diff (p)	Significant	T2–T1 diff (p)	Significant
Temperature	-1.63 (0.0257)	*	-1.06 (0.124)	ns	0.57 (0.458)	ns
O_2(%)	-99.5 (0.000464)	**	-89.17 (0.000845)	**	10.33 (0.693)	ns
Salinity	3.63 (9.1e-07)	***	4.89 (2.14e-07)	***	1.25 (0.000359)	**
pH	-0.38 (0.00017)	**	-0.29 (0.000802)	**	0.09 (0.122)	ns
N-NH_4	4.64 (0.0268)	*	4.73 (0.0246)	*	0.09 (0.997)	ns
N-NO_2	-0.61 (4.85e-05)	***	-0.64 (3.67e-05)	***	-0.03 (0.829)	ns
N-NO_3	-8.82 (6.39e-06)	***	-9.86 (3.23e-06)	***	-1.04 (0.194)	ns
P-PO_4	0 (1)	ns	0.05 (0.28)	ns	0.05 (0.28)	ns
Si-$Si(OH)_4$	8.99 (0.114)	ns	10.21 (0.0749)	ns	1.22 (0.943)	ns
Chl *a*	0.51 (0.00204)	**	-0.32 (0.0201)	*	-0.83 (0.000143)	**
BP	11.69 (0.0257)	*	-8.93 (0.0727)	n.s.	-20.63 (0.00168)	**
Diatoms	7.43 (0.048)	*	-4.23 (0.258)	ns	-11.66 (0.0067)	**
Dinoflagellates	4.19 (0.162)	ns	-0.45 (0.972)	ns	-4.64 (0.121)	ns
Coccolithophores	0.07 (0.126)	ns	0 (1)	ns	-0.07 (0.126)	ns
Flagellates	0 (1)	ns	-4.26 (0.0271)	*	-4.25 (0.0272)	*
GPPw	7.61 (0.00115)	**	-0.33 (0.953)	ns	-7.94 (0.000914)	**
HCPw	-1.34 (0.69)	ns	-1.18 (0.746)	ns	0.16 (0.995)	ns
Clay	-2.26 (0.533)	ns	3.27 (0.305)	ns	5.53 (0.0735)	ns
Silt	-5.87 (0.385)	ns	5.8 (0.392)	ns	11.67 (0.0659)	ns
Sand	8.13 (0.422)	ns	-9.07 (0.354)	ns	-17.2 (0.0654)	ns
TN	-0.15 (0.883)	ns	-0.48 (0.346)	ns	-0.33 (0.579)	ns
TC	-3.16 (0.0266)	*	-2.94 (0.0357)	*	0.22 (0.966)	ns
TOC	-1.88 (0.691)	ns	-3.23 (0.375)	ns	-1.35 (0.821)	ns
C/N	-0.24 (0.917)	ns	0.67 (0.531)	ns	0.91 (0.342)	ns
MPB	5.34 (0.993)	ns	52.93 (0.554)	ns	47.59 (0.615)	ns
CRs	9.58 (0.011)	*	13.3 (0.00216)	**	3.72 (0.279)	ns
GPPs	-10.37 (0.0184)	*	-12.25 (0.00855)	**	-1.88 (0.767)	ns
NPPs	-0.8 (0.946)	ns	1.04 (0.91)	ns	1.84 (0.753)	ns
HCPs	0.44 (0.924)	ns	0.74 (0.802)	ns	0.3 (0.963)	ns

Table 10.S3 Spearman correlation tests performed on the measured variables in water and sediment, reporting only significant correlations. The correlation coefficient ρ, the p-value, and statistical significance, with *** for p < 0.001, ** for p < 0.01, and * for p < 0.05 are indicated

WATER COLUMN				
Var1	**Var2**	**ρ**	**p-value**	**Significant**
O_2(%)	Temperature	0.79	3.75×10^{-3}	**
Salinity	Temperature	–0.67	2.33×10^{-2}	*
pH	Temperature	0.83	1.43×10^{-3}	**
N-NH_4	Temperature	–0.66	2.60×10^{-2}	*
Si-$Si(OH)_4$	Temperature	–0.62	4.26×10^{-2}	*
Dinoflagellates	Temperature	–0.66	2.60×10^{-2}	*
GPPw	Temperature	–0.75	8.45×10^{-3}	**
N-NH_4	O_2(%)	–0.87	4.55×10^{-4}	***
N-NH_4	Salinity	0.61	4.67×10^{-2}	*
O_2(%)	pH	0.93	2.60×10^{-5}	***
N-NH_4	pH	–0.82	2.22×10^{-3}	**
N-NH_4	N-NO_2	–0.66	2.79×10^{-2}	*
N-NH_4	N-NO_3	–0.69	1.86×10^{-2}	*
N-NO_2	N-NO_3	0.79	4.11×10^{-3}	**
N-NO_3	P-PO_4	–0.67	2.39×10^{-2}	*
Chl *a*	P-PO_4	–0.72	1.20×10^{-2}	*
Flagellates	P-PO_4	–0.77	5.11×10^{-3}	**
O_2(%)	Si-$Si(OH)_4$	–0.83	1.68×10^{-3}	**
pH	Si-$Si(OH)_4$	–0.79	3.96×10^{-3}	**
N-NH_4	Si-$Si(OH)_4$	0.98	8.40×10^{-8}	***
N-NO_2	Si-$Si(OH)_4$	–0.76	6.79×10^{-3}	**
N-NO_3	Si-$Si(OH)_4$	–0.72	1.28×10^{-2}	*
Chl *a*	Diatoms	0.81	2.56×10^{-3}	**
Chl *a*	Dinoflagellates	0.72	1.28×10^{-2}	*
Diatoms	Dinoflagellates	0.78	4.47×10^{-3}	**
Chl *a*	Flagellates	0.70	1.65×10^{-2}	*
Diatoms	Flagellates	0.69	1.86×10^{-2}	*
Chl *a*	GPPw	0.73	1.12×10^{-2}	*
Dinoflagellates	GPPw	0.65	2.89×10^{-2}	*
SEDIMENT				
Var1	**Var2**	**ρ**	**p-value**	**Significant**
Clay	Silt	0.94	1.35×10^{-5}	***
Sand	Silt	–1.00	1.71×10^{-10}	***
C/N	TN	–0.62	4.20×10^{-2}	*
NPPs	TN	–0.61	4.82×10^{-2}	*
CRs	TC	–0.76	7.14×10^{-3}	**
GPPs	TC	0.75	8.23×10^{-3}	**
NH4	Si-$Si(OH)_4$	0.98	8.40×10^{-8}	***
CRs	GPPs	–0.64	3.31×10^{-2}	*
C/N	NPPs	0.66	2.60×10^{-2}	*

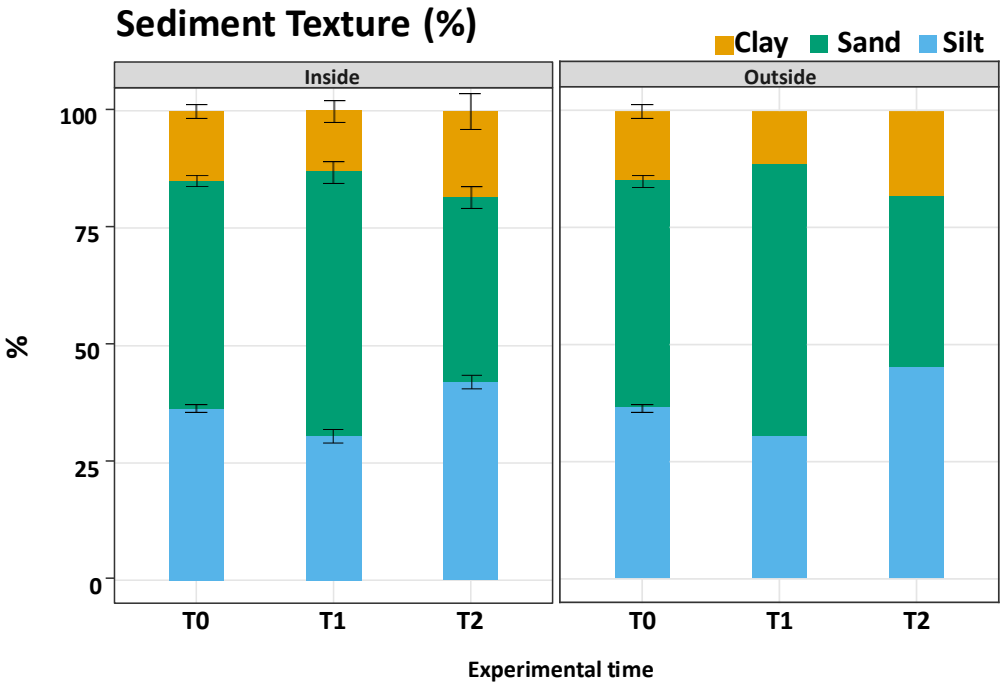

Figure 10.S1 At T_0, the sample was the same for inside and outside conditions. Mean grain size composition (clay, sand, and silt, expressed as %) of surface sediments inside and outside the mesocosms, averaged across all sampling times